Development and Application of a RTX protein-based production platform for peptides and small proteins

Inaugural-Dissertation

zur Erlangung des Doktorgrades

der Mathematisch-Naturwissenschaftlichen Fakultät

der Heinrich-Heine-Universität Düsseldorf

vorgelegt von

Bach-Ngan Wetzel

aus Düren

Düsseldorf, Januar 2024

aus dem Institut für Biochemie

der Heinrich-Heine-Universität Düsseldorf

Gedruckt mit der Genehmigung der

Mathematisch-Naturwissenschaftlichen Fakultät der

Heinrich-Heine-Universität Düsseldorf

Berichterstatter:

1. Prof. Dr. Lutz Schmitt

2. Prof. Dr. Karl-Erich Jaeger

Tag der mündlichen Prüfung:

16. November 2023

„Ein Gelehrter in einem Laboratorium ist nicht nur ein Techniker, er steht auch vor den Naturvorgängen wie ein Kind vor einer Märchenwelt.“

– Marie Curie

Abstract

Strategies for recombinant protein production are frequently associated with challenges including proteolytic degradation, aggregation and cytotoxicity towards host cells or high production cost hampering application in various industries. This dissertation describes the development of a new and unique biochemical production platform for peptides, proteins and a new proteogenic family named "pepteins" that solves the above-mentioned challenges in many cases – Numaswitch^{TM}. This technology is based on so-called "Switchtags", a group of GG repeats containing fragments of RTX proteins which include the C-terminal fragment of α-hemolysin (HlyA), namely HlyA1. Target peptides fused to the C-terminus of HlyA1 were produced as inclusion bodies (IBs) in the absence of the HlyA type 1 secretion system (T1SS) in *E. coli* but extracted from cells and solubilized in chaotropic salts they were found to efficiently refold to highly soluble and functional proteins in the presence of Ca^{2+} ions. This approach was developed for peptides firstly and subsequently for pepteins up to 300 amino acids and complex structure proteins harboring up to three disulfide bridges. Remarkably, truncated HlyA1 variants in fusion to selected candidates led to higher renaturation efficiencies than HlyA1 wild type, and efficient release of targets from HlyA1 backbone was confirmed by analytical and biochemical methods after site-specific proteolysis. It was demonstrated that optimized HlyA1 fragments and other GG repeats containing fragments of RTX proteins are efficient and reliable protein tags granting access to advantages of IBs and solve the bottleneck of efficient refolding of IBs into functional proteins. Pilot scale production of one of the selected candidates, namely Teriparatide, demonstrated the capability of the Numaswitch^{TM} approach to produce peptides in industrial-relevant scales and high qualities. Furthermore, this dissertation focused on the design of antimicrobial-adhesive peptides which may serve as foundation for the functionalization of Resomer®-based implant coatings to prevent bacterial growth in combat against implant-associated infections (IAIs). To identify peptide motifs with adhesive properties against Resomer® phagemid libraries displaying randomized peptides were constructed and used in biopanning experiments against the biopolymer. The emerging Resomer® binding peptide 2 (RBP2) were fused to three selected antimicrobial peptides (AMPs) extensively studied in the literature and produced by the Numaswitch^{TM} technology. Different assays were established to determine whether the antimicrobial and adhesive functions in the bifunctional peptide were preserved. The bifunctional peptides HBD3-RBP2 and reference peptide DS-THA were demonstrated to exhibit antimicrobial activity against *B. subtilis* and adhesive properties against Resomer®. Proof-of-concept was demonstrated with DS-THA, which effectively inhibited the growth of *E. coli* PKL1162 strains on Resomer® coatings after incorporation.

Zusammenfassung

Strategien zur Herstellung rekombinanter Proteine sind häufig mit Problemen wie proteolytischem Abbau, Aggregation und Zytotoxizität gegenüber Wirtszellen oder hohen Produktionskosten verbunden, die ihren industriellen Einsatz in verschiedenen Bereichen erschwert. Diese Dissertation beschreibt die Entwicklung einer neuen und einzigartigen biochemischen Produktionsplattform für Peptide, Proteine und einer neuen proteinogenen Familie namens „Pepteine“, die viele der oben genannten Herausforderungen löst – Numaswitch™. Diese Technologie basiert auf so genannte „Switchtags“, einer Gruppe von Fragmenten aus RTX-Proteinen mit charakteristischen Glycin-reichen Sequenzwiederholungen. Darunter zählt insbesondere das C-terminale Fragment von α-Hämolysin (HlyA), nämlich HlyA1. Zielpeptide, die an den C-Terminus von HlyA1 fusioniert sind, werden in Abwesenheit des Typ-1-Sekretionssystems (T1SS) für HlyA in *E. coli* als unlösliche Proteinaggregate produziert, die sich aber nach der Extraktion aus Zellen und Solubilisierung in chaotrope Agenzien in Gegenwart von Ca^{2+} effizient zu hochlöslichen und funktionellen Proteinen zurückfalten. Dieser Ansatz wurde zunächst für kleinere Peptide und anschließend für Pepteine mit bis zu 300 Aminosäuren entwickelt, die strukturell komplexer sind und bis zu drei Disulfidbrücken enthalten können. Bemerkenswert ist, dass die Fusion von verkürzten HlyA1-Varianten mit den ausgewählten Kandidaten zu höheren Renaturierungseffizienzen führen als mit dem Wildtyp HlyA1. Die Freisetzung der Peptide von HlyA1 nach proteolytischer Spaltung konnte erfolgreich durch analytische und biochemische Methoden nachgewiesen werden. Es konnte gezeigt werden, dass optimierte HlyA1 aber auch andere Fragmente aus RTX-Proteinen mit Glycin-reichen Sequenzwiederholungen als effiziente Protein-Tags fungieren können. Sie ebnen den Weg zu Vorteilen von Proteinaggregaten und lösen die gegenwärtige Problematik der effizienten Rückfaltung. Die Produktion von Teriparatid im Pilotmaßstab demonstriert das Potential der Numaswitch™-Technologie Peptide im industriellen Maßstab und in höchster Qualität herzustellen. Des Weiteren liegt der Fokus dieser Dissertation auf der Entwicklung von antimikrobiell-adhäsiven Peptiden, die als Grundlage für die Funktionalisierung von Resomer®-basierten Implantatbeschichtungen zur Reduktion von Bakterienbesiedlung im Kampf gegen Implantat assoziierte Infektionen (IAIs) dienen können. Zur Identifikation von Peptidmotiven mit adhärenten Eigenschaften gegen Resomer® wurden Phage Display-Peptid-Bibliotheken erstellt und gegen Resomer®-Oberflächen gescreent. So wurde das Resomer®-bindende Peptid 2 (RBP2) entdeckt, welches mit drei ausgewählten antimikrobiellen Peptiden aus der Literatur fusioniert und mit der Numaswitch™-Technologie hergestellt wurde. Die Erhaltung der antimikrobiellen und adhäsiven Eigenschaften der bifunktionellen Peptide wurden in verschiedenen Assays überprüft. Dabei zeigte sich, dass die bifunktionelle Peptide HBD3-RBP2 und DS-THA antimikrobielle Wirkung gegen *B. subtilis* und adhäsive Eigenschaften gegenüber Resomer® aufwiesen. In ersten Machbarkeitsstudien konnte gezeigt werden, dass DS-THA nach Inkorporation in Resomer®-Beschichtungen erfolgreich das Wachstum von *E. coli* PKL1162 auf Oberflächen inhibierte.

Table of Contents

I. Abbreviations

Abbreviation	Meaning
Aβ	β amyloid
aa	amino acid
ABC	ATP-binding cassette
AEX	anion exchange chromatography
AMP	antimicrobial peptide
Amp	ampicillin
ATP	adenosine triphosphate
API	active pharmaceutical ingredients
Aβ40	human ß-amyloid (1-40)
B. subtilis	*Bacillus subtilis*
bp	base pair(s)
BSA	bovine serum albumin
cAMP	cyclic adenosine monophosphate
CEX	cation exchange chromatography
cfu	colony forming units
CLD	C39 peptidase-like domain
ColE1	Colicin E1 origin
CT	C-terminal domain
Ctrl	Control
Da	Dalton
DAPI	4,6-Diamidino-2-phenylindole
DCD-1L	dermcidin-1L
ddH_2O	double-distilled water
DNA	Deoxyribonucleic acid
dsDNA	double stranded DNA
DS-THA	Dermaseptin-Thanatin
EC_{50}	half maximal effective concentration
E_{max}	maximal effective concentration
E. coli	*Escherichia coli*
EGF	Epidermal growth factor
EGFR	Epidermal growth factor receptor
ELISA	enzyme-linked immunosorbent assay
EPS	extracellular polymeric substances
epPCR	error-prone PCR
ESI-MS	Electrospray ionization mass spectrometry
ESI-TOF	Electrospray ionization time-of-flight

FA	formic acid
FDA	Food and Drug Administration
Ff	family of filamentous *E. coli* phage
g	relative centrifugal force
GG repeats	glycine-rich repeats
GuHCl	guanidium hydrochloride
GST	glutathione S-transferase
HBD3	beta-defensin-3
hEGF	human epidermal growth factor
HTN3	human histatin-3
HlyA	hemolysin A
HlyA1	C-terminal 218 aa of hemolysin A
HlyB	hemolysin B
HlyC	hemolysin C
HlyD	hemolysin D
HlyBD	complex consisting of HlyB and HlyD
HlyBD-TolC	complex consisting of HlyB, HlyD and TolC
HM	host membrane
hND	hydrophobic N-terminal domain
IAI	implant-associated infections
IEX	ion exchange chromatography
IB	inclusion body
IG	intergenic region
IgG2	Immunoglobin G2
IM	inner membrane
IMAC	immobilized metal affinity chromatography
IBS-C	irritable bowel syndrome with constipation
IPTG	Isopropyl β-D-1-thiogalactopyranoside
kan	kanamycin
K_d	dissociation constant
kDa	kilo Dalton
kV	kilovolt
LA	Lactic acid
LAL	Limulus amebocyte lysate
LB medium	Luria-Bertani medium
LPS	Liposaccharide
M	molar
MalE	Maltose binding protein
MFP	membrane fusion protein

mg	milligram
MIC	minimal inhibitory concentration
min	minute
mL	milliliter
MOI	multiplicity of infection
MRSA	methicillin-resistant *S. aureus*
MW	molecular weight
m/z	mass-to-charge ratio
NBD	nucleotide binding domain
OD_{600}	optical density (absorbance) at 600 nm
OM	outer membrane
OMP	outer membrane protein
ORF	open reading frame
p3	filamentous phage minor capsid protein
p8	filamentous phage major capsid protein
PEG	polyethylene glycol
pro-HlyA	precursor form of HlyA
PBS	Phosphate-buffered saline
PBS-T	PBS containing 0.1% (v/v) Tween-20
pelB	pectate lyase B from *Erwinia carotovora*
PLLA	poly-L-lactic acid
PDLLA	Poly-D, L-lactic acid
Plac	lac promotor
PTH	Parathyroid hormone
QCM	quartz crystal microbalance
RBP	Resomer binding protein
rHCD	residual host cell DNA
rHCP	residual host cell protein
RBP	Resomer binding peptide
RF DNA	replicate form DNA
RP-HPLC-MS	reversed phase high performance liquid chromatography mass spectrometry
RPM	rounds per minute
RT	room temperature
RTK	receptor tyrosine kinase
RTX	Repeats in Toxins
SAA3	Serum amyloid A3
scFv	single-chain variable fragment
SDS-PAGE	sodium dodecyl sulfate polyacrylamide gel electrophoresis
SD	standard deviation

sec	seconds
SEC	size exclusion chromatography
ssDNA	single stranded DNA
S. aureus	*Staphylococcus aureus*
SOC medium	super optimal broth with catabolite repression medium
SPPS	solid-phase peptide synthesis
SPR	surface plasmon resonance spectroscopy
SUMO	small ubiquitin-like modifiers
Tat	Twin-arginine translocation
TB	Terrific Broth
TBS	Tris-buffered saline
TBE	Tris-borate-EDTA
TE	Transformation efficiency
TEV	tobacco etch virus
TFA	trifluoro acetic acid
TMD	transmembrane domain
T1SS	type I secretion system
UPEC	uropathogenic *Escherichia coli*
UPLC-MS	ultraperformance liquid chromatography-tandem mass spectrometry
µL	microliter
µM	micromolar
UTI	urinary tract infections
UV/VIS	Ultraviolet–visible spectroscopy
VH	variable fragment heavy chain
VL	variable fragment light chain
VHH	camelid heavy chain antibody fragment
V	Volt
2YT medium	2x Yeast Extract Tryptone medium
2YT-AG	2YT medium supplemented with 100 µg/mL ampicillin and 100 mM glucose
2YT-AK	2YT medium supplemented with 100 µg/mL ampicillin and 30 µg/mL kanamycin

List of amino acids

Amino acid	three letter code	one letter code
Alanine	Ala	A
Arginine	Arg	R
Asparagine	Asn	N
Aspartic acid	Asp	D
Cysteine	Cys	C
Glutamic acid	Glu	E
Glutamine	Gln	Q
Glycine	Gly	G
Histidine	His	H
Isoleucine	Ile	I
Leucine	Leu	L
Lysine	Lys	K
Methionine	Met	M
Phenylalanine	Phe	F
Proline	Pro	P
Serine	Ser	S
Threonine	Thr	T
Tryptophan	Trp	W
Tyrosine	Tyr	Y
Valine	Val	V

List of nucleotides

Bases	one letter code
Adenine	A
Guanine	G
Cytosine	C
Thymine	T

II. List of Figures

III. List of Tables

1 Introduction

1.1 Secretion systems in Gram-negative bacteria

Gram-negative bacteria are a group of bacteria characterized by a complex cell wall structure including an inner membrane and a thin peptidoglycan cell wall that is enveloped by an outer membrane consisting of liposaccharides. In contrast, Gram-positive bacteria lack an outer membrane but have a thicker cell wall consisting of peptidoglycans and teichoic acid (Beveridge, 1999). Gram-negative bacteria are a considerable concern in the healthcare sector because they can cause various illnesses that are difficult to treat due to antibiotic resistance. During evolution, these bacteria have developed various secretion systems allowing them to transport different substances across the cell wall which contributed to the development of antibiotic resistances. These substrates range from small molecules like antibiotics or toxins, DNA to small or large proteins (Green and Mecsas, 2016). So far, eleven different secretion systems have been discovered in Gram-negative bacteria. Some of these systems, such as the type I secretion system (T1SS), T3SS, T4SS, and T6SS, transport substrates across both cell membranes in a one-step process. Other systems, such as T2SS, T5SS, T7SS, T8SS, T9SS, T10SS, and T11SS require substrates to be translocated to the periplasm by secretory pathways including Sec, twin-arginine translocation (Tat) and holin systems firstly before completing the secretion process (Filloux, 2022). For the understanding of this dissertation exclusively T1SS of *E. coli* is of particular importance, hence detailed descriptions of its assembly and function are given in the following chapters.

1.2 Type 1 secretion system

The type 1 secretion system (T1SS) is widespread among Gram-negative bacteria and known to secrete high diversity substrates (e.g. toxins, protease, lipases, adhesins) of different sizes ranging from 10 to 900 kDa from the cytoplasm to the exterior in a single step without periplasmic stop (Lenders et al., 2015, Smith et al., 2018). The T1SS is a tripartite complex consisting of the IM ATP-binding cassette (ABC) transporter, a membrane fusion protein (MFP) and an outer membrane pore (OMP) (Kanonenberg et al., 2018). T1SS substrates are often acidic in nature and harbor glycine-rich repeats (GG repeats) which bind Ca^{2+} (Baumann et al., 1993). Furthermore, almost all known T1SS substrates contain a C-terminal 50-60 amino acid (aa) long secretion signal that directs the unfolded substrate to the IM complex composed of the ABC transporter and MFP. The ABC transporter recognizes the secretion signal and the OMP is recruited to the translocation site which enables the secretion of the unfolded substrate to the exterior space. Unlike other secretion systems the signal peptide is not cleaved from the substrate upon release. When the secretion process is completed the transport complex dissociates and the next translocation cycle is initiated (Smith et al., 2018). Since the secretion signal is located at the C-terminal region it is assumed that T1SS substrates are exported post-translationally rather than co-translationally (Masi and Wandersman, 2010). The most prominent

substrate of the T1SS is the toxin hemolysin A belonging to the repeats in toxin (RTX) protein family (Zhao et al., 2022, Lenders et al., 2015) (section 1.2.5).

1.2.1 The hemolysin A T1SS of *E. coli*

Hemolysin A (HlyA) is one of the best characterized substrates of the T1SS and a major virulence factor secreted by uropathogenic *Escherichia coli* (UPEC) which is the primary cause for chronic urinary tract infections (UTIs) (Johnson, 1991). HlyA is secreted by the HlyA1 T1SS in similar fashion as described in section 1.2. The secretion signal of unfolded HlyA is recognized by the IM HlyBD complex which consist of ABC transporter hemolysin B (HlyB) and the MFP hemolysin D (HlyD). This leads to the recruitment of OMP TolC which is an essential component of several efflux systems (section 1.2.4). The resulting tripartite HlyBD-TolC complex exports HlyA across both cell membranes in a single step. Outside the cell Ca^{2+} ions bind to so-called GG repeats which are nonapeptide stretches of the consensus sequence GGxGxDxUx (where x can be any amino acid and U is a large hydrophobic amino acid) inducing the correct folding of HlyA into a soluble, stable and functional protein (Kanonenberg et al., 2018, Baumann et al., 1993).

Most components of the HlyA T1SS are encoded by the *hly* operon present in bacterial chromosomes or on plasmids. The *hly* operon consist of the four genes *hlyC, hlyA, hlyB* and *hlyD* (Felmlee et al., 1985). While the genes *hlyA*, *hlyB* and *hlyD* encode HlyA, HlyB and HlyD, respectively, the gene *hlyC* encodes the acyltransferase HlyC which is not related to the secretion process, but it catalyzes the acylation reaction of the HlyA precursor (pro-HlyA) at two lysine residues. Acylations are important for the biological activity of HlyA (Thomas et al., 2014b, Stanley et al., 1994). The gene of OMP TolC is not included in the *hly* operon, but essential for the HlyA secretion process (Wandersman and Delepelaire, 1990). A terminator region in form of a hairpin-loop is located between the genes *hlyA* and *hlyB* and the transcriptional anti-terminator factor RfaH is required to read through it. In the absence of RfaH the transcription level of *hly* operon significantly decreases (Leeds and Welch, 1997).

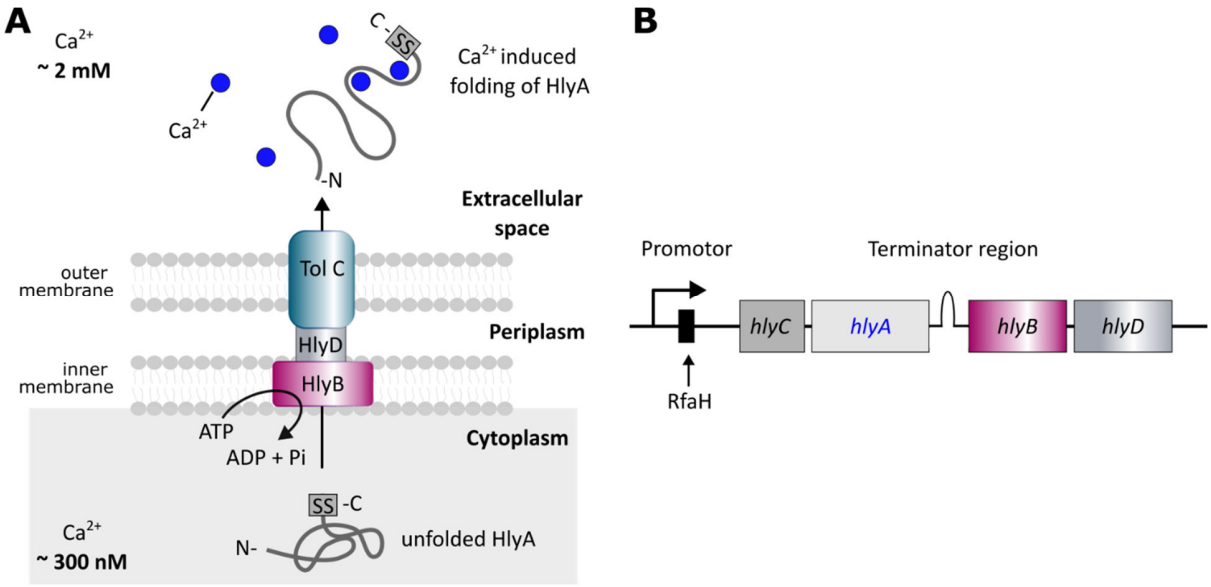

Figure 1 | Schematic illustration of HlyA T1SS in *E. coli* and the *hly* operon

(A) The HlyA T1SS is a tripartite transport complex consisting of the outer membrane TolC, the membrane fusion protein HlyD and the ATP-binding cassette (ABC) transporter HlyB. Secretion of unfolded HlyA substrate is energized by ATP hydrolyses by the HlyBD complex. In the extracellular space Ca^{2+} induce the correct folding of HlyA to biological active protein (Kanonenberg et al., 2018). IM: inner membrane; OM: outer membrane. N and C mark the N- or C- terminal end of the HlyA protein. **(B)** The *hly* operon consist of the genes *hlyC*, *hlyA*, *hlyB* and *hlyD*. Downstream of the promotor (angled black arrow) is the anti-terminator factor RfaH (indicated) located that is required to read through the terminator region (indicated as kink) between *hlyA* and *hlyB* (Thomas et al., 2014b, Pourhassan et al., 2022).

1.2.2 HlyB – the ABC transporter

The ABC-transporter HlyB is located at the IM of *Escherichia coli* (*E. coli)* and forms a functional homodimer of approximately 82 kDa per monomer. Each subunit contains a N-terminal C39 peptidase-like domain (CLD), a transmembrane domain (TMD) and a C-terminal nucleotide binding domain (NBD) essential for protein secretion. The binding of ATP to a monomeric NBD triggers dimerization of HlyB subunits and subsequent ATP hydrolyses by NBDs trigger conformational changes in TMDs that form a channel in the IM for substrate translocation (Zaitseva et al., 2005, Pan et al., 2016). For substrate translocation, HlyB homodimers form a stable IM complex with HlyD subunits. The resulting IM HlyBD complex consist of three HlyB homodimers and six HlyD subunits that are symmetrically arranged to a pseudo-trimer (Zhao et al., 2022).

Besides ATP hydrolysis the NBDs were found to specifically interact with the C-terminal fragment of HlyA substrate, the so-called HlyA1, indicating the importance of the secretion signal for HlyA-NBD association (Benabdelhak et al., 2003). Furthermore, HlyB contains an N-terminal CLD (~ 130 aa) which interacts with unfolded HlyA independently from the secretion signal and brings it in position for the translocation process

(Lecher et al., 2012, Balakrishnan et al., 2001). C39 peptidases belong to a subfamily of the papain superfamily of cysteine proteases and located in ABC transporters (e.g. Colicin V in *E. coli*). They use the catalytic triad (consisting of Cys, His and Asp) to cleave off the C-terminal signal peptide from substrates during or upon translocation (Havarstein et al., 1995, Hwang et al., 1997). However, many T1SS ABC transporters such as HlyB from *E. coli* harbor a Tyr residue instead of a Cys residue in the catalytic triad which makes the domain proteolytically inactive. The HlyB ABC transporter forms a stable inner complex with the MFP HlyD (Lecher et al., 2012).

1.2.3 HlyD – the membrane fusion protein

HlyD is a member of the MFP family and exclusively present in Gram-negative bacteria. They are characterized by a single TMD, a short N-terminal cytosolic domain (~ 60 aa) and a large periplasmic domain (Zhao et al., 2022, Balakrishnan et al., 2001). While the cytosolic domains of hexameric HlyD as part of the HlyBD complex interact with HlyA substrate, the periplasmic domains transiently interact with homotrimeric outer membrane TolC forming a tunnel-like channel that enables direct export of substrates across both cell membranes (Zhao et al., 2022, Balakrishnan et al., 2001, Andersen et al., 2002).

1.2.4 TolC – the outer membrane protein

The OMP TolC in *E. coli* is a multifunctional protein involved in several multidrug efflux pump mechanisms and is an integral part of the T1SS. The gene of TolC is not directly linked with the *hly* operon, hence TolC is not exclusively dedicated to HlyA secretion, but also involved in colicin import (Jakes, 2017) or efflux of antibiotics (Piddock, 2006b, Ayhan et al., 2016) and bile salts (Hamner et al., 2013, Cremers et al., 2014). In fact, the efflux of antibacterial drugs from cells is considered as problematic as it promotes multidrug resistances of bacterial strains (Piddock, 2006a). When HlyA interacts with the cytosolic domain of HlyD and the CLD of HlyB (Lecher et al., 2012, Zhao et al., 2022), TolC is recruited to the translocation site and forms a transient 140 Å long homotrimeric channel consisting of a short ß-barrel domain which span the outer membrane and a long α-helical periplasmic domain (Andersen et al., 2001, Koronakis et al., 2000). In resting state the periplasmic tunnel entrance is closed (~ 3.5 Å) but upon interaction with inner membrane transport systems such as HlyBD the channel opens in an iris-like manner (~ 30 Å) allowing the export of HlyA or other substrates of different sizes (Andersen et al., 2002, Koronakis et al., 2000).

1.2.5 HlyA – the RTX toxin and substrate of HlyA T1SS

The toxin HlyA (110 kDa), a prominent member of the RTX protein family and key virulence factor of UPEC and other pathogens induces different responses in epithelial cells like intracellular Ca^{2+} oscillation (Uhlen et al., 2000, Koschinski et al., 2006), cell polarity changes (Schulz et al., 2021), modulation of NF-kB, MAPK, and AKT signaling pathways (Dhakal and Mulvey, 2012, Bhushan et al., 2011, Kloft et al., 2009) or modification of histone acetylation and phosphorylation patterns (Hamon et al., 2007, Ratner et al., 2006). Furthermore, HlyA causes the lysis of eukaryotic cells including red blood cells by formation of pores in epithelial plasma membranes (Cavalieri et al., 1984). HlyA consists of three functional domains: a hydrophobic N-terminal domain (hND), a RTX domain characterized by the presence of six GG repeats and an about 60 aa long C-terminal secretion signal (Kanonenberg et al., 2018) (Figure 2).

Upon expression in *E. coli* cells, HlyA toxins are produced as non-toxic precursor forms (pro-HlyA), and two essential events are necessary to obtain mature and biological active HlyA. Firstly, HlyA activation is initiated by lysine fatty acylation: long-chain acyl groups (myristic (C_{14}) or palmitic acid (C_{16})) are attached to two internal lysine residues (Lys564 and Lys690) by amide bond formation. This reaction is mediated by the co-synthesized acyltransferase HlyC and the acylated form of acyl-carrier protein (Nicaud et al., 1985, Stanley et al., 1994). Secondly, outside the cell the secreted HlyA binds Ca^{2+} at the C-terminal RTX domain which triggers the proper folding of HlyA into soluble, stable and biological active protein. Since the cytoplasmic Ca^{2+} concentration (~ 300 nM) is below the K_d value of this binding event (~ 100 µM), folding happens exclusively after transport in the cell surrounding ($Ca^{2+} \geq 2$ mM) (Thomas et al., 2014a, Lenders et al., 2016). To this date, no chaperone is known to be involved in the HlyA secretion process, presumably due to the interaction of the CLD of HlyB with HlyA (Lecher et al., 2012).

1.2.6 HlyA1 – a versatile carrier for heterologous protein expression

HlyA1 is a C-terminal fragment (~ 218 aa) of HlyA and contains the C-terminal secretion signal of HlyA (~ 60 aa) along with three of the six conserved GG repeats of the RTX domain (Figure 2). Despite reduction in size (24 vs. 110 kDa) and number of GG repeats the secretion levels and Ca^{2+} binding affinities of HlyA1 and full-length HlyA comparable which suggest that all necessary information are included in the C-terminal fragment (Nicaud et al., 1986, Kenny et al., 1991). Since decades, the HlyA1 fragment has been employed as carrier protein for the transport of heterologous fusion proteins (Blight and Holland, 1994, Kenny et al., 1991, Mackman et al., 1987). For secretion, the genes encoding heterologous proteins were N-terminally fused to HlyA1 fragments and co-expressed with genes of the inner membrane components HlyB and HlyD (Kenny et al., 1991, Bakkes et al., 2010). TolC is constitutively expressed by recombinant host *E. coli* strains (Tikhonova and Zgurskaya, 2004). Although the export of fusion proteins were successful low secretion titers and narrow substrate ranges prevented broad application of HlyA1 as a universal secretion platform

(Schwarz et al., 2012, Ruano-Gallego et al., 2019, Fernandez et al., 2000). This changed by the finding of an A/U-rich enhancer sequence encoded on the C-terminal gene of HlyC (Khosa et al., 2018) increasing expression and secretion levels up to 1000-fold allowing production of HlyA1 in titers up to 30 g per fermentation liter (unpublished data). Furthermore, large heterologous proteins not able to be produced before were able to be efficiently expressed in the soluble, functional form now (Schwarz et al., 2012, Pelzer et al., 2015). The company Numaferm GmbH currently applies this secretion approach successfully to produce peptides and small proteins under the brand name Numasec™. Here, HlyA1 serves as protein tag enabling efficient transportation of heterologous fusion proteins to the extracellular medium and facilitates the folding into soluble and functional proteins in the presence of Ca^{2+}.

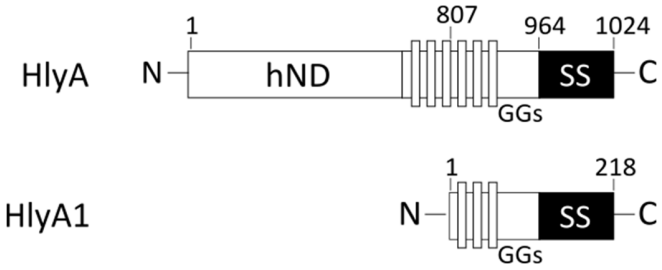

Figure 2 | Schematic view of HlyA and HlyA1

HlyA consist of a hydrophobic N-terminal domain (hND), a RTX domain characterized by the presence of six GG repeats (GGs) and a C-terminal secretion signal (SS, ~ 60 aa). HlyA1 is a C-terminal fragment of HlyA (~ 218 aa) and contains three of the six GGs and the SS (Nicaud et al., 1986). Numbers indicate the position in the corresponding amino acid sequence.

However, in the absence of HlyB and HlyD both HlyA and HlyA1 are not secreted but form IBs in the cytoplasm, presumably due to low Ca^{2+} concentration inside cells leading to formation of (partially) unfolded and aggregation prone proteins (Bakas et al., 1998, Bumba et al., 2016, Pimenta et al., 2005). Remarkably, HlyA and HlyA1 IBs extracted from cells and denatured in chaotropic agents such as urea or guanidium-hydrochloride (GuHCl) were found to efficiently refold into soluble and functional protein again promoted by the presence of Ca^{2+} (Lecher et al., 2012, Sanchez-Magraner et al., 2007, Pimenta et al., 2005). In the extracellular environment high concentrations of Ca^{2+} ($\geq$ 2 mM) bind to the GG repeats located in the RTX domains of HlyA and HlyA1 and induce the formation of parallel β-roll structures which is critical for the tertiary conformation of RTX domains (Baumann et al., 1993, Lenders et al., 2016). Furthermore, this behavior has been demonstrated to be conserved when peptides and small proteins were fused to the C-terminus of HlyA1 fragments (Figure 3) (unpublished data). Here, HlyA1 functions as a bifunctional protein tag forcing the formation of intracellular IBs in *E. coli.* Upon extraction and solubilization, HlyA1 efficiently induces the refolding process to highly soluble and functional proteins in the presence of Ca^{2+}.

In this dissertation, the term "Switchtags" refers to a group of protein tags containing different GG repeat numbers and variations sourced from RTX proteins, in particular HlyA. They were named "Switchtags" due to their ability to convert insoluble IB aggregates into soluble proteins in a switch-like manner in the presence of Ca^{2+}. The workflow of the Numaswitch™ technology employing Switchtags for peptide and protein production is illustrated in Figure 3.

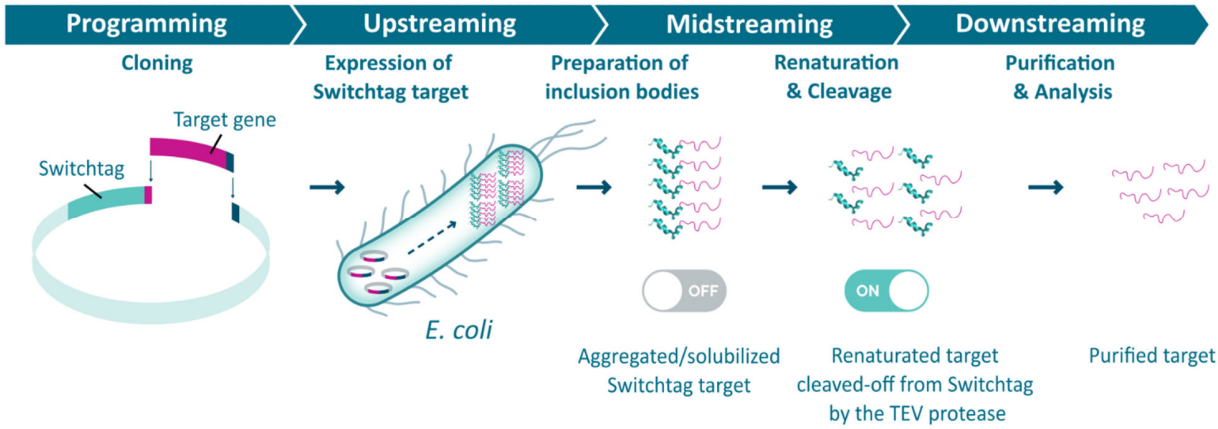

Figure 3 | Numaswitch™ – An efficient platform for heterologous protein expression

The expression plasmid contains a N-terminal HlyA1 fragment (also referred to as “Switchtag”) genetically fused to the target gene encoding the desired peptide or protein. After the plasmid DNA is transformed into *E. coli*, the fusion proteins are produced as IBs inside the cells due to the absence of the HlyBD inner membrane complex. The IBs can be extracted from cells, solubilized in chaotropic agents and the fusion proteins can be efficiently refolded after dilution in Ca^{2+}-containing buffer. Separation of target peptide or protein from HlyA1 occurs by site-specific proteolytic cleavage between both domains and purified targets can be obtained by standard chromatographic methods.

1.3 Recombinant protein production strategies

1.3.1 Peptides and pepteins

Peptides and pepteins combine pharmacological advantages of small molecule and protein-based drugs and are used as active pharmaceutical ingredients (APIs) in therapeutic applications (Zompra et al., 2009). Peptides are conventionally defined as molecules consisting of 2–50 aa (Friedberg et al., 1947) while the term “pepteins” (deriving from peptide and proteins) refer to polypeptide chains made of 30–300 aa in this dissertation. The important role of pepteins including e.g. growth factors, antibody fragments or nanobodies in biological functions and cellular processes was not recognized until recently (Su et al., 2013, Storz et al., 2014). The demand of peptide and peptein-derived drugs in the pharmaceutical industry considerably grew in the last years due to their high activity, great chemical and biological properties and low cytotoxicity (Lau and Dunn, 2018, Wang et al., 2022). Peptides smaller than 50 aa are conventionally synthesized by chemical synthesis, but pepteins in the range of 30–300 aa are considered as to be challenging to produce due to

intrinsic disadvantages and limitations of this method (e.g. inefficient coupling and deprotection reactions, accumulation of byproducts and aggregation of growing peptide chains) (Hou et al., 2017, Pedersen et al., 2012, Schnölzer et al., 1992, King et al., 1990). In addition, chemical synthesis is associated with the use of harmful chemicals, limited scalability and cost-of-goods which prevents broad commercial application (Isidro-Llobet et al., 2019). Reliable recombinant expression systems face other challenges as many peptides and pepteins are prone to degradation, post-translational modifications or aggregation inside cells. Furthermore, cytotoxic effects of targets towards host cells decrease the efficiency and product yield of most systems (Rivera-de-Torre et al., 2021). Various expression strategies were developed to circumvent such limitations based on the fusion with protein tags, for example IB tags, solubility tags or transport signals (Wegmuller and Schmid, 2014). The strategies are successfully applied for various peptides, but the establishment of efficient production processes is often time consuming and costly due to intrinsic disadvantages. IB peptide fusions are typically produced as proteolysis resistant aggregates in *E. coli* at high titers, but low refolding efficiencies hamper downstream steps and thus the production of functional products at high yields (Singh and Panda, 2005, Singh et al., 2015). Approaches using solubility tags most often aim for intracellular peptide production in a soluble form. However, these approaches are limited by proteolytic degradation in the cytoplasm, low expression titers or extensive downstream efforts to reach high purity levels (Costa et al., 2014). The transport into the cell surrounding by Gram-positive bacteria or yeast is an alternative that is universally applied for the industrial production of proteins. However, significant efforts are needed, e.g. for cloning, analysis of different signal sequences, definition of a suitable host and depletion of host proteases (Tripathi and Shrivastava, 2019). So far, robust and efficient transport systems for the industrial standard host *E. coli* are not available or limited to few examples and the reliability and applicability of the systems for efficient production of peptides has yet to be demonstrated (Rivera-de-Torre et al., 2021).

1.3.2 Disulfide-rich peptides and proteins

Disulfide bond formations in peptides and proteins play a crucial role for folding into the native state as it influences their stability, function, and activity (Zavodszky et al., 2001). Production of disulfide bonds containing protein-derived bioactive compounds, such as antimicrobial peptides, growth factors, antibody fragments or nanobodies often occur in yeast systems based on *Saccharomyces cerevisiae* or *Pichia pastoris* as they are cost-efficient, easy to manage, and high product titers can be reached. However, unfavorable N-glycosylation can occur leading to hyper-mannosylation reducing the protein's activity and eliciting immune reactions (Wu et al., 2018, Ma et al., 2020). Alternative systems including mammalian calls or baculovirus expression systems contain enzymatic machineries and/or chaperones assisting correct protein folding and enable other post-translational modifications, but they are associated with high production costs, laborious and time-consuming cell line developments and low production yields (Bulleid, 2012, Ma et al., 2020). Bacterial expression systems based on *E. coli* are fast, cost-efficient, simple and the most widely utilized (Rivera-de-Torre et al., 2021). Around 30 % of the currently approved recombinant therapeutic peptides or proteins are produced by this expression host. Especially for large scale production of recombinant proteins *E. coli* is the host-of-choice for the biotechnology industry (Baeshen et al., 2015). However production of disulfide-rich peptides and proteins in *E. coli* has been difficult as the reducing environment in the cytoplasm and the absence of appropriate chaperones most often prevent the formation of proper disulfide bonds (Costa et al., 2014, Manta et al., 2019). Several systems and procedures have been developed to optimize the formation of disulfide bonds, including modified *E. coli* host cells for enhanced oxidative folding in the cytoplasm (Lobstein et al., 2012) or the translocation of targets to the oxidative environment of the *E. coli* periplasm (Bardwell et al., 1991, Manta et al., 2019). In both cases, native disulfide bond formation relies on correct *de novo* disulfide bond formation or the subsequential isomerization to the correct isomer. Despite successful examples, many of such targets tend to accumulate as insoluble aggregates due to incomplete or mismatched formation of disulfide bonds resulting in low overall production yields (Bhatwa et al., 2021, Teilum et al., 1999).

1.3.3 Selected peptide and peptein candidates

In this dissertation different peptides and pepteins were selected to demonstrate the applicability of the Numaswitch™ technology to produce structurally challenging candidates of varying molecular masses, biological functions, and number of disulfide bridges. An overview of the selected peptides and pepteins and their role in biological processes is given in Table 1.

Table 1 | Overview of selected peptide and peptein candidates produced by Numaswitch™

Selected peptides or pepteins	Biological functions	Reference
Teriparatide	N-terminal and biologically active peptide fragment (1-34 aa) of the human parathyroid hormone (PTH, 1-84 aa) used as therapeutic drug to stimulate bone formation and for treatment of osteoporosis.	Holick (2005)
Linaclotide	Synthetic peptide (14 aa) and agonist of the guanylate cyclase C mainly applied as therapeutic drug to treat irritable bowel syndrome with constipation (IBS-C).	Hannig et al. (2014)
Dermaseptin-Thanatin (DS-THA)	Peptide-peptide conjugate consisting of the antimicrobial peptide dermaseptin (DS) and thanatin (THA). Bifunctional peptide described to adhere on wax layer of soybean leaves and to prevent the germination of *Phakopsora pachyrhizi* spores. Applied in combat against the plant disease Asian soybean rust.	Schwinges et al. (2019)
human β-amyloid (1–40) (Aβ40)	C-terminal peptide isomer of the β-amyloid (Aβ) (40 aa) mainly found in plaques in the brains of Alzheimer's patients. Aggregation of Aβ is implicated in the pathogenesis of the Alzheimer's disease.	Gu and Guo (2013)
Serum amyloid A3 (SAA3)	Murine SAA3 is an acute-phase protein and hallmark for inflammation and infection diseases.	Meek et al. (1992)
human epidermal growth factor (hEGF)	Growth factor (53 aa) which binds to EGF receptors (EGFR, ErB1) and activates the intrinsic tyrosine kinase. The EGF signaling pathway regulates cellular events including cell differentiation, proliferation, or motility.	Zeng and Harris (2014)
camelid heavy chain antibody fragment (VHH)	Nanobody which specifically binds to red fluorescent protein mCherry.	Wang et al. (2021) Fridy et al. (2014)
single-chain variable fragment (scFv) clone F2C	A single-chain variable fragment (scFv) which specifically binds to α-tubulin. It is a fusion protein of the variable regions of the heavy (VH) and light chains (VL) of immunoglobulins.	Nizak et al. (2003)

1.4 Implant-associated infections

Orthopedic implants play a critical role in medical treatments as they restore the function of bone impairments or deformations in the human body such as hips, joints, and limbs. In 2014, about 1.55 % of the total hospitalizations were related to implant-associated infections (IAIs) occurred post-surgically after implant insertion (Pirisi et al., 2020). In prospect of the increase of ageing population world-wide the demand on implant insertions and related surgeries are expected to rise (Mastnak et al., 2022, Amin Yavari et al., 2020). Implant failures caused by IAIs lead to high morbidity and mortality rates and are a significant

financial burden to health care systems. Failure to adequately treat IAIs lead to revision surgeries for implant removal, amputations or delayed wound healing (Mastnak et al., 2022, Arciola et al., 2012).

IAIs are predominantly caused by *Staphylococcus* species due to their excellent ability to produce biofilms (Mastnak et al., 2022, Arciola et al., 2012). Typically, the formation of biofilms can be categorized into four stages. The first stage involves initial attachment of bacteria to implant surfaces facilitated by hydrophobic, electrostatic, or Van der Waals forces. In the second stage, the adherent bacteria proliferate and create a layer that firmly anchors the cell mass to the implant surface. As the biofilm matures, it consists of a highly hydrated extracellular matrix that encapsulates the bacteria providing them with efficient protection against antibiotics (Arciola et al., 2012). Bacteria in biofilms tolerate antibiotic concentrations up to 500 to 1000 times higher than planktonic ones (Anwar et al., 1990). The last stage involves the detachment of bacteria from the biofilm triggering a new cycle of bacterial colonization elsewhere (Arciola et al., 2012).

Prevention of biofilm formation on implant surfaces has been the primary goal of numerous strategies developed over the years. This is because treating infections associated with biofilm formation is considerably more difficult than preventing the initial development of the biofilm (Amin Yavari et al., 2020, Arciola et al., 2012). The most common strategies involve surface functionalization or coating of the implants. Coatings applied to implant surfaces can have two primary purposes. The first is to improve the surface properties of the implant, leading to decreased bacterial attachment and subsequent prevention of biofilm formation. The second is to eliminate bacteria in a direct contact killing mechanism, which can be achieved by loading or immobilization of drugs such as antibiotics, antimicrobial peptides (AMPs), inorganic materials (e.g. chitosan) or inorganic ions (e.g. silver, copper, zinc metal nanoparticles) (Amin Yavari et al., 2020). The use of biopolymers for implant surface coating has become a promising approach due to their ease of application on several types of implant materials without altering their inherent properties. Although most biopolymers do not possess intrinsic antimicrobial properties, they are frequently utilized in combination with antimicrobial agents as drug delivery systems to combat infections at the implant site (Campoccia et al., 2013, Song et al., 2020).

1.5 The biopolymer Poly-D, L-lactic acid

In this dissertation, the biopolymer Poly-D, L-lactic acid (PDLLA) also referred to as Resomer® R203 by Evonik was chosen to create surface coatings (Evonik, 2023). These coatings were assessed for their antimicrobial effect after incorporation of antimicrobial-adhesive peptides (section 1.7). PDLLA is an amorphous biopolymer already widely applied as scaffold in the field of tissue engineering (Lin et al., 2006, Gierej et al., 2019) or as microparticles in controlled drug delivery systems (Xu et al., 2013). PDLLA is composed of L- and D-lactic acid isomers that are covalently linked by ester groups. With molecular weights (MWs) ranging from 18,000 to 28,000 Da, it displays exceptional biocompatibility and has been declared

safe for human applications by the US Food and Drug Administration (FDA) for clinical use (Gierej et al., 2019, Lee et al., 2016).

The advantage of PDLLA is that it is biodegradable, i.e. in the human body the biopolymer degrades by ester group hydrolysis catalyzed by water. The long polymer chains gradually break down into lactic acid (LA) monomers. Typically, two models describe the degradation behaviors of biopolymers. In the bulk degradation model, the surrounding water penetrates the bulk material faster than the conversion of PDLLA oligomers to monomeric LA. Thus, the biopolymer swells up and degrades from the inside out. Eventually, the polymer scaffold collapses, and LA monomers are metabolized into CO_2 and H_2O, which are cleared out as urine through the kidney. In the surface degradation model, PDLLA degradation occurs only on the polymer surface while the bulk material remains intact. Over the time the polymeric devices becomes increasingly thinner (von Burkersroda et al., 2002). According to the manufacturer's information, Resomer® R203 is in particular designed for microparticles and drug-loaded implants and the rate of degradation varies from a few weeks to nine months highly depending on the coating thickness, temperature and chemical stability (Evonik, 2023).

To prepare PDLLA coatings, the biopolymer can be dissolved in organic solvents such as chloroform, ethyl acetate, or methylene chloride. Different techniques can be used to form PDLLA coatings including solution casting technique (Siemann, 2005), spin-coating (Albarahmieh et al., 2018) or dip-coating methods (Zhang et al., 2022). In this dissertation the solution casting technique was applied to coat wells of microtiter plates due to the simplicity of this method. For this, PDLLA was dissolved in an organic solvent and equal volumes of the resulting biopolymer solution were added to wells of microtiter plates. The organic solvent evaporates and a thin PDLLA film remains.

1.6 Antimicrobial peptides

Antibiotics are commonly used in routine procedures to combat IAIs, but their excessive usage is leading to the emergence of antibiotic-resistant bacteria, i.e. methicillin-resistant *Staphylococcus aureus* (MRSA) which becomes increasingly problematic in combat against bacterial infections (Brumfitt and Hamilton-Miller, 1989). In prospect of the necessity to find novel alternative drug compounds, antimicrobial peptides (AMPs) emerged as a promising class of biomolecules. AMPs are short peptides (10-50 aa) present in the innate immune systems of various organisms and they exhibit broad antimicrobial activity against different bacteria, fungi, and viruses (Huan et al., 2020). More than 3200 AMPs have been discovered to date, and many AMPs are being assessed in clinical trials underlining their potential to replace conventional antibiotics (Chen et al., 2022). Most AMPs are positively charged (net charge range from +2 to +11) and contain hydrophobic regions (up to 50 %). They typically exhibit α-helical or β-helical structures, while random-coiled structures are less prevalent (Mahlapuu et al., 2016, Huan et al., 2020).

AMPs have two primary modes of action. In the first one, they directly target the bacterial cell membrane which leads to their disruption and subsequent cell death. It is proposed that cationic AMPs are attracted to negatively charged phosphate groups of liposaccharides (LPS) by electrostatic interactions which results in pore formation and destabilization of the cell membrane. Three distinct models describe how AMPs permeabilize bacterial cell membranes, referred to as barrel starve model, the carpet model and the toroidal pore model (Huan et al., 2020) (Figure 4). In the second mode of action, AMPs enter the cell without membrane disruption and target certain cell host DNA or proteins which blocks nucleic acid or protein biosynthesis, protease activity or cell division. Due to the mode of action of AMPs it is more difficult for bacteria to develop resistances compared to conventional antibiotics (Huan et al., 2020, Peschel and Sahl, 2006).

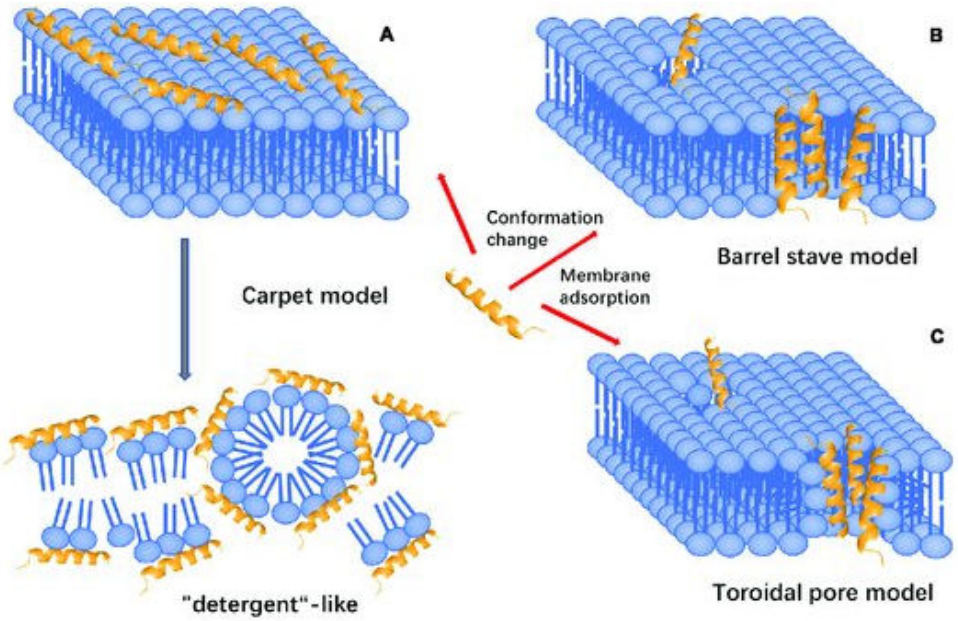

Figure 4 | Mode of action of AMPs

The AMPs are depictured as yellow spirals, while the bacterial cell membrane consisting of phospholipids are illustrated in blue. **(A)** In the carpet model, AMPs accumulate on the surface of cell membranes and act like a "detergent" for disruption. **(B)** In the barrel stave model the AMPs aggregate to multimers which penetrate the cell membrane in parallel alignment to phospholipids and create a channel. **(C)** In the toroidal pore model the AMPs vertically embed into the cell membrane forming a ring-shaped hole. The figure was adapted from Huan et al. (2020).

1.7 Resomer® coatings with bifunctional peptides

One major objective of this dissertation was to design of antimicrobial-adhesive peptides, also referred to as bifunctional peptides, that can be incorporated in Resomer® coatings (section 1.5) to prevent bacterial

growth on surfaces (Figure 5). Bifunctional peptides embedded in polymeric matrices for implant surface coatings can have the following advantages: Firstly, the adhesive properties of the bifunctional peptides are directed against Resomer® and ensure proper immobilization within the matrix. Unlike typical drug delivery systems, the peptides might not be immediately released upon insertion in the human body but stay for an elongated time inside. This may potentially reduce the risk of cytotoxic effects and lead to prolonged antimicrobial effects at the implant site. Secondly, immobilizing bifunctional peptides within the polymeric matrix might protect them from proteolytic degradation by enzymes or cells in human sera. Thirdly, surface coating strategies, such as direct peptide immobilization on implant surfaces through chemical methods, can face issues such as low effective concentrations due to low coupling efficiencies (Silva et al., 2016). Embedding bifunctional peptides in Resomer® coatings may overcome this issue as the loading capacity is increased resulting in higher effective concentration per implant surface area.

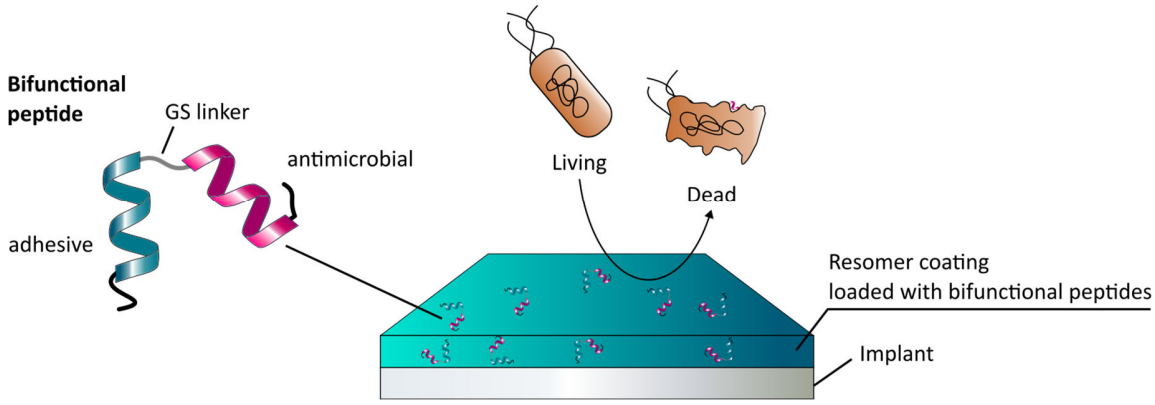

Figure 5 | Resomer® coatings loaded with bifunctional peptides

The bifunctional peptide consists of an antimicrobial and adhesive peptide covalently linked to each other by a short GS linker. Resomer® coatings loaded with bifunctional peptides mediate antimicrobial activity against different bacteria. Upon adhesion of living bacteria on the Resomer® surface, they are immediately killed by the coating's antimicrobial effect. The adhesive domain of the bifunctional peptide shall be directed against the Resomer® coating and ensure that the compounds are immobilized within the polymeric matrix for prolonged antimicrobial effect.

1.8 The phage display technology

Phage display is a versatile selection technology developed by George P. Smith 1985 where peptides, proteins, antibodies or antibody fragments are genetically fused to the coat proteins of bacteriophages, recombinantly expressed in bacterial hosts, and displayed on the viral surface (Smith, 1985). A major advantage of this technology is that the target displaying phages harbor the respective DNA sequence also in their genome providing a physical linkage between phenotype and genotype. A collection of such recombinant phage clones is a peptide or protein phage library and can include up to 10^{11} individual clones

(library diversity), each of them displaying different targets on the phage's surface (Almagro et al., 2019, Smith and Petrenko, 1997).

In selection processes, also referred to as biopanning, phage libraries are screened against target molecules or surfaces to find strong binding targets. They are effectively isolated from non-specific or weak binders by repetitive washing steps. Strong-binding phage clones are amplified by infecting bacterial host, recovered, and subjected to another cycle of target screening and amplification in host cells (Wu et al., 2016, Parmley and Smith, 1988). Repetition of the biopanning cycle three to four times allow stepwise enrichment of desired targets which can be identified by DNA sequence analyses of infected bacterial host (phenotype/genotype linkage) (Smith and Petrenko, 1997, Smith, 1985). The biopanning procedure is illustrated in Figure 6 for a peptide phage library screened against PDLLA surfaces.

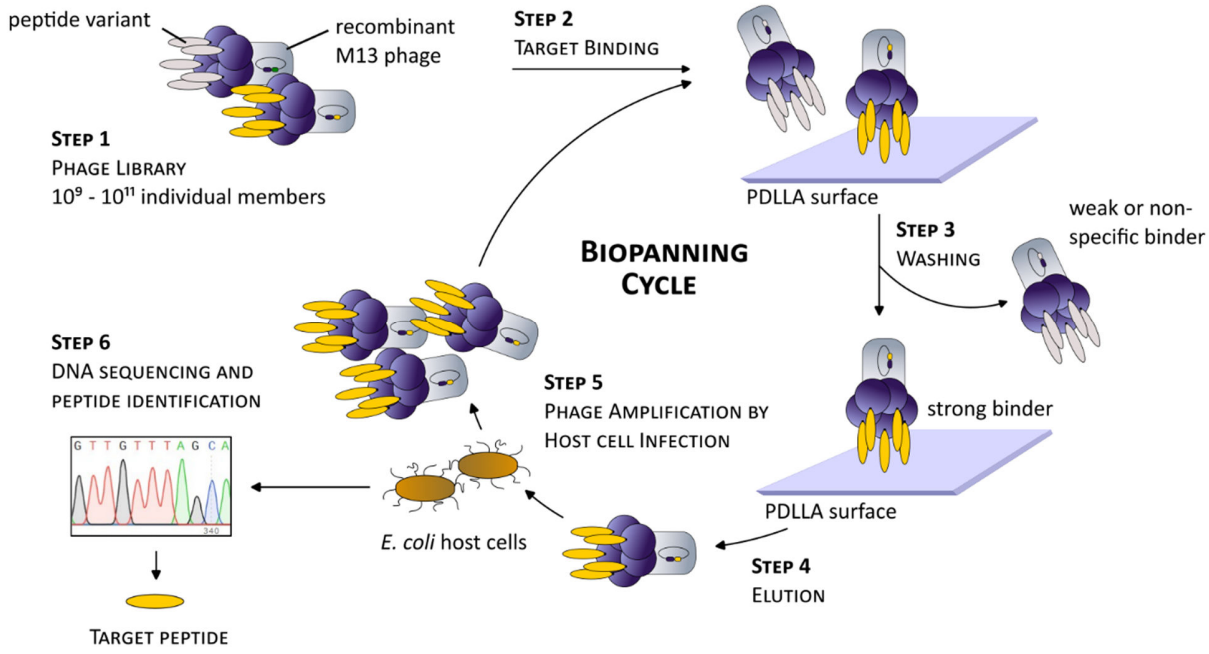

Figure 6 | Screening of peptide phage library against PDLLA surfaces

Steps included in the biopanning procedure are shown exemplarily based on recombinant M13 bacteriophages displaying different peptides on their surface. **Step 1**: Preparation of phage libraries consisting of 10^9-10^{11} individual members. **Step 2**: Incubation of the phage library with the target surface PDLLA. **Step 3**: Non-specific and weak binders are removed during repetitive washing steps. **Step 4**: Strong-binding phages are eluted by pH shift or by proteolytic cleavage. **Step 5**: Phages in the elution pool are amplified by *E. coli* host cell infection. The resulting phage pool is ready for the next biopanning cycle. Typically, 3 to 4 rounds are applied to gradually enrich strong binders. **Step 6**: As the genetic information of the binder peptide is preserved within the phage, its sequence can be identified by DNA sequencing of infected host cell clones.

In general, phage display technology is a powerful tool for the analyses of binding interactions between peptides/proteins and ligands or material surfaces (Liu et al., 2010), epitope mapping (Qi et al., 2021) or therapeutic drug discovery and development (Rami et al., 2017). The library size, so the number of individual phage clones in a repertoire, and the amino acid diversity in the library are two key criterions shaping the library quality. High-diversity libraries should contain between 10^9-10^{11} individual phage clones to increase the chances of finding targets with desired properties (Sloth et al., 2022). Adequate amino acid distribution eliminates the probability of false-positive clones (e.g. due to bias towards non-binding targets with high propagation rates, censorship of peptide sequences etc.) (Sloth et al., 2022, Zade et al., 2017).

1.8.1 M13 bacteriophage

The M13 bacteriophage belongs to the family of Ff filamentous phages and together with other members (f1, fd) they are known to infect *E. coli* strains expressing F-pili. M13 bacteriophage is 800-2000 nm long and has a width of 6 nm (O'Callaghan et al., 1973). The single stranded (ss) M13 bacteriophage vector (6,407 bp) (Van Wezenbeek et al., 1980) consist of nine genes encoding 11 different proteins. Five of those are coat proteins (p8, p3, p6, p7 and p9) while the other six are mostly involved in phage replication and assembly (Berkowitz and Day, 1976). The capsid protein p8 is with 2700 copies the most abundant coat protein and responsible for the encapsulation of the phage genome. The minor coat proteins p3 and p6 are present in 3-5 copies at one phage particle's end while p7 and p9 are located in the same copy numbers at the other end (Ledsgaard et al., 2018). The structures of M13 bacteriophage and its p3 coat protein are shown in Figure 7.

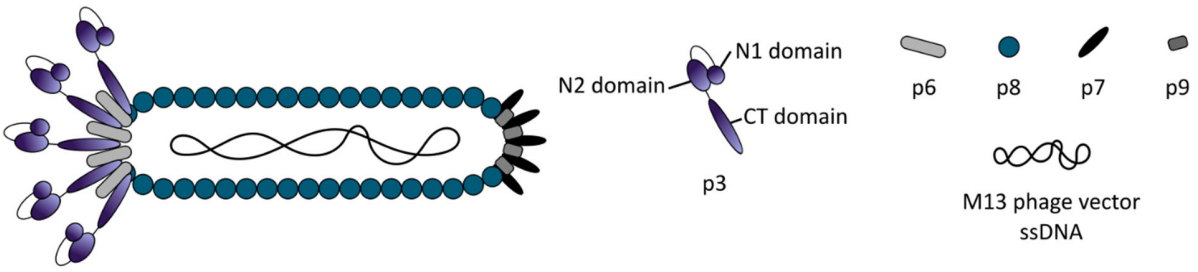

Figure 7 | M13 bacteriophage and p3 coat protein structure

More detailed information on the M13 bacteriophage structure and the p3 coat protein can be found in section 1.8.1 and 1.8.2.

1.8.2 M13 bacteriophage life cycle in *E. coli*

The M13 bacteriophage life cycle consists of four essential stages including infection of *E. coli*, replication of the phage genome, assembly, and release of progeny phage particles from the host cells (Kuhn and Wickner, 1985, Smeal et al., 2017).

Infection: M13 bacteriophages exclusively infect *E. coli* cells expressing F-pili. The coat protein p3 is crucial for the phage infectivity and release of phage particles after assembly. The coat protein p3 consists of three domains: two N-terminal domains (N1 and N2) and a C-terminal domain (CT) which functions as membrane anchor (Riechmann and Holliger, 1997, Bennett et al., 2011) (Figure 7). In the first step of M13 infection the N2 domain binds to the F-pilus tip of *E. coli* host cell leading to retraction of the F-pilus and bringing the phage closer to the host cell. This allows the N1 domain to bind the TolA receptor, an IM protein of *E. coli* anchored on its surface. TolA is important for the membrane integrity and is part of the TolQRA complex spanning the periplasmic space of *E. coli* (Riechmann and Holliger, 1997, Bennett et al., 2011). The role of the TolQRA complex in M13 infection is still under investigation, but N1-TolA interaction triggers integration of p8 capsid proteins into the IM of *E. coli* enabling the translocation of the ss M13 genome is translocated into the cell's cytoplasm (Ledsgaard et al., 2018, Carmen and Jermutus, 2002).

Replication: The first step of replication after release of the ssDNA genome of M13 bacteriophage is the synthesis of the antisense (-) DNA strand since the M13 ssDNA genome represents the sense (+) DNA strand and therefore cannot serve as template for mRNA synthesis. The resulting double stranded (ds) DNA composed of (+) and (-) DNA stands is referred to as replicative form DNA (RF DNA) and serves as template for phage gene replication and expression (Stassen et al., 1994, Smeal et al., 2017). The expressed p2 protein nicks the RF DNA (+) strand at the F1 intergenic region (IR) and the host DNA polymerase III elongates the 3' end of the nicked strand by rolling circle mechanism using the (-) strand as template. When the round of replication is finished the original (+) strand which is displaced by the Rep helicase is closed by the p2 protein and converted to RF DNA again (Stassen et al., 1994, Smeal et al., 2017). During the early stage of infection, when RF DNA and phage protein concentration are still low both strands are immediately converted to RF DNA. When DNA and phage protein (especially p5) concentration reaches a certain threshold, thousands of p5 proteins coat the newly synthesized (+) strands blocking further RF DNA conversion leading to decrease of protein and DNA synthesis rates. The p5 proteins bound to the (+) strand form dimers in a back-to-back arrangement leading to the collapse of circular ssDNA structure to a more rod-like one. The packaging signal in the p5 coated ssDNA initiates packaging of (+) DNA strands into progeny phages (Stassen et al., 1994, Smeal et al., 2017).

Assembly and Release of M13 bacteriophages progenies: M13 bacteriophage assembly occurs in the cytoplasmic membrane of *E. coli* and phage progenies are secreted while they assemble. A membrane spanning phage assembly complex consisting of p1, p11 and p4 recognize the p5 coated (+) DNA strand, attach p7 and p9 at the tip of the complex before transporting the DNA though the membrane-spanning channel (Rakonjac et al., 1999, Rakonjac and Model, 1998). Host cell thioredoxin, usually involved in reduction of disulfide bonds in proteins, is assumed to play a major role in stripping p5 dimers off DNA strands for replacement with p8 coat proteins during translocation (Loh et al., 2019). When the phage genome is completely encapsulated by p8 minor coat proteins p3 and p6 are incorporated at the end of the phage particle. p3 and p6 form stable complexes and initiate the release of progeny phages from cells by conformational change (Rakonjac and Model, 1998, Rakonjac et al., 1999).

In contrast to other phages (e.g. lambda, T4 or T7), members of the Ff family follow a non-lytic life cycle which means that they inject their genome into *E. coli* cells, initiate DNA replication, phage production and secretion without killing their host (Stassen et al., 1994, Smeal et al., 2017). A schematic overview of M13 bacteriophage life cycle in *E. coli* is shown in Figure 8.

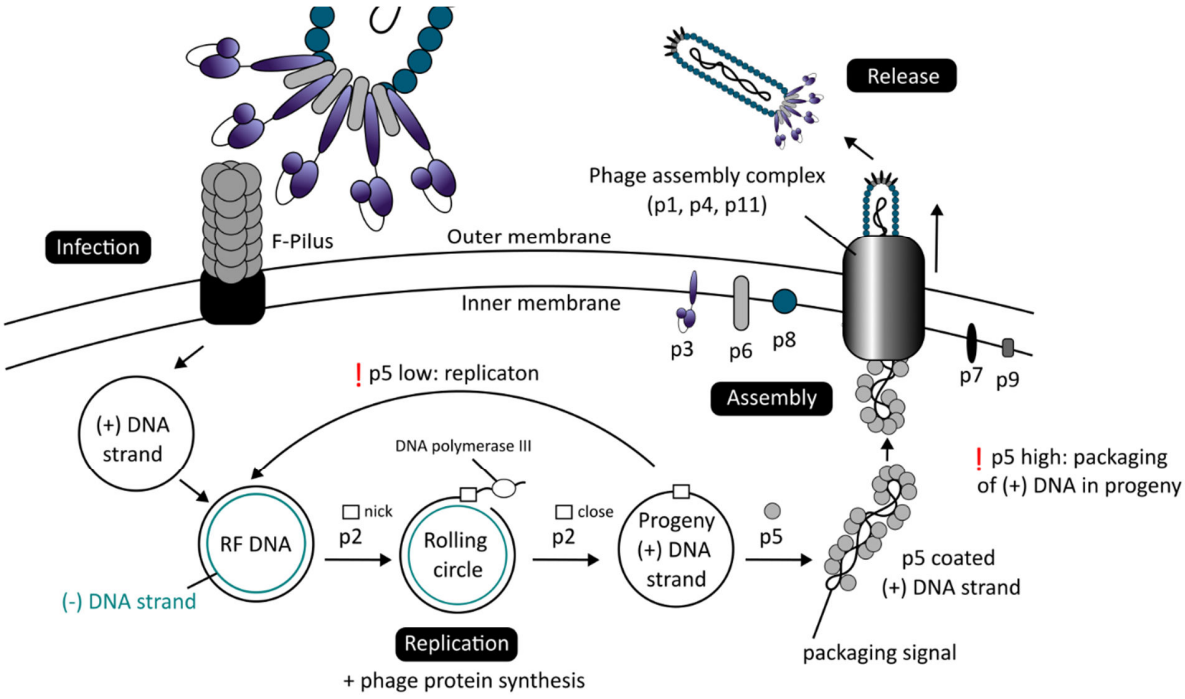

Figure 8 | M13 bacteriophage life cycle in *E. coli*

Illustration of the M13 bacteriophage life cycle from cell entry by infection of *E. coli* host cells to release of M13 bacteriophage progenies. More detailed information on the stages of M13 bacteriophage life cycle can be found in section 1.8.2.

1.8.3 M13 bacteriophage display systems

To use the M13 bacteriophage for display of randomized peptides, the respective genes have to be genetically fused to the N-terminus of one of the M13 coat proteins. Each of the five M13 coat proteins (p8, p3, p6, p7 and p9) has already been used to display protein or peptide sequences, however, p3 and p8 are most commonly applied (Smith and Petrenko, 1997, Clackson and Lowman, 2004). Typically, the genes encoding the randomized peptides are directly inserted into the phage vector in between the pelB leader sequence and the coding sequence of the mature M13 coat protein (e.g. p3). *E. coli* cells infected with recombinant M13 bacteriophages express the peptide-p3 fusion proteins and nascent phage progenies display the target peptides on their viral surface (Hoogenboom et al., 1991, Clackson and Lowman, 2004).

M13 bacteriophages harbor 2700 copies of major coat protein p8 and five copies of minor coat protein p3. Typically, p8 only allows the display of relatively short peptide sequences (6-8 aa residues) because peptides of larger sizes disturb the phage assembling process (Iannolo et al., 1995, Clackson and Lowman, 2004). For p3 the display of peptides of 50 residues (Cwirla et al., 1990) or even 100 residues (Noren and Noren, 2001) has been reported without affecting p3 infection functionality. Nevertheless, large peptides in p3 fusions may sterically hinder p3 and F-pilus interaction and preservation of the M13 bacteriophage infectivity is crucial for the propagation of phage clones selected in biopanning processes (Clackson and Lowman, 2004).

Since each copy of the engineered coat protein (e.g. p3 or p8) is produced as fusion protein and each bacteriophage contains about 3-5 copies of p3 it is proposed that the targets are display in a multivalent manner on the viral surface. Consequently, relatively low copy numbers of p3 fusions incorporated in the viral structure typically allow the selection of peptides with higher binding affinities to the respective targets compared to approaches using p8 as carrier (~ 2700 copy numbers). Therefore, p3 is the favored system for selection of high-affinity peptides especially those which are larger in size (up to 50 residues) (Ledsgaard et al., 2018, Deng et al., 2018). Alternatively to conventional M13 phage vectors, M13 phagemid systems can be applied to produce recombinant M13 bacteriophages (section 1.8.4). M13 phagemid systems offer several advantages compared to M13 phage vectors which are explained in more detail in the following sections.

1.8.4 M13 phagemid systems

Phagemids are basically plasmids used for standard recombinant protein productions with all common inherent features, i.e. antibiotic resistance marker, origin of replication (ori), promotor, enzyme recognition sites. The difference is that phagemids additionally harbor a 508-nucleotide long F1 intergenic region (IR) which is a phage-derived ori and contains a packaging signal crucial for the incorporation of ssDNA into nascent phage progenies (Dotto et al., 1981, Breitling et al., 1991). Furthermore, phagemids usually contain

the coding sequence of at least one of the M13 coat proteins. Insertion of genes encoding target peptides in between the pelB leader sequence and M13 coat protein ensure that the fusion protein (peptide:M13 coat protein) is translocated to the periplasm of host cells for assembly of phages and that the target peptide is displayed on the viral surface (Qi et al., 2012, Breitling et al., 1991). Since phagemids usually harbor only one gene of the phage coat protein and none of the other phage genes they are not able to produce infectious phagemid particles by themselves. The missing phage genes crucial for production of viable phagemid particles are delivered by helper phages or hyperphages (Rondot et al., 2001, Vieira and Messing, 1987). By superinfection of host cells they bring in the genes important for phage replication, assembly and propagation and the phage proteins are produced by the translation machinery of host cells (Qi et al., 2012, Rondot et al., 2001) (Figure 9). This way, recombinant M13 bacteriophages can be produced displaying the desired targets on the viral surface. M13 bacteriophages originating from phagemid systems are also referred to as phagemid particles (Chasteen et al., 2006, Breitling et al., 1991).

Helper phages such as M13K07 are based on wild type M13 bacteriophages with several differences: Their genome harbors an additional ori and antibiotic resistance marker (e.g. kan^R). In addition, the packaging signal in the F1 IR is defective. When *E. coli* cells containing the phagemid are infected by M13K07 (superinfection), phagemids containing intact packaging signals are packaged more efficiently in nascent phage progenies (Ledsgaard et al., 2018, Vieira and Messing, 1987). Furthermore, the p3 wild type proteins from M13K07 compete with p3 fusion proteins from phagemids for incorporation in nascent phagemid particles. As a result, the phagemid particles produced are heterogeneous, with p3 proteins and genomes derived either from the helper phage or the phagemid (Chasteen et al., 2006, Vieira and Messing, 1987). Although the disabled packaging signal in the helper phage genome should theoretically reduce the proportion of wild type M13 bacteriophages in the nascent phagemid particle population, in reality, only 1–10 % of the phagemid particles carry one or two copies of the p3 fusion proteins (Rondot et al., 2001, Ledsgaard et al., 2018). Using helper phages for phagemid particle packaging promote monovalent display of target proteins and facilitate the selection of high-affinity binders in biopanning processes (Lowman et al., 1991, Ledsgaard et al., 2018).

Hyperphages, like M13K07Δp3 are modified helper phages harboring a truncated or missing p3 gene in the phage genome. As they still carry the p3 protein phenotypically, hyperphages are able to infect *E. coli* cells expressing F-pili (Rondot et al., 2001). For *E. coli* cells superinfected with both the phagemid and hyperphage the only source of intact p3 protein available for assembly of phages stems from p3 fusion proteins from phagemids. The chances of incorporating p3 fusion proteins in phagemid particles are much higher in comparison to helper phage preparations increasing the proportion of recombinant phagemid particles in the pool (Rondot et al., 2001, Ledsgaard et al., 2018).

Similar to M13 phage vectors, phagemid particle progenies can carry up to five copies of the p3 fusion protein, which promote multivalent display of targets on the viral surface. Employing M13K07Δp3 hyperphage systems in biopanning processes can improve the display efficiency of peptides by two to three orders of magnitude (Rondot et al., 2001, Breitling et al., 2010). Compared to helper phage systems, the background of bald M13 bacteriophages is relatively low, which increases the chances of finding candidates with desired properties, especially those that are usually represented by low copy numbers. However, it is important to note that the multivalent display format also favors the selection of low affinity targets due to avidity effects (Rondot et al., 2001). The different display formats based on helper phage and hyperphage systems is schematically shown in Figure 9.

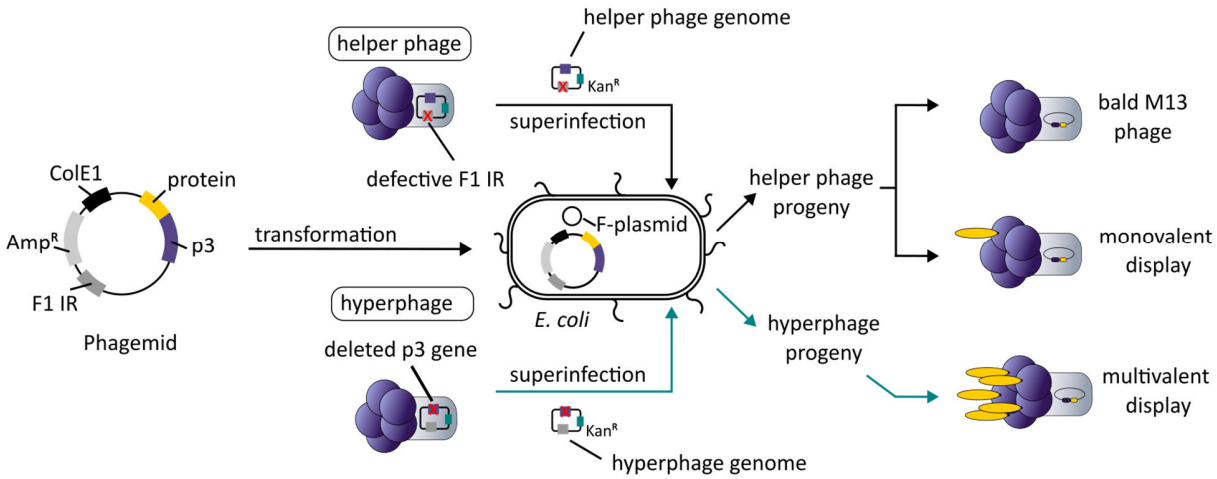

Figure 9 | Target display formats on M13 bacteriophages by employing helper or hyperphages

Phagemids containing genes of p3 fusion protein are transformed in *E. coli* cells expressing F-pili. When *E. coli* cells are infected by helper phages, their genome is not efficiently packed compared to the phagemids due to the defective packaging signal in the F1 intergenic region (IR). Consequently, most of the phagemid progenies produced are either bald or display the target peptide in a monovalent form with just one or two copies on the surface of phagemid particles (Ledsgaard et al., 2018, Lowman et al., 1991). On the other hand, when *E. coli* cells are infected with hyperphages which lack the p3 gene in their genome, the p3 fusion protein expressed by the phagemids is the only source of intact p3 for assembly of phagemid particles. As a result, all p3 fusion proteins are incorporated into nascent phagemid progenies leading to multivalent display of target peptides on the viral surface (Rondot et al., 2001, Breitling et al., 2010). Further features: ColE1, Colicin E1 origin of replication; Amp^R, ampicillin resistance gene; Kan^R, Kanamycin resistance gene.

Concluding, phage display systems using phagemids have several advantages compared to M13 vectors. Firstly, since p3 fusion proteins are externally provided by phagemids the process of recombinant protein expression is uncoupled from phage propagation. The expression level of p3 fusion proteins can be modulated before phage propagation is initiated by helper or hyperphage infection (Rondot et al., 2001, Qi

et al., 2012, Hust et al., 2006). Secondly, higher transformation efficiencies are reached using phagemids since they are smaller in size compared to M13 vectors (~ 4 kb vs. 6.4 kb) which facilitates the construction of large libraries (Hust and Dubel, 2005, Hoogenboom et al., 1991). Furthermore, dsDNA from phagemids is easier to handle than ssDNA of phages, especially in terms of DNA preparation, cloning and DNA analysis (Hust and Dubel, 2005, Chasteen et al., 2006). Employing phagemid systems, it is easy to switch between monovalent (helper phage) or multivalent (hyperphage) display formats of target peptides (Rondot et al., 2001, Lowman et al., 1991). Lastly, in multiple propagations, phagemids are more stable than M13 phage vectors because they are less prone to deletion events caused by selection pressure (Chasteen et al., 2006, Qi et al., 2012).

1.8.5 Advantages of phagemid libraries displaying long-chained peptides

In scope of this dissertation phagemid libraries displaying randomized long-chained peptides (≥ 20 aa) were constructed and employed to screen against Resomer® surfaces to identify strong binding peptide motifs. Although libraries displaying short peptides (< 20 aa) in M13 bacteriophages are commercially available (e.g. New England BioLabs, Creative Biolabs, ThermoFisher), those displaying long-chained peptides are highly underrepresented in the market. High cost-of-goods associated with long-chained peptides limit the broad application of these molecules. Typically, short linear oligopeptides are conventionally synthesized by chemical synthesis (Merrifield, 1963, Dawson et al., 1994) and robust recombinant strategies are missing to produce long-chained ones at high quantities and at attractive prices (Gaskin et al., 2001). Furthermore, libraries displaying more than seven amino acids are considered inadequately covered. For instance, libraries displaying heptapeptide sequences have 1.28 x10^9 (20^7) different sequence possibilities, which is near the upper limit of technically feasible phage display libraries. It is evident that the phagemid libraries displaying long-chained peptide sequences represent an infinitely small fraction of the possible peptide sequences. Despite the fact that it is not feasible to achieve full sequence coverage, using libraries displaying long-chained peptides have several advantages. These peptides are large enough to adopt tertiary structures, allowing identification of peptide candidates that bind to targets using discontinuously located key residues rather than contiguous amino acid stretches, which is not possible with short peptides (McConnell et al., 1996). Short peptide libraries have been extensively studied over the last few decades due to the availability of commercially available phage libraries, whereas studies on long-chained peptide libraries are scarce, making them potentially useful for discovering new biological functionalities. Importantly, the evolved Numaswitch™ technology can be applied to produce this class of biomolecules at substantial product yields, ensuring high quality, all while maintaining reasonable pricing.

2 Aims

This dissertation investigates the potential of GG repeat-containing fragments, in particular HlyA1, as protein tags for production of recombinant peptides and pepteins. N-terminal HlyA1 fragments fused to target peptides form in the absence of the T1SS transporter inclusion bodies (IBs) inside *E. coli* cells, but after extraction and solubilization in chaotropic salts they refold efficiently to soluble and functional protein in Ca^{2+}-containing buffers (section 1.2.6). One objective of this dissertation was to investigate whether HlyA1 fragments with different truncations at the C-terminal secretion signal exhibit the same refolding behavior as HlyA1 wild type and/or potentially lead to even higher renaturation efficiencies. For this study, HlyA1 and HlyA1 truncations were fused to five selected peptide or peptein candidates (Teriparatide, Linaclotide, DS-THA, Aβ40, and SAA3) (section 1.3.3) which vary in MWs and physicochemical characteristics. The fusion proteins were produced as IBs in *E. coli* cells, extracted, solubilized, and refolded in the presence of Ca^{2+}. Biochemical methodologies were applied to compare the refolding efficiency of each construct and assess target release from HlyA1 backbones after proteolytic cleavage. Finally, the applicability of the Numaswitch™ approach to produce peptides and pepteins at high scales and in high qualities shall be evaluated by establishing a pilot scale production process for the therapeutic peptide Teriparatide. Furthermore, the potential of the Numaswitch™ technology as a universal biochemical platform for peptide and pepteins production shall be highlighted on candidates usually challenging to produce in the correctly folded and functional form in *E. coli*. For this purpose, Switchtags (section 1.2.6) were fused to four selected candidates of varying MWs (< 300 aa), number of disulfide bridges (≤ 3 Cys-Cys) and biological functions (e.g. AMPs, antibody fragments). The candidates selected were hEGF, VHH, scFv clone F2C and DS-THA (section 1.3.3). After expression of the fusion proteins as IBs in *E. coli,* individual high-scale production processes were established for each candidate and different analyses were applied to assess the purity, the oxidized state, and biological functions of the purified targets.

In scope of this dissertation it was aimed to design bifunctional peptides, specifically peptide-peptide fusions combining antimicrobial and adhesive domains against the biopolymer Resomer® with each other. These molecules may serve as foundation for the functionalization of Resomer® coatings to prevent bacterial growth on implant surfaces in combat against IAIs (section 1.4). While the AMPs were selected from literature, it was an integral part of this work to identify peptides binding to Resomer®. Phagemid libraries displaying randomized peptides were constructed and screened against Resomer® surfaces in biopanning experiments to identify Resomer®-binding peptides (RBPs). The RBPs shall be fused to the three selected AMPs, namely human beta-defensin-3 (HBD3), human histatin-3 (HTN3) and dermcidin-1L (DCD-1L) and produced by the Numaswitch™ technology. Different assays were established to determine whether the antimicrobial and adhesive properties in the novel bifunctional peptides were preserved. For proof-of-concept, a bifunctional peptide was selected and incorporated into Resomer® coatings to evaluate its capability to prevent bacterial growth on the surface.

3 Material & Methods

3.1 Cloning, Expression and IB extraction of HlyA1 and HlyA1 fusions

The DNA fragments encoding, HlyA1, HlyA1 truncations and HlyA1 fusion peptides including Teriparatide, Linaclotide, Dermaseptin–Thanatin (DS-THA), human β-amyloid (1–40) (Aβ40) and Serum amyloid A3 (SAA3) were cloned into the expression plasmid pSU2726 (Khosa et al., 2018). The structure of the resulting HlyA1 fusion protein is shown Figure 10. The plasmid contains an ampicillin resistance (Amp^R) gene for selection of positive clones and the *lac* promotor is inducible with isopropyl β-d-1-thiogalactopyranoside (IPTG). The plasmid constructs were transformed in *E. coli* BL21 (DE3) chemically competent cells by heat shock (Dagert and Ehrlich, 1979). After regeneration in 200 µL of 2YT medium at 37 °C and 1,150 rpm for 45 min cell suspension was spread on Luria-Bertani (LB) agar plates containing 100 µg/mL ampicillin and incubated at 37 °C overnight for selection of positive clones.

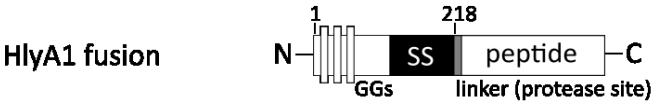

Figure 10 | Schematic illustration of HlyA1 fusion protein constructs

HlyA1 consist of a RTX domain characterized by the presence of three GG repeats (GGs) and a C-terminal secretion signal (SS, ~ 60 aa). For heterologous protein expression HlyA1 is fused as a N-terminal protein tag to the target peptide. Between HlyA1 and the target peptide is a *Tobacco etch virus* (TEV) cleavage site (ENLYFQ) that allows separation of target peptides from HlyA1 backbone after site-specific proteolytic cleavage.

For initial expression studies, pre-cultures were grown from single colonies at 37 °C for 16 h and used to inoculate 25 mL 2YT medium containing 100 µg/mL ampicillin in 250 mL shaking flasks to a final OD_{600} of 0.1. The expression cultures were cultivated at 37 °C and 180 rpm until the cells reached OD_{600} 0.4–0.6 and protein production was induced by addition of 1 mM IPTG. The cells were cultivated for 16 h (37 °C, 180 rpm) and afterwards harvested by centrifugation (4,696 *g*, 15 min, 4 °C, Legend™ X1 Centrifuge, ThermoFisher). The extraction of IBs from cells was conducted by BugBuster® Master Mix Kit (Novagene) according to manufacturer's protocol. Recombinant protein production was checked before and 16 h after IPTG induction. For this, 0.5-1 mL of cell culture were pelleted by centrifugation (16,000 *g,* 5 min, RT) and the cell pellets were adjusted to a final OD_{600} of 5 with 1:5 diluted 5x SDS-PAGE sample loading buffer (100 mM Tris-HCl pH 6.8, 16 % (w/v) SDS, 40 % (v/v) glycerol, 0.2 % (w/v) Bromophenol Blue) before heated at 95 °C for 5 min. For SDS-PAGE analyses 5 µL samples were loaded on a 15 % (w/v) polyacrylamide gel. The SDS-PAGE gels were run at 160 V for 1 h and protein bands were visualized by colloidal Coomassie Blue G-250 staining (Dyballa and Metzger, 2009). The gels were destained in water until the backgrounds were clear. Gram scale production of HlyA1 Δ165–218 Teriparatide IBs was

performed via high cell density fermentation by the Upstream division of Numaferm GmbH using an extended fed batch approach. For IB preparation, the cells were disrupted by high pressure homogenization for three cycles at 1,200 bar (LM-20, Microfluidics). After subsequent centrifugation (16,000 *g*, 30 min, 4 °C, Avanti® JXN-26, Beckman Coulter), the IBs were washed with buffer (10 mM Tris-HCl pH 7.3, 120 mM NaCl, 2 mM EDTA, 0.1 % Triton-X-100) and sedimented by centrifugation.

3.2 Refolding and TEV protease cleavage of HlyA1 fusions

The IBs of HlyA1, HlyA1 truncations and HlyA1 fusion proteins were solubilized in 6 M GuHCl (1:4, w/v). Protein concentrations were determined by UV/VIS spectroscopy at 280 nm (NanoDrop™ One/One C, ThermoFisher) using the calculated MWs and extinction coefficients (ProtParam, Expasy). Protein concentrations of solubilized proteins were adjusted to 1 mM with 6 M GuHCl. For renaturation studies, denatured HlyA1 and HlyA1 fusions were diluted to 0.05 mM final concentration using renaturation buffer (20 mM Tris-HCl buffer, pH 8.0, 150 mM NaCl, 0.5 mM EDTA) in absence or presence of 10 mM $CaCl_2$. Renaturation reactions were incubated for 20 min at RT, then centrifugated at 13,200 *g* for 10 min. Renaturation efficiencies were determined by dividing the protein concentration in the cleared supernatant by the maximal expected value of the protein concentration adjusted for the renaturation reaction (i.e. 0.05 mM). Target releases from HlyA1 backbones were triggered by adding TEV protease in a molar enzyme to target protein ratio of 1:25 and incubation at 30 °C for 3 h.

For SDS-PAGE analyses, 80 µL of renaturation and cleavage samples were mixed with 20 µL 5x SDS-PAGE sample loading buffer. The samples were heated at 95 °C for 5 min and 10 µL were loaded on 15 % polyacrylamide gels for analysis. For visualization of protein bands, the SDS-PAGE gels were stained and destained as described in section 3.1. Analytical scale RP-HPLC-MS (reversed phase high performance liquid chromatography coupled to a mass spectrometer) analyses were performed with the Alliance™ HPLC system (Waters) using the ZORBAX 300SB-C18 column (4.6 mm × 250 mm, 5 µm, Agilent). To stop the TEV protease activity the cleavage samples were mixed 1:1 (v/v) with 6 M GuHCl and 80 µL of the mixtures were injected into the HPLC system, respectively. Components of the cleavage reactions were eluted by applying a linear gradient of water and acetonitrile (5–60 % over 30 min) in presence of 0.1 % (v/v) TFA. The runs were performed at a flow rate of 1 mL/min and RT. The UV absorbances were monitored at 205 nm. Following electron spray ionization (ESI) in positive ion mode the molecular masses of elution signals were determined by the quadrupole mass analyzer (ACQUITY QDa Detector, Waters) and the Empower 3 chromatography data software.

3.3 Production of Teriparatide

HlyA1 Δ165–218 Teriparatide IBs were produced, extracted from cells and washed as described in section 3.1. Renaturation of fusion proteins was performed in HEPES-based buffer (20 mM, pH 8.0, 10 mM

$CaCl_2$) adjusting the protein concentration to 2 mg/mL using solubilized IBs in 8 M urea (1:8, w/v). TEV protease was added in a molar enzyme to protein ratio of 1:200 and the cleavage reaction was incubated at RT for 3 h. For SDS-PAGE analysis, 4 µL of IB solution were mixed with 20 µL 8 M urea, 56 µL 1 M Tris-HCl pH 7.3 and 20 µL 5x SDS-PAGE loading buffer. SDS-PAGE and RP-HPLC-MS analyses of renaturation and cleavage samples were conducted as described in section 3.1. SDS-PAGE samples were heated at 95 °C for 5 min before 10 µL of samples were loaded on 15 % polyacrylamide gels, respectively. The target peptide Teriparatide was purified by cation exchange chromatography (CEX, Capto SP ImpRes, Cytiva) using a NaCl gradient in 20 mM Na-acetate buffer pH 6.5. Teriparatide-containing elution fractions were further purified on a RP-FLASH column (Aquarius C18AQ, BGB) using a linear gradient of water and acetonitrile in presence of 0.1 % TFA. TFA to acetic acid exchange was performed by washing the Teriparatide loaded RP-FLASH column in presence of 3 % (v/v) acetic acid. After elution, Teriparatide containing fractions were pooled, shock-frozen in liquid nitrogen and lyophilized (Martin Christ Freeze Dryer Alpha 2-4 LD plus) at 0.1 mbar for 48 h. Afterwards, the lyophilized product was post-dried at 0.01 mbar for 2 h before stored at -80°C.

3.4 Analysis of purified Teriparatide

3.4.1 Purity and identity analyses of Teriparatide by RP-HPLC-MS

The purity of the lyophilized Teriparatide (section 3.3) was analyzed by analytical scale RP-HPLC-MS with the same device as mentioned in section 3.2. Here, between 5–7 µg of Teriparatide reconstituted in water was loaded onto a ZORBAX 300SB-C18 column (4.6 mm × 250 mm, 5 µm, Agilent). Teriparatide was eluted by applying a linear gradient of water and acetonitrile (5–80 % over 30 min) in presence of 0.1 % (v/v) TFA. The runs were performed at a flow rate of 1 mL/min and RT. The UV absorbances were monitored at 215 nm. Following ESI in positive ion mode the molecular masses of elution signals were determined by the quadrupole mass analyzer (ACQUITY QDa Detector, Waters). The molecular masses of elution signals were analyzed by electron spray ionization mass spectroscopy (ESI-MS) using the quadrupole mass analyzer (ACQUITY QDa Detector, Waters). The purity of Teriparatide was determined by employing the ApexTrack algorithm implemented in the Empower 3 chromatography data software by integration of chromatographic target and impurity elution peaks.

3.4.2 Glu-C digestion for peptide mapping analysis

The lyophilized Teriparatide (section 3.3) was compared to the commercial drug products FORSTEO® (Lilly) and TERROSA® (Gedeon Richter) by peptide mapping. For this, the different Teriparatide peptides were reconstituted in water and the protein concentrations were determined by UV/VIS spectroscopy. For peptide digestion, Glu-C from *Staphylococcus aureus* strain V8 (Sigma-Aldrich) was added in a final enzyme to protein ratio of 1:16 (w/w), respectively, and the reactions were incubated at 37 °C and 300 rpm for 4 h. Glu-C is a endoproteinase that specifically cleaves at the C-terminus of either aspartic or glutamic acid residues (Drapeau et al., 1972). Around 20 µg peptide samples were injected into the Alliance™ HPLC system (Waters), respectively, and digested peptide fragments were separated from each other by the ZORBAX 300SB-C18 column (4.6 mm × 250 mm, 5 µm, Agilent). Peptide fragments were eluted in a linear gradient of water and acetonitrile (5–80 % over 150 min) in the presence of 0.1 % (v/v) TFA. The runs were performed at a flow rate of 1 mL/min and RT. The UV absorbances were monitored at 215 nm. The molecular masses of elution signals were analyzed by ESI-MS using the quadrupole mass analyzer (ACQUITY QDa Detector, Waters) and the Empower 3 chromatography data software.

3.4.3 Quantification of contaminants in purified Teriparatide samples

The lyophilized Teriparatide (section 3.3) were subjected to different analyses to further assess the product quality. The bacterial endotoxin content in the sample was determined by a Limulus amebocyte lysate (LAL) assay performed by BioChem (Karlsruhe). Furthermore, the Downstream Processing & Analytics Division of Numaferm GmbH determined the concentrations of counterions (anions) such as TFA, acetate and Cl^- ions in samples by ion chromatography. Residual host cell DNA (rHCD) was determined by real-time PCR using the innuMIX qPCR SyGreen Sensitive Master Mix (Analytik Jena) and the qTOWER^3 qPCR Thermal Cycler (Analytik Jena). Residual host cell proteins (rHCP) were determined by using the commercially available Cygnus™ HCP ELISA Kit (Cygnus technologies). The gross/net weight of the product was determined by reconstitution of a weighed lyophilized fraction in water and determination of the protein concentration by UV/VIS spectroscopy using the respective MW and extinction coefficient (ProtParam, Expasy). The biological activity of purified Teriparatide was confirmed in a cell-based cyclic adenosine monophosphate (cAMP) assay performed by Charles River Laboratories Germany GmbH.

3.5 Cloning, Expression and IB preparation of Switchtag protein fusions

Genes encoding the peptides and pepteins Dermaseptin-Thanatin (DS-THA), a camelid heavy chain antibody fragment (VHH), the scFv clone F2C and the human epidermal growth factor (hEGF) were fused to N-terminal Switchtag proteins (Table 6) and cloned into pBAD-derived expression plasmids (Guzman et al., 1995). The expression plasmids contain a gene for kanamycin resistance (Kan^R) that enables selection for positive clones. The bidirectional araBAD promoter is tightly regulated and inducible by addition of

arabinose. *E. coli* BL21 cells transformed with recombinant expression plasmids were cultivated in high cell density fermentations performed by the Upstream division of Numaferm GmbH. In short, the fermentations were performed in a BioFlo® 320 Bioreactor. For this, 750 mL of media (17.7 g/L KH_2PO_4, 5.3 g/L $(NH_4)_2HPO_4$, 2.5 g/L citric acid, 10 mM $MgSO_4$) containing trace elements ($CaCl_2$, Fe_3Cl, $CoCl_2$, $MnCl_2$, $CuCl_2$, H_3BO_3, Na_2MoO_4, zinc acetate), 30 µg/mL kanamycin and glucose (20 g/L) were inoculated with pre-cultures of *E. coli* BL21 transformed with recombinant expression plasmids to a OD_{600} of 0.25. The temperatures, pH and dissolved oxygen (DO) levels were maintained at 37 °C, 7.0 and 20 %, respectively. Growth phases were extended by adding glucose pulses of 20 g (feed) when the DO level exceeded 40 %. Arabinose was added to the cultures in a final concentration of 2 g/L for expression induction. Afterwards a constant glucose feed rate of 0.57 g/min was applied and cell growth was monitored by release of CO_2 (CO_2 out) and measurement of the OD_{600}. After cell harvesting, the Switchtag fusion protein IBs were isolated and washed as described in section 3.1. For SDS-PAGE analyses, 500 µL of cell cultures were centrifuged (16,000 *g,* 5 min, RT) and adjusted to OD_{600} of 5 with 1x SDS-PAGE sample loading buffer diluted in water. The samples were heated at 95 °C for 5 min and 2 µL were loaded on 15 % polyacrylamide gels along different protein amounts of bovine serum albumin (BSA, ThermoFisher Scientific). The protein band intensities were analyzed by ImageJ software (Image Processing and Analysis in Java). The amounts of produced Switchtag fusion protein IBs were determined by a BSA protein standard curve.

3.6 Refolding and TEV protease cleavage of Switchtag protein fusion IBs

The extracted Switchtag fusion protein IBs (section 3.5) were either solubilized in 6 M GuHCl or 8 M urea in IB to solvent ratios of 1:4 to 1:8 (w/v). Protein concentrations were determined by UV/VIS spectroscopy using the calculated MWs and extinction coefficients (ProtParam, Expasy). Renaturations were performed in Tris-HCl or HEPES-based buffer (pH 8, 20 mM, 10 mM $CaCl_2$, 0.5 mM EDTA) adjusting the protein concentration to 1.1–1.7 mg/mL using the solubilized IBs. The renaturation efficiencies were determined as described in 3.2. The Switchtags were removed from the targets by proteolytic cleavage by adding the Numacut TEV protease (Numaferm GmbH, Düsseldorf) in a molar enzyme to protein ratio of 1:25–50. The cleavage reactions were incubated at RT for 3–24 h. Solubilized IBs, refolded Switchtag fusion proteins and cleavage reactions were analyzed by SDS-PAGE and/or RP-HPLC-MS analyses as described in section 3.1 and 3.3.

3.7 Purification of hEGF, VHH, scFv clone F2C and DS-THA

Purifications of hEGF, VHH and scFv clone F2C by ion exchange (IEX) chromatography and/or immobilized metal affinity chromatography (IMAC) were conducted using the ÄKTA™ pure chromatography system. The cleavage reactions of VHH and scFv clone F2C were cleared by centrifugation

(16,000 *g*, 20 min, 4 °C) and/or syringe filtration (0.45 µm, Sarstedt). Negative mode IMAC runs (HisTrap™ FF, Cytiva) were performed in 50 mM Tris-HCl pH 8.0, 10 mM $CaCl_2$ to separate the His_6-tagged Switchtags and TEV protease from the non-tagged VHH and scFv clone F2C, respectively. Elution of VHH and scFv clone F2C in the flow through fractions was monitored by UV absorbance at 280 nm. The VHH and scFv clone F2C-containing fractions were pooled, concentrated and the buffer were exchanged for TBS (50 mM Tris-HCl, pH 8.0, 150 mM NaCl) by ultrafiltration (Millipore, Amicon Ultra-15, 3 kDa cut-off), respectively.

Purification of hEGF was performed in a two-step chromatographic strategy to isolate the correct hEGF isomer. After cleavage of the Switchtag from hEGF, the cleavage reaction was cleared by syringe filtration (0.45 µm, Sarstedt) before loaded on an anion exchange chromatography (AEX) column (HiTrap Capto Q ImpRes, Cytiva) pre-equilibrated in 20 mM Tris-HCl pH 8.0. Elution of bound hEGF was performed by a linear gradient of 0–500 mM NaCl. Elution signals were monitored by UV absorbance at 280 nm. The hEGF-containing elution fractions were analyzed by analytical scale RP-HPLC-MS as described in section 3.2. To determine which elution peak represents the correct isomer commercially purchased hEGF (Bachem) was employed as reference standard. Fractions containing correctly folded hEGF isomers were pooled and further purified by negative-mode IMAC (HisTrap™ FF, Cytiva). As above, the hEGF-containing flow through fractions were pooled, concentrated by ultrafiltration (Sartorius, Vivaspin 15 R, 2 kDa cut-off) and buffer was exchanged for PBS (137 mM NaCl, 2.7 mM KCl, 8 mM Na_2HPO_4, and 2 mM KH_2PO_4) by gel filtration (PD-10 Sephadex G-25, Cytiva).

Purification of DS-THA was performed by RP FLASH chromatography using the BUCHI Pure C-850 Flash/Prep chromatography system. The cleavage reaction was supplemented with 3 M urea, 5 % acetonitrile, acidified by addition of 0.1 % TFA and loaded on a Scorpius Flash Cartridge (Cyano, 100 Å, 30 µm, BGB). DS-THA was eluted by a linear gradient of water and acetonitrile (5–60 %) in the presence of 0.1 % (v/v) TFA. Elution signals were monitored by UV absorbance at 205 nm. DS-THA-containing fractions were pooled and lyophilized (Martin Christ Freeze Dryer Alpha 2-4 LD plus) at 0.1 mbar for 24 h. Afterwards, lyophilized DS-THA was post-dried at 0.01 mbar for 2 h. The purity and identity of purified DS-THA were analyzed and verified by analytical scale RP-HPLC-MS analyses as described in section 3.4.1. The gross/net weight was determined by reconstitution of a weighted lyophilized DS-THA fraction in water and determination of the protein concentration by UV/VIS spectroscopy using the calculated MWs and extinction coefficients (ProtParam, Expasy).

3.8 UPLC-MS analysis

Lyophilized hEGF, VHH, scFv clone F2C and DS-THA (section 3.7) were analyzed by the BioAccord ultraperformance liquid chromatography (UPLC) system equipped with an ESI source and time-of-flight

(TOF) mass spectrometer (ACQUITY RDa, Waters) (UPLC-MS) to confirm the identities and oxidative state of targets. They were reconstituted in water, the protein concentration was determined by UV/VIS spectroscopy and between 1–3 µg was loaded on a BioResolve RP mAb Polyphenyl (450 Å, 2.7 µm, 2.1 x 50 mm) or an ACQUITY UPLC CSH C18 (130 Å, 1.7 µm, 2.1 mm x 100 mm) column, respectively. The peptides and pepteins were eluted by a linear gradient of water and acetonitrile (5–80 % over 150 min) in the presence of 0.1 % (v/v) formic acid (FA). The flow rate was constantly set on 0.4 mL/min and the column temperature hold on 60 °C. The UPLC chromatograms were monitored by UV absorbance at 215 nm. ESI was operated in positive ion mode and the molecular ions were analyzed by full scan with fragmentation method (400–2,000 *m/z*) at 2 hertz acquisition rates. The capillary voltage was set at 1.2 kV and the cone voltage at 30 V, and the desolvation temperature was maintained at a temperature of 350 °C. The UPLC-MS data were analyzed by the UNIFI Scientific Information System software (Waters) employing the MaxEnt deconvolution algorithm.

3.9 Functional analysis

The biological activity of purified DS-THA, VHH, scFv clone F2C and hEGF were investigated in different assays further described in the sections 3.9.1 to 3.9.4.

3.9.1 Minimal inhibitory concentration assay for DS-THA

The minimal inhibitory concentration (MIC) assay was performed to assess the antimicrobial activity of purified DS-THA. Lyophilized DS-THA was reconstituted in water supplemented with 0.1 % (v/v) acetic acid. The protein concentration was adjusted to 2 mM by determining the protein concentration by UV/VIS spectroscopy. Serials of 2-fold peptide dilutions were prepared in a 96-well microtiter plate. *E. coli* and *B. subtilis* cultures were grown in Mueller Hinton Broth (MHB) medium to OD_{600} of 0.6 before diluted to the required number of cells with 1.6 x 10^6 cfu/mL, respectively. For the assay, 10 µL of serial diluted peptide solutions were added to 90 µL of diluted bacterial culture, respectively, and the final tested peptide concentrations ranged from 0.1 to 100 µM. As control, 90 µL of diluted bacterial cultures were added to 10 µL of 0.01 % acetic acid. Growth of cells was initiated by incubation of the plate at 37 °C for 24 h. Afterwards, the OD_{600} was measured (FLUOstar Optima, BMG Labtech) to determine the lowest peptide concentration which resulted in ≥ 95 % inhibition of cell growth compared to the control without DS-THA (referred to as MIC value).

3.9.2 mCherry binding assay for VHH

The biological activity of purified VHH was checked in a binding assay. The monomeric red fluorescent protein mCherry (Nanotag Biotechnologies GmbH) was used as target for VHH binding (Wang et al., 2021). For the assay, VHH was added in 2-fold molar excess to mCherry in TBS buffer (50 mM Tris-HCl pH 7.4,

150 mM NaCl). The protein mixture was incubated on ice for 1 h, cleared by centrifugation (20,000 *g*, 5 min, RT) and the supernatant was analyzed by size exclusion chromatography (SEC) for the formation of VHH-mCherry complexes. SEC analyses were performed using the Agilent Infinity II LC system and the Agilent Bio SEC-5 column (5 µm, 300 Å, 4.6 mm x 300 mm) pre-equilibrated in TBS buffer. Chromatographic peaks were monitored by UV absorbance at 280 nm and a constant flow rate of 0.2 mL/min was applied.

3.9.3 Target engagement assay for hEGF

To evaluate the biological activity of hEGF, Eurofins DiscoverX Corporation (Fremont, USA) performed a cell-based receptor tyrosine kinase (RTK) assay (Catalog ref., 86-0006P-2742AG). Determination of the potency and efficacy (E_{max}) of purified hEGF for the human EGFR (ErbB1) receptor was conducted using stably transfected U2OS cells. For the assay, the U2OS cells were incubated in presence of different hEGF dilutions and response induction of the ErbB1 receptor was measured by chemiluminescent signal detection. The efficacy and compound concentrations were fitted in a dose response curve for determination of the half maximal effective concentration (EC_{50}). Measurements were conducted in duplicates.

3.9.4 Detection of α-tubulin in COS-7 cells by Atto 647 conjugated scFv clone F2C

The functional assay of anti-α-tubulin scFv clone F2C was performed by Nanotag Biotechnologies GmbH (Göttingen, Germany). For this, 250 µg of purified scFv clone F2C was labeled with fluorescent dye Atto 647 NHS ester (Atto-TEC) according to the manufacturer´s protocol. The degree of labelling (DOL, dye-to-protein ratio) was determined to be 1.5. Excessive dye was removed by desalting of the conjugate using a gravity flow column (Cytiva, Catalog Nr. 17085101). For epifluorescence imaging, COS-7 cells were fixed in 4 % paraformaldehyde (w/v) at RT for 30 min. Cells were blocked and permeabilized in PBS containing 10 % (v/v) normal goat serum and 0.1 % (v/v) Triton X-100 for 15 min at RT. The Atto 647 conjugated scFv clone F2C was diluted 1:500 in PBS containing 3 % (v/v) normal goat serum and 0.1 % (v/v) Triton-X 100. The cells were incubated in the staining solution for 1 h at RT and washed three times for 5 min with PBS subsequently. To stain the nucleus, DAPI (4′,6-diamidino-2-phenylindole, 0.4 µg/L) was included in one of the PBS washing steps. Cover slips were mounted on glass-slides using Mowiol solution, dried at 37 °C, and imaged.

3.10 Phagemid library construction

3.10.1 Preparation of pSEX81 vector fragment

Pre-culture of *E. coli* XL1-Blue transformed with pSEX81 phagemid was grown from 5 µL cryo culture in 2YT medium supplemented with 100 µg/mL ampicillin at 37 °C for 16 h and used to inoculate 500 mL selective TB medium in a 5 L shaking flask to a starting OD_{600} of 0.1. Cells were grown at 37 °C for 16 h

before harvested by centrifugation (5000 *g*, 15 min, 4 °C). The pSEX81 phagemids were isolated from cells using the NucleoBond® Xtra Midi Prep Kit (Qiagen) according to the manufacturer's protocol. Correct size of isolated pSEX81 phagemids were verified by 0.8 % (w/v) agarose gel electrophoresis. The scFv antibody fragment cassettes of pSEX81 flanked by *Not*I and *Nco*I restriction sites were removed by double restriction digestion using *Nco*I-HF® and *Not*I-HF® (New England Biolabs, NEB) restriction enzymes. The digestion reaction was incubated at 37 °C for 5 h before loaded on 0.8 % (w/v) agarose gels to separate desired pSEX81 fragments from released scFv antibody fragments. Gels were stained in GelRed® Nucleic Acid Gel stain (Biotium), DNA bands were visualized by UV light and pSEX81 fragment containing bands were excised and purified by Zymoclean Gel DNA Recovery Kit (Zymo Research). Residual gel impurities in the DNA sample were removed by Sera^{TM} Magnetic Beads (Cytiva) purification (Hawkins et al., 1994). Correct size of desired pSEX81 fragments were verified by agarose gel electrophoresis analyses. The library DNA was cloned into pSEX81 phagemids using the *Nco*I and *Not*I restriction sites (detailed in section 3.10.3). The plasmid maps of the original and recombinant pSEX81 phagemids are shown in Figure 11.

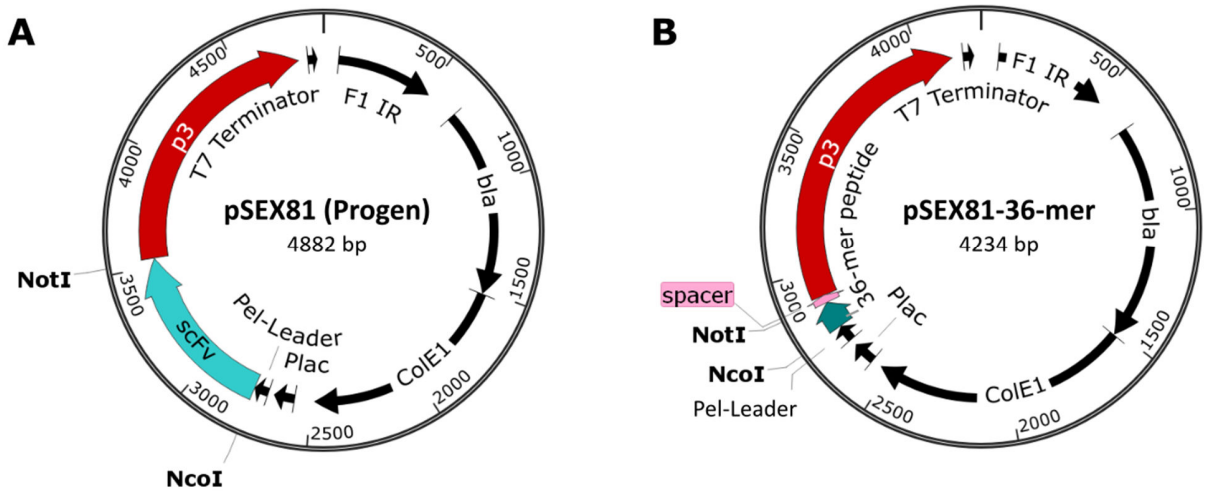

Figure 11 | Plasmid maps of original and recombinant pSEX81 phagemid vector

(A) Original pSEX81 phagemids (Progen) were designed to express single-chain variable fragments (scFv). **(B)** Recombinant pSEX81-36-mer phagemid vector. The restriction sites *Not*I and *Nco*I were used to insert the 36-mer library DNA between the pelB leader sequence (Pel-Leader) and p3 coat protein. The Pel-Leader sequence is important for the transport of p3-peptide fusion protein to the periplasm. The spacer sequence (GAAAGSKDIR) between the 36-mer library DNA and p3 contains a trypsin cleavage site which allows elution of recombinant phagemid particles from targets by proteolytic cleavages in biopanning experiments. The ß-lactamase gene (bla) enables selection of ampicillin-resistant clones. Further features: F1 IR, F1 intergenic region; ColE1, Colicin E1 origin; Plac, lac promotor; T7 Terminator, terminator from T7 bacteriophage.

3.10.2 Preparation of the 36-mer library DNA

Single-stranded library oligonucleotides containing 36 degenerate NNM codons (where N represent A, C, G, T nucleotides and M equimolar amounts of A and C nucleotides) were purchased from Integrated DNA Technologies, Inc. (IDT). The sequence is inverse, so correct insertion into pSEX81 phagemids resulted in the translation of NNK codons. The library oligonucleotides were synthesized in 2 nmol scale and purified by polyacrylamide gel electrophoresis (PAGE). The extension primer complementary to the fixed 3' region of the library oligonucleotide was purchased from Microsynth and was crucial to convert the library oligonucleotide to double stranded library DNA. The DNA sequences of the extension primer and the 36-mer library oligonucleotide are shown in (Supplementary Material, Table S 1). Annealing of the extension primer to the library oligonucleotide was initiated by preparation of reaction mix (0.68 nmol library oligonucleotide, 2.1 nmol extension primer, 10 mM Tris-HCl pH 8.0, 1 mM EDTA pH 8.0 and 20 mM NaCl, filled up to 250 µL with ddH_2O) and starting the program (Table 2) in a thermocycler (Biometra).

Table 2 | Thermocycler program for library oligonucleotide and extension primer annealing

Step	Temperature (°C)	Time	Remark
1	95 °C	5 min	
2	94 °C	30 sec	Decreased by 1 °C per 30 sec
3-59	37 °C	30 sec	
60	36 °C	15 sec	Decrease by 1 °C per 15 sec
66	30 °C	15 sec	
67	25 °C	15 sec	
68	4 °C	∞	

After the annealing reaction was completed, 100 µL of 10x CutSmart buffer, 0.4 mM dNTPs and 15 µL of Klenow fragment (5000 U/mL, NEB) were added. The reaction was filled up to 1 mL with ddH_2O, mixed and equally split in 0.2 mL PCR tubes. Klenow fill-in reaction was started by incubation at 37 °C for 10 min, then stopped by heat inactivation (75 °C for 15 min). The ORFs of the randomized peptide inserts in the library DNA were now flanked by *Nco*I and *Not*I restriction sites. Reactions were pooled and the library DNA was digested with *Nco*I®-HF and *Not*I-HF® (NEB) at 37 °C for 5 h. To decrease the reaction volume the library DNA was concentrated by binding to Sera-Mag™ Magnetic Beads and subsequently eluted in low volumes of 5 mM Tris-HCl pH 8.5. The library DNA was loaded on 8 % polyacrylamide gels and run at low voltage (TBE buffer, 8 V/cm) to get rid of DNA impurities (e.g. parental DNA, uncomplete digestion products). Gels were incubated in GelRed® Nucleic Acid Gel stain (Biotium), visualized by UV light and gel bands containing desired library DNA fragments were excised. The gel bands were crushed in small pieces using a spatula to destroy the gel structure and increase the surface area to facilitate DNA diffusion

from the gel. Diffusion buffer (0.5 M ammonium acetate, 10 mM magnesium acetate, 1 mM EDTA pH 8.0, 0.1 % SDS) was added (400 µL/ 100 mg gel) and the mixture was incubated at 37 °C, 1,500 rpm and for 4 h. Gel pieces were sedimented by centrifugation (17,000 *g*, 5 min, RT) and the library DNA containing supernatant was removed and filtered (Whatman GC/C filter, 0.25 µm). Library DNA fragments were purified by Sera-Mag™ Magnetic Beads (Hawkins et al., 1994) and the correct size was confirmed by 8 % (w/v) PAGE.

3.10.3 Production of bacterial 36-mer phagemid library

Optimized ligation and transformation conditions were used for library preparation to reach transformation efficiencies > 1 x10^7 cfu per µg DNA. Large scale ligation reaction was set up as follows: 17 µg pSEX81, 2.5 µg 36-mer library DNA (5-fold molar excess), 240 µL of T4 DNA ligase buffer, 170 µL of T4 DNA ligase were mixed and filled up to 3.4 mL with ddH_2O. The ligation mixture was incubated at 25 °C for 30 min before heat-inactivated (70 °C for 25 min). The resulting pSEX81-36-mer phagemids were purified by Sera™ Magnetic Beads (Cytiva), analyzed by 0.8 % (w/v) agarose gel electrophoresis and DNA concentration was determined by UV/VIS spectroscopy at 260 nm (NanoDrop™ One/One C, ThermoFisher). To prepare the transformation reactions, 200 ng of pSEX81-36-mer phagemids were mixed with 50 µL of *E. coli* TG1 electrocompetent cells (Lucigen) in pre-chilled 0.2 cm gap cuvettes (BioBudget). After electroporation (3 kV pulse, Ec3 program, Bio-Rad Micropulser™) cells were recovered in super optimal medium with catabolic repressor (SOC) medium (37 °C for 45 min, 1,150 rpm) before spread on agar plates based on 2YT supplemented with 100 µg/mL ampicillin and 100 mM glucose (2YT-AG) (150 mm x 20 mm). Growth of library clones was initiated by incubation at 37°C overnight. The transformation efficiency (number of library clones in cfu per µg of library DNA, cfu/µg) and the total number of library clones (cfu) were determined in every third transformation reaction. For this, serial dilutions of recovered cell cultures were prepared, and they were spread on 2YT-AG agar plates. After overnight incubation at 37°C the library colonies were counted. The average transformation efficiency provides information on how well the pSEX81-36-mer phagemids were taken up by *E. coli* TG1 electrocompetent cells. The theoretical library diversity, so the estimated number of individual library clones in the pool, was projected by multiplying the average total number of library clones (µg) with the total number of transformation reactions performed. In summary, for the construction of the 36-mer library 80 transformation reactions were performed, but batches of maximal 6 to 8 transformation reactions were simultaneously handled to avoid long processing times. The next day, all library clones grown on 2YT-AG plates were scratched off, pooled, supplemented with glycerol to a final concentration of 25 % (v/v) and thoroughly mixed. The bacterial solution was aliquoted in 2 mL cryo tubes, shock-frozen in liquid nitrogen and the tubes were stored at -80 °C until further use.

3.10.4 Phagemid library analysis

To assess the quality of the phagemid libraries the 36-mer (section 3.10.3) and 24-mer (prepared by Numaferm GmbH) were further analyzed. Small samples of both libraries were spread on 2YT-AG agar plates for growth of library clones. Roughly 60 clones for each library were randomly picked and sent for DNA sequence analyses (Microsynth). For this, a -221 sequencing forward primer was employed that anneals 221 bp upstream of the randomized peptide sequence (Supplementary Material, Table S 1). The proportions of correct clones (i.e. containing in-frame peptide inserts and translated in the right orientation) and incorrect ones (i.e. containing frameshifts due to nucleotide deletions, multiple peptide concatemers and/or pSEX81 wild type contaminations) were determined for each library. The ratio of incorrect clones provides insights into the quantity of functional library clones within the phagemid pool, also referred to as actual library diversity.

In other analyses, the ORFs encoding randomized peptides were further analyzed regarding their frequency of amino acids in the sequence. Here, only peptide inserts were considered that were cloned correctly into pSEX81 phagemids. Microsoft Excel was used for the evaluation. As described in section 3.10.2, both libraries were constructed based on the NNK randomization strategy. NNK codons still enable the coding of all 20 canonical amino acids, but bias towards certain residues was still expected because the number of codons for each amino acid varied. The expected frequency of each amino acid can be calculated based on the number of available codons derived from the NNK randomization strategy (number of codons for each amino acid divided by 32 codons x 100 %), i.e. the expected frequencies for L, R, S lies at 9.4 %, for A, G, P, Q, T and V at 6.2 % and for the remaining residues at 3.1 % (Yang et al., 2008).

3.11 Production of phagemid particles

The recombinant pSEX81 phagemids in *E. coli* TG1 cells can be converted to phagemid particles displaying randomized peptides on their surface. To produce these phagemid particles, pre-cultures of the bacterial 24-mer or 36-mer library were grown from 2 mL cryo culture aliquot stocks (section 3.10.3) in 200 mL 2YT-AG at 37 °C overnight. Afterwatds, 5 mL of the respective pre-culture was used to inoculate 500 mL of 2YT-AG in 5 L shaking flasks for the main cultures. When glucose is present, the p3-peptide expression is repressed to facilitate cell growth due to the toxicity of p3 to the cells (Clackson and Lowman, 2004). The cultures were grown to OD_{600} 0.4–0.6 before M13K07Δp3 hyperphages (1.3x 10^{12} particles/mL, Progen) were added to a multiplicity of infection (MOI) of 20:1. The MOI represents the ratio of infectious phages to bacterial cells estimated by measuring the OD_{600} (Implen OD600 DiluPhotometer; OD_{600} of 1 corresponds to approximately 5 x10^8 cells per mL (Implen, 2022)). For superinfection, the cells were incubated at 37 °C without shaking, then 30 min with shaking (250 rpm) before pelleted by centrifugation (3,200 *g*, 10 min, 4 °C). The cell pellets were gently resuspended in 500 mL of 2YT supplemented with 100 µg/mL ampicillin

and 30 µg/mL kanamycin (2YT-AK) for selection of *E. coli* TG1 cells harboring the pSEX81-24-mer phagemid or pSEX81-36-mer phagemid (Amp^R), respectively, and hyperphage genome (Kan^R). Here, the absence of glucose in 2YT triggers p3-peptide expression in cells and the other phage proteins deriving from the hyperphage genome were produced by the host cell machinery. Typically, the formation of recombinant phagemid particles takes place within the cell, and subsequently, they are released into the culture supernatant without killing the host (Roy and Mitra, 1970). Productions of phagemid particles were performed by overnight cultivation at 37 °C and 250 rpm.

3.12 Purification of phagemid particles

Phagemid particles were separated from host cells by centrifugation (3,220 *g*, 4 °C for 10 min) and precipitated by addition of 17 % (v/v) of ice-cold aqueous PEG/NaCl solution (20 % (w/v) PEG-8000/2.5 M NaCl) to the culture supernatant. After incubation on ice for 5 h the phagemid particles were pelleted by centrifugation (12,000 *g*, 1 h, 4 °C) and washed in 2 % of the initial volume in Tris-HCl buffer (10 mM, 20 mM NaCl, 2 mM EDTA, pH 7.5) supplemented with a Pierce™ protease inhibitor tablet (ThermoFisher) to prevent proteolytic degradation of p3-peptide. The solution containing phagemid particles was syringe filtered (0.45 µm, Sarstedt) and precipitated again by addition of 17 % (v/v) ice-cold PEG/NaCl solution. Incubation on ice was conducted for 2 h before phagemid particles were harvested by centrifugation at 12,000 *g* and 4 °C for 1 h. The pellets were resuspended in 1 mL of Tris-HCl buffer (10 mM, 20 mM NaCl, 2 mM EDTA, pH 7.5) and phagemid particle titers in the resulting stock solutions were determined by phagemid titration assay (section 3.15.1) and UV/VIS spectroscopy (section 3.15.2).

3.13 Biopanning of 24-mer phagemid library for identification of RBPs

Resomer® surfaces were sterilized in 70 % EtOH for 1 h and washed three times with sterile PBS before unspecific binding sites were blocked by incubation in PBS containing 1 % (w/v) BSA for 1 h. Afterwards, the surfaces were washed five times with PBS in 1 min intervals before the first biopanning round was conducted. About 2.4 $x10^{11}$ phagemid particles deriving from the 24-mer library phagemid stock solution (corresponds to ~ 100-fold representation of the actual library diversity) were mixed with human plasma (Sigma-Aldrich, P9523) reconstituted in PBS and incubated at 37 °C for 1 h to eliminate peptides susceptible to proteolytic degradation. Then, 1 % (w/v) BSA was added before the mixture was incubated in presence of the Resomer® surface for 2 h at RT to select for strong binders resistant to proteolytic degradation. The non- and weak binding phagemid particles were removed by rigorous washing steps. The surface was washed three times with PBS containing 0.1 % Tween 20 (PBS-T), three times with Trypsin-EDTA solution (Gibco™, R001100) and three times with PBS-T for 5 min, respectively. The vessel containing the Resomer® surface was exchanged against new ones after each washing step to minimize the risk of false positive selection. Bound phagemid particles on the Resomer® surface were eluted by

incubation in an acidic buffer (200 mM glycine-HCl pH 2.2) for 10 min before neutralized with 1 M Tris-HCl pH 9.1. The phagemid particle titer in the elution fraction was determined by phagemid titration assay (section 3.15.1) and the entire solution was added to 100 mL of *E. coli* TG1 culture grown to OD_{600} 0.4–0.6 for host cell infection. The cells were harvested by centrifugation (3,220 *g*, and 4 °C for 10 min) and the cell pellet was gently resuspended in 2 mL of PBS before plated on 2YT-AG agar plates for growth of enriched library clones. On the next day, the colonies were scraped off the plate and used to inoculate 50 mL of 2YT-AG (1:250, v/v) in a 250 mL shaking flask. The culture was grown to OD_{600} 0.4–0.6 and M13K07Δp3 hyperphage (1.3 $x10^{12}$ particles/mL, Progen) was added to 5 mL of bacterial culture at a MOI of 20:1. For infection, the culture was incubated at 37 °C without shaking, then 30 min with shaking (250 rpm). The cells were pelleted by centrifugation at (3,200 *g* and 4 °C for 10 min) and the resulting cell pellet was resuspended in 30 mL of 2YT-AK. Production of phagemid particles was performed by cultivation at 37 °C and 250 rpm overnight.

Phagemid particles in the culture supernatant were purified as described in section 3.12. In the last step, the phagemid particle pellet was resuspended in 1.8 mL of Tris-HCl buffer (10 mM, 20 mM NaCl, 2 mM EDTA, pH 7.5) containing Pierce™ protease inhibitor solution (ThermoFisher). The phagemid particle titer was determined by UV/VIS spectroscopy (section 3.15.1) and phagemid titration assay (section 3.15.2). The phagemid library was used for the next round of selection in the same manner as previously described. Altogether four rounds of selection were performed, and while in the 1st and 2nd biopanning round M13 KO7ΔpIII (Progen) hyperphages were used for the rescue of phagemid particles the stringency of selection was increased in the 3rd round by employing M13 KO7 helper phages (Progen). After the 4th biopanning round the eluted phagemid particles were shock-frozen in liquid nitrogen and stored at – 80 °C. Around 20 *E. coli* TG1 colonies derived from host cell infection of the 3rd and 4th elution fraction were randomly picked and further analyzed by DNA sequencing (Microsynth) (section 3.10.4) to identify enriched peptide motifs.

3.14 Biopanning of 36-mer phagemid library for streptavidin binding peptides

To assess the functionality of the 36-mer library the prepared phagemid particle solution (section 3.11) was screened against 96-well microtiter plates coated with the molecular target streptavidin. Biopanning experiments should yield peptide sequences containing the consensus motifs HPQ and HPM (Devlin et al., 1990). To coat the wells, about 1.5 µg/well streptavidin in 0.1 M $NaHCO_3$ was added and the plate was incubated at 4 °C overnight. On the next day, the wells were washed with TBS and incubated with blocking buffer (0.1 M $NaHCO_3$, 5 mg/mL BSA, 1 mg/mL streptavidin, 0.02 % NaN_3) at 4 °C for 3 h. Again, the wells were washed six times with TBS-T (0.1 % v/v Tween 20). Control wells without streptavidin were exclusively treated with blocking buffer and washed with TBS-T. About 1.2 $x10^{11}$ phagemid particles from the 36-mer library phagemid particle solution (corresponds to ~ 100-fold representation of the actual library diversity) were added to streptavidin-coated and non-coated wells and incubated at RT for 1 h. The

phagemid particle solutions were removed, and the wells were washed ten times with TBS-T in 5 min intervals to remove non-binders. Bound phagemids were eluted by incubation of the wells in presence of 0.1 µg/mL biotin in TBS at 37 °C for 30 min. To determine the phagemid particle titer in the elution fraction the phagemid titration assay was performed (section 3.15.1). The remaining elution fraction was used to infect 1 mL of *E. coli* TG1 culture grown to OD_{600} 0.4–0.6. After incubation at 37 °C for 30 min the cells were pelleted by centrifugation (3,200 *g*, 10 min, 4 °C), resuspended in 500 µL of PBS and plated on 2YT-AG agar plates for growth of library clones. On the next day, the colonies were scraped off from the plate and used to inoculate 30 mL of 2YT-AG. Phagemid particles were rescued by addition of M13K07 helper phages at a MOI of 20:1. After incubation at 37 °C for 30 min the medium was exchanged to 2YT-AK to allow the production of phagemid particles overnight. Purification of phagemid particles was performed as described in section 3.12. In the last step, the phagemid particle pellet was resuspended in 200 µL of TBS containing Pierce™ protease inhibitor solution. After the phagemid particle titer was determined by phagemid titration assay (section 3.15.1) and UV/VIS spectroscopy (section 3.15.2) the 2nd round of selection against streptavidin-coated and non-coated wells was conducted in the same manner as previously described. Altogether two biopanning rounds were performed and ~10 to 15 library clones derived from host cell infection of the 2nd round elution fraction were analyzed by DNA sequencing (Microsynth) to determine the proportion of HPQ and/or HPM-containing clones in the phagemid particle pool.

3.15 Phagemid particle titer determination

3.15.1 Phagemid titration assay

To determine the titer of infective phagemid particles in a solution 10-fold serial dilutions were prepared and 10 µL were added to 90 µL of *E. coli* TG1 culture grown to OD_{600} 0.4–0.6, respectively. For infection, the culture was incubated at 37°C for 30 min without shaking. Afterwards, 10 µL aliquots of infected cells were spotted in triplicates on selective LB agar containing 100 µg/mL ampicillin and 100 mM glucose for growth of colonies. Only infected *E. coli* cells harboring phagemids are resistant to ampicillin. Therefore, the titer of infective phagemid particles in the solution is based on the number of grown colonies and is indicated as cfu/mL.

3.15.2 Estimation of phagemid titer based on UV/VIS spectroscopy

The titer of phagemid particles in a solution can be estimated by measuring the OD of different dilutions at 260 nm (OD_{260}, NanoDrop™ One/One C, ThermoFisher). The following empirical formula can be used for calculation of the titer: Phagemid particles per mL = OD_{260} x dilution factor x 22.14 x10^{10} (Lee et al., 2007).

3.16 Cloning, expression and IB preparation of Switchtag fusions

The ORFs encoding HBD3-RBP2, HTN3-RBP2, DCD-1L-RBP2, RBP2-HBD3, RBP2-HTN3 and RBP2-DCD-1L fused to N-terminal Switchtags (Supplementary Material, Table S 7) were cloned into pBAD-derived expression plasmids (Guzman et al., 1995). Chemically competent *E coli* BL21 cells were transformed with recombinant expression plasmids, respectively, by heat shock (1 min, 42 °C) (Dagert and Ehrlich, 1979). The cells were regenerated in 200 µL of 2YT at 37 °C and 1,150 rpm for 45 min before spread on LB plates containing 30 µg/mL kanamycin for growth of selective clones. Renaturation efficiencies were determined by dividing the protein concentration in the cleared supernatant by the maximal expected value of the protein concentration adjusted for the renaturation reaction. Pre-cultures of *E. coli* BL21 cells harboring recombinant plasmids were grown from single colonies in 5 mL of 2YT containing 30 µg/mL kanamycin and cultivated at 37 °C and 180 rpm overnight. On the next day, 25 mL of selective 2YT in 250 mL shaking flasks were inoculated with pre-cultures to a starting OD_{600} of 0.1. The cultures were incubated at 37 °C and 180 rpm until OD_{600} 0.4–0.6 was reached and the production of IBs was induced by addition of 2 g/L arabinose. The cells were cultivated at 37 °C and 180 rpm overnight before harvested by centrifugation at 4,696 g and 4 °C for 15 min (Legend^{TM} X1 Centrifuge, ThermoFisher). The production of Switchtag fusion IBs before and after expression induction were checked by SDS-PAGE analysis as described in section 3.1. The IBs were extracted from the cells by using the BugBuster® Master Mix Kit (Novagene) according to the manufacturer's protocol.

For large scale IB production, pre-cultures of *E. coli* BL21 cells harboring recombinant plasmids were grown from single colonies in 25 mL selective 2YT using 250 mL shaking flasks. The cultures were incubated at 37 °C and 180 rpm overnight before used to inoculate 1 L of selective terrific broth (TB) medium in 5 L shaking flasks. To produce the Switchtag fusion IBs, 2 g/L arabinose was added to the cultures, respectively, when the OD_{600} reached 0.4–0.6. The cultures were incubated at 37 °C and 180 rpm for further 4 h before the cells were harvested by centrifugation at 16,000 *g* and 4 °C for 20 min (Beckman Avanti JXN-26). The production of Switchtag fusion IBs before and after expression induction were checked by SDS-PAGE analysis. Here, the IBs were isolated from cells by high pressure homogenization as described in section 3.1.

3.17 Renaturation and TEV protease cleavage of Switchtag fusions

Switchtag fusion IBs were solubilized in 6 M GuHCl in a protein to solvent ratio of 1:6 (w/v) and protein concentrations were determined by UV/VIS spectroscopy at 280 nm (NanoDrop™ One/One C, ThermoFisher) using calculated MWs and extinction coefficients (ProtParam, Expasy). Renaturations were performed in Tris-HCl or HEPES-based buffer (pH 8.0, 20 mM, 10 mM $CaCl_2$, 0.5 mM EDTA) adjusting the protein concentration to 1 mg/mL using the solubilized IBs. The renaturation efficiencies

To remove the Switchtags from the target peptides the TEV protease (Numaferm GmbH, Düsseldorf) was added in a molar enzyme to protein ratio of 1:25 and cleavage reactions were incubated at RT for 3 h. Solubilized and refolded Switchtag fusions, and the cleavage samples were analyzed by SDS-PAGE analysis (section 3.1 and 3.3). Refolded Switchtag fusions and cleavage samples were additionally analyzed by RP-HPLC-MS (section 3.2).

3.18 Purification of HBD3-RBP2, HTN3-RBP2 and DCD-1L-RBP2

After TEV protease cleavage, HBD3-RBP2, HTN3-RBP2 and DCD-1L-RBP2 were purified by RP-HPLC using the Knauer HPLC chromatography system. Crude cleavage reactions of HBD3-RBP2, HTN3-RBP2 and DCD-1L-RBP2 were supplemented with 4 M GuHCl, 5 % acetonitrile and 0.1 % TFA before cleared by syringe filtration (0.45 µm, Sarstedt). Samples were loaded on a preparative ZORBAX 300SB-C18 column (9.4 mm x 250 mm, 5 µm, Agilent) and the targets were eluted by a linear gradient of water and acetonitrile (5–60 %) in presence of 0.1 % TFA to achieve optimal separation from the Switchtag. The elution fractions were analyzed by RP-HPLC-MS (section 3.2) and target-containing fractions were pooled and lyophilized (Martin Christ Freeze Dryer Alpha 2-4 LD plus) at 0.1 mbar for 24 h. Afterwards, the lyophilized peptides were additionally post-dried at 0.01 mbar for 2 h before stored at -80 °C.

To conduct different analyses the lyophilized peptides were reconstituted in water and the protein concentration was determined by UV/VIS spectroscopy. Roughly 4 µg of each target was loaded on Tricine-SDS-PAGE gels (Schagger and von Jagow, 1987) to assess the apparent MWs. Furthermore, the targets were analyzed by RP-HPLC-MS (section 3.4.1) to determine the purities and verify the target identities. In addition the oxidized state of HBD3-RBP2 which contains six cysteine residues was further analyzed by RP-UPLC-MS using the ACQUITY UPLC CSH C18 column (130 Å, 1.7 µm, 2.1 mm x 100 mm) (section 3.8).

3.19 Functional analysis of HBD3-RBP2, HTN3-RBP2 and DCD-1L-RBP2

3.19.1 Pulldown assay

To assess the binding of peptides to the target surface, 40 µM of reconstituted peptides (section 3.18) in Tris-HCl buffer (10 mM, 20 mM NaCl, 2 mM EDTA, pH 7.5) were added to 200 mg of Resomer® beads in 1.5 mL tubes (Eppendorf). After incubation for 15 min the beads were sedimented by centrifugation (16,000 *g*, RT, 5 min) and peptide excess in the supernatant was removed. The beads were washed four times with Tris-HCl buffer (10 mM, 20 mM NaCl, 2 mM EDTA, pH 7.5) before bound peptides on Resomer® beads were eluted by addition of 150 µL of 200 mM glycine-HCl pH 2.2. The supernatant obtained after centrifugation (16,000 *g*, 5 min, RT) was neutralized with 1 M Tris-HCl pH 9.1 (1:10, v/v). For SDS-PAGE analyses, 80 µL of the supernatant, wash and elution fractions were mixed with 5x SDS-PAGE sample loading buffer and heated at 95 °C for 5 min. Then, 15 µL of SDS-PAGE samples were loaded on Tricine-SDS-PAGE gels (Schagger and von Jagow, 1987) and protein bands were visualized by colloidal Coomassie Blue G-250 staining (Dyballa and Metzger, 2009).

3.19.2 Minimal inhibitory concentration assay

The MIC assay was performed to assess the antimicrobial activity of HBD3-RBP2, HTN3-RBP2, DCD-1L-RBP2 and control peptides HBD3 (PeproTech), HTN3 (MCE), DCD-1L (Eurogentec), DS-THA (section 3.7) and RBP2 (ProteoGenix) against *E. coli* and *B. subtilis*. The assay was conducted as described in section 3.9.1 with the difference that the lyophilized peptides were reconstituted in MOPS buffer (10 mM, 120 mM $NaCl_2$, 10 mM $CaCl_2$) instead of aqueous 0.01 % acetic acid solution. Peptide concentrations ranging from 0.1 to 100 µM were assessed. Since the availabilities of HBD3-RBP2 and HBD3 peptides were limited, lower test concentrations were selected (0.1 to 25 µM). The same was true for DCD-1L-RBP2 and DCD-1L (0.2 to 50 µM). All measurements were conducted in duplicates.

3.20 Bacterial adhesion assay

Resomer® beads (R203, Poly-D, L-lactic acid, Evonik) were dissolved in ethyl acetate (133 mg/mL) under slow agitation for 3 h. Then, 0.3 %, 0.5 %, 2 % and 5 % (w/v) lyophilized DS-THA was added to the coating solutions, respectively. Resomer® coating solutions without DS-THA and with kanamycin (100 µg/mL) served as controls. Black 96-well microtiter plates (Greiner Bio-One, Frickenhausen) were coated by solution casting technique (section 1.5). Briefly, 30 µL of homogenously mixed coating solution was added to wells and left to dry at RT overnight. The coatings were additionally dried at 37 °C for 24 h to make sure that no residual organic solvent remained. Afterwards, the coatings were washed three times with PBS to remove peptide excess. All steps were performed under laminar flow.

Pre-cultures of expressing *E. coli* PKL1162 were grown from 5 µL cryo stock in LB containing 100 µg/mL ampicillin and 25 µg/mL chloramphenicol at 37 °C and 180 rpm overnight. The *E. coli* PKL1162 cells were kindly provided by Jun.-Prof. Dr. Stephan Schmidt and Prof. Dr. Laura Hartmann from the Institute for Macromolecular Chemistry in the University of Freiburg. For the main culture, 25 mL of selective MHB medium was inoculated with the pre-culture to a starting OD_{600} of 0.1 in a 250 mL shaking flask. The culture was incubated at 37 °C and 180 rpm until an OD_{600} 0.4–0.6 was reached before pelleted by centrifugation at 2,000 *g*, 4 °C and for 5 min. The cells were washed two times in PBS by gentle resuspension and centrifugation (2,000 *g*, 4 °C, 5 min) before the bacterial solution was adjusted to an OD_{600} of 0.004 with PBS, which corresponds to a final concentration of 3.2×10^6 cells/mL (Implen OD600 DiluPhotometer). According to the manufacturer's protocol an OD_{600} of 1 corresponds to about 5×10^8 cells per mL (Implen, 2022).

To promote cell adhesion on Resomer® coatings, 50 µL of the bacterial solution was dropped on the surface and incubated at 37 °C for 2 h. Precautions were taken to avoid contact between the bacterial solution and the non-coated regions of microtiter plate wells and prevent non-specific bacterial binding. After incubation, the bacterial solution was removed, and the surfaces were rigorously washed three times with 300 µL PBS to remove non-adherent bacteria from coated wells. Afterwards, 200 µL of MHB containing 100 µg/mL ampicillin and 25 µg/mL chloramphenicol were added and growth of adherent cells was initiated by incubation at 37°C overnight. Cell growth was monitored by measuring the fluorescence intensity at Ex/Em = 485 nm/535 nm every hour for 16 h (FLUOstar Optima, BMG). Furthermore, cells attached to Resomer® coatings in the absence of DS-THA were exposed to selective MHB containing 1.56 µM DS-THA reconstituted in PBS, aiming to assess the stability and antimicrobial efficacy of the peptide in solution.

4 Results

It should be mentioned that the results obtained in section 4.1 to 4.8 were previously published in the listed publications shown in section 7.

4.1 Renaturation studies on HlyA1

The first study provides information on the renaturation behavior of HlyA1 in the absence or presence of 10 mM Ca^{2+} (Figure 12). HlyA1 was recombinantly produced as IBs in *E. coli* BL21 (DE3) cultures. After isolation of the HlyA1 IBs from cells, they were denatured in 6 M GuHCl before refolded in buffer with and without Ca^{2+} (section 3.2).

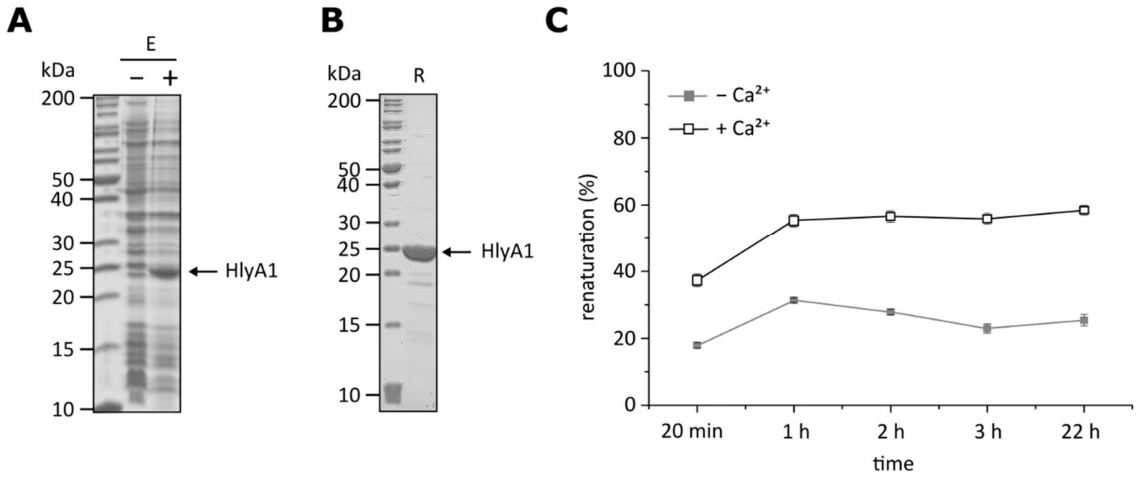

Figure 12 | Expression and renaturation of HlyA1 in absence or presence of Ca^{2+}

(A) Coomassie-stained SDS-PAGE gel analysis of *E. coli* BL21 (DE3) cells before (–) and after (+) induction of the expression (E). **(B)** Refolded (R) HlyA1 in Ca^{2+}-containing buffer using solubilized HlyA1 IBs. SDS-PAGE analyses were performed as described in section 3.1 and 3.2. The arrows indicate the location of HlyA1 (24 kDa). **(C)** Quantification of time-dependent renaturation efficiencies in absence and presence of Ca^{2+}. Error bars indicate the standard deviations (SD), and all measurements were performed in triplicates.

The presence of a strong protein band at about 24 kDa after expression induction indicated that intracellular production of HlyA1 IBs in *E. coli* BL21 (DE3) was successful (Figure 12A). Furthermore, renaturation of solubilized HlyA1 IBs in presence of Ca^{2+} led to substantial amounts of soluble HlyA1 with good initial purities as indicated in the absence of impurity bands (Figure 12B). Remarkably, the data suggest that the renaturation efficiency of HlyA1 IBs is higher in presence of 10 mM Ca^{2+} (~ 60 %) than in absence (~ 25 %) (Figure 12C). After incubation of the renaturation reactions for 1 h at RT no further increase of the renaturation efficiency was observed for none of the conditions.

4.2 Expression and renaturation of HlyA1 and HlyA1 fusions

Next, it was investigated whether the observed renaturation behavior (section 4.1) is conserved for HlyA1 fused to the N-terminus different peptides or pepteins. The selected targets differed in MWs (1.5–12.3 kDa), physicochemical characteristics (e.g. antimicrobial, hydrophobic, number of Cys) and biological functions. Detailed information on the biological functions of the selected peptides and pepteins can be found in section 1.3.3. The amino acid sequences and MWs of the selected candidates are illustrated in Table 3.

Table 3 | Overview of selected peptides and pepteins fused to HlyA1

Name of selected peptide and peptein	Amino acid sequence (one letter code)	MW (kDa)
Teriparatide	SVSEIQLMHNLGKHLNSMERVEWLRKKLQDVHNF	4.2
Linaclotide	CCEYCCNPACTGCY	1.5
Dermaseptin-Thanatin (DS-THA)	GLWSTIKQKGKEAAIAAAKAAGQAALGALGSKKPVPI IYCNRRTGKCQRM	5.2
Human ß-amyloid A3 (1-40 aa, Aß40)	DAEFRHDSGYEVHHQKLVFFAEDVGSNKGAIIGLMVG GVV	4.3
Serum amyloid A3 (SAA3)	QGWGTFLREAGQGAKDMWRAYRDMKEANYKGADK YFHARGNYDAAQRGPGGVWAAEVIREALQGITDPLFK GMTRPQVREDTKADQFANEWGQSGKDPNHFGPAALP DKY	12.3

The different peptide and pepteins were fused to N-terminal HlyA1 (Figure 10) in pSU2726 expression plasmids. The HlyA1 fusions were produced as IBs in *E. coli* BL21 (DE) cells (section 3.1) and cell samples obtained before and after expression induction were further analyzed by SDS-PAGE to evaluate target protein production (Figure 13).

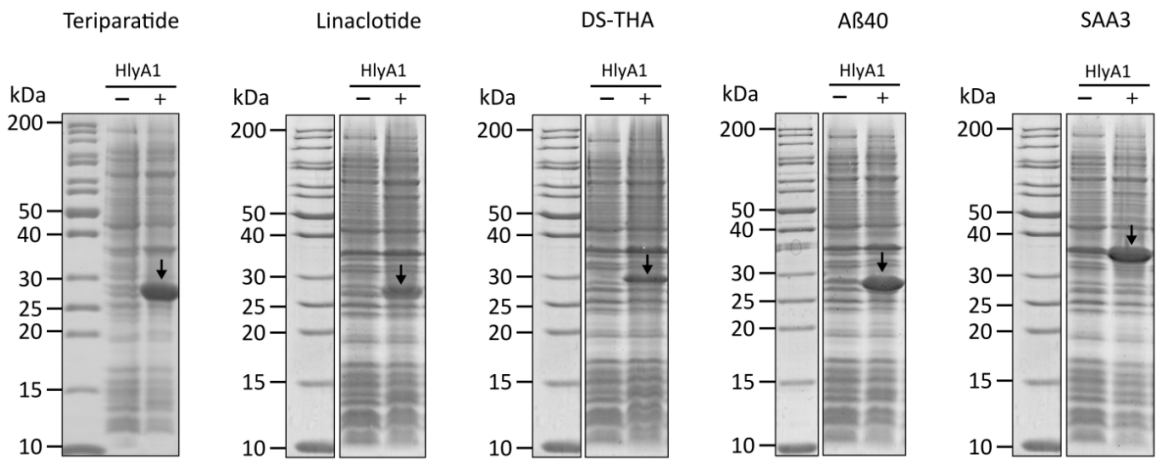

Figure 13 | Expression analysis of HlyA1 fusions

Coomassie-stained SDS-PAGE gel analyses of *E. coli* BL21 (DE) cells before (-) and after (+) expression induction of HlyA1 fusion genes. SDS-PAGE analyses and sample preparations were conducted as described in section 3.1. The arrows indicate the location of the HlyA1 fusions (HlyA1-Teriparatide, 28.0 kDa; HlyA1-Linaclotide, 26.4 kDa; HlyA1-DS-THA, 30.1 kDa; HlyA1-Aβ40, 29.2 kDa; HlyA1-SAA3, 37.2 kDa).

SDS-PAGE analyses of cell pellet samples indicate that all HlyA1 fusion IBs were successfully produced in *E. coli* BL21 (DE3) as the respective protein bands were found for all targets (Figure 13). The signal intensities of indicated target bands vary and this suggest that the expression levels differ depending on the target peptide or peptein. As before, the IBs were isolated from cells, the IBs were denatured in 6 M GuHCl and HlyA1 fusions were refolded in presence or absence of Ca^{2+} (section 3.2). The renaturation efficiencies were assessed based on UV/VIS spectroscopy measurements (Figure 14A). The soluble and renaturated HlyA1 fusions were subjected to TEV protease cleavage which resulted in the separation of target peptides or pepteins from HlyA1 backbone. The renaturation and cleavage reactions were further analyzed by SDS-PAGE and RP-HPLC-MS (Figure 14B-C).

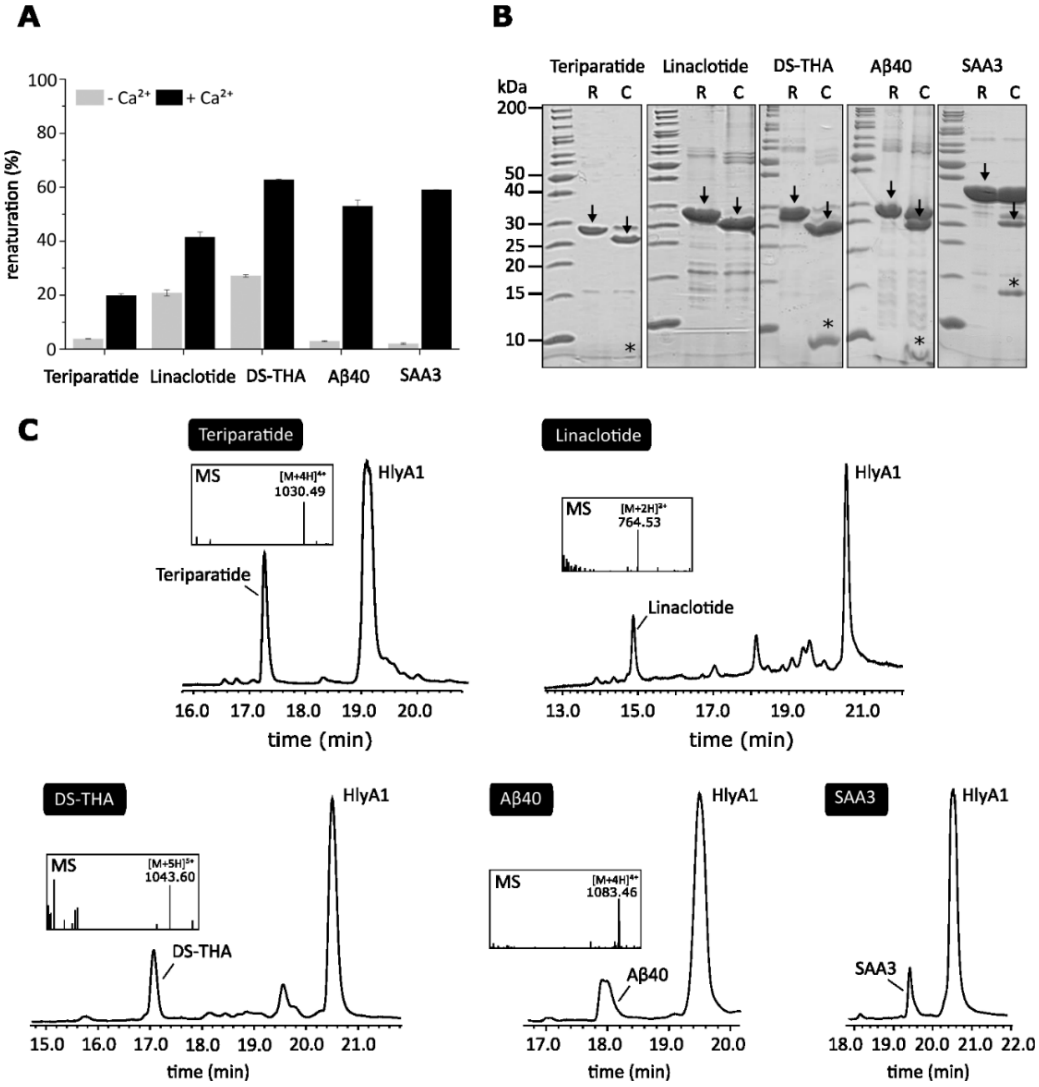

Figure 14 | Renaturation and TEV protease cleavage of HlyA1 fusions

(A) Renaturation efficiencies (%) of HlyA1 fusion proteins in presence or absence of 10 mM Ca^{2+} after 1 h incubation. 100 % renaturation efficiency corresponds to the maximal protein concentration adjusted for the renaturation reaction. Error bars indicate the SD, measurements were performed in triplicates. Measurements were conducted as described in section 3.2. **(B)** Coomassie-stained SDS-PAGE gel analyses of renatured HlyA1 fusion proteins prior to and after TEV protease cleavage. The samples were prepared as described in section 3.2. The arrows indicate the location of HlyA1 fusions after renaturation (R) and HlyA1 after TEV protease cleavage (C). Signals were found for each target but Linaclotide. Due to visualization limits of Coomassie staining, the locations of the target peptide or pepteins are highlighted (*). (**C**) RP-HPLC-MS analysis of HlyA1 fusions cleaved with TEV protease. Preparation and analyses of the samples were conducted as described in section 3.2. The retention time of HlyA1 backbone varied as different acetonitrile in water gradients were employed to achieve optimal peak separation. Molecular masses of the elution signals were determined by ESI-MS. Chromatograms show the UV absorption at 205 nm. For SAA3, no mass signals could be detected by the applied methods.

As previously observed (section 4.1) the renaturation efficiencies in absence of Ca^{2+} were lower (between 4–25 %) than in the presence of Ca^{2+} (20–63 %) (Figure 14A). Evidently, Ca^{2+} improved the renaturation efficiencies for HlyA1, but also HlyA1 fusions. After treatment of renaturated HlyA1 fusions with TEV protease each target peptide or peptein should be cleaved off from HlyA1 backbone. However, this occurred with varying efficiencies: Efficient cleavage from HlyA1 backbone was observed for Teriparatide, Linaclotide and DS-THA (about 90 %) while for Aß40 about 50 % and for SAA3 about 10–20 % cleavage efficiencies were observed. For all targets but Linaclotide respective protein bands were detected by Coomassie staining (Figure 14B). Target peptide or peptein releases in cleavage reactions were further analyzed by RP-HPLC-MS (Figure 14C). The formation of distinct elution signals was observed for each target and the identities of Teriparatide, Linaclotide, DS-THA and Aβ40 were confirmed by ESI-MS. For SAA3, no mass signals could be detected by mass spectrometric measurements but the protein band at 13 kDa in the Coomassie-stained SDS-PAGE gel (Figure 14B) correlated with the expected MW of SAA3.

4.3 Optimization of renaturation efficiencies

As the initial studies (section 4.2) showed renaturation efficiencies below 63% for all tested HlyA1 fusions, optimization experiments were undertaken using truncated HlyA1 variants. Previous studies have shown that the C-terminal secretion signal of HlyA1 contains regions prone to degradation (unpublished data). Therefore, three different HlyA1 variants were designed lacking the secretion signal partially (HlyA1 Δ185–218), almost entirely (HlyA1 Δ165–218) or containing an even longer C-terminal depletion (HlyA1 Δ135–218) (Table 4). The RTX domain of all HlyA1 variants was preserved as it is relevant for the Ca^{2+}-assisted refolding of fusion proteins (Lecher et al., 2012). The previously selected target peptides and pepteins (Table 3) were fused to N-terminal HlyA1 truncations and the fusion proteins were produced in *E. coli* BL21 (DE3) as IBs (section 3.1). As previously described, cells before and after expression induction were analyzed by SDS-PAGE for the presence of target proteins (Figure 15).

Table 4 | Amino acid sequences and MWs of HlyA1 and HlyA1 truncations

HlyA1 variant	Amino acid sequences (one letter code)	MW (kDa)
HlyA1	GNSLAKNVLFGGKGNDKLYGSEGADLLDGGEGDDLLKG GYGNDIYRYLSGYGHHIIDDDGGKEDKLSLADIDFRDVAF KREGNDLIMYKAEGNVLSIGHKNGITFRNWFEKESGDISN HQIEQIFDKSGRIITPDSLKKALEYQQRNNKASYVYGNDA LAYGSQGDLNPLINEISKIISAAGSFDVKEERTAASLLQLSG NASDFSYGRNSITLTTSA	23.7
HlyA1 Δ185-218	GNSLAKNVLFGGKGNDKLYGSEGADLLDGGEGDDLLKG GYGNDIYRYLSGYGHHIIDDDGGKEDKLSLADIDFRDVAF KREGNDLIMYKAEGNVLSIGHKNGITFRNWFEKESGDISN HQIEQIFDKSGRIITPDSLKKALEYQQRNNKASYVYGNDA LAYGSQGDLNPLINEISKIISAAGSF	20.1
HlyA1 Δ165-218	GNSLAKNVLFGGKGNDKLYGSEGADLLDGGEGDDLLKG GYGNDIYRYLSGYGHHIIDDDGGKEDKLSLADIDFRDVAF KREGNDLIMYKAEGNVLSIGHKNGITFRNWFEKESGDISN HQIEQIFDKSGRIITPDSLKKALEYQQRNNKASYVYGNDA LAYGSQ	18.1
HlyA1 Δ135-218	GNSLAKNVLFGGKGNDKLYGSEGADLLDGGEGDDLLKG GYGNDIYRYLSGYGHHIIDDDGGKEDKLSLADIDFRDVAF KREGNDLIMYKAEGNVLSIGHKNGITFRNWFEKESGDISN HQIEQIFDKSGRIITP	14.7

Underlined: GG repeats (GGxGxDxUx, where x can be any amino acid and U is a large hydrophobic amino acid); Grey: Last C-terminal 60 amino acid residues of HlyA1 which comprise the secretion signal (Nicaud et al., 1986).

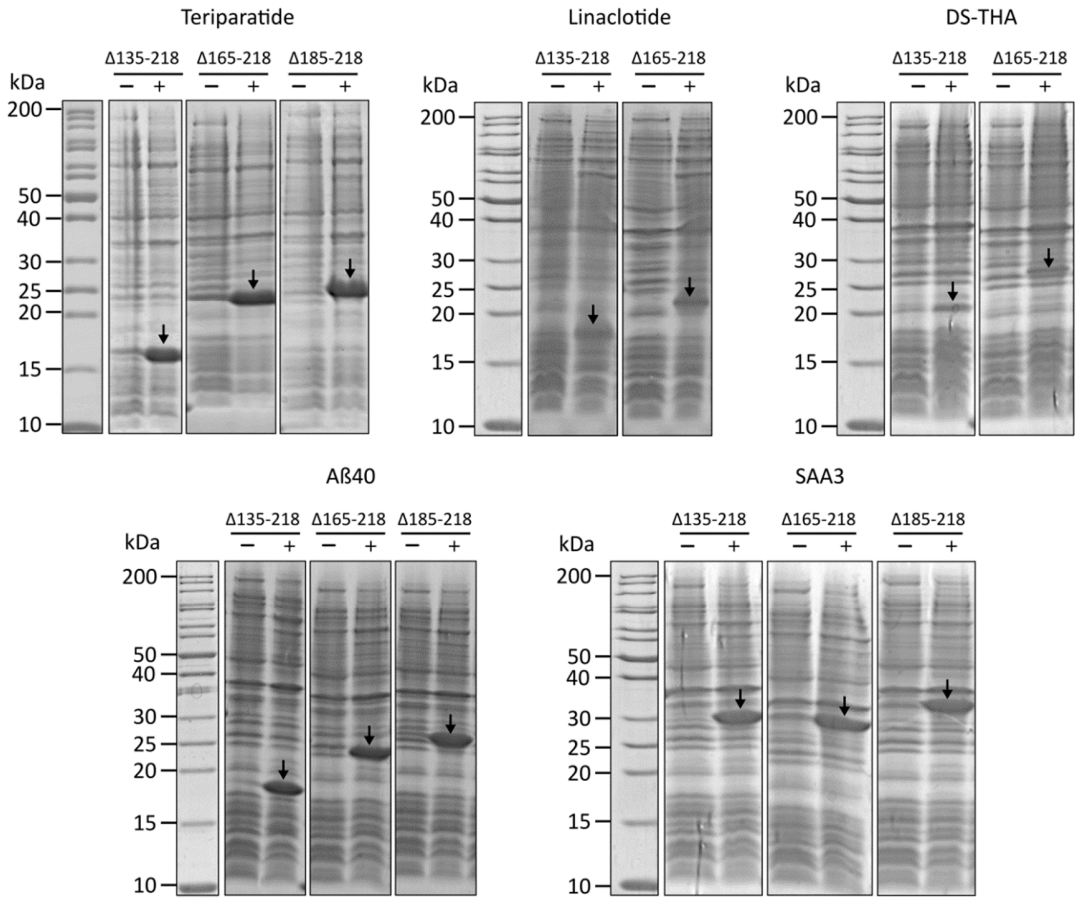

Figure 15 | Expression analysis of truncated HlyA1 fusions

Coomassie-stained SDS-PAGE gel analyses of *E. coli* BL21 (DE3) cells before (-) and after (+) expression induction. SDS-PAGE analyses and sample preparations were conducted as described in section 3.1. The arrows indicate the location of truncated HlyA1 fusions. For each of the target peptides or pepteins, three different HlyA1 truncations (Δ135-218, Δ165-218, Δ185-218) were evaluated as fusion partner. For Linaclotide and DS-THA no expression study for HlyA1 Δ185-218 could be conducted because cloning failed.

SDS-PAGE analyses indicated that all truncated HlyA1 fusions were intracellularly produced as IBs as respective protein bands were observed for all constructs (Figure 15). As previously observed for Teriparatide, Aß40 and SAA3 (section 4.2) the protein bands of these candidates were more dominant than DS-THA and Linaclotide. The IBs of truncated HlyA1 fusions were extracted from cells, denatured in 6 M GuHCl and renaturated in the presence of 10 mM Ca^{2+}. The renaturation efficiencies of truncated HlyA1 fusions were calculated based on UV/VIS spectroscopy and compared to full-length HlyA1 fusions (Figure 16).

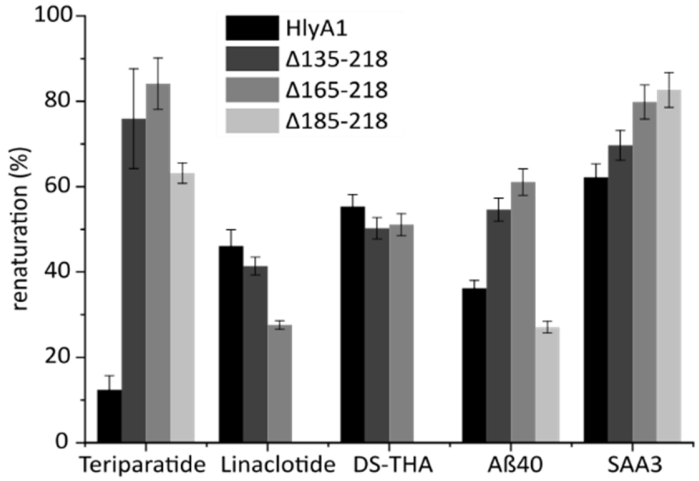

Figure 16 | Renaturation efficiencies of HlyA1 fusions and truncated HlyA1 fusions

Renaturation efficiencies (%) in Tris-HCl-based buffer in presence of 10 mM Ca^{2+} were determined for HlyA1 fusions and truncated HlyA1 fusions (section 3.2). Error bars indicate the SD, measurements were performed in triplicates.

Renaturation efficiencies of truncated HlyA1 fusions increased 6.8-fold for Teriparatide (84 %), 1.7-fold for Aβ40 (61 %) and 1.3-fold for SAA3 (80 %) compared to full length HlyA1 fusions. For DS-THA the renaturation efficiency did not substantially change and for Linaclotide renaturation efficiencies decreased with all truncated HlyA1 variants (Figure 16). Furthermore, all fusion proteins were treated with TEV protease to cleave off the target peptides or pepteins from truncated HlyA1 backbones. The renaturation and cleavage reactions were analyzed by SDS-PAGE (Supplementary Material, Figure S 1). For all targets, but Linaclotide respective protein bands were detected in Coomassie-stained SDS-PAGE gels. The release of Linaclotide in cleavage reactions was confirmed by RP-HPLC-MS. As the highest refolding efficiency was observed for HlyA1 Δ165-218 (84 %) fused to Teriparatide it was selected for the next study.

4.4 Gram scale production of Teriparatide

Here, the main objective was to establish a pilot scale production protocol for Teriparatide to demonstrate the scalability of the Numaswitch™ technology. Teriparatide is a therapeutic peptide used to stimulate the growth of osteoblast cells and to treat osteoporosis (Minisola et al., 2019). A fed-batch high cell density fermentation protocol was established by the Upstream division of Numaferm GmbH (Supplementary Material, Figure S 2) which yielded 21 g HlyA1 Δ165-218 Teriparatide IBs net weight per liter fermentation broth (63 g wet weight). Pilot scale production of Teriparatide is detailed in section 3.3. Under optimized conditions with HEPES-based buffer solubilized IBs of HlyA1 Δ165-218-Teriparatide were efficiently renatured (> 95 %). In addition, separation of Teriparatide from HlyA Δ165-218 backbone by TEV protease cleavage occurred efficiently (> 95 %) within 3 h of reaction time (Figure 17A). Released Teriparatide was

purified by CEX reaching high purity levels. RP-FLASH chromatography was applied for further purification, salt removal and for TFA/acetate exchange before Teriparatide was lyophilized (data not shown). Lyophilized Teriparatide was determined to have a purity of > 99.6 % employing RP-HPLC. The target identity was confirmed by ESI-MS (Figure 17B) and peptide mapping (Supplementary Material, Figure S 3).

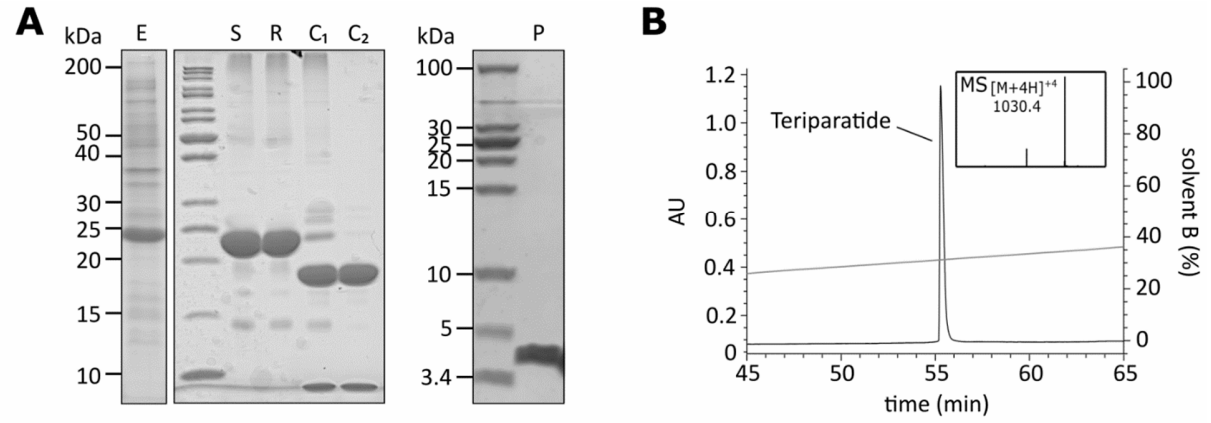

Figure 17 │Analysis of pilot scale production of Teriparatide using HlyA1 Δ165-218

(A) Coomassie-stained SDS-PAGE gel analyses of different process steps: Expression analysis of *E. coli* cells from high cell density fermentation (E), solubilized HlyA1 Δ165-218-Teriparatide IBs (S), after renaturation step (R), after TEV protease cleavage (C_1: crude, C_2, cleared) and purified Teriparatide after CEX, RP-FLASH chromatography and TFA/acetate exchange (P) (section 3.3). (**B)** RP-HPLC-MS analysis of purified Teriparatide revealed > 99.6 % purity of lyophilized Teriparatide. The identity of Teriparatide was confirmed by RP-HPLC-MS (section 3.4.1).

Further analyses were performed to assess the quality of purified Teriparatide (section 3.4.3). The endotoxin level in the sample was determined in a LAL assay conducted by BioChem (Karlsruhe). The actual Teriparatide content in the sample was analyzed by UV/VIS spectroscopy (gross/net weight). Ion chromatography was performed to determine the concentration of residual acetate, TFA and Cl^- ions in the Teriparatide sample. The content of residual host cell proteins (rHCP) was determined by the Cygnus™ HCP ELISA Kit (Cygnus technologies) and purified Teriparatide were analyzed for residual host cell DNA (rHCD) by real-time PCR using the innuMIX qPCR SyGreen Sensitive Master Mix (Analytik Jena) (data not shown). The biological activity of purified Teriparatide was confirmed in a cell-based cAMP assay performed by Charles River. The results of all analyses are summarized in Table 5. Altogether, from 1 L fermentation broth roughly 2 g of Teriparatide was produced meeting common specifications of active pharmaceutical ingredients for human applications.

Table 5 | Specification analyses of Teriparatide products

Property	Specification	Measured
Identity (4117.7 Da)	1030.4 $[M+4H]^{+4}$	1030.4 $[M+4H]^{+4}$
Peptide mapping (aa)	23-30, 23-34, 5-22, 5-19	confirmed
Purity	≥ 95 %	99.6 %
Net/ Gross weight	> 80 %	88.7 %
Acetate/TFA/Cl	> 95 % acetate	96/3/1 (mol %)
Endotoxins	< 5 EU/mg	< 0.4 EU/mg
rHCP	< 500 ng/mg	< 100 ng/mg
rHCD	< 200 pg/mg	< 10 pg/mg
Biological activity	As WHO standard	confirmed

4.5 Cloning, expression and renaturation of Switchtag fusions

In the next study the focus was set on the production of peptides and pepteins usually challenging to produce in *E. coli*. The selected candidates vary in their MWs (5.2–26.9 kDa), number of cysteine residues (2–6 Cys) and biological functions (e.g. growth factor, scFv, nanobody). The selected peptides and pepteins were Dermaseptin-Thanatin (DS-THA), human epidermal growth factor (hEGF), a camelid heavy chain antibody (VHH) and the scFv clone F2C (section 1.3.3). In previous studies of Numaferm GmbH other truncated HlyA1 variants were tested for their suitability as protein tags for recombinant expression by the Numaswitch™ technology. In addition, other GG repeats-containing fragments derived from alternative RTX proteins and exported by the T1SS were included. Previous studies indicated that some GG repeats-containing fragments exhibited similar renaturation capabilities as HlyA1 and HlyA1 truncations (unpublished data). “Switchtags” refer to a collective group of protein tags harboring varying numbers of GG repeats used in the Numaswitch™ technology to produce recombinant peptides and pepteins. Many of these Switchtags, in particular those based on HlyA are still under investigation. As the data in section 4.3 already indicated, it is hard to predict how a given Switchtag performs in renaturation reactions when fused to different targets. Therefore, in previous studies DS-THA, hEGF, VHH and scFv clone F2C were fused to different Switchtags to assess their refolding performance in trial-and-error approaches (unpublished data). The Switchtag-target combination that demonstrated the highest renaturation efficiency were chosen to develop protocols for large scale production. It should be mentioned that criteria including expression level

of different Switchtag fusions in *E. coli* or target recovery after TEV protease cleavage were also considered for selection. The amino acid sequences and MWs of the selected Switchtag fusions are shown in Table 6.

Table 6 | Structure and MWs of Switchtag fusion proteins

Switchtag fusion	Amino acid sequence (one letter code)	MW (kDa)
Switchtag-DS-THA	Switchtag– ENLYFQGLWSTIKQKGKEAAIAAAKAAGQAALGALGSK KPVPIIYCNRRTGKCQRM	30.1
Switchtag-hEGF	Switchtag– ENLYFQNSDSECPLSHDGYCLHDGVCMYIEALDKYACN CVVGYIGERCQYRDLKWWELR	29.5
Switchtag-VHH	Switchtag– ENLYFQSGDASDSAQVQLVESGGGLVQAGGSLRLSCAT SGFTFSDYAMGWFRQAPGKEREFVAAISWSGHVTDYAD SVKGRFTISRDNVKNTVYLQMNSLKPEDTAVYSCAAAK SGTWWYQRSENDFGSWGQGTQVTVSSGSTGENSSGTG	38.6
Switchtag-scFv clone F2C	Switchtag– ENLYFQSGDASDSAEVQLVESGGGLVQPGGSLRLSCAAS GFTFSSYAMSWVRQAPGKGLEWVSAISGSGGSTYYADS VKGRFTISRDNSKNTLYLQMNSLRAEDTAVYYCARPTIN SIAPQLWGQGTLVTVSSGGGGSGGGGSGGGSALQSVLTQ PPSASGTPGQRVTISCSGSSSNIGSNYVYWYQQLPGTAP KLLIYRNNQRPSGVPDRFSGSKSGTSASLAISGLRSEDEA DYYCAAWDDSLASVVFGGGTKLTVLGSGSTGENSSGTG	38.8

ENLYFQ: Cleavage site of the TEV protease; Underlined: Amino acid sequence of the target peptide or peptein

The targets DS-THA, hEGF, VHH and scFv clone F2C were fused to N-terminal Switchtags, and the resulting fusion proteins were produced as IBs in high cell density fermentations employing *E. coli* BL21 as hosts. The IBs were extracted from the cells by high pressure homogenization, washed and solubilized in either 8 M urea or 6 M GuHCl. The Switchtag fusions were renaturated in Ca^{2+}-containing buffer and the renaturation efficiencies were assessed by SDS-PAGE and UV/VIS spectroscopy. Separation of target peptides or pepteins from Switchtags was performed by TEV protease cleavage (section 3.6). The

expression of targets in *E. coli*, the solubilized IBs, the renaturated Switchtag fusions and the cleavage reactions were analyzed by SDS-PAGE (Figure 18).

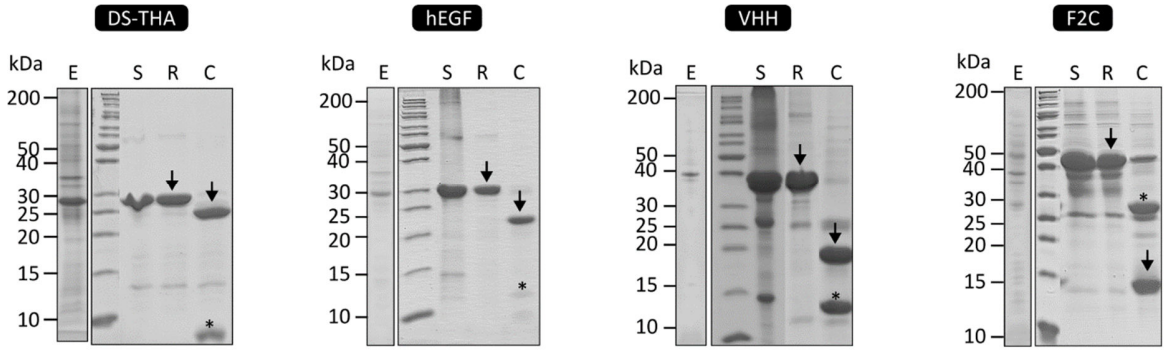

Figure 18 | Expression, solubilization, renaturation and cleavage of Switchtag fusions

Coomassie-stained SDS-PAGE gel analyses of Switchtag fusions from expression to the cleavage reaction. Target protein genes were expressed (E) in *E. coli* and produced as IBs in high cell density fermentations (section 3.5). The IBs were isolated from cells and solubilized in 8 M urea or 6 M GuHCl (S). After the renaturation step (R) the Switchtags were cleaved off from targets by TEV protease cleavage (C). The arrows indicate the location of renaturated Switchtag fusions and released Switchtags prior to and after TEV protease cleavage. SDS-PAGE analyses were performed as described in section 3.3. The positions of target peptides or proteins are highlighted (*) (DS-THA, 5.2 kDa; hEGF 6.2 kDa; VHH, 15.3 kDa; scFv clone F2C, 26.9 kDa).

SDS-PAGE analyses showed that all Switchtag fusions were successfully produced as IBs in *E. coli* BL21 cells (Figure 18, see lanes "E"). Expression titers of Switchtag fusions were determined by SDS-PAGE analysis using BSA protein standard (section 3.5) and revealed titers ranging from 10-19 g per liter fermentation broth. Furthermore, all Switchtag fusions were efficiently renaturated in the presence of Ca^{2+} as demonstrated by SDS-PAGE analyses (Figure 18, compare lanes "S" and "R") and by UV/VIS spectroscopy. The renaturation efficiencies ranged between 52 and 90 % (Table 7). The Switchtags were efficiently removed from the target peptide or peptein by TEV protease cleavage (Figure 18, see lanes "C"). For DS-THA, hEGF, and VHH the protein bands of Switchtag fusions were very weak after TEV protease treatment, indicating efficient cleavage. However, scFv clone F2C exhibited an estimated cleavage efficiency between 80-90% based on SDS-PAGE gel analysis. Protein bands correlating with the expected MWs confirmed the presence of the released targets, but the signal intensities varied. The protein band intensity was the weakest for hEGF, moderately so for DS-THA, while the strongest signals were detected for VHH and the scFv clone F2C.

4.6 Purification of target proteins hEGF, VHH, scFv clone F2C and DS-THA

To purify hEGF, VHH, scFv clone F2C and DS-THA from crude cleavage reactions individual production process strategies were developed. The antibody fragments VHH and scFv clone F2C were purified by

negative mode IMAC where His_6-tagged Switchtag and TEV protease were captured from crude cleavage reactions by binding to a Ni^{2+}- charged column. Both targets VHH and scFv clone F2C eluted in the flow through fractions, respectively. They were concentrated and buffer exchanged for TBS before analyzed by SDS-PAGE. In case of hEGF a two-step chromatographic strategy was required to isolate the correct hEGF isomer. RP-HPLC analysis of the cleavage reaction revealed the presence of various hEGF isomers which resulted in product heterogeneity within the sample (data not shown). To separate the desired hEGF isomer from the others, AEX was performed as initial purification step. Then, negative mode IMAC was conducted to remove residual impurities including the His_6-tagged Switchtag and TEV protease. The hEGF in the flow through fractions were pooled, concentrated, buffer exchanged for PBS and analyzed by SDS-PAGE. In case of the bifunctional peptide DS-THA, RP-FLASH chromatography was conducted to separate the target from Switchtag backbone. The chromatograms of the individual production processes and SDS-PAGE analyses of all four targets are shown in Supplementary Material, Figure S 4 – S 7. The key characteristics of the production processes including expression titer of Switchtag fusions, renaturation efficiency, product yield or the purity of targets are shown in Table 7.

Table 7 | Key characteristics of production processes of DS-THA, VHH, scFv clone F2C and hEGF

	DS-THA	VHH	scFv clone F2C	hEGF
Expression titer of Switchtag fusions (g/L) [A]	10	17.7	11.9	19.7
Renaturation efficiency (%) [B]	52	58	90	90
Product yield (g/L) [C]	≥ 1.6	≥ 2.5	≥ 4.5	≥ 1.1
Purity (%)	≥ 98[D]	≥95[E]	≥ 95[E]	≥ 95[E]

[A] Expression titer for Switchtag fusions derived from high cell density fermentations were calculated by SDS-PAGE using BSA protein standard (section 3.5). [B] Renaturation efficiencies were determined by UV/VIS spectroscopy (section 3.6). [C] Product yields were determined by UV/VIS spectroscopy after chromatographic purification or reconstitution of lyophilized targets (section 3.7). The product yield per liter fermentation broth was calculated retroactively. Purity of targets were either determined by [D] RP-HPLC or estimated from a [E] Coomassie-stained SDS-PAGE gel using BSA protein standard.

4.7 Identification of the oxidative state

Purified hEGF, VHH, scFv clone F2C and DS-THA were further analyzed by RP-UPLC-MS to confirm their identity and to evaluate the oxidative state of the products. RP-UPLC-MS analyses were performed as described in section 3.8. The UPLC chromatograms and mass spectra of each target are presented in Figure 19.

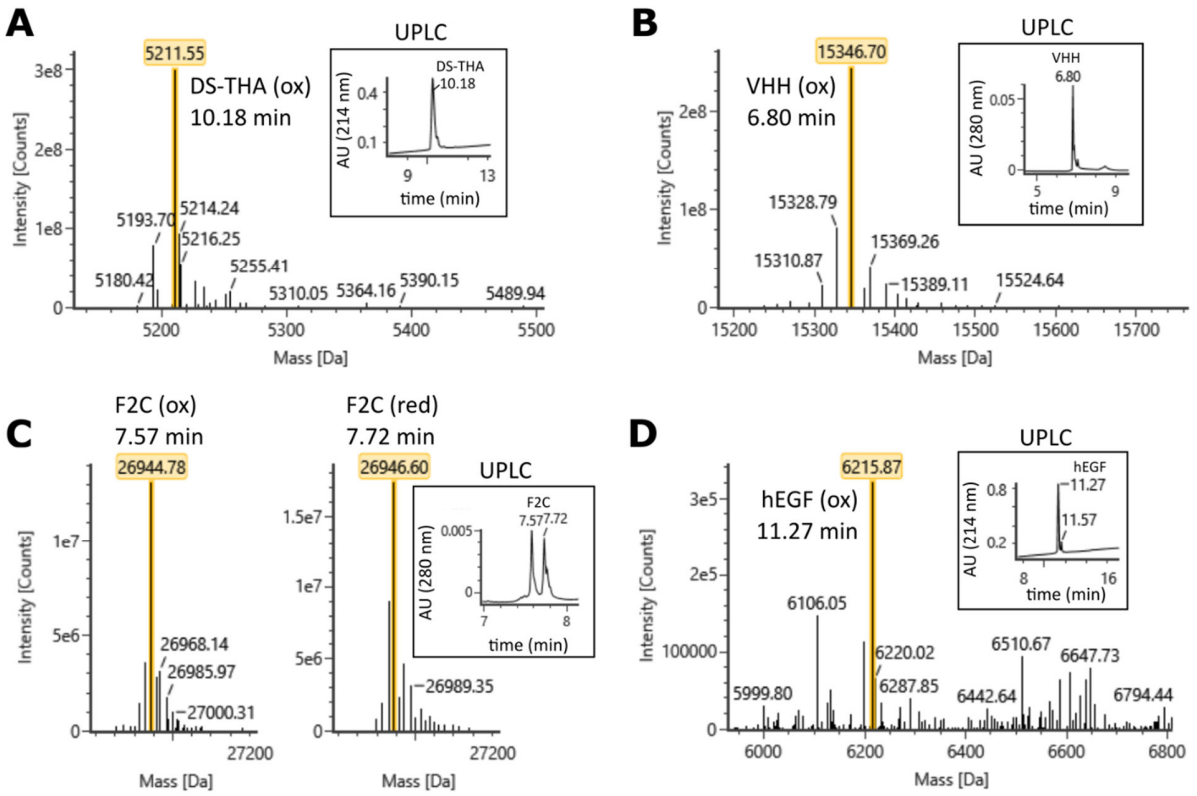

Figure 19 | Oxidative state analysis of purified DS-THA, VHH, scFv clone F2C and hEGF

RP-UPLC-MS analyses of purified **(A)** DS-THA, **(B)** VHH, **(C)** scFv clone F2C and **(D)** hEGF were performed as described in section 3.8. In the UPLC chromatograms, the target retention times and wavelengths of UV absorption are indicated. Molecular mass analyses of the elution signals were performed by ESI time-of-flight (TOF) mass spectrometry (ACQUITY RDa, Waters). Insight into the oxidative state (red, reduced or ox, oxidized) of the purified targets were provided. The molecular masses of each target are highlighted in yellow.

The observed molecular masses of VHH and DS-THA corresponded to the expected MWs when oxidized which confirmed the presence of an intramolecular disulfide bond (Figure 19A–B). For scFv clone F2C, a difference of -2 Da compared to the theoretical mass of a completely reduced form was observed which may result from the formation of intermediate isomers (Figure 19C). Treatment of scFv clone F2C with the oxidizing reagent Copper (II)-phenanthroline (Kobashi, 1968) yielded the fully oxidized mass (Supplementary Material, Figure S 8). The growth factor hEGF contains six cysteine residues and RP-UPLC-MS analyses revealed the presence of fully oxidized protein (Figure 19D). Detailed information on the expected and observed MWs of each target is shown in Table 8.

Table 8 | Analysis of the oxidative state of purified DS-THA, VHH, scFv clone F2C and hEGF

Compound	Number of expected disulfide bonds (Cys – Cys)	MW (Da)		
		Expected		Observed
		reduced	oxidized	
DS-THA	1	5,213.16	5,211.15	5,211.55
VHH	1	15,348.49	15,346.47	15,346.70
scFv clone F2C	2	26,947.17	26,945.15	26,944.78 / 26,946.60
hEGF	3	6,221.98	6,215.98	6,215.87

4.8 Analysis of the biological function of DS-THA, VHH, scFv clone F2C, hEGF

Different assays were performed to assess the biological functionality of purified targets (section 3.9.1). The antimicrobial activity of DS-THA against *E. coli* and *B. subtilis* was analyzed in a MIC assay. The MIC value was determined to be 1.6 µM for both species (Supplementary Material, Figure S 9). Furthermore, the binding of a single chain antibody fragment VHH to red fluorescent protein mCherry (Wang et al., 2021) was analyzed by SEC. Indeed, after co-incubation of VHH and mCherry the formation of VHH-mCherry heterodimers were observed which confirmed the functional fold of the purified VHH (Supplementary Material, Figure S 10). The biological functionality of the recombinantly purified scFv clone F2C was analyzed by epifluorescence imaging operated by NanoTag Biotechnologies GmbH. The scFv clone F2C was coupled to an Atto 647 NHS ester dye and binding to α-tubulin present in COS-7 cells was confirmed by imaging which confirmed the functionality of the purified antibody fragment (Supplementary Material, Figure S 11). The hEGF activity was evaluated in a cell-based EGFR human receptor tyrosine kinase (RTK) assay performed by Eurofins DiscoverX Corporation. The data revealed that the potency (EC_{50}) and efficacy (E_{max}) of purified hEGF were in line with Eurofin's internal EGF control compound which emphasizes that the produced hEGF is biologically active (Table 9, Supplementary Material, Figure S 12).

Table 9 | Results of hEGF activity assay

Assay type	Target	Purified hEGF	EGF control compound of Eurofins DiscoverX Corporation
Cell-based RTK assay (Agonist binding)	ErbB1	EC_{50} 0.70 ng/mL E_{max} 107.13	EC_{50} 0.54 ng/mL E_{max} 101.05

4.9 Construction of the 36-mer phagemid library

The following section of this dissertation focuses on the design of bifunctional peptides that may serve as foundation for the functionalization of Resomer® implant coatings. The resulting peptide-peptide conjugates shall exhibit antimicrobial properties against a wide range of pathogens and adhesive properties against the biopolymer Resomer® for immobilization. To identify Resomer®-binding peptides (RBPs) it was an integral part of this work to construct phagemid libraries displaying randomized peptides on the surface. These phagemid libraries can be employed to identify RBPs in biopanning experiments. In previous studies, phagemid libraries displaying 24 aa long peptides (24-mer library) were constructed by Numaferm GmbH (unpublished data). Therefore, the focus of this dissertation was set on to construct phagemid libraries presenting 36 aa long peptides (36-mer library). A general overview of all working steps involved to construct the 36-mer library is illustrated in Figure 20. Detailed insight into the process of library construction can be found in the sections 4.9.1 and 4.9.2.

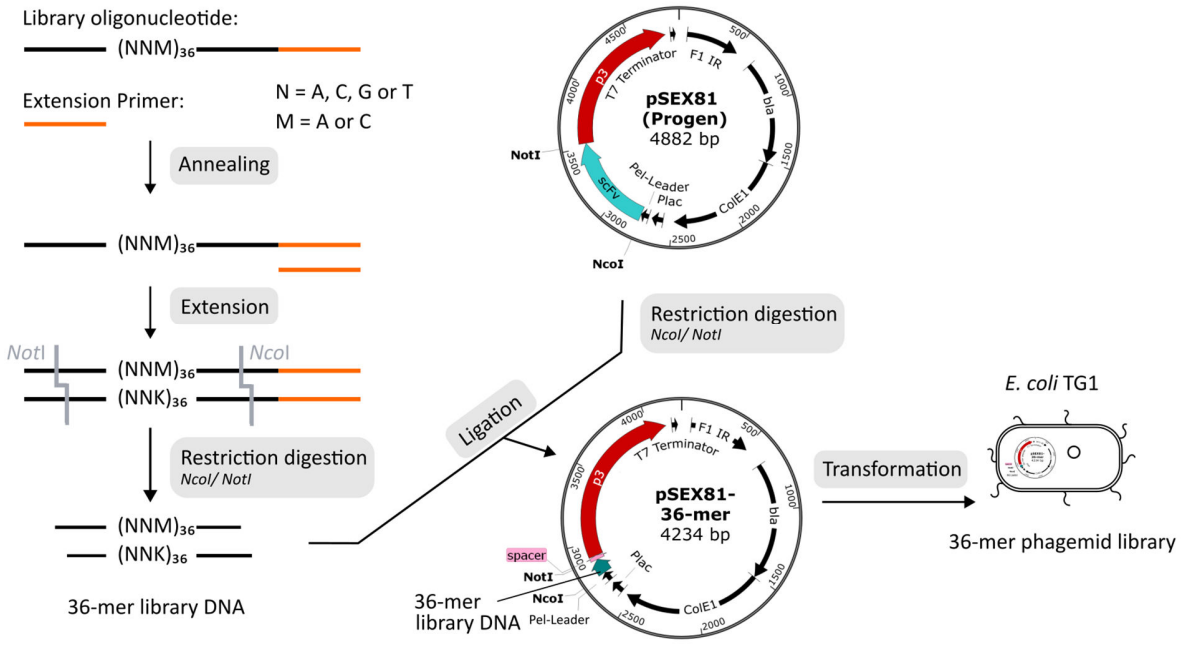

Figure 20 | General overview of working steps required to construct the 36-mer library

The scFv gene cassette was removed from original pSEX81 phagemid (Progen) by *Nco*I and *Not*I restriction digestion. Each single-stranded library oligonucleotide contains 36 degenerate NNM (N = A, C, G or T, M = A or C) codons encoding unique 36 aa long peptides. The extension primer was annealed to the library oligonucleotide and Klenow fill-in reaction lead to the formation of the double stranded 36-mer library DNA which was cloned into the prepared pSEX81 phagemid using *NcoI* and *NotI* restriction sites. Electrocompetent amber suppressor (supE) *E. coli* TG1 cells were transformed with recombinant pSEX81-36-mer phagemids to construct the 36-mer phagemid library.

4.9.1 Preparation of pSEX81 and 36-mer library DNA

The pSEX81 phagemid was used to produce randomized peptides in fusion to the phage coat protein p3 for display on the surface of M13 bacteriophages. The 36-mer library DNA (section 3.10.2) obtained by Klenow-fill in reaction was cloned into pSEX81 phagemids (section 3.10.1) by using the restriction sites *NcoI* and *NotI* (section 3.10.3). The fragment sizes of *Nco*I/*Not*I digested pSEX81 phagemids and 36-mer library DNA were confirmed by agarose gel electrophoresis and PAGE, respectively (Figure 21A–B). The recombinant pSEX81-36-mer phagemids after ligation were analyzed by agarose gel electrophoresis (Figure 21C).

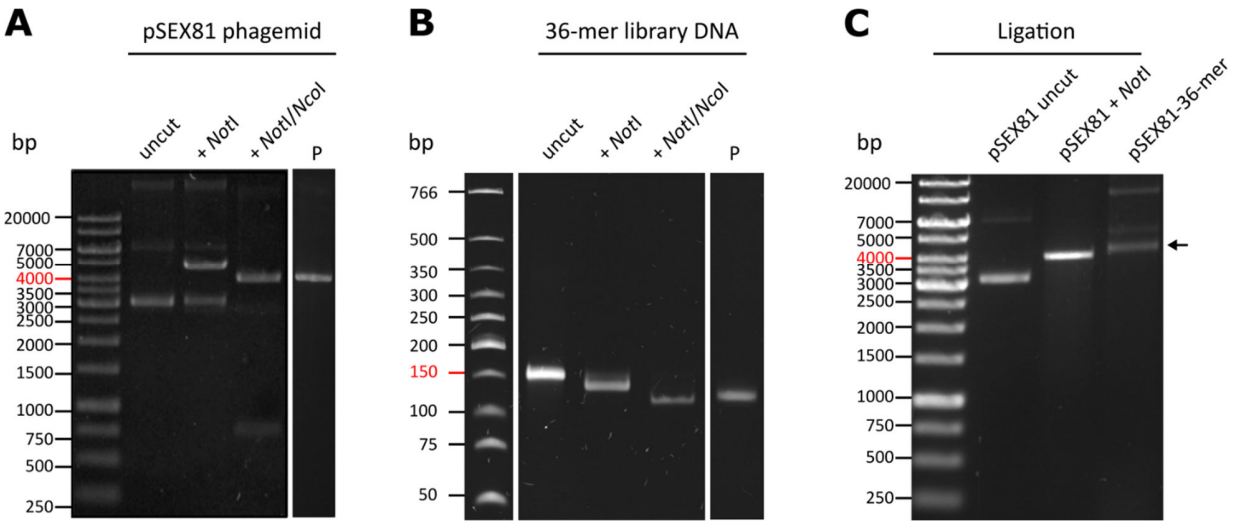

Figure 21 | Construction of recombinant pSEX81-36-mer phagemids

(A) Agarose gel electrophoresis of pSEX81 phagemids digested by *Not*I (4882 bp) and *Not*I/*Nco*I (4114 bp). *Not*I/*Nco*I digested pSEX81 fragments were isolated from the scFv gene cassette (768 bp) by agarose gel extraction and purified (P) as described in section 3.10.1. **(B)** PAGE of 36-mer library DNA (156 bp) digested by *Not*I (140 bp) and *Not*I/*Nco*I (116 bp). Target library DNA fragments were isolated and purified (P) as described in section 3.10.2. **(C)** Ligation of *Not*I/*Nco*I treated pSEX81 and 36-mer library DNA. The 36-mer library DNA was added in 5-fold molar excess to the pSEX81 fragment in presence of T4 DNA ligase. Ligation conditions are described in section 3.10.3. The arrow indicates the location of resulting pSEX81-36-mer phagemid (4234 bp).

The desired *Not*I/*Nco*I digested pSEX81 phagemids and 36-mer library DNA were obtained in high purities, respectively (Figure 21A–B). Ligation of both fragments led to the presence of a dominant band slightly higher than linearized pSEX81 fragment which corresponds to the correct size of recombinant pSEX81-36-mer phagemid (4234 bp) (Figure 21C). However, the presence of bands at ~ 5000 bp or ~ 10.000 bp indicate the formation of high molecular weight DNA products during ligation reaction.

Electrocompetent *E. coli* TG1 cells were transformed with recombinant pSEX81-36-mer phagemids to determine the initial transformation efficiency and to analyze the resulting library clones. The transformation efficiencies obtained with self-prepared electrocompetent *E. coli* TG1 cells were quite low but were substantially increased up to 7-fold by using commercially available ones (Supplementary Material, Figure S 13A). Moreover, diverse ratios of vector insertion (1:5, 1:10, 1:15), varying amounts of transformed DNA (100–300 ng), alterations in ligation duration (15, 30 or 60 min) and ligation temperatures (4, 16, 25 or 30 °C) were tested to enhance the transformation efficiency. However, only slight improvements were achieved (Supplementary Material, Figure S 13C–E). Purification of the ligated DNA product prior to electro-transformation was found to increase the transformation efficiency by 5-fold (Supplementary Material, Figure S 13B). In summary, the optimized ligation process involved applying a vector to insert ratio of 1:5 and incubation of the ligation reaction at 25 °C for 30 min. The ligated DNA product was purified prior to electro-transformation and roughly 200 ng of DNA was transformed in electrocompetent *E. coli* TG1 cells (Lucigen). Under optimized conditions the transformation efficiency was successfully improved from about 10^5 cfu/µg to 10^7-10^8 cfu/µg. Ten randomly picked library clones were analyzed by DNA sequencing (Microsynth) and correct insertions of 36-mer library DNA in pSEX81 phagemids were confirmed.

4.9.2 Comparison of the 24- and 36-mer library production

Production of the 36-mer library at large scales was conducted in two steps (section 3.10.3). Firstly, *Not*I/*Nco*I digested pSEX81 phagemids were ligated with 36-mer library DNA in a large scale preparation. The ligated DNA products were purified and correct sizes of pSEX81-36-mer phagemids were confirmed by agarose gel electrophoresis (Figure 21C). In the second step, purified pSEX81-36-mer phagemids were transformed in electrocompetent *E. coli* TG1 cells (Lucigen). In total, 80 transformation reactions were performed, and the library clones were grown on selective LB agar plates. The key characteristics of the 24-mer (constructed by Numaferm GmbH) and 36-mer library productions are summarized in Table 10. All colonies from the agar plates were scraped off, pooled, and prepared for storage at -80°C (section 3.11).

Table 10 | Key characteristics of 24-mer and 36-mer library production

	24-mer library [A]	36-mer library
number of performed transformation reactions	52	80
transformed DNA amount	200 – 500 ng	200 ng
average transformation efficiency	1.2 x10^8 cfu/µg	7 x10^7 cfu/µg [B]
average number of total library clones	4.6 x10^7 cfu	2 x10^7 cfu [C]
theoretical library diversity	2.4 x10^9 library clones	1.6 x10^9 library clones [D]

[A] Constructed by Numaferm GmbH. [B] Average transformation efficiency determined from 27 of 80 transformation reactions. [C] Average number of library clones determined by colony counting of transformation plates. [D] Average number of library clones multiplied by the number of transformation reactions.

In theory, the bacterial 36-mer library consists of 1.6 x10^9 unique clones derived from 80 transformation reactions. During library production average transformation efficiencies of 7 x10^7 cfu/µg were achieved, slightly lower compared to values obtained by 24-mer library production (Table 10, 1.2 x10^8 cfu/µg). In case of the 36-mer library more transformation reactions were required to achieve a library diversity of $\geq 10^9$. It should be mentioned that during the 24-mer library production varying DNA amounts (200–500 ng) were employed for electro-transformation which may strongly affect the number of library clones and the transformation efficiency. For the production of the 36-mer library 200 ng DNA was constantly applied, therefore a direct comparison of both library productions was not possible. The theoretical diversity of the bacterial 24-mer library was estimated to consist of 2.4 x10^9 unique clones.

4.9.3 Phagemid library Analysis

4.9.3.1 Verification of DNA sequences and library diversity

To obtain insight into the actual library diversity, so the proportion of library clones containing correctly inserted peptide sequences, roughly 60 clones of each library were randomly picked and analyzed by DNA sequencing (section 3.10.4). In general, only library clones containing in-frame peptide inserts are expected to produce functional phagemid particles displaying randomized peptides on the phage's surface (Sloth et al., 2022). DNA sequence analyses of clones derived from the 24-mer library indicated that 47 of 60 clones (78.3 %) harbored correct 24-mer peptide inserts. One clone contained a 23-mer peptide insert in frame with the p3 coat protein (1.7 %) probably a resulted of codon deletion. (Figure 22A). Taking both values together, the percentage of clones containing in-frame peptide inserts (and expected to form functional phagemid particles) was 80 %. Thus, the 24-mer library was expected to yield 1.9 x10^9 functional clones (80 % of 2.4 x10^9) also referred to as the actual library diversity. DNA sequence analyses of clones derived from the

36-mer library suggested that 44 of 64 picked clones (68.8 %) contained correct 36-mer peptides inserts. In addition, 4 clones (6.2 %) harbored truncated but in-frame peptide inserts (33 or 35 aa). Consequently, the 36-mer library was calculated to consist of functional 1.2 x10^9 clones (75 % of 1.6 x10^9) encoding unique peptide sequences (Figure 22B). The percentage of incorrect clones, so those which harbored frameshifts due to e.g. nucleotide deletions or multiple peptide inserts totaled about 20 % in both libraries. The proportion of pSEX81 wild type contaminants, so phagemids still containing the original scFv gene cassette (Figure 11A) was 4.7 % in the 36-mer library further decreasing the actual library diversity. For the 24-mer library no pSEX81 wild type contamination was observed. The proportions of correct and incorrect clones found in the 24-mer and 36-mer library are summarized in pie charts illustrated in Figure 22. Furthermore, the amino acid sequences of the correct peptide inserts are listed in Supplementary Material, Table S 2 and Table S 3.

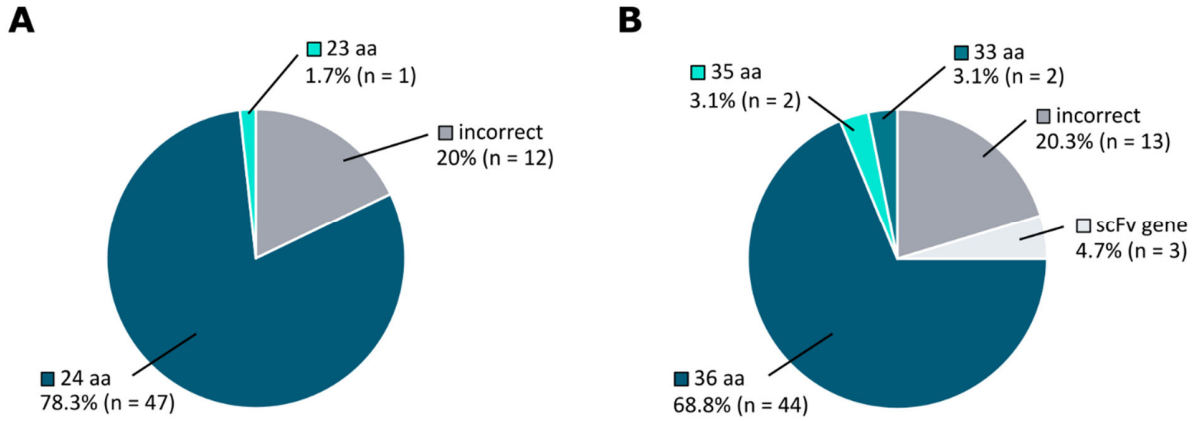

Figure 22 | DNA sequencing analyses of library clones derived from the 24- and 36-mer library

Proportions of correct and incorrect clones found in the **(A)** 24- and **(B)** 36-mer library are illustrated in pie charts. Correct clones represent peptides which were cloned in-frame in pSEX81 phagemids and incorrect clones harbored frameshifts (resulted from nucleotide deletions or multiple peptide inserts). The proportion of pSEX81wild type contaminants (scFv gene) is also indicated. The 24-mer library analysis involved 60 picked clones, while the 36-mer library analysis included 64 chosen ones. The percentage of each proportion and total number of clones are indicated (n).

4.9.3.2 Analysis of the amino acid composition

To obtain insight into the sequence diversity, i.e. the discrepancy between expected and observed amino acid frequency in both libraries, 48 correctly inserted peptide sequences (Supplementary Material, Table S 2 and Table S 3) were analyzed regarding their amino acid composition (section 3.10.4). Ideally, the observed amino acid frequencies should be close to the expected ones. Deviations from it indicate under or

overrepresentation of certain amino acids in the phagemid library. Analyses of amino acid frequencies of peptide inserts derived from the 24-mer and 36-mer library are presented in Figure 23.

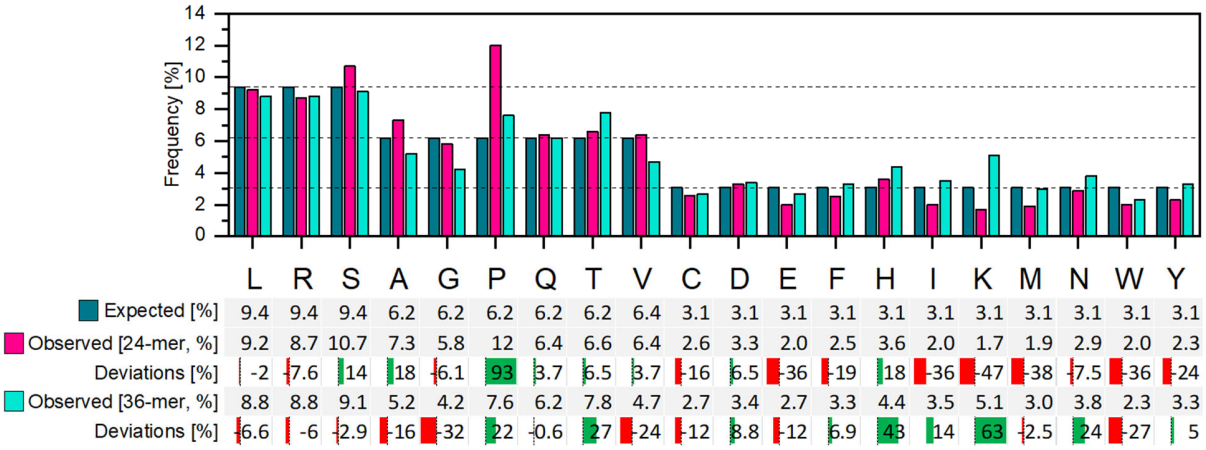

	L	R	S	A	G	P	Q	T	V	C	D	E	F	H	I	K	M	N	W	Y
Expected [%]	9.4	9.4	9.4	6.2	6.2	6.2	6.2	6.2	6.4	3.1	3.1	3.1	3.1	3.1	3.1	3.1	3.1	3.1	3.1	3.1
Observed [24-mer, %]	9.2	8.7	10.7	7.3	5.8	12	6.4	6.6	6.4	2.6	3.3	2.0	2.5	3.6	2.0	1.7	1.9	2.9	2.0	2.3
Deviations [%]	-2	-7.6	14	18	-6.1	93	3.7	6.5	3.7	-16	6.5	-36	-19	18	-36	-47	-38	-7.5	-36	-24
Observed [36-mer, %]	8.8	8.8	9.1	5.2	4.2	7.6	6.2	7.8	4.7	2.7	3.4	2.7	3.3	4.4	3.5	5.1	3.0	3.8	2.3	3.3
Deviations [%]	-6.6	-6	-2.9	-16	-32	22	-0.6	27	-24	-12	8.8	-12	6.9	43	14	63	-2.5	24	-27	5

Figure 23 | Analyses of the amino acid frequency of peptide sequences of the 24- and 36-mer library

Correctly inserted peptide inserts found in the 24-mer and 36-mer library were analyzed for their amino acid frequencies (Supplementary Material, Table S 2 and Table S 3). In total, 48 peptide sequences were analyzed, respectively. The table below the bar graph provides information on the observed, expected amino acid frequencies and the deviation of both values in % which results in under (**red**) or overrepresentation (**green**) of certain amino acids.

The amino acid frequencies observed for most amino acids were found to be close to the expected values like in case of L, R, S, A, Q, C, D, or F. The deviations ranged between 2–19 % indicating an overall fair representation of amino acids in line with the NNK randomization strategy. However, in the 24-mer library P was considerably overrepresented (93 %, roughly twice the expected value) which was not as pronounced in the 36-mer library (22 %, about 1.2 times the expected value). Thus, other residues were underrepresented including E, I, K, M, W and Y which show deviations ranging from 24 to 47 %. Interestingly, in the 36-mer library K was slightly overrepresented K (63 %) but depleted in the 24-mer library (47 %). Furthermore, the residues T, H and N were slightly overrepresented in the 36-mer library (24–47 %).

4.10 Phagemid particle production

To produce phagemid particles the bacterial 24- and 36-mer libraries were grown from frozen cryo cultures, respectively (section 4.10). Phagemid particles were rescued by M13K07Δp3 hyperphage superinfection to promote multivalent display of randomized peptides (section 3.11). After production in *E. coli* TG1 host cells the phagemid particles were harvested and purified by PEG/NaCl precipitation. Finally, the titers of the phagemid particles in the solution were estimated by phagemid titration assay (section 3.15.1) and

UV/VIS spectroscopy (section 3.15.2), respectively. The phagemid particle titers in the solutions are summarized in Table 11.

Table 11 | Phagemid particle titers obtained by 24- and 36-mer library preparation

	Titer determination		Ratio
	UV/VIS spectroscopy [A]	Phagemid titration assay	(titer $_{UV/VIS}$ / titer$_{titration}$)
24-mer library	1.4 x10^{12} phage/mL	5.6 x10^{11} cfu/mL	2.5
36-mer library	9.1 x10^{12} phage/mL	8 x10^{11} cfu/mL	11.4

[A] phage/mL = OD_{260} x dilution factor x 22.14 x10^{10} (Lee et al., 2007)

Notably, the phagemid particle titers obtained by UV/VIS spectroscopy were higher than the titers determined by phagemid titration assay (~ 2.5 to 11.4-fold). The phagemid particle solutions may contain contaminants which influenced the UV absorption of the sample leading to overestimation of the titer. Phagemid particle titers obtained by the titration assay were considered to be more reliable as this method provides insight into the actual number of functional and infectious phagemid particles. Therefore, these titers were considered for calculation of the input phagemid particle amount for forthcoming biopanning experiments. The phagemid particle solutions were used to infect mid-log phase grown *E. coli* TG1 cells. DNA sequence analyses of ten randomly picked library clones confirmed the presence of correct peptide inserts. Biopanning is a time-consuming process including repetitive and tedious manual procedures to select for strong binding peptides. Initially, it was planned to use both phagemid libraries to screen for RBPs, but due to lack of time, biopanning was only performed with the 24-mer library. Nevertheless, the functionality of the 36-mer library was evaluated by biopanning against streptavidin-coated microtiter plate wells (section 4.12).

4.11 Biopanning of 24-mer library against Resomer® surfaces

The 24-mer library was screened against Resomer® surfaces in biopanning experiments to identify RBPs (section 3.13). Altogether, four biopanning rounds were performed and the titers of phagemid particles obtained after each elution step were quantified by phagemid titration assay (section 3.15.1). An overview of the number of phagemid particles used (input) in each biopanning round, the number of phagemid particles obtained after each elution step (output) and information on which helper phage was employed for phagemid particle rescue is given in Table 12.

Table 12 | Enrichment of phagemid particles during four biopanning rounds

Round	Input [A] (phagemid particles)	Output [B] (phagemid particle)	Helper phage variant
1	2.4 x10^{11}	1.3 x10^{4}	M13K07Δp3 hyperphage
2	2.4 x10^{11}	2.4 x10^{4}	M13K07Δp3 hyperphage
3	2.4 x10^{11}	3.3 x10^{6}	M13K07 helper phage
4	2.4 x10^{11}	3.2 x10^{4}	–

[A] Number of input phagemid particles used for selection. [B] Number of phagemid particles obtained after elution step determined by phagemid titration assay (section 3.15.1).

The number of phagemid particles employed in each biopanning round was 2.4 x10^{11} constantly. The numbers of phagemid particles obtained after the first two rounds of selection were significantly decreased (1.3 x10^{4} and 2.4 x10^{4} phagemid particles) due to loss of many non- or weak binders during the biopanning procedure and low enrichment levels of binder candidates. The phagemid particles were rescued by M13K07Δp3 hyperphage superinfection, respectively, to promote multivalent display of peptides and to reduce the risk of losing promising candidates represented by low copy numbers. After the 3rd round, a slight increase of output phagemid particles (about 3.3 x10^{6} phagemid particles) indicate slow enrichment of binder candidates. The stringency of selection was increased in the final round by employing M13K07 helper phages for phagemid particle rescue to promote monovalent display and select for phagemid particles binding with high affinity instead of high avidity effects. As expected, the number of recovered phagemid particles decreased in the final round since weak binders were ejected (3.2 x10^{4} phagemid particles). After the 3rd and 4th biopanning round about 20 library clones obtained after re-infection of *E. coli* TG1 cells with respective elution fractions were analyzed by DNA sequencing to evaluate the enrichment of potential RBP candidates (Figure 24).

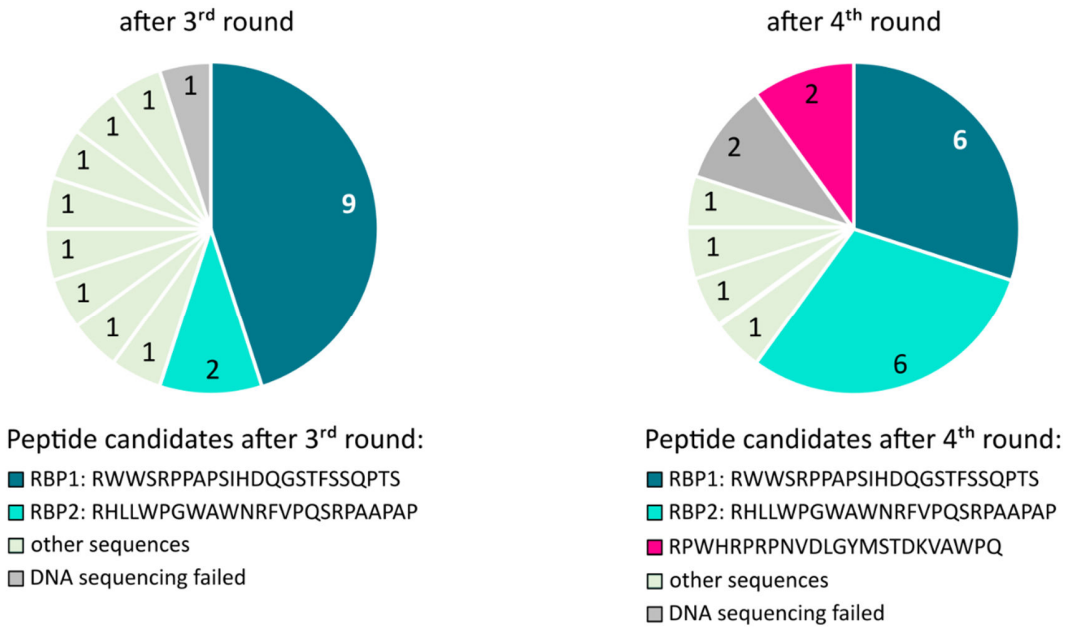

Figure 24 | Enriched peptide sequences obtained after the 3rd and 4th biopanning round

Numbers of found peptide sequence after the 3rd and 4th biopanning round are indicated.

Following the 3rd biopanning round, nine of 20 clones exhibited an identical motif for the peptide sequence referred to as RBP1 which indicated that this peptide binds to Resomer®. Furthermore, the peptide motif RBP2 was detected twice, and the remaining sequences were found only once, respectively. In the 4th biopanning round, more stringent conditions were applied when M13K07 helper phages were employed for phagemid particle rescue. Analyses of the DNA sequence of library clones obtained after the final selection revealed that both peptide motifs RBP1 and RBP2 were still dominantly present (six of 20 clones, respectively). One peptide motif not observed before was found twice. A summary of the amino acid sequences for the enriched peptide sequences can be found in Supplementary Material, Table S 4 and Table S 5. Enrichment of RBP1 and RBP2 during biopanning point towards high affinity binding to Resomer®. Therefore, lyophilized samples for both peptides were ordered by ProteoGenix to analyze their binding capabilities to Resomer® exclusively of the phagemid particle body.

4.12 Biopanning of 36-mer library against streptavidin

In scope of this dissertation the 36-mer library was not screened against Resomer® but the functionality of the phagemid library was analyzed anyway by biopanning employing streptavidin-coated microtiter plate wells. Previous studies reported that that biopanning of peptide libraries against the molecular target streptavidin led to phages bearing HPQ and/or HPM motifs in enriched peptide sequences (Devlin et al., 1990, Krumpe et al., 2006). Indeed, it was confirmed that HPQ is a functional mimicry of biotin recognized by the streptavidin binding pocket (Weber et al., 1992). To test the functionality of the 36-mer library,

microtiter plate wells were coated with streptavidin (section 3.14) and the 36-mer phagemid library (section 4.9.2) was added for binding. After rigorous washing, potentially bound phagemid particles were competitively eluted from the wells using biotin. Eluted phagemid particles were rescued by helper phage superinfection and the next biopanning round was performed. Two biopanning rounds were conducted *E. coli* TG1 cells were infected with the final elution pool. About 15 library clones were analyzed by DNA sequencing to look for HPM and/or HPQ motifs in enriched peptide sequences. The amino acid sequences, lengths and number of HPM and HPQ hits are shown in Table 13.

Table 13 | Peptide sequences obtained after the 2nd biopanning round against streptavidin

Nr.	Peptide sequence	Length (aa)	HPM	HPQ
1	EYPDRGEEMGDHPQFAAAHNKPR*RPPNHRPHGQAQ	36	0	1
2	PWTWVRFTAPKPQTGR*EVLIQAA*NPETLARVRAN	36	0	0
3	TRDASLRSTFGSNPWEYE*LSDHP*NYTNNVTDM	34	0	1
4	LTQAQSMSRANAVTASNQR*NLPSK*TGLSHT*VSC	36	0	0
5	NQPPRRT*DPWTAGPSYFLAPFHGGFANGPESWRPN	36	0	0
6	PPQDPTMNVGLHDLFPHNHPQNPSNGTRYDSWT	33	0	1
7	RSAAAHGTPDGV*SNRRAPYYPMSWPWMTFEHPQNP	36	0	1
8	HK*LQLAQLPTQFDIDWLNFDHPQAGSNSSKHPK*T	36	0	1
9	ILQTLQI*EIWWWRFHPQGIQAEPSAGHSF*DIPSQ	36	0	1
10	SCCPLAKYSLQMTSHFFELSPQHHWYMHTKHP*GDD	36	0	1
11	LPALERATSLSP*TRDGHETALTAIPRWTWNHPMFQ	36	1	0
12	ER*FAHHMPWRMEHSGICHPQGDTVCYRTERTTTML	36	0	1
13	HPLPSYRPEAQFETWHPMAPHHPMQTLRTRSQ*PSV	36	1	0
14	LGPLERTKWQSNPQIYHP*GDRLEQRCSPKDKICEN	36	0	1
15	TLM*LTFAPLISNHP*ADHCSPKTCLDRLGHFPPNS	36	0	1

*Glutamine (Q) residues encoded by TAG stop codons. HPQ motifs are highlighted in red and HPM motifs in blue.

The data revealed that 12 of 15 identified peptide sequences (80 %) harbored the streptavidin-binding motifs HPQ or HPM (Table 13) which demonstrated that biopanning worked as expected. The number of HPQ-containing peptides is obviously higher than HPM-containing peptides (~ 66 % vs. 13 %) which suggest that HPQ may be the stronger binding motif. In control biopanning experiments employing microtiter plate wells without streptavidin coating none of the obtained library clones show, as expected, the HPQ or HPM

motif (Supplementary Material, Table S 6). The biological functionality of the 36-mer library was confirmed by this experiment and showcasing its immense potential for future applications.

4.13 Functional analysis of RBP1 and RBP2

In a pulldown assay the binding capabilities of RBP1 and RBP2 to Resomer® was tested without attachment to the phagemid particle (section 3.19.1). Lyophilized RBP1 and RBP2 were reconstituted in Tris-HCl-based buffer and incubated with Resomer® beads, respectively. Excess of peptides were removed by repetitive washing and potentially bound peptides were eluted from Resomer® beads by pH shift. The bifunctional peptide DS-THA, which seem to adhere on hydrophobic surfaces in literature (Schwinges et al., 2019) and previously produced by the Numaswitch™ technology (section 4.6) was included in this study. All fractions obtained during the pulldown assay were analyzed by Tricine-SDS-PAGE, respectively (Figure 25).

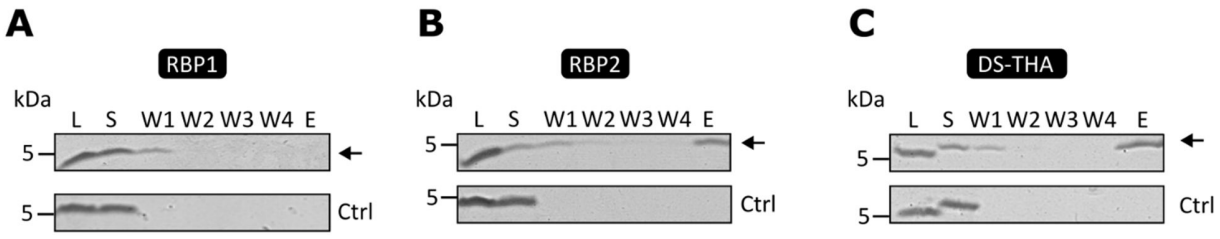

Figure 25 | Analysis of RBP1, RBP2 and DS-THA binding to Resomer® beads

Coomassie-stained Tricine-SDS-PAGE gel analyses of fractions obtained by pulldown assays performed with RBP1, RBP2 and DS-THA (section 3.19.1). Lyophilized peptides were resuspended in Tris-HCl-based buffer (L, load) and incubated in presence of Resomer® beads. Supernatants (S) were removed, and the beads were washed four times (W1–4) to get rid of peptide excess. Bound peptides on Resomer® beads were eluted by pH shift (E). The arrows indicate the location of peptide targets after elution. To exclude the possibility that emerging protein bands in the elution fraction derived from unspecific binding to the tubes the pulldown assay was simultaneously performed without Resomer® beads (Ctrl, control).

The absence of a protein band in the elution fraction as observed for RBP1 (Figure 25A) indicate that no interaction with Resomer® beads occurred either because it actually does not bind to Resomer® or because of unfavorable binding conditions. However, for RBP2 a clear protein band at the expected location indicated that it binds to Resomer® (Figure 25B). As expected, in the control experiment no band in the elution fraction was observed which strongly confirmed that RBP2 specifically binds to Resomer® and not to the tube (Figure 25B). Remarkably, DS-THA was also found to bind to Resomer® as indicated by the protein band in the elution fraction (Figure 25C). Another heptapeptide (QLMHDYR) reported to recognize the α form of poly-L-lactic acid (PLLA) crystalline films (Matsuno et al., 2008) was included in this study but no interaction with Resomer® was observed (data not shown). In summary, RBP2 identified by biopanning seemed to exhibit adhesive properties against Resomer®. In summary, RBP2 identified through

biopanning showed adhesive properties against Resomer®, confirming the functionality of the constructed 24-mer library.

4.14 Design, expression, renaturation and cleavage of bifunctional peptides

To design bifunctional peptides, RBP2 was fused to three different AMPs reported to exhibit broad antimicrobial activity against a wide range of different pathogens. In between the peptide-peptide fusions a short G-linker (GGGGS) was included which connected both functional domains with each other and increased the flexibility of the molecule. The selected AMPs were human beta-defensin-3 (HBD3), human histatin-3 (HTN3) and dermcidin-1L (DCD-1L). As it is unclear which domains of the AMPs mediate antimicrobial activity, RBP2 was C- and N-terminally fused to the AMPs, respectively, resulting in altogether six different constructs (Table 14).

Table 14 | Overview of bifunctional peptide constructs

Bifunctional peptide candidate	Amino acid sequence (one letter code)	MW (kDa)
RBP2-HBD3	RHLLWPGWAWNRFVPQSRPAAPAPGGGGSGIINTLQKYYC RVRGGRCAVLSCLPKEEQIGKCSTRGRKCCRRKK	8.3
RBP2-HTN3	RHLLWPGWAWNRFVPQSRPAAPAPGGGGSDSHAKRHHGY KRKFHEKHHSHRGYRSNYLYDN	7.2
RBP2-DCD-1L	RHLLWPGWAWNRFVPQSRPAAPAPGGGGSSSLLEKGLDGA KKAVGGLGKLGKDAVEDLESVGKGAVHDVKDVLDSVL	7.9
HBD3-RBP2	GIINTLQKYYCRVRGGRCAVLSCLPKEEQIGKCSTRGRKCC RRKKGGGGSRHLLWPGWAWNRFVPQSRPAAPAP	8.3
HTN3-RBP2	DSHAKRHHGYKRKFHEKHHSHRGYRSNYLYDNGGGGSR HLLWPGWAWNRFVPQSRPAAPAP	7.2
DCD-1L-RBP2	SSLLEKGLDGAKKAVGGLGKLGKDAVEDLESVGKGAVHD VKDVLDSVLGGGGSRHLLWPGWAWNRFVPQSRPAAPAP	7.9

Underlined: GS-linker

The DNA sequences encoding six bifunctional peptide candidates (Table 14) were cloned in pBAD plasmids in fusion to N-terminal Switchtags. The amino sequences of the resulting Switchtag fusions are shown in Supplementary Material, Table S 7. The Switchtag fusions were produced as IBs in *E. coli* BL21, extracted and solubilized in 6 M GuHCl. Refolding of Switchtag fusions was performed in Ca^{2+}-containing buffers and TEV protease was added to cleave off the Switchtags from target peptides (section 3.16 and 3.17).

Intracellular production of Switchtag IBs, the solubilization, renaturation and cleavage reactions were analyzed by SDS-PAGE and/or RP-HPLC (Figure 26).

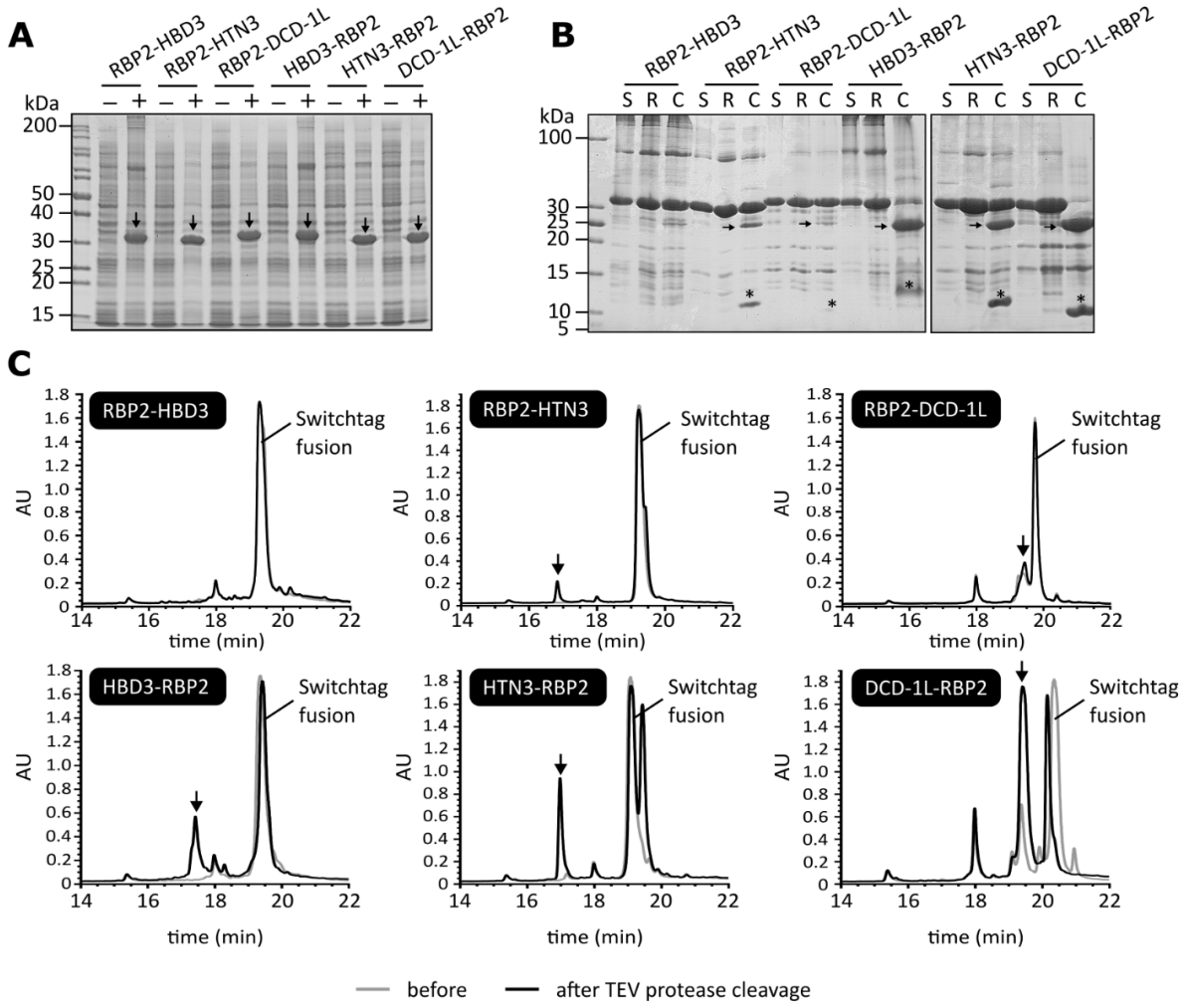

Figure 26 | Expression, Solubilization, Renaturation and Cleavage of Switchtag fusions

(A) Coomassie-stained SDS-PAGE gels showing *E. coli* cells before (–) and after (+) expression induction. SDS-PAGE samples of cells were prepared as described in section 3.1. The arrows indicate the location of produced Switchtag fusions (Switchtag-RBP2-HBD3 or Switchtag-HBD3-RBP2, 33.2 kDa; Switchtag-RBP2-HTN3 or Switchtag-HTN3-RBP2, 32.1 kDa; Switchtag-RBP2-DCD-1L or Switchtag-DCD-1L-RBP2, 32.9 kDa). **(B)** SDS-PAGE analysis of solubilized (S), renaturated (R) and TEV protease cleaved (C) Switchtag fusions. Arrows indicate the location of Switchtag backbones after cleavage. The released target peptides are highlighted (*). **(C)** RP-HPLC analysis of renaturation and cleavage reactions of all six Switchtag fusions. Shown are the chromatograms monitored at 205 nm before (grey) and after TEV protease cleavage (black) (section 3.17).

Expression analyses show that all six Switchtag fusion proteins were produced as IBs at high levels (Figure 26A). The solubilized IBs were efficiently refolded (about 75−100 %) determined by UV/VIS spectroscopy, but also confirmed by SDS-PAGE analyses (Figure 26B). Cleavage of Switchtags from target peptides after TEV protease treatment occurred with varying efficiencies. Notably, for Switchtag-RBP2-HBD3, Switchtag-RBP2-HTN3 and Switchtag-RBP2-DCD-1L only low cleavage efficiencies were observed (0−5 %) but for Switchtag-HBD3-RBP2, Switchtag-HTN3-RBP2 and Switchtag-DCD-1L-RBP2 the efficiencies ranged from 50−90 %. (Figure 26B). Low cleavage efficiencies observed were most likely due to the RBP2 sequence immediately following the TEV protease cleavage site. As RBP2 begins with a R which fills in the P1' position of the TEV cleavage site efficient peptide bond hydrolyses was hampered (see discussion, section 5.3). Furthermore, target peptide releases after TEV protease cleavage were confirmed by RP-HPLC analyses (Figure 26C). In line with observations from SDS-PAGE analyses, relatively small target peptide peaks were detected for RBP2-HBD3, RBP2-HTN3 and RBP2-DCD-1L after cleavage. The emergence of high elution peaks for HBD3-RBP2, HTN3-RBP2 and DCD-1L-RBP2 after cleavage indicated that the cleave off from Switchtags occurred efficiently. In summary, only HBD3-RBP2, HTN3-RBP2, and DCD-1L-RBP2 exhibited notably high refolding and cleavage efficiencies, enabling efficient production of these candidates through Numaswitch^{TM} technology. As the cleavage efficiencies and resulting product yield were considered insufficient for RBP2-HBD3, RBP2-HTN3 and RBP2-DCD-1L, it was decided to focus solely on purifying the bifunctional peptides HBD3-RBP2, HTN3-RBP2 and DCD-1L-RBP2.

4.15 Purification of HBD3-RBP2, HTN3-RBP2 and DCD-1L-RBP2

To purify HBD3-RBP2, HTN3-RBP2 and DCD-1L-RBP2 the Switchtag fusions were firstly produced as IBs in *E. coli* BL21 cells using 5 L shaking flasks (section 3.18) The IBs were isolated from cells by high pressure homogenization and subsequently solubilized in 6 M GuHCl, respectively. After addition of the TEV protease the crude cleavage reactions were firstly analyzed by analytical scale RP-HPLC chromatography to check on the release of target peptides before all three candidates were purified by preparative RP-HPLC, respectively (section 3.18). The chromatogram and all analyses of the fractions obtained during the HTN3-RBP2 purification are exemplarily shown in Figure 27A–B. After purification, elution fractions containing HTN3-RBP2 were pooled, lyophilized and analyzed by SDS-PAGE and RP-HPLC-MS (Figure 27C–F). Purifications of HBD3-RBP2 and DCD-1L-RBP2 were conducted in the same manner as described for HTN3-RBP2.

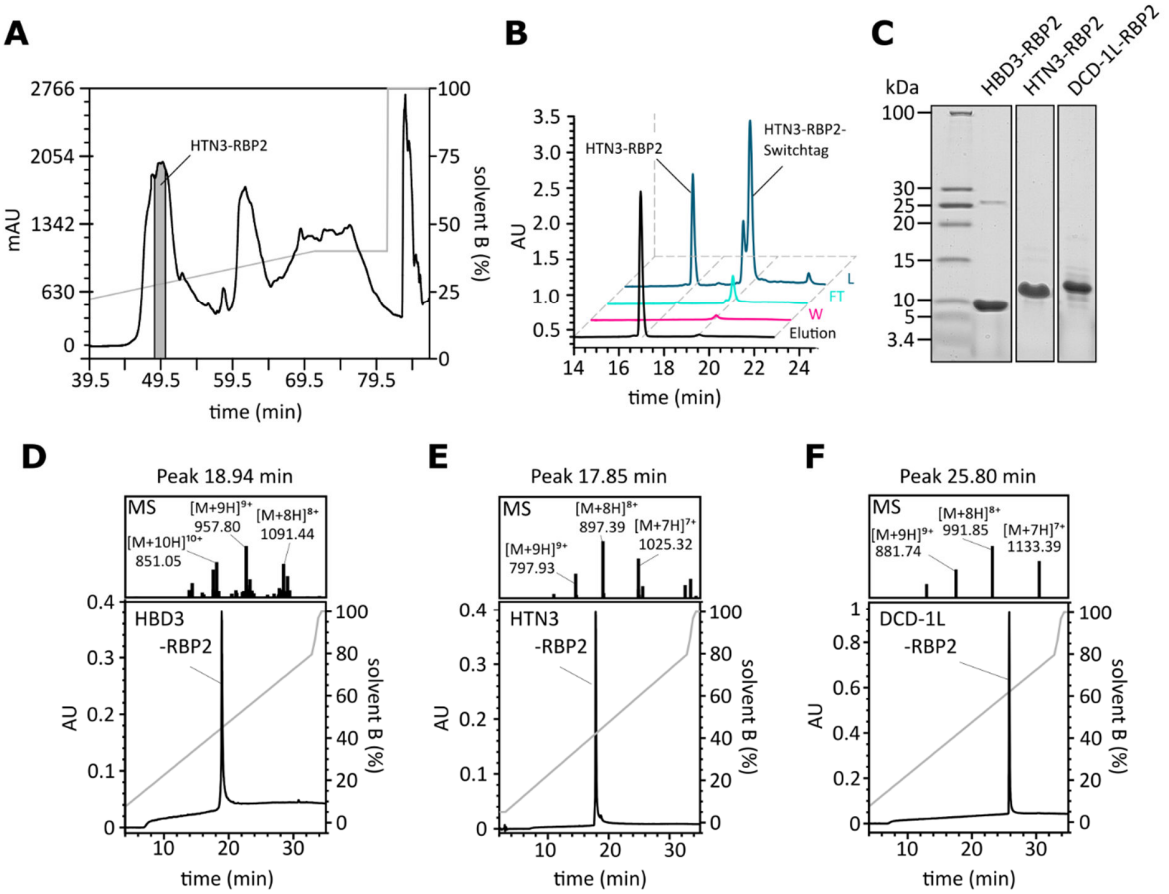

Figure 27 | Purification of HBD3-RBP2, HTN3-RBP2 and DCD-1L-RBP2

(A) Purification of target peptides by preparative RP-HPLC is shown exemplarily for HTN3-RBP2 (section 3.18). The chromatograms show the UV absorption at 205 nm. HTN3-RBP2-containing elution fraction is indicated. **(B)** The load (L), flow through (FT), wash (W) and pooled elution fractions during HTN3-RBP2 purification were analyzed by RP-HPLC. **(C)** Tricine-SDS-PAGE analysis of purified HBD3-RBP2 (8.3 kDa), HTN3-RBP2 (7.2 kDa) and DCD-1L-RBP2 (7.9 kDa) after lyophilization and reconstitution in water (section 3.18). **(D–F)** Analytical scale RP-HPLC-MS analysis of purified HBD3-RBP2, HTN3-RBP2 and DCD-1L-RBP2 after lyophilization and reconstitution in water. Molecular masses of the elution signals were determined by ESI-MS. Chromatograms show the UV absorption at 205 nm (section 3.18).

All Switchtag fusions exhibited high renaturation efficiencies (41–90 %) and cleavage efficiencies (≥ 90 %) (Table 16, Supplementary Material, Figure S 15). The target peptides were purified by preparative RP-HPLC, respectively (section 3.18) and analyses of elution fractions revealed that the target peptides were effectively isolated from the Switchtags (shown exemplarily for HTN3-RBP2, Figure 27B). Tricine-SDS-PAGE analyses revealed that the protein band of HBD3-RBP2 corresponded well to the expected MW

(7.2 kDa). In contrast, the protein bands of purified HTN3-RBP2 and DCD-1L-RBP2 run on Tricine-SDS-PAGE gels higher as expected (~ 12 kDa, Figure 27C). However, the identities of all purified bifunctional peptides were confirmed by RP-HPLC-MS and/or RP-HPLC-MS, respectively. The mass spectrometric data of HBD3-RBP2, HTN-3-RBP3 and DCD-1L-RBP2 obtained by RP-HPLC-MS analyses are shown in Table 15.

Table 15 | Mass spectrometric data of HBD3-RBP2, HTN3-RBP2 and DCD-1L-RBP2

Target peptide	Ion name	*m/z* (expected)	*m/z* (observed)	Mass (Da, expected) [A]	Mass (Da, observed) [B]	Discrepancy (Da)
HBD3-RBP2	$[M+8H]^{8+}$	1034.72	1091.60		8724.80	455.08
	$[M+9H]^{9+}$	919.87	957.83		8611.47	341.75
	$[M+9H]^{9+}$		945.35	8269.64 (red)	8499.20	229.40
	$[M+10H]^{10+}$	827.98	839.40	8263.59 (ox)	8384.00	114.28
	$[M+10H]^{10+}$		850.86		8498.60	228.90
	$[M+11H]^{11+}$	752.80	763.09		8382.99	113.27
HTN3-RBP2	$[M+7H]^{7+}$	1025.43	1025.32		7169.82	0.69
	$[M+8H]^{8+}$	897.37	897.40		7170.24	0.27
	$[M+9H]^{9+}$	797.78	797.85	7170.83	7171.20	0.72
	$[M+10H]^{10+}$	718.10	718.27		7171.65	1.77
	$[M+11H]^{11+}$	652.91	639.51		7172.70	4.32
DCD-1L-RBP2	$[M+7H]^{7+}$	1133.44	1133.39		7926.73	0.3
	$[M+8H]^{8+}$	991.88	991.85		7926.80	0.2
	$[M+9H]^{9+}$	881.79	881.74	7926.91	7926.66	0.4
	$[M+10H]^{10+}$	793.71	793.76		7927.60	0.6
	$[M+11H]^{11+}$	721.65	721.59		7926.49	0.5

[A] Calculated by the formula: [m/z ratio (expected) multiplied by the charged state] minus number of protons;
[B] Calculated by the formula: [m/z ratio (observed) multiplied by the charged state] minus number of protons;
red: reduced; ox: oxidized

The mass data of purified target peptides show that the observed *m/z* fragment ions of HTN3-RBP2 and DCD-1L-RBP2 corresponded well with the expected values which confirmed their target identities. The mass errors, i.e. the discrepancies between observed and expected *m/z* fragments were mostly within the acceptable range of ESI-MS employing quadrupole mass analyzer (> 1 ppm). However, the observed *m/z* fragment ions of HBD3-RBP2 were higher as expected. Ion mass increments of 113 Da, 229 Da and 342 Da point towards the formation of HBD3-RBP2-TFA adducts (M + 114n). Indeed, TFA in the mobile phase is reported to improve peak shape characteristics but in ESI-MS known to cause ionization suppression and TFA adduct formation (McIndoe and Vikse, 2019, Wouters et al., 2021). The identity of HBD3-RBP2 was confirmed by RP-UPLC-MS where formic acid (FA) was used in the mobile phase (section 3.18). Here, the observed masses corresponded to the calculated values of fully reduced protein (Supplementary Material, Figure S 16). Altogether, product amounts ranging from 1-15 mg lyophilized peptides were obtained reaching purity levels of ≥ 95 % were obtained. The key characteristics of the purification processes of HBD3-RBP2, HTN3-RBP2 and DCD-1L-RBP2 are summarized in Table 16.

Table 16 | Key characteristics of purification processes of bifunctional peptides

	HBD3-RBP2	HTN3-RBP2	DCD-1L-RBP2
Cell pellets (wet weight) [A]	4.6 g	5.4 g	4.8 g
IBs (wet weight)	1.3 g	1.2 g	0.8 g
Renaturation efficiency [B]	41 %	90 %	87 %
Cleavage efficiency [C]	≥ 95 %	≥ 95 %	≥ 95 %
Product yield [D]	6.9 mg	15 mg	1 mg
Purity [E]	95 %	97 %	95 %
Identity [F]	confirmed	confirmed	confirmed

[A] Cell pellets derived from 5 L shaking flask cultures. [B] Determined by UV/VIS spectroscopy (section 3.17). [C] Assessed by SDS-PAGE analyses. [D] Lyophilized peptides were weighed using a precision scale (gross weight). [E] Determined by RP-HPLC (section 3.4.1). [F] Target identities were confirmed by RP-HPLC-MS or RP-UPLC-MS (section 3.18).

4.16 Determination of minimal inhibitory concentrations

The antimicrobial activities of purified HBD3-RPB2, HTN3-RBP2 and DCD-1L-RBP2 were evaluated in MIC assays against *E. coli* and *B. subtilis*. Final peptide concentrations between 0.1–100 µM were tested (section 3.19.2). The antimicrobial peptides HBD3, HTN3, DCD-1L and RBP2 were included in this study as controls. Furthermore, DS-THA whose antimicrobial activity was confirmed in previous studies (section 4.8) was taken as assay control. The MIC values of all tested peptides are summarized in Table 17. The corresponding graphs are shown in Supplementary Material, Figure S 17.

Table 17 | MICs of different peptides against *E. coli* and *B. subtilis*

	MIC values in µM*	
Peptides	*E. coli*	*B. subtilis*
HBD3-RBP2	no activity	12.5; 25
HTN3-RBP2	no activity	6.2
DCD-1L-RBP2	no activity	no activity
HBD3	no activity	1.6
HTN3	no activity	50
DCD-1L	no activity	no activity
DS-THA	1.6	1.6
RBP2	no activity	100

*Measurements were conducted in duplicates. If only one MIC is specified, the same value was obtained in both duplicates.

The MIC assay revealed that none of the three designed bifunctional peptides exhibited antimicrobial activity against *E. coli.* These data were in line with control peptides HBD3, HTN3, DCD-1L and RBP2 which also showed no antimicrobial activity against *E. coli.* The MIC value of HBD3-RBP2 against *B. subtilis* was determined to range between 12.5–25 µM, considerably higher than of control peptide HBD3 (1.6 µM). This means that the antimicrobial activity of the bifunctional peptide is reduced most probably caused by RBP2 fusion to HBD3. In contrast, the MIC value of HTN3-RBP2 against *B. subtilis* was 6.2 µM which was about 8-fold higher than of control peptide HTN3 (50 µM) suggesting improved antimicrobial activity. For DCD-1L-RBP2 and control peptide DCD-1L no antimicrobial activity against *E. coli* nor *B. subtilis* was observed in the MIC assay. The MIC value of DS-THA against *E. coli* and *B. subtilis* was confirmed to be 1.6 µM as determined in previous studies (section 4.8). As expected, the adhesive peptide RBP2 did not display antimicrobial activity against *E. coli* but concentrations of > 100 µM seem to hamper

B. subtilis growth. Thus, it is to be expected that RBP2 has no influence on the antimicrobial activity of HBD3-RBP2 and HTN3-RBP2. In summary, two of three designed bifunctional peptides exhibited antimicrobial activity against *B. subtilis* which demonstrated that the functional domains of the respective AMPs were well preserved in the molecule despite RBP2 fusion. As DCD-1L-RBP2 did not show antimicrobial activity against *E. coli* and *B. subtilis* in the MIC assay, only HBD3-RBP2 and HTN3-RBP2 were selected for the subsequent study.

4.17 Analyses of the adhesive properties by pulldown assays

Pulldown assays were performed to evaluate whether HBD3-RBP2 and HTN3-RBP2 bind to Resomer® beads (section 3.19.1). Lyophilized HBD3-RBP2 and HTN3-RBP2 were reconstituted in binding buffer and incubated in the presence of Resomer® beads. The supernatants were removed and the Resomer® beads were extensively washed and bound peptides were eluted by pH shift. All fractions obtained during pulldown assay were analyzed by Tricine-SDS-PAGE (Figure 28).

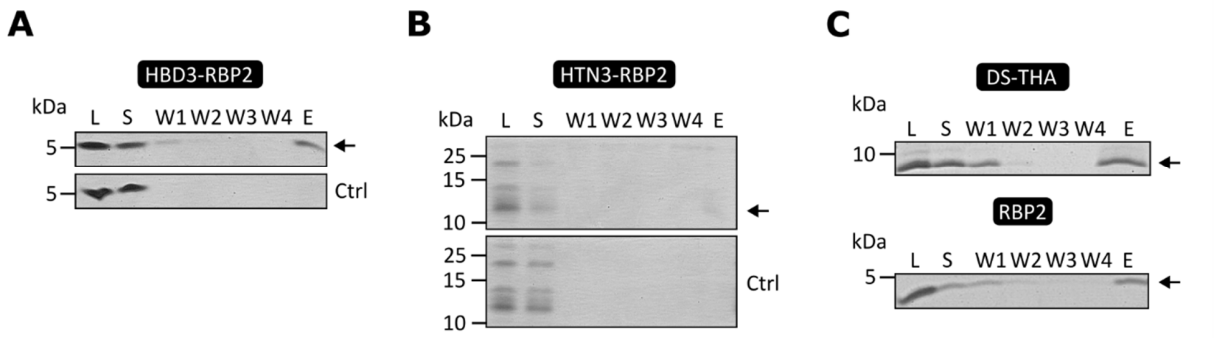

Figure 28 | Binding analysis of HBD3-RBP2 and HTN3-RBP2 to Resomer® beads

Tricine-SDS-PAGE analyses of fractions obtained after pulldown assay (section 3.19.1). The assay was performed with **(A)** HBD3-RBP2, **(B)** HTN3-RBP2 and control peptides **(C)** DS-THA and RBP2. Lyophilized peptides were reconstituted in Tris-HCl-based buffer (L, load) and incubated in the presence of Resomer® beads. Supernatants (S) were removed, the beads were washed four times (W1–4) to remove peptide excess. Bound peptides on Resomer® beads were eluted by pH shift (E). The arrows indicate the location of target peptides after elution. To exclude the possibility that the emerging protein bands in the elution fraction stem from unspecific binding of target peptides to tubes the pulldown assay was also performed in the absence of Resomer® beads (Ctrl, control).

The pulldown assay indicated that HBD3-RBP2 binds specifically to Resomer® beads as a clear protein band in the elution fraction was observed (Figure 28A). As expected, no protein band emerged in the control experiment without Resomer® beads which further confirmed the observation. However, no binding of HTN3-RBP2 to Resomer® beads was observed as no protein band appeared in the elution fraction. Additional protein bands at higher MWs in the load and supernatant suggested the formation of HTN3-RBP2 aggregation products which may explain why no binding to Resomer® beads was observed

(Figure 28B). RBP2 bound to Resomer® as expected, and also DS-THA was found to bind to the biopolymer (Figure 28C). In summary, out of the three designed bifunctional peptides, only HBD3-RBP2 displayed retained adhesive and antimicrobial properties. MIC assays revealed that HBD3-RBP2 exhibited decreased antimicrobial activity against *B. subtilis* than the control peptide HBD3 (section 4.16). The remaining bifunctional peptides, HTN3-RBP2 and DCD-1L-RBP2, either did not bind to Resomer® beads in pulldown assays or show no antimicrobial activity against the tested bacteria. Remarkably, the bifunctional peptide DS-THA showed high antimicrobial activity against both *E. coli* and *B. subtilis* and was found to have adhesive properties against Resomer®. This peptide clearly outperforms the HBD3-RBP2 peptide as it exhibited antimicrobial activity against *E. coli* and has higher MIC values against *B. subtilis.*

4.18 Bacterial adhesion assay

In a proof-of-concept experiment, the antimicrobial effect of bifunctional peptides was tested after incorporation in Resomer® coatings. A bacterial adhesion assay was established (section 3.20) employing the fimbriated *E. coli* PKL1162 strain which constitutively expressed the green fluorescent protein (GFP) and known to specifically adhere on mannan-coated surfaces (Hartmann et al., 2010).

In a pre-study, it was investigated how *E. coli* PKL1162 adhered to Resomer® surfaces, both in the presence and absence of the plant polysaccharide mannan. For the bacterial adhesion assay, it is important that the strain adheres on Resomer® surfaces without mannan. Mannan's presence on Resomer® coatings may form a barrier, reducing the antimicrobial effect and affecting the contact-killing capabilities of the bifunctional peptides in Resomer® coatings. The studies showed that the cell growth rates of adherent bacteria in the presence and absence of mannan on Resomer® surfaces were very similar rendering the *E. coli* PKL1162 strain suitable for the bacterial adhesion assay (Supplementary Material, Figure S 18).

Regarding the choice of bifunctional peptide, as HBD3-RPB2 did not exhibit antimicrobial activity against *E. coli* in MIC assays (section 4.16) this peptide was deemed unsuitable for the bacterial adhesion assay. Therefore, DS-THA was employed in this assay as it was found to exhibit excellent antimicrobial activity against *E. coli* (section 4.16) and to adhere on Resomer® beads (section 4.17).

Resomer® coatings loaded with different concentrations of DS-THA were prepared as described in section 3.20. The coatings were washed with PBS to remove excessive peptides and bacterial solution was added to enable bacterial adhesion on the coatings. Following incubation, the non-adherent cells were removed by rigorous washing steps before MHB medium was added to induce growth of adherent bacteria. Cell growth was monitored by fluorescence readout for 16 h and the results are shown in Figure 29.

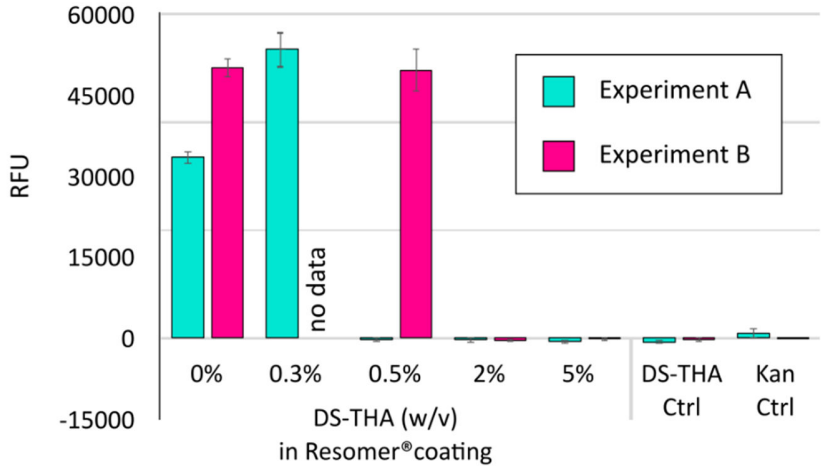

Figure 29 | Bacterial growth on DS-THA loaded Resomer® coatings

Growth of adherent *E. coli* PKL1162 cells on Resomer® coatings containing different concentrations of DS-THA (0.3 %, 0.5 %, 2 % and 5 %, w/v) were monitored by fluorescence readout in two experimental set-ups (A and B). Resomer® coating containing 0.3 % DS-THA was excluded in experiment B. Shown in bars are the RFUs (Relative Fluorescence Unit) after 16 h of incubation at 37 °C. Resomer® coatings without DS-THA (0 %) and with kanamycin (Kan Ctrl) served as controls. In another control, cells which adhered on Resomer® coatings were incubated with MHB supplemented with 1.56 µM DS-THA (DS-THA Ctrl). Error bars indicate the SD. Three technical replicates were carried out for each experimental set-up.

In two experiments the impact of Resomer® coatings loaded with different concentrations of DS-THA on the growth of adherent *E. coli* PKL1162 was investigated. As expected, bacterial growth was observed on Resomer® coatings without DS-THA while coatings containing kanamycin inhibited bacterial growth efficiently. Data of experiment A indicated that incorporation of ≥ 0.3 % DS-THA in the coating was not sufficient to inhibit bacterial growth. For Resomer® coatings containing 0.5 % DS-THA contradictory results existed. Bacterial growth was successfully inhibited in experiment A, but not in experiment B (Figure 29). Different results may be attributed to high error rates of the assay further elaborated in the discussion section (section 5.3). Notably, coatings containing ≥ 2% DS-THA effectively inhibited growth of adherent *E. coli* PKL1162 in both experiments. This confirms that the antimicrobial effect of bifunctional peptides remained potent within Resomer® coatings, effectively inhibiting bacterial growth on surfaces.

5 Discussion

5.1 Numaswitch™ – An efficient production platform for peptides and small proteins

Over the past decade, the importance of therapeutic peptides within the pharmaceutical sector has increased, largely owing to their compatibility within the human body and their exceptional bioactivity. Worldwide, about 80 peptide drugs have been approved and more are currently developed (Wang et al., 2022). Equally of great interest are small proteins, also referred to as "pepteins" ranging between 50 and 300 aa (section 1.3.1). They exhibit unique biological functions and are involved in many cellular processes (Su et al., 2013, Storz et al., 2014) including molecules such as growth factors or antibody fragments. The demand for peptide or peptein-based drugs in the pharmaceutical industry rapidly grew in the last years due to their high activity, great chemical and biological properties and low cytotoxicity (Lau and Dunn, 2018, Wang et al., 2022).

For the production of peptides, only a few reliable recombinant expression platforms exist so far making chemical synthesis the preferred method in most cases despite its drawbacks. Disadvantages including high cost, limited scalability, and the use of hazardous chemicals are associated with chemical synthesis making industrial scale peptide production challenging (Isidro-Llobet et al., 2019). On the other hand, the production of pepteins by chemical synthesis is difficult, often hampered by technical limitations (Hou et al., 2017). Here, recombinant expression systems are the method-of-choice, but the development of efficient production processes is cumbersome adding a time and price tag, particularly due to intrinsic characteristics of pepteins including proteolytic degradation, aggregation and cytotoxicity (Otvos and Wade, 2014, Hancock et al., 1995).

In this dissertation the Numaswitch™ technology (section 1.2.6) was introduced, a novel recombinant expression system capable to overcome the aforementioned limitations of conventional systems. It offers the potential to produce challenging peptides and pepteins efficiently and cost-effectively in *E. coli*. The Numaswitch™ technology is based on HlyA1 which is a C-terminal fragment of HlyA. The RTX protein HlyA serves as the allocrite of the dedicated HlyA T1SS in Gram-negative bacterium *E. coli.* Previous studies have shown that when HlyA1 is N-terminally fused to target peptides and expressed without the T1SS transport complex in *E. coli* the resulting fusion proteins form IBs inside the cytoplasm. After extraction of the IBs from cells and solubilization in chaotropic agents they refold efficiently to highly soluble and biologically active proteins in the presence of Ca^{2+} (section 1.2.6). This technology is currently applied by the company Numaferm GmbH successfully for the production of peptides and proteins.

One major aim of this dissertation was to explore whether different HlyA1 variants with C-terminal truncations at the secretion signal (SS) exhibited similar refolding characteristics when fused to different

peptides and pepteins, in comparison to HlyA1 wild type. Smaller protein tags may lead to higher expression titers and/or product titers, as the stoichiometric proportion of the target in the fusion protein is increased (Vargas-Cortez et al., 2017, Yadav et al., 2016). As the RTX domain is located at the N-terminal part of HlyA1 and is crucial for Ca^{2+} binding and the refolding process, it was assumed that the SS at the C-terminus does not influence the functionality of the protein tag. Therefore, the C-terminal secretion signal of HlyA1 was partially deleted in HlyA1 Δ185–218, nearly entirely deleted in HlyA1 Δ165–218 and the HlyA1 Δ135–218 contains an even longer C-terminal depletion (Table 4).

HlyA1 wildtype and all three HlyA1 truncations were fused as N-terminal protein tags to the five selected targets Teriparatide, Linaclotide, DS-THA, Aß40 and SAA3, respectively. Expression analyses of *E. coli* BL21 (DE3) transformed with recombinant plasmids encoding HlyA1 fusions and truncated HlyA1 fusions revealed that all fusion proteins were produced as IBs in *E. coli* cells at high levels (Figure 13 and Figure 15). Differences in protein band intensities observed among the targets implied that certain peptides or pepteins were more preferably expressed in cells than others (e.g. compare lanes of Teriparatide with DS-THA and Linaclotide, Figure 15). Variations in gene expression levels might stem from inherent properties of the targets as some IBs can retain their biological activity even when aggregated (Slouka et al., 2019). In scope of this work it was demonstrated that the bifunctional peptide DS-THA exhibited antimicrobial activity against *E. coli* and *B. subtilis* (Table 17). It is assumed that lower expression levels of DS-THA compared to the other targets might be caused by cytotoxic effects of DS-THA IBs on host cells, but further studies are necessary to confirm this.

Refolding of HlyA1 and truncated HlyA1 fusions in the presence of Ca^{2+} led to soluble proteins with high initial purities (estimated to be > 80 %, Figure 14 and Supplementary Material, Figure S 1). However, the renaturation efficiencies varied between 12 and 84 % (Figure 16) highly depending on the employed HlyA1 variant in combination to the fused targets. Comparing the three HlyA1 truncations with HlyA1 wild type, in three of five cases the renaturation efficiencies could be substantially increased (see Teriparatide, Aß40 and SAA3, Figure 16). The highest increase was observed for Teriparatide where the renaturation efficiency was increased by about 6.8-fold employing the HlyA1 Δ165-218 variant. It is important to highlight that the renaturation efficiency is a crucial factor to achieve high product titers, so in case of Teriparatide, Aß40 and SAA3 it could be considerably improved. For DS-THA the refolding efficiency was not enhanced when truncated HlyA1 variants were employed and for Linaclotide, the renaturation efficiencies were even lower than HlyA1 wild type. Overall, it is difficult to assess whether deletions at the C-terminal SS affect the renaturation efficiency due to conflicting data. What is recognizable, however, is that the renaturation efficiency strongly depends on the attached target peptide or protein.

To address the question of how HlyA1 manages to induce efficient renaturation of fusion proteins, there are several assumptions. In previous studies it was confirmed that the refolding process is highly dependent on

Ca^{2+} as the renaturation efficiency of HlyA1 wild type was about 3-fold higher with Ca^{2+} than without (Figure 12). This phenomenon can be explained by the presence of three conserved GG repeats within the RTX domain of HlyA1 which form the binding sites for Ca^{2+} (Ludwig et al., 1988, Baumann et al., 1993). Glycine and aspartate residues of GG repeats coordinate the Ca^{2+} ion leading to alternating turns of ß strands which form ß-roll structures typical for RTX domains. In earlier reports it was proposed that the number of GG repeats correlates with the protein's MW and can vary between four to more than 50 GG repeats (Baumann, 2019). Remarkably, reducing the GG repeats in HlyA from six to three did not affect the Ca^{2+} binding capacity at all as the K_d values remained highly similar at around 100 µM (Thomas et al., 2014a). The formation of Ca^{2+} loaded ß-roll structures in RTX domains induces proper conformation of the entire protein, thereby enhancing the protein's solubility and stability (Baumann et al., 1993, Bumba et al., 2016). As the Ca^{2+} ions are integrated in the RTX domain and are only partially accessible to solvents they reliably keep the protein soluble and enhances their stability also after Ca^{2+} removal. Only the addition of EDTA or denaturing agents like urea or GuHCl lead to removal of Ca^{2+} from RTX domains and decreasing the protein's stability (Meier et al., 2007, Baumann, 2019). In previous studies the impact of the HlyA1 domain on the folding of fusion proteins was assessed, specifically involving the core domain of maltose binding protein (MalE). Insights derived from time-resolved intrinsic tryptophan fluorescence spectroscopy indicated that HlyA1 reduces the folding rate of the MalE domain within MalE-HlyA1 fusion proteins (Bakkes et al., 2010). It is possible that HlyA1 is able to decelerate the folding rate of the linked target peptide or protein while promoting the formation of native folded structures. In another theory it was proposed that RTX domains exhibit chaperone-like characteristics in the cytoplasm which maintain the post-translational RTX protein in an unfolded state mandatory for the T1SS secretion process (Baumann, 2019). Similar to solubility tags such as MalE (di Guan et al., 1988) or GST (Smith and Johnson, 1988), it is possible that HlyA1 exhibits chaperone-like properties that prevent intermolecular protein aggregation during refolding and improve its solubility. However, further studies are needed to confirm the theory.

Refolded HlyA1 and truncated HlyA1 fusions were treated with TEV protease to release the targets from HlyA1 backbones. SDS-PAGE analyses revealed that fusion protein cleavage varied considerably (Figure 14 and Supplementary Material, Figure S 1). Generally, the TEV cleavage site (ENLYFQ) is located between the N-terminal HlyA1 variant and the target protein (Figure 10). Peptide hydrolysis typically occurs between Q and the initial N-terminal amino acid residue of the target also referred to as P1' position. Previous studies demonstrated that the TEV protease exhibits optimal cleavage when small amino acid residues like S or G fill in the P1' position (Dougherty et al., 1989, Parks et al., 1994). Replacement of S and G against other residues including for example N, Q, K, R, V or I can hamper the TEV protease cleavage efficiencies to varying degrees (Kapust et al., 2002). In line with these studies, SDS-PAGE analyses of cleavage reactions revealed nearly complete cleavage (90–100 %) for Teriparatide, Linaclotide and DS-

THA (which contain S, C or G in P1' position), around 50 % for Aß40 (D in P1' position) and around 20 % for SAA3 (Q in P1' position) (compare "C" lanes in Figure 14B). Release of target peptides or pepteins, except for SAA3, from HlyA1 backbones after TEV protease cleavage was confirmed by RP-HPLC-MS, respectively. SDS-PAGE analyses indicated the presence of SAA3 in the cleavage reaction.

HlyA1 wild type and truncated HlyA1 variants can be employed as bifunctional protein tags, also referred to as "Switchtags" (section 1.2.6) for efficient production of target peptides and pepteins. The first functionality refers to the capability of HlyA1 fusions to form intracellular IBs which protects the targets from proteolytic degradation in the cytoplasm independent of their physicochemical properties and biological functions. The second functionality refers to the ability of Switchtags to act as Ca^{2+}-induced "renaturation tags" outside the cells promoting efficient refolding of denatured HlyA1 fusions to soluble and biologically active protein. Efficient refolding is a major bottleneck in IB-based production processes, yet Switchtags alleviate this hurdle while offering additional advantages such as high-titer expression, high initial purities, easy separation from host cell proteins and protection of the host cell from cytotoxic target functionalities (Singhvi et al., 2020, Bhatwa et al., 2021). High initial purities of > 80 % estimated from SDS-PAGE gels were already reached after the refolding step (see Figure 14 and Supplementary Material, Figure S 1) and demonstrate the benefit of IBs to separate them easily from host cell contaminants decreasing downstream efforts and process complexity.

The study effectively showcased the applicability of Switchtags across five different targets, indicating that Numaswitch™ technology could serve as a versatile and universal platform for peptide and peptein production. To showcase the scalability of the Numaswitch™ technology HlyA1 Δ185-218 was employed as Switchtag (section 1.2.6) to produce > 2 g Teriparatide per liter fermentation broth in high quality (Table 5). Compared to state-of-the-art production strategies (Abbaszadeh et al., 2019) this represents an about 20-fold product yield increase. This underlines the potential of Numaswitch™ technology for industrial-scale peptide production, delivering purified products meeting pharmaceutical industry standards. This advance not only facilitates the production of existing peptides, but also enables the development of new peptides for pharmaceutical applications. The studies demonstrate the potential of this reliable and cost-efficient approach to act as a universal platform that can be used for the large-scale production of high quality peptides and pepteins.

5.2 Numaswitch™ – An efficient production platform for disulfide-rich pepteins

Many pharmaceutical and biological relevant peptides and pepteins harbor disulfide bonds which are important for their stability, biological function and activity (Zavodszky et al., 2001, Ishikawa et al., 2007). In general, disulfide-rich peptides or proteins are difficult to produce in recombinant *E. coli* systems as the reducing environment of the cytoplasm hinders proper formation of disulfide bonds. While progress has

been achieved in this context, e.g. the improvement of disulfide bond formation by translocation of targets into the oxidizing periplasm (Bardwell et al., 1991, Manta et al., 2019), the development of *E. coli* shuffle strains (Lobstein et al., 2012) or application of redox shuffle systems (Rivera-de-Torre et al., 2021, Lobstein et al., 2012) the formation of undesired isomers still remains challenging and leads to aggregation or low yields of functional targets (Lobstein et al., 2012, Bhatwa et al., 2021). *E. coli* shuffle strains contain an oxidative cytoplasmic environment but challenges like slow growth rates or limited scalability hinder their broad application in the pharmaceutical industry (Lobstein et al., 2012).

In another study of this dissertation, the potential of the Numaswitch™ technology to produce disulfide-rich peptides and proteins was explored. Different Switchtags (section 1.2.6) were fused to disulfide-rich candidates including hEGF, VHH, scFv clone F2C and DS-THA (Table 1) to evaluate their potential to produce these candidates in their correctly folded and functional form. The resulting Switchtag fusions (Table 6) were produced as IBs in *E. coli* at high levels employing fed-batch high density fermentations. Product yields of 10–19 g Switchtag fusions per liter fermentation broth were achieved (Table 7). After extraction of IBs from cells and solubilization in chaotropic agents, the Switchtag fusions were refolded in Ca^{2+}-containing buffers achieving high renaturation efficiencies ranging from 52 to 90 %. Once more, the data demonstrate the capability of Switchtags to efficiently convert insoluble protein aggregates to highly soluble proteins. All target peptides or pepteins were removed from Switchtags by TEV protease cleavage at high efficiencies (≥ 90 %, estimated from SDS-PAGE gels). SDS-PAGE analyses confirmed the presence of all targets in the cleavage reactions. It should be noted that the hEGF protein band did not appear in the 6.2 kDa region as expected but emerged at a slightly higher MW of about 12 kDa (Figure 18). The difference of expected and apparent MW most likely resulted from the presence of three intramolecular disulfide bonds in hEGF, which affected their migration behavior in the SDS-PAGE gel. This theory was confirmed by treatment of purified hEGF with the reducing reagent TCEP prior to SDS-PAGE analysis which led to a shift of the hEGF proteins bands to lower MWs (Supplementary Material, Figure S 5D).

Individual production strategies were developed for all targets reaching product yields of 1.1 to 4.5 g/L culture. In contrast, cytoplasmic expression led to reported yields of up to 30 mg per liter fermentation broth for scFv clone F2C and 250 mg per liter for hEGF. The production strategies relied on the use of solubility tags like thioredoxin (Shams et al., 2019), the small ubiquitin-like modifier (SUMO) (Ma et al., 2016) or the CyDisCo system (Kim et al., 2021) to purify hEGF in their natively folded form.

This shows that the Numaswitch™ technology is also capable of producing disulfide-rich peptides and pepteins at large scales in *E. coli*. The approach worked efficiently not only for small peptides but also for proteins up to 27 kDa. High purities were reached (≥ 95 %) (Table 7) confirming the high quality of the products. Remarkably, RP-UPLC-MS analyses confirmed the oxidative state of all targets (Figure 19). As mentioned before, disulfide bond formations are important for the correct folding and stability of many

peptides and proteins, in particular for those exhibiting biological activities (Ishikawa et al., 2007, Zavodszky et al., 2001). For DS-THA and VHH which each harbor two cysteines, the presence of an intramolecular disulfide bond was confirmed by RP-UPLC-MS. The growth factor hEGF contains six cysteines and natively forms three intramolecular disulfide bonds (Cys_6-Cys_{20}, Cys_{14}-Cys_{31}, Cys_{33}-Cys_{42}) (Carpenter and Cohen, 1990). Incomplete formation of disulfide bonds or the formation of undesired isomers are present challenges when dealing with this compound (Chang et al., 2001). Notably, employment of Switchtags as protein tags enabled the purification of the fully oxidized functional protein. For scFv clone F2C masses of the oxidized and reduced form were observed. So far, no profound explanation was found why scFv clone F2C was not fully oxidized like the other targets but after treatment of the product with the oxidizing catalyst Copper (III) phenanthroline the oxidized form was yielded (Supplementary Material, Figure S 8). Furthermore, the biological activities of the purified targets were confirmed in different assays showing that the targets were yielded at large scales and in their natively functional forms (section 4.8).

The obtained data back up the theory that Switchtags are efficient solubility tags. On the one hand, they act chaperon-like and help the fused target peptide or protein to adopt their native confirmation. On the other hand, it is assumed that they prevent intermolecular interaction and thus aggregation of fusion proteins. As interaction of HlyA1 with the MalE domain in MalE-HlyA1 fusion proteins was confirmed in previous studies (Bakkes et al., 2010), it is possible that Switchtags slow down the folding process of their fusion partner, allowing gradual folding of proteins along the thermodynamical energy landscape until they achieve their native state. Upon refolding of fusion proteins, the disulfide bonds are most likely formed by auto-oxidation triggered by the oxidative environment of the refolding buffer. It is possible that slower protein folding rates favor the formation of the correct disulfide bonds, but further studies are necessary to confirm these theories.

Importantly, the application of Switchtags may not only limited to dedicated *E. coli* strains as it can be regarded as a biochemical toolbox. If Switchtags induce the production of fusion protein IBs the evolved approach may be applicable in other expression hosts. In future studies, the focus will be set on the production of even larger proteins ($\geq$ 300 aa) characterized by complex tertiary structures (e.g. enzymes, antibodies). However, first studies in this direction indicated that the renaturation efficiencies, hence the product yields decreased in correlation with larger protein MWs when attached to Switchtags (unpublished data). This clearly draws out the limitations of the Numaswitch^{TM} technology. Moreover, Switchtags may not only be restricted to HlyA1-derived fragments, but other GG repeats containing fragments of alternative RTX proteins may also perform well. A broad range of alternative Switchtags deriving from the > 1000 members of the RTX protein family (Linhartova et al., 2010) are currently under investigation for their applicability to reach higher renaturation efficiencies for challenging candidates (unpublished data). If successful, Switchtags may grant access to an even broader class of proteins.

In summary, this dissertation demonstrated the applicability of the Numaswitch™ technology not only on small peptides but also on disulfide-rich pepteins of up to 26.9 kDa. The selected targets were purified at large scales and high purities showcasing the potential of this approach to be an universal production platform for peptide and peptein production. Switchtags solve the major bottleneck of low renaturation efficiency and ensure that the fusion proteins IBs are efficiently converted to soluble and functional proteins. Since the production of Switchtag fusion IBs and the renaturation step were shown to be reliable, efficient production process strategies for novel targets can be developed within weeks. Numaswitch™ emerges as a highly effective production platform compared to chemical synthesis and alternative recombinant expression platforms.

5.3 Development of bifunctional peptides for implant coatings

Novel alternatives to conventional antibiotics are urgently needed to stop the expansion of methicillin-resistant *S. aureus* (MRSA) strains. In view of the global demographic trend it is expected that more and more elderly people need orthopedic implants in the future due to bone impairments and deformations (Bruellhoff et al., 2010, Chen et al., 2023). Implant failure caused by the development of implant-associated infections (IAIs) is a major problem in orthopedic surgeries leading to high morbidity and mortality rates as well as high financial burden of health care systems (Portillo et al., 2013, Weinstein, 2001, Hedrick et al., 2006). IAIs originate from bacterial adhesion on implant surfaces, which is a critical factor in the formation of biofilms (Chen et al., 2023). To date, numerous coating strategies have been developed to enhance antimicrobial properties of implant surfaces to prevent bacterial adhesion and reduce the risk of IAIs. These implant coatings often involve the incorporation of antibiotics (Ma et al., 2012), organic compounds, metal ions like silver (Soma et al., 2022) or the attachment of antimicrobial peptides to the implant surface (Costa et al., 2011). Although these strategies were demonstrated to decrease bacterial adhesion on implant surfaces challenges like the requirement of complicated immobilization techniques, short-lived antimicrobial effects, concerns regarding the development of bacterial resistance or cytotoxicity effects still persist (Chen et al., 2023, Li et al., 2023).

Addressing the above-mentioned challenges one objective of this dissertation was to develop bifunctional peptides comprising an antimicrobial and adhesive property. They shall be incorporated in Poly-D, L-lactic acid-based coatings, referred to as Resomer® to prevent bacterial growth on implant surfaces. Incorporation of bifunctional peptides in polymer matrices shall help to achieve the following benefits: Firstly, by embedding these peptides within the coating, they are shielded from extracellular proteases in human sera resulting in a prolonged half-life of the molecules. Secondly, the adhesive domain of the peptide shall immobilize the molecule within the coating and prevent rapid release. This way, the antimicrobial effect at the implant site is extended while the risks of potential cytotoxicity are lowered. Thirdly, compared to methods where AMPs are linked to bare implant surfaces, incorporating peptides into Resomer® coatings

could potentially enhance their density per surface area, thereby increasing the overall antimicrobial effect at the implant site.

AMPs exhibiting broad-spectrum activity against different pathogens are extensively described in the literature (Wang et al., 2022, Huan et al., 2020). In contrast, peptides specifically binding to the biopolymer Resomer® were rarely found. Thus, in scope of this dissertation phagemid libraries were constructed which display randomized 24 aa or 36 aa peptides, respectively. These phagemid libraries shall be used to identify peptides which specifically bind to Resomer® surfaces. As the 24-mer phagemid library was constructed by Numaferm GmbH before this dissertation focused on the construction of the 36-mer library. In short, the process of phagemid library construction involved the cloning of degenerate library DNA into phagemid vectors which were subsequently transformed into electrocompetent *E. coli* TG1 cells in multiple rounds until the desired library size was achieved (section 4.9).

In reference to section 4.9.1, during ligation of pSEX81 and 36-mer library DNA a dominant band slightly higher than the linearized parental vector indicated the correct formation of recombinant pSEX81-36-phagemid vector (Figure 21). However, weak DNA bands at ~5000 bp or ~10,000 bp suggest the formation of high molecular weight DNA products probably caused by formation of vector-multiple-insert or vector-vector events. Transformation of high molecular weight DNA products may lead to a slight decrease of the library diversity, but the resulting phagemid particles are most likely non-viable (Sloth et al., 2022). Previous studies demonstrated that the transformation efficiency drops with the increase of DNA size (Szostkova and Horakova, 1998). Even if these large DNA products enter the cell, further challenges including in-frame translation with the p3-protein or translocation of the fusion protein across cell membranes for assembly of phagemid particles need to be overcome before viable particles are produced (Sloth et al., 2022, Noren and Noren, 2001).

For the majority of phage libraries available on the market diversities in the order of 10^9–10^{11} are described (Grieco et al., 2009). High-diversity libraries increase the chances of finding promising peptide candidates during biopanning experiments. To create libraries of such high diversity, it is crucial to attain high transformation efficiencies during library construction. In the scope of this work different experimental conditions were tested to achieve maximal transformation efficiency (Supplementary Material, Figure S 13). Two crucial factors were discovered that enhanced the transformation efficiency considerably. Firstly, the employment of commercially available electrocompetent *E. coli* TG1 cells and secondly, purification of the transformed library DNA before transformation. The transformation efficiency is closely related to the state of the electrocompetent cells, specifically the permeability of the cell membrane, and it is evident that commercially available cells exhibit superior performance (~ 7-fold) compared to self-prepared ones (Supplementary Material, Figure S 13A). Furthermore, purification of the library DNA before transformation improved the transformation efficiency by factor 5 and indicate that the presence of

impurities such as proteins or salts may decrease the electroporation efficiency. Employing optimized conditions, transformation efficiencies in the order of 10^7– 10^8 cfu/µg were achieved.

The most important key parameter to assess the quality of the constructed phagemid library is the diversity, i.e. the proportion of all possible peptide sequences in the library pool (Smith and Petrenko, 1997). Estimation of the library diversity based on colony counts of the transformed library or the transformation efficiency is a widely accepted approach (Sloth et al., 2022, Clackson and Lowman, 2004). It was estimated that the bacterial 24-mer peptide library consist of approximately 2.4 x10^9 unique transformants, while the bacterial 36-mer peptide library contains about 1.6 x10^9 individual clones. Notably, for the preparation of the 24-mer library a higher average transformation efficiency (1.2 x10^8 cfu/µg) was achieved compared to the 36-mer library (7 x10^7 cfu/µg), resulting in fewer number of transformation reactions required to obtain library sizes of ≥ 10^9. However, the reason for this difference remains unclear and hard to evaluate since different amounts of library DNA were used to transform *E. coli* TG1 cells in both preparations. Several factors, such as the state of electrocompetent cells (Wu et al., 2010, Liu et al., 2018), size or purity of transformed library DNA (Szostkova and Horakova, 1998) or practical differences in execution potentially affected the transformation efficiency.

The DNA sequences of ≥ 60 randomly picked library transformants of each phagemid library were examined to provide insight into the actual library diversities, i.e. the proportion of variants containing in-frame peptide inserts and capable of forming viable phagemid particles (Sloth et al., 2022). Incorrect clones represent those containing stop codons (except of UAG) or frameshifts (due to e.g. nucleotide deletions or multiple peptide inserts) leading to a premature termination of the translation or it is unlikely that viable phagemid particles are produced at all. In any case, incorrect clones result in a decrease of the library diversity (Noren and Noren, 2001, Sloth et al., 2022). Notably, the proportion of incorrect clones was about 20 % in both phagemid libraries, hence it can be estimated that the 24-mer phagemid library contains about 1.9 x10^9 and the 36-mer phagemid library about 1.2 x10^9 correct transformants (actual library diversity). Frameshifts caused by nucleotide deletions in the variable region most likely were introduced during chemical synthesis of randomized oligonucleotides. The deletion rate during oligonucleotide synthesis can range between 0.1–0.5 % per coupling reaction (Hecker and Rill, 1998), and the coupling efficiency has been found to decrease with increasing oligonucleotide length. The 24-mer and 36-mer library oligonucleotides synthesized were close to the upper limit of oligonucleotide synthesis capabilities (150–200 bp) (LeProust et al., 2010). In addition, the presence of wild type pSEX81 phagemids, which still harbor the original scFv cassette, was found exclusively found in the 36-mer phagemid library. Wild type pSEX81 phagemid contamination most likely resulted from incomplete digestion reactions during vector preparation further decreasing the actual library diversity. All analyzed DNA sequences did not contain any undesired stop codons (except of UAG) that may lead to premature termination of peptide-p3 translation. A small

number of incorrect clones carried three or five coherent inserts, confirming the presence of vector-multiple-insert events formed during ligation reaction.

Although inferring the library diversity by the transformation efficiency and DNA sequencing has been the traditional route for a long time, limitations of this method are clearly drawn out by its superficial nature and low throughput (Ravn et al., 2010, Matochko et al., 2012). It should be noted that this approach provides limited insights into the actual diversity due to the small sample size and the library complexity does not necessarily increase proportionally with the size of the sample (Fantini et al., 2017). Most display platforms rely on libraries of 10^9 or higher diversity, but conventional DNA sequencing tools struggle to efficiently cover this diversity range (He et al., 2018). High-throughput sequencing methods, known as next-generation-sequencing (NGS) overcome current limitations and enable the screening of $\geq 10^6$ library clones in parallel providing a more reliable and detailed picture on the actual library diversity (Sloth et al., 2022, McCombie et al., 2019, Goodwin et al., 2016). NGS in combination with phage display is a powerful tool to characterize phage or phagemid libraries, but also to monitor enrichment of potential binders during biopanning (Plessers et al., 2021). Every NGS platform has their own strengths and limitations, e.g. the Roche 454 pyrosequencing method was found to provide read lengths of 300–400 bp but is mostly associated with high error rates (~ 0.5 % per base) and low throughput (10^4 –10^5). Alternative systems, like PacBio are able to sequence lengths of 8,500 bp but have a low throughput (10^4) and a high error rate (Fantini et al., 2017).

To assess the amino acid composition of the peptide inserts is another important factor to evaluate the library quality (Fagerlund et al., 2008, Sloth et al., 2022, Ryvkin et al., 2018). Amino acid diversity of peptides displayed in phagemid libraries was achieved by using randomized library oligonucleotide DNA. The correct clones of the 24- and 36-mer libraries were further analyzed regarding their amino acid composition. The aim was to evaluate how well the observed amino acid frequency aligned with the expected values derived from the NNK randomization strategy. Interestingly, the 24-mer library showed prominent overrepresentation of proline, approximately twice the expected value, which is consistent with other reports where high proline contents in libraries were observed (Sloth et al., 2022, Krumpe et al., 2007, ’t Hoen et al., 2012). The cause of this inclination towards proline remains unclear, but since the sequences encoding randomized peptides were analyzed prior packaging of phagemid particles bias attributed to biological selection (i.e. censorship of amino acids due to M13 bacteriophage life cycle) can be excluded (Rodi et al., 2002). Proline is known to act as a structural disruptor preventing the formation of both α-helical and β-sheet structures in peptides and proteins (Morgan and Rubenstein, 2013). Thus, increased occurrence of proline in peptide inserts is assumed to largely impact the structural conformation of peptides and possibly affects binding capacities during biopanning. Naturally, overrepresentation of certain amino acids leads to depletion elsewhere increasing deviations from the NNK randomization strategy. However, as the majority

of amino acids were found to be in line with the NNK randomization strategy both phagemid libraries provide an excellent foundation to identify strong binding peptides in biopanning experiments.

In scope of this dissertation the 36-mer library was not employed to screen against Resomer® surfaces, but the library functionality was confirmed by biopanning experiments against streptavidin-coated microtiter wells (section 3.14). Firstly discovered by Devlin et al. (1990) the screening of peptide libraries against streptavidin led to isolation of peptide sequences mostly exhibiting a His-Pro convergence. Indeed, binding of the motifs HPQ and HPM to streptavidin was confirmed in other studies. It is assumed that HPQ and HPM mimic the functional properties of biotin and bind to the same streptavidin binding site (Weber et al., 1992). After the second round of selection against the target molecule streptavidin 12 of 15 isolated peptide sequences harbored the HPQ or HPM motif confirming the functionality of the 36-mer library.

The 24-mer library was employed to screen against Resomer® surfaces to identify strong binding peptide sequences (section 3.13). After four rounds of selection, potential strong binding peptide sequences were identified by DNA sequencing of re-infected *E. coli* cells following the 3rd and 4th round of biopanning. The frequency of a peptide sequence in a phagemid pool is generally considered indicative of specific binding to the target, as strong binding phagemid clones are gradually propagated in subsequent rounds of selection and amplification (Smith and Petrenko, 1997). Analysis of library clones from re-infected cells after the 3rd and 4th round of biopanning demonstrated that two peptide sequences, referred to as Resomer® binding peptides 1 (RBP1) and RBP2 (Supplementary Material, Figure S 14), dominated the enriched phagemid pool.

It is important to consider that each round of biopanning carries the risk of not only selecting for strong binding peptides, but also for sequences that bind to non-target materials, e.g. plastics or BSA. Furthermore, the risk of amplifying non-selective clones with propagation advantages increases with every biopanning round (Vodnik et al., 2011). These so-called background phages increase the chances of false positive hits, which is a frequent problem in phage display screenings (’t Hoen et al., 2012, Vodnik et al., 2011). To minimize the selection of background phages, the tubes containing the Resomer® surface were constantly exchanged after each washing step. Successful identification of strong binding peptides also depends on the experimental conditions employed in the washing and binding procedures during biopanning, such as the buffer composition, pH, incubation time, and temperature (Clackson and Lowman, 2004). Hyperphages were used for the packaging of phagemid particles in the first two rounds to promote multivalent display of peptides on the phage’s surface while reducing the risk of losing promising candidates at the same time. In the third round of biopanning, helper phages were employed for the packaging of phagemid particles resulting in monovalent display of peptides. The switch from hyperphage to helper phage shall increase the stringency of the selection procedure and facilitate the identification of peptides binding with high affinity

to the target surface. A population of strong binding phagemid particles can typically be enriched with three to four rounds of biopanning (Smith and Petrenko, 1997).

Taking a closer look at the amino acid sequence of RBP1 and RBP2 revealed that both peptides begin with a charged arginine (R) residue and contain high proportions of hydrophobic residues such as A, I, L, H, T, F, W, V (RBP1, 33.33 % and RBP2, 50 %) (Supplementary Material, Figure S 14). While RBP1 harbors many S (25 %) residues, RBP2 contains an abundance of W (12.5 %), A (16.7 %) and R (12.5 %) residues. Furthermore, both peptide motifs are rich in P (16.7–20 %) while other residues (e.g. K, Y or E) are missing completely.

To address how these biases might arise, it is crucial to consider the following information. In the beginning of phagemid library production, a repertoire of unbiased peptides is available, but as selection pressure increases during biopanning, bias and censorship of certain amino acids can occur on many levels (Sloth et al., 2022). For instance, bias can arise from the propagation of preferred peptide sequences or amino acid positions, resulting in the gradual dominance of "fast-growing" clones in pools of successive amplification rounds (Matochko et al., 2012). Biological censorship is a term used to describe the loss of specific peptide sequences caused by incompatibility between the host and phage during the M13 life cycle. Certain amino acid positions or peptide sequences can affect various processes such as host cell infection, phage particle packaging, proteolytic processing of p3, or release phagemid particles from the cell (Krumpe et al., 2007, Rodi et al., 2002).

Censorship of R through the Sec pathway is well known in literature. A previous study reported that phage production rate reversely correlates with the number of positively charged residues (R and K) in the peptide sequence (Peters et al., 1994). In particular N-terminal R residues of peptides are known to be censored as positively charged residues near the signal peptide cleavage site hamper translocation of p3 across the inner membrane to the periplasm and prevent the secretion of phage particles (Yamane and Mizushima, 1988, Andersson and von Heijne, 1991). Contrary to these findings, both peptides RBP1 and RBP2 start with R, a phenomenon for which an explanation has yet to be found. Other peptide sequences strongly affect the processing at the signal peptidase cleavage site. The first amino acid after the signal peptide cleavage site has a strong impact on the cleavage rate of the signal peptide determining the display level of peptides fused to p3 (Shen et al., 1991). Peptide sequences suppressing cleavage are most likely not dominantly represented in the library whereas sequences well cleaved are favored and well propagated in the library. In libraries where the randomized peptide sequence follows the signal peptidase cleavage site the presence of P in the beginning (+1 position) is notably scarce. Proline is known to inhibit efficient peptidase cleavage and hence proper proteolytic processing of p3 (Blond-Elguindi et al., 1993, Cwirla et al., 1990). Indeed, none of the peptide sequences found after biopanning (Supplementary Material, Table S 4 and Table S 5) started with P supporting these notions. Rodi et al (2002) found that α-helical and ß-sheet conformations delay the

periplasmic export of peptides decreasing the chances of display on the phage's surface. In line with these findings it was indicated in another study that folded proteins are generally not well translocated by the Sec pathway (Steiner et al., 2006). Furthermore, sequence bias against unpaired cysteine residues was reported leading to censorship of this residue throughout the peptide sequence. Unpaired cysteine residues tend to form intramolecular disulfide bridges with intrinsic cysteines of p3 which interfere with processes of phage assembly and/or infection (McConnell et al., 1996). In line with these theories, the majority of peptide sequences found after biopanning contained two cysteines or no cysteine residues at all (Supplementary Material, Table S 4 and Table S 5).

To evaluate the binding of RBP1 and RBP2 to Resomer® in a qualitative manner, a pulldown assay was developed (section 4.13). The results of the pulldown assay revealed that RBP2 specifically binds to Resomer® surfaces, whereas no binding was observed for RBP1 (Figure 25). Enrichment of RBP1 during biopanning may result from propagation advantages of phagemid particles harboring this sequence or from non-target-related binding events during selection. A heptapeptide, QLMHDYR, which was reported to recognize the α form of poly-L-lactic acid (PLLA) crystalline films (Matsuno et al., 2008) was included in the pulldown assay. However, no interaction with Resomer® was observed (unpublished data). Peptides recognizing polymers are known to bind through π–π interactions, hydrophobic and/or electrostatic interactions (Rubsam et al., 2018). In general, binding of peptides to polymers can be affected by various peptide properties, such as conformation, amino acid content, structure or chemical composition (Hnilova et al., 2008). For instance, peptides binding to polystyrene typically contain aromatic residues (F, Y, W) and motifs such as WXXW (X = any amino acid) (Menendez and Scott, 2005) which was also present in RBP2. The nature of binding most likely occurs by π–π interactions, so stacking of aromatic ring systems present in the side chains of aromatic residues and the benzene ring of polystyrene (Adey et al., 1995, Serizawa et al., 2011). As mentioned before, RBP2 has an exceptionally high proportion of hydrophobic residues (50 %). Since benzene rings are missing in PDLLA biopolymers binding of RBP2 to Resomer® is assumed to occur by hydrophobic interaction but further studies are necessary to confirm this theory. Important to note is that peptide binding to polymers can also be affected by experimental conditions such as salt content, solvation and intra-peptide forces (Horinek et al., 2008). The pulldown assay only indicates whether the RBPs bind to Resomer® or not. Alternative methods such as quartz crystal microbalance (QCM) or surface plasmon resonance spectroscopy (SPR) can provide more detailed information on the binding affinities and kinetics (Thyparambil et al., 2012).

To design bifunctional peptides, RBP2 was fused to three selected AMPs at the N- and C-termini, respectively. The chosen AMPs, human defensin-3 (HBD3), human histatin-3 (HTN3), and dermcidin-1L (DCD-1L), have been extensively studied in the literature and are known for their broad antimicrobial activity against a wide range of pathogens (Hoover et al., 2003, Blotnick et al., 2017, Lai et al., 2005). All

three peptides are of human origin decreasing the risks of cytotoxicity (Wang, 2014). HBD3 and DCD-1L are even reported to exert antimicrobial activity against MRSA strains (Midorikawa et al., 2003, Steffen et al., 2006). To enhance the peptide's flexibility and keep the two activity domains separated a short GS linker was inserted between the two peptide-peptide conjugates. This way, the likelihood of unfavorable intramolecular interactions are minimized while the specific peptide functions are hopefully retained (Arai et al., 2001).

All six bifunctional peptides were fused to N-terminal Switchtags and produced by the Numaswitch™ technology (section 4.14). The fusion proteins were produced as IBs at high levels in *E. coli* (Figure 26A) and the refolding efficiencies ranged between 41–87 % (Figure 26B). However, TEV protease cleavage for removal of the Switchtag from bifunctional peptides was only successful for HBD3-RBP2, HTN3-RBP2, and DCD-1L-RBP2 as cleavage efficiencies of 50–90 % were reached. For the remaining constructs, RBP2-HBD3, RBP2-HTN3 and RBP2-DCD-1L, no or very low cleavage efficiencies were observed (0–5 %) (Figure 26B–C). Here, as the RBP2 begins with a R and simultaneously represents the P1' position of the upstream TEV cleavage site (ENLYFQ) efficient cleavage from the Switchtag is obviously inhibited. This finding is in line with other reports where substitution of amino acids in the P1' position with R led to reduced cleavage efficiencies (Kapust et al., 2002). The canonical recognition sequence of the TEV protease with the highest catalytic efficiency is reported to be ENLYGQ-G/S where cleavage occurs between QG or QS (Parks et al., 1994). To overcome this issue, insertion of small residues such as G or S to the N-terminal end of the RBP2 to release non-native but potentially functional targets might be the solution. Alternatively, application of the Numacut™ TEV protease which was engineered to cleave the ENLYFQ sequence independently of the amino acid P1' position. Its cleavage efficiency on hard-to-cleave amino acids at P1' was demonstrated on different substrates (unpublished data). The Numacut™ TEV protease was not launched to the market until recently.

It was decided to only produce the bifunctional peptides HBD3-RBP2, HTN3-RBP2, and DCD-1L-RBP2 as they could be efficiently cleaved off from the Switchtag. All three bifunctional peptides were successfully produced from 5 L cultures in amounts of 1–15 mg. High purities of ≥ 95 % have been confirmed for each protein (Table 16). In addition, the identities of the targets were confirmed by RP-HPLC and/or RP-UPLC-MS analyses (Figure 27 and Supplementary Material, Figure S 16). The results emphasize the potential of the Numaswitch™ technology to produce a broad range of challenging peptides and pepteins including AMPs. Typically, AMPs are produced by chemical synthesis as current recombinant production platforms are hindered due to the cytotoxicity of AMPs towards host cells. Furthermore, AMPs are susceptible to proteolytic degradation in the cytoplasm, complicating large scale production and leading to high production costs (Roca-Pinilla et al., 2020). Fusion of Switchtags to AMPs induce the formation of IBs inside cells. This state deactivates the bioactivity of most peptides and proteins allowing high-titer expression without

harming the host cells. After IB extraction from cells, the biological functions can be effectively restored by refolding as demonstrated for HBD3-RBP2 and HTN3-RBP2 (Table 17).

Different assays were performed to assess whether the antimicrobial and adhesive functions of HBD3-RBP2, HTN3-RBP2 and DCD-1L-RBP2 remained intact. MIC assays confirmed the antimicrobial activity of HBD3-RBP2 and HTN3-RBP2 against *B. subtilis* but not *E. coli* strains (Table 17). HBD3-RBP2 exhibited lower antimicrobial efficacy against *B. subtilis* compared to the reference peptide HBD3. The mechanism of action for HBD3 entails binding to lipid-II-rich regions of the cell wall resulting in the inhibition of membrane synthesis (Sass et al., 2008). It is assumed that C-terminal fusion of RBP2 to HBD3 disrupts this interaction reducing the antimicrobial activity of HBD3. Consistent with this hypothesis, previous studies revealed the importance of two C-terminal R residues for the antimicrobial activity of HBD3 (Sakagami-Yasui et al., 2017). HBD3 harbors six cysteine residues forming three intramolecular disulfide bridges. However, several reports confirmed that the antimicrobial activity takes place regardless of disulfide bond formation (Wu et al., 2003, Dhingra et al., 2021).

In contrast, the MIC values obtained for HTN3-RBP2 indicated increased antimicrobial activity against *B. subtilis* in comparison to reference peptide HTN3. The mechanism of action for HTN3 involves binding of the N-terminal peptide domain to metal ions like Cu^{2+} or Ni^{2+} to generate reactive oxygen species which damage the cell membrane and lead to cell death (Melino et al., 2013). Since RBP2 was fused to the C-terminus of HTN3, it was anticipated that the antimicrobial activity would stay unaffected, a hypothesis supported by obtained MIC data (Table 17). The reason HBD3-RBP2 and HTN3-RBP2 exhibited antimicrobial activity against *B. subtilis* but not *E. coli* is most likely attributed to different compositions of the bacterial cell walls. Typically, Gram-negative bacteria are more resistant against AMPs than Gram-positive bacteria as they harbor an outer membrane that needs to be penetrated firstly before reaching the inner membrane (Huan et al., 2020). However, MIC values of ≥ 1 µM were described for HBD3 against *B. subtilis* inconsistent with our data (Joly et al., 2004). MIC assays indicated that neither DCD-1L-RBP2 nor DCD-1L displayed antimicrobial activity against *B. subtilis* or *E. coli*, despite earlier reports indicating MIC values of 10 µg/mL for *E. coli* with DCD-1L (Schittek et al., 2001). However, the lack of uniformity in the conduction of MIC assays makes it challenging to compare MIC values across different experiments.

Pulldown assay confirmed specific binding of HBD3-RBP2 to Resomer® beads, while HTN3-RBP2 did not seem to bind (Figure 28). Reconstitution of HTN3-RBP2 in Tris-HCl-based buffer seem to induce protein aggregation as distinct protein bands at higher MWs in the load and supernatant fractions were observed. This might explain why no binding to Resomer® beads was observed. So far, other reconstitution buffers have not yet been tested for HTN3-RBP2. Among three designed and tested bifunctional peptides, only HBD3-RBP2 displayed retained antimicrobial and Resomer® binding properties. This underlines the suitability of HBD3-RBP2 to functionalize Resomer® coatings to inhibit bacterial growth on surfaces.

For proof-of-concept, the bacterial adhesion assay was established employing the *E. coli* PKL1162 strain which was shown to grow on Resomer® surfaces in the absence of mannan (Supplementary Material, Figure S 18). One key benefit of this strain over other *E. coli* variants is that it constitutively expresses GFP, enabling the monitoring of bacterial growth on surfaces by fluorescence readout (Hartmann et al., 2010). As the bifunctional peptide HTN3-RBP2 did not exhibit antimicrobial activity against *E. coli* in MIC assays (Table 17) this compound was deemed not suitable for the established bacterial adhesion assay. Therefore, the focus was shifted to the bifunctional peptide DS-THA which not only showed excellent antimicrobial activity against *E. coli* and *B. subtilis* in MIC assays (Table 17) but also bound to Resomer® beads (Figure 25). Indeed, DS-THA surpasses HBD3-RBP2 due to its antimicrobial properties against *E. coli* and lower MIC values against *B. subtilis* suggesting increased potency in combating pathogens. It is important to note that the antimicrobial activity of HBD3-RBP2 and DS-THA against primary pathogens in IAIs, specifically *S. epidermis* and *S. aureus*, still needs to be validated in future experiments (Kreis et al., 2022).

To assess whether DS-THA retains its antimicrobial property also after incorporation in Resomer® coatings different concentrations of DS-THA were integrated. The results from the bacterial adhesion assay indicated that incorporation of DS-THA at concentrations of ≥ 2 % (w/v) effectively inhibited growth of *E. coli* PKL1162 (Figure 29). Resomer® coatings loaded with 0.5 % (w/v) DS-THA yielded inconsistent results. It should be noted that the lyophilized DS-THA or kanamycin powder were poorly soluble in the organic solvent ethyl acetate. Therefore, it was assumed that the compounds were incorporated into Resomer® coatings in the form of small drug aggregates. After the Resomer® coating dried the surfaces were washed three times with PBS to remove peptide excess. However, this washing step is highly unpredictable and error-prone leading to different peptide washouts and thus to inconsistencies in experiment outcomes (Gollwitzer et al., 2003). It was difficult to determine the amount of DS-THA remaining in the coating after PBS washing, as the deviations varied significantly (unpublished data). The process of drug release from coatings is a more predictable process since the drug compounds are embedded deeper within the coating (Gollwitzer et al., 2003). Determining the amount of DS-THA remaining in the Resomer® coating was difficult and led to inconsistent results (unpublished data). In other experiments antibiotics like gentamicin, teicoplanin or vancomycin were incorporated in Resomer® biopolymers as drug carriers to prevent bacterial infections since it does not possess inherent antimicrobial activity (Gollwitzer et al., 2003, Thamvasupong and Viravaidya-Pasuwat, 2022). Although the experimental results were promising alternative drugs are required to prevent the spread of MRSA strains (Brumfitt and Hamilton-Miller, 1989). Windolf et al. (2014) demonstrated that Resomer® coatings containing the antibacterial enzyme lysostaphin efficiently prevented bacterial infection by *S. aureus* in mouse models. In similar approaches like in this work, bifunctional peptides comprising of an AMP and a titanium binding peptide were designed to coat titanium implants. The potential of this approach to reduce bacterial growth on titanium implants was confirmed in *in vitro*

experiments (Yazici et al., 2016). In our approach, the adhesive property of bifunctional peptide was not directed against the implant material but the biopolymer Resomer® aiming to retain them within the polymer matrix to enhance their antimicrobial effectiveness. Further studies are needed before considering its application in human medical use. Subsequent sections elaborate on the required studies to use Resomer® coatings containing bifunctional peptides in human medical contexts.

In forthcoming experiments the elution profiles of DS-THA from Resomer® coatings need to be investigated. In theory, the peptides should reside inside the coating immobilized by the Resomer® binding domain within bifunctional peptides. However, whether they remain in the Resomer® coating in *in vitro* or even *in vivo* systems, and if so, for how long, still needs to be proven in additional experiments. The release profiles of compounds from Resomer® coatings are highly influenced by the ratio of polymer, solvent and drug, allowing for the adjustment of either immediate or prolonged release profiles (Strobel et al., 2011). Burst release models include rapid release of incorporated drugs over short time periods which lead in a sudden concentration surge that might induce local cytotoxicity. This process is difficult to control and generally considered as undesirable (Bhattacharjee, 2021). In contrast, sustained release profiles provide enhanced predictability and enable prolonged drug delivery. By regulating the gradual release of drugs in coatings sustained release formulations can uphold a steady drug concentration level in the bloodstream or targeted tissues (Sun et al., 2014, Bhattacharjee, 2021).

Furthermore, the upcoming experiments should also investigate the duration of the antimicrobial effect. In general, IAIs can occur in early stages (within 3 months of surgery), in delayed stages (between 3 to 24 months after surgery) or even in late stages (more than 2 years after surgery) (Davidson et al., 2019). Therefore, developing implant coatings capable of delivering continuous antimicrobial efficacy over prolonged periods would be advantageous.

The key requirement for implant coatings in human medical use is their biocompatibility (Huzum et al., 2021). To ensure that the coating does not hinder the healing process and exert any cytotoxic effects towards eukaryotic cells is mandatory. Following implant insertion, a commonly known phrase referred to as the "race for the surface" ensues involving a competition between host eukaryotic cells and bacteria to interact with the implant surface (Gristina et al., 1988). If eukaryotic cells win tissue integration on the implant surface begins leading to reduced susceptibility to bacterial infection and improved ingrowth of bone to the implant surface (osseointegration). On the other hand, if bacteria dominate the implant surface biofilms are formed leading to bacterial infection and tissue damage caused by bacterial virulence factors and toxins (Gristina et al., 1988). Alternative to strategies targeting bacteria reduction, many implant coating approaches focus on promoting the adhesion of eukaryotic cells in order to counteract bacterial colonization. Here, incorporation of bioactive minerals like hydroxyapatite (Ajami et al., 2021), cell-adhesion promoting RGD peptides (Ferris et al., 1999) or different growth factors (Bjelic and Finsgar, 2021) in implant coatings

stimulates osteoblast cell growth fostering bone regeneration and improving the efficacy of implant integration.

Last but not least, indispensable for medical application in humans are studies that validate the antimicrobial effect of the developed implant coating in complex *in vivo* animal models rather than simplified *in vitro* systems. Notably, not all implant coatings exhibiting favorable outcomes in *in vitro* experiments are capable of preventing biofilm formation in *in vivo* models (Arciola et al., 2012). For clinical use, it is important to understand how the antimicrobial coating functions within the complexity of a living organism, where various biological interactions and physiological conditions may influence its performance (Saeidnia et al., 2015). For example, PLGA (poly D, L-lactic-co-glycolic acid) nanofibers loaded with vancomycin demonstrated a prolonged drug release *in vivo* compared to *in vitro* systems presumably due to a slower metabolic rate in the *in vivo* environment (Liu et al., 2015).

To conclude, in this dissertation phagemid libraries were constructed displaying long-chained peptides with randomized sequences. These libraries were utilized to identify peptide motifs that bind to Resomer® surfaces, and one of the candidates, RBP2, was found to specifically bind to this biopolymer in binding assays. Bifunctional peptides were designed by fusing RBP2 with three different AMP candidates to create antimicrobial-adhesive peptide molecules. Various assays were conducted to determine if the biological functionalities of the respective domains were retained, and HBD3-RBP2 was found to be effective. Although HBD3-RBP2 and DS-THA bifunctional peptides demonstrated the ability to inhibit microbial activity and bind to Resomer®, further investigations are necessary to confirm their antimicrobial activity against the pathogens *S. epidermis* and *S. aureus* (Kreis et al., 2022). Nonetheless, HBD3-RBP2 displays promising potential in reducing bacterial adhesion on Resomer® coatings. Proof-of-concept was established with the bifunctional peptide DS-THA, which effectively inhibited *E. coli* PKL1162 strain growth on Resomer® coatings after incorporation.

6 Bibliography

'T Hoen PA, Jirka SMG, Ten Broeke BR, Schultes EA, Aguilera B, Pang KH, Heemskerk H, Aartsma-Rus A, Van Ommen GJ & Den Dunnen JT (2012) Phage display screening without repetitious selection rounds. *Anal Biochem.* 421**,** 622-31. doi: 10.1016/j.ab.2011.11.005

Abbaszadeh S, Bakhtiari N & Amini-Bayat Z (2019) Simple and effective purification of recombinant peptide drug, hPTH (1-34), expressed in *E. coli* host. *Int J Pept Res Ther.* 25**,** 419-25. doi: 10.1007/s10989-018-9685-x

Adey NB, Mataragnon AH, Rider JE, Carter JM & Kay BK (1995) Characterization of phage that bind plastic from phage-displayed random peptide libraries. *Gene.* 156**,** 27-31. doi: 10.1016/0378-1119(95)00058-e

Ajami E, Fu C, Wen HB, Bassett J, Park SJ & Pollard M (2021) Early bone healing on hydroxyapatite-coated and chemically-modified hydrophilic implant surfaces in an ovine Model. *Int J Mol Sci.* 22**,** 9361. doi: 10.3390/ijms22179361

Albarahmieh E, Albarahmieh M & Alkhalidi BA (2018) Fabrication of hierarchical polymeric thin films by spin coating toward production of amorphous solid dispersion for buccal drug delivery system: preparation, characterization, and *in vitro* release investigations. *J Pharm Sci.* 107**,** 3112-3122. doi: 10.1016/j.xphs.2018.08.019

Almagro JC, Pedraza-Escalona M, Arrieta HI & Perez-Tapia SM (2019) Phage display libraries for antibody therapeutic discovery and development. *Antibodies.* 8**,** 44. doi: 10.3390/antib8030044

Amin Yavari S, Castenmiller SM, Van Strijp JaG & Croes M (2020) Combating implant infections: Shifting focus from bacteria to host. *Adv Mater.* 32**,** e2002962. doi: 10.1002/adma.202002962

Andersen C, Hughes C & Koronakis V (2001) Protein export and drug efflux through bacterial channel-tunnels. *Curr Opin Cell Biol.* 13**,** 412-6. doi: 10.1016/s0955-0674(00)00229-5

Andersen C, Koronakis E, Hughes C & Koronakis V (2002) An aspartate ring at the TolC tunnel entrance determines ion selectivity and presents a target for blocking by large cations. *Mol Microbiol.* 44**,** 1131-9. doi: 10.1046/j.1365-2958.2002.02898.x

Andersson H & Von Heijne G (1991) A 30-residue-long "export initiation domain" adjacent to the signal sequence is critical for protein translocation across the inner membrane of *Escherichia coli*. *PNAS.* 88**,** 9751-4. doi: 10.1073/pnas.88.21.9751

Anwar H, Dasgupta MK & Costerton JW (1990) Testing the susceptibility of bacteria in biofilms to antibacterial agents. *Antimicrob Agents Chemother.* 34**,** 2043-6. doi: 10.1128/AAC.34.11.2043

Arai R, Ueda H, Kitayama A, Kamiya N & Nagamune T (2001) Design of the linkers which effectively separate domains of a bifunctional fusion protein. *Protein Eng.* 14**,** 529-32. doi: 10.1093/protein/14.8.529

Arciola CR, Campoccia D, Speziale P, Montanaro L & Costerton JW (2012) Biofilm formation in *Staphylococcus* implant infections. A review of molecular mechanisms and implications for biofilm-resistant materials. *Biomaterials.* 33**,** 5967-82. doi: 10.1016/j.biomaterials.2012.05.031

Ayhan DH, Tamer YT, Akbar M, Bailey SM, Wong M, Daly SM, Greenberg DE & Toprak E (2016) Sequence-specific targeting of bacterial resistance genes increases antibiotic efficacy. *PLoS Biol.* 14**,** e1002552. doi: 10.1371/journal.pbio.1002552

Baeshen MN, Al-Hejin AM, Bora RS, Ahmed MM, Ramadan HA, Saini KS, Baeshen NA & Redwan EM (2015) Production of biopharmaceuticals in *E. coli*: Current scenario and future perspectives. *J Microbiol Biotechnol.* 25**,** 953-62. doi: 10.4014/jmb.1412.12079

Bakas L, Veiga MP, Soloaga A, Ostolaza H & Goni FM (1998) Calcium-dependent conformation of *E. coli* alpha-haemolysin. Implications for the mechanism of membrane insertion and lysis. *Biochim Biophys Acta.* 1368**,** 225-34. doi: 10.1016/s0005-2736(97)00181-8

Bakkes PJ, Jenewein S, Smits SH, Holland IB & Schmitt L (2010) The rate of folding dictates substrate secretion by the *Escherichia coli* hemolysin type 1 secretion system. *J Biol Chem.* 285**,** 40573-80. doi: 10.1074/jbc.M110.173658

Balakrishnan L, Hughes C & Koronakis V (2001) Substrate-triggered recruitment of the TolC channel-tunnel during Type I export of hemolysin by *Escherichia coli*. *J Mol Biol.* 313**,** 501-10. doi: 10.1006/jmbi.2001.5038

Bardwell JC, Mcgovern K & Beckwith J (1991) Identification of a protein required for disulfide bond formation *in vivo*. *Cell.* 67**,** 581-9. doi: 10.1016/0092-8674(91)90532-4

Baumann U (2019) Structure-function relationships of the repeat domains of RTX toxins. *Toxins.* 11**,** 657. doi: 10.3390/toxins11110657

Baumann U, Wu S, Flaherty KM & Mckay DB (1993) Three-dimensional structure of the alkaline protease of *Pseudomonas aeruginosa*: a two-domain protein with a calcium binding parallel beta roll motif. *EMBO J.* 12**,** 3357-64. doi: 10.1002/j.1460-2075.1993.tb06009.x

Benabdelhak H, Kiontke S, Horn C, Ernst R, Blight MA, Holland IB & Schmitt L (2003) A specific interaction between the NBD of the ABC-transporter HlyB and a C-terminal fragment of its transport substrate haemolysin A. *J Mol Biol.* 327**,** 1169-79. doi: 10.1016/s0022-2836(03)00204-3

Bennett NJ, Gagic D, Sutherland-Smith AJ & Rakonjac J (2011) Characterization of a dual-function domain that mediates membrane insertion and excision of Ff filamentous bacteriophage. *J Mol Biol.* 411**,** 972-85. doi: 10.1016/j.jmb.2011.07.002

Berkowitz SA & Day LA (1976) Mass, length, composition and structure of the filamentous bacterial virus fd. *J Mol Biol.* 102**,** 531-47. doi: 10.1016/0022-2836(76)90332-6

Beveridge TJ (1999) Structures of gram-negative cell walls and their derived membrane vesicles. *J Bacteriol.* 181**,** 4725-33. doi: 10.1128/JB.181.16.4725-4733.1999

Bhattacharjee S (2021) Understanding the burst release phenomenon: toward designing effective nanoparticulate drug-delivery systems. *Ther Deliv.* 12**,** 21-36. doi: 10.4155/tde-2020-0099

Bhatwa A, Wang W, Hassan YI, Abraham N, Li XZ & Zhou T (2021) Challenges associated with the formation of recombinant protein inclusion bodies in *Escherichia coli* and strategies to address them for industrial applications. *Front Bioeng Biotechnol.* 9**,** 630551. doi: 10.3389/fbioe.2021.630551

Bhushan S, Hossain H, Lu Y, Geisler A, Tchatalbachev S, Mikulski Z, Schuler G, Klug J, Pilatz A, Wagenlehner F, Chakraborty T & Meinhardt A (2011) Uropathogenic *E. coli* induce different immune response in testicular and peritoneal macrophages: implications for testicular immune privilege. *PLoS One.* 6**,** e28452. doi: 10.1371/journal.pone.0028452

Bjelic D & Finsgar M (2021) The role of growth factors in bioactive coatings. *Pharmaceutics.* 13**,** 1083. doi: 10.3390/pharmaceutics13071083

Blight MA & Holland IB (1994) Heterologous protein secretion and the versatile *Escherichia coli* haemolysin translocator. *Trends Biotechnol.* 12**,** 450-5. doi: 10.1016/0167-7799(94)90020-5

Blond-Elguindi S, Cwirla SE, Dower WJ, Lipshutz RJ, Sprang SR, Sambrook JF & Gething MJ (1993) Affinity panning of a library of peptides displayed on bacteriophages reveals the binding specificity of BiP. *Cell.* 75**,** 717-28. doi: 10.1016/0092-8674(93)90492-9

Blotnick E, Sol A, Bachrach G & Muhlrad A (2017) Interactions of histatin-3 and histatin-5 with actin. *BMC Biochem.* 18**,** 3. doi: 10.1186/s12858-017-0078-0

Breitling F, Broders O, Helmsing S, Hust M & Dübel S (2010) Improving phage display throughput by using hyperphage, miniaturized titration and pVIII (g8p) ELISA. In: Kontermann R & Dübel S (eds.) *Antibody Engineering,* Springer Protocols Handbooks, vol 2. Springer, Berlin, Heidelberg. 197-206, doi: 10.1007/978-3-642-01144-3_14

Breitling F, Dubel S, Seehaus T, Klewinghaus I & Little M (1991) A surface expression vector for antibody screening. *Gene.* 104**,** 147-53. doi: 10.1016/0378-1119(91)90244-6

Bruellhoff K, Fiedler J, Moller M, Groll J & Brenner RE (2010) Surface coating strategies to prevent biofilm formation on implant surfaces. *Int J Artif Organs.* 33**,** 646-53. doi: 10.1177/039139881003300910

Brumfitt W & Hamilton-Miller J (1989) Methicillin-resistant *Staphylococcus aureus*. *N Engl J Med.* 320**,** 1188-96. doi: 10.1056/NEJM198905043201806

Bulleid NJ (2012) Disulfide bond formation in the mammalian endoplasmic reticulum. *Cold Spring Harb Perspect Biol.* 4**,** a013219. doi: 10.1101/cshperspect.a013219

Bumba L, Masin J, Macek P, Wald T, Motlova L, Bibova I, Klimova N, Bednarova L, Veverka V, Kachala M, Svergun DI, Barinka C & Sebo P (2016) Calcium-driven folding of RTX domain beta-rolls ratchets translocation of RTX proteins through Type I secretion ducts. *Mol Cell.* 62**,** 47-62. doi: 10.1016/j.molcel.2016.03.018

Campoccia D, Montanaro L & Arciola CR (2013) A review of the biomaterials technologies for infection-resistant surfaces. *Biomaterials.* 34**,** 8533-54. doi: 10.1016/j.biomaterials.2013.07.089

Carmen S & Jermutus L (2002) Concepts in antibody phage display. *Brief Funct Genomic Proteomic.* 1**,** 189-203. doi: 10.1093/bfgp/1.2.189

Carpenter G & Cohen S (1990) Epidermal growth factor. *J Biol Chem.* 265**,** 7709-12.

Cavalieri SJ, Bohach GA & Snyder IS (1984) *Escherichia coli* alpha-hemolysin: characteristics and probable role in pathogenicity. *Microbiol Rev.* 48**,** 326-43. doi: 10.1128/mr.48.4.326-343.1984

Chang JY, Li L & Lai PH (2001) A major kinetic trap for the oxidative folding of human epidermal growth factor. *J Biol Chem.* 276**,** 4845-52. doi: 10.1074/jbc.M005160200

Chasteen L, Ayriss J, Pavlik P & Bradbury AR (2006) Eliminating helper phage from phage display. *Nucleic Acids Res.* 34**,** e145. doi: 10.1093/nar/gkl772

Chen CH, Bepler T, Pepper K, Fu D & Lu TK (2022) Synthetic molecular evolution of antimicrobial peptides. *Curr Opin Biotechnol.* 75**,** 102718. doi: 10.1016/j.copbio.2022.102718

Chen X, Zhou J, Qian Y & Zhao L (2023) Antibacterial coatings on orthopedic implants. *Materials Today Bio.* 19**,** 100586. doi: 10.1016/j.mtbio.2023.100586

Clackson T & Lowman HB (eds) (2004) Phage Display: A Practical Approach. *Oxford University Press*, New York

Costa F, Carvalho IF, Montelaro RC, Gomes P & Martins MC (2011) Covalent immobilization of antimicrobial peptides (AMPs) onto biomaterial surfaces. *Acta Biomater.* 7**,** 1431-40. doi: 10.1016/j.actbio.2010.11.005

Costa S, Almeida A, Castro A & Domingues L (2014) Fusion tags for protein solubility, purification and immunogenicity in *Escherichia coli*: the novel Fh8 system. *Front Microbiol.* 5**,** 63. doi: 10.3389/fmicb.2014.00063

Cremers CM, Knoefler D, Vitvitsky V, Banerjee R & Jakob U (2014) Bile salts act as effective protein-unfolding agents and instigators of disulfide stress *in vivo*. *PNAS.* 111**,** E1610-9. doi: 10.1073/pnas.1401941111

Cwirla SE, Peters EA, Barrett RW & Dower WJ (1990) Peptides on phage: a vast library of peptides for identifying ligands. *PNAS.* 87**,** 6378-82. doi: 10.1073/pnas.87.16.6378

Dagert M & Ehrlich SD (1979) Prolonged incubation in calcium chloride improves the competence of *Escherichia coli* cells. *Gene.* 6**,** 23-8. doi: 10.1016/0378-1119(79)90082-9

Davidson DJ, Spratt D & Liddle AD (2019) Implant materials and prosthetic joint infection: the battle with the biofilm. *EFORT Open Rev.* 4**,** 633-639. doi: 10.1302/2058-5241.4.180095

Dawson PE, Muir TW, Clark-Lewis I & Kent SB (1994) Synthesis of proteins by native chemical ligation. *Science.* 266**,** 776-9. doi: 10.1126/science.7973629

Deng X, Wang L, You X, Dai P & Zeng Y (2018) Advances in the T7 phage display system. *Mol Med Rep.* 17**,** 714-20. doi: 10.3892/mmr.2017.7994

Devlin JJ, Panganiban LC & Devlin PE (1990) Random peptide libraries: a source of specific protein binding molecules. *Science.* 249**,** 404-6. doi: 10.1126/science.2143033

Dhakal BK & Mulvey MA (2012) The UPEC pore-forming toxin alpha-hemolysin triggers proteolysis of host proteins to disrupt cell adhesion, inflammatory, and survival pathways. *Cell Host Microbe.* 11**,** 58-69. doi: 10.1016/j.chom.2011.12.003

Dhingra H, Kaur K & Singh B (2021) Engineering and characterization of human beta-defensin-3 and its analogues and microcin J25 peptides against Mannheimia haemolytica and bovine neutrophils. *Vet Res.* 52**,** 83. doi: 10.1186/s13567-021-00956-4

Di Guan C, Li P, Riggs PD & Inouye H (1988) Vectors that facilitate the expression and purification of foreign peptides in *Escherichia coli* by fusion to maltose-binding protein. *Gene.* 67**,** 21-30. doi: 10.1016/0378-1119(88)90004-2

Dotto GP, Enea V & Zinder ND (1981) Functional analysis of bacteriophage f1 intergenic region. *Virology.* 114**,** 463-73. doi: 10.1016/0042-6822(81)90226-9

Drapeau GR, Boily Y & Houmard J (1972) Purification and properties of an extracellular protease of *Staphylococcus aureus*. *J Biol Chem.* 247**,** 6720-6. doi: 10.1016/S0021-9258(19)44749-2

Dyballa N & Metzger S (2009) Fast and sensitive colloidal coomassie G-250 staining for proteins in polyacrylamide gels. *J Vis Exp.* 1431. doi: 10.3791/1431

Evonik (2023) Biodegradable polymers for controlled release [Online]. Accessed: 23 Apr 2023. Available: https://healthcare.evonik.com/en/drugdelivery/parenteral-drug-delivery/parenteral-excipients/bioresorbable-polymers/standard-polymers

Fagerlund A, Myrset AH & Kulseth MA (2008) Construction and characterization of a 9-mer phage display pVIII-library with regulated peptide density. *Appl Microbiol Biotechnol.* 80**,** 925-36. doi: 10.1007/s00253-008-1630-z

Fantini M, Pandolfini L, Lisi S, Chirichella M, Arisi I, Terrigno M, Goracci M, Cremisi F & Cattaneo A (2017) Assessment of antibody library diversity through next generation sequencing and technical error compensation. *PLoS One.* 12**,** e0177574. doi: 10.1371/journal.pone.0177574

Felmlee T, Pellett S & Welch RA (1985) Nucleotide sequence of an *Escherichia coli* chromosomal hemolysin. *J Bacteriol.* 163**,** 94-105. doi: 10.1128/jb.163.1.94-105.1985

Fernandez LA, Sola I, Enjuanes L & De Lorenzo V (2000) Specific secretion of active single-chain Fv antibodies into the supernatants of *Escherichia coli* cultures by use of the hemolysin system. *Appl Environ Microbiol.* 66**,** 5024-9. doi: 10.1128/AEM.66.11.5024-5029.2000

Ferris DM, Moodie GD, Dimond PM, Gioranni CW, Ehrlich MG & Valentini RF (1999) RGD-coated titanium implants stimulate increased bone formation *in vivo*. *Biomaterials.* 20**,** 2323-31. doi: 10.1016/s0142-9612(99)00161-1

Filloux A (2022) Bacterial protein secretion systems: Game of types. *Microbiology.* 168. doi: 10.1099/mic.001193

Fridy PC, Li Y, Keegan S, Thompson MK, Nudelman I, Scheid JF, Oeffinger M, Nussenzweig MC, Fenyo D, Chait BT & Rout MP (2014) A robust pipeline for rapid production of versatile nanobody repertoires. *Nat Methods.* 11**,** 1253-60. doi: 10.1038/nmeth.3170

Friedberg F, Winnick T & Greenberg DM (1947) Peptide synthesis *in vivo*. *J Biol Chem.* 169**,** 763.

Gaskin DJ, Starck K, Turner NA & Vulfson EN (2001) Phage display combinatorial libraries of short peptides: ligand selection for protein purification. *Enzyme Microb Technol.* 28**,** 766-772. doi: 10.1016/s0141-0229(01)00330-1

Gierej A, Vagenende M, Filipkowski A, Siwicki B, Buczynski R, Thienpont H, Van Vlierberghe S, Geernaert T, Dubruel P & Berghmans F (2019) Poly(D,L-Lactic Acid) (PDLLA) biodegradable and biocompatible polymer optical fiber. *Journal of Lightwave Technology.* 37**,** 1916-23. doi: 10.1109/JLT.2019.2895220

Gollwitzer H, Ibrahim K, Meyer H, Mittelmeier W, Busch R & Stemberger A (2003) Antibacterial poly(D,L-lactic acid) coating of medical implants using a biodegradable drug delivery technology. *J Antimicrob Chemother.* 51**,** 585-91. doi: 10.1093/jac/dkg105

Goodwin S, Mcpherson JD & Mccombie WR (2016) Coming of age: ten years of next-generation sequencing technologies. *Nat Rev Genet.* 17**,** 333-51. doi: 10.1038/nrg.2016.49

Green ER & Mecsas J (2016) Bacterial secretion systems: An overview. *Microbiol Spectr.* 4. doi: 10.1128/microbiolspec.VMBF-0012-2015

Grieco SH, Lee S, Dunbar WS, Macgillivray RT & Curtis SB (2009) Maximizing filamentous phage yield during computer-controlled fermentation. *Bioprocess Biosyst Eng.* 32**,** 773-9. doi: 10.1007/s00449-009-0303-3

Gristina AG, Naylor P & Myrvik Q (1988) Infections from biomaterials and implants: a race for the surface. *Med Prog Technol.* 14**,** 205-24.

Gu L & Guo Z (2013) Alzheimer's Aβ42 and Aβ40 peptides form interlaced amyloid fibrils. *J Neurochem.* 126**,** 305-11. doi: 10.1111/jnc.12202

Guzman LM, Belin D, Carson MJ & Beckwith J (1995) Tight regulation, modulation, and high-level expression by vectors containing the arabinose PBAD promoter. *J Bacteriol.* 177**,** 4121-30. doi: 10.1128/jb.177.14.4121-4130.1995

Hamner S, Mcinnerney K, Williamson K, Franklin MJ & Ford TE (2013) Bile salts affect expression of *Escherichia coli* O157:H7 genes for virulence and iron acquisition, and promote growth under iron limiting conditions. *PLoS One.* 8**,** e74647. doi: 10.1371/journal.pone.0074647

Hamon MA, Batsche E, Regnault B, Tham TN, Seveau S, Muchardt C & Cossart P (2007) Histone modifications induced by a family of bacterial toxins. *PNAS.* 104**,** 13467-72. doi: 10.1073/pnas.0702729104

Hancock RE, Falla T & Brown M (1995) Cationic bactericidal peptides. *Adv Microb Physiol.* 37**,** 135-75. doi: 10.1016/s0065-2911(08)60145-9

Hannig G, Tchernychev B, Kurtz CB, Bryant AP, Currie MG & Silos-Santiago I (2014) Guanylate cyclase-C/cGMP: an emerging pathway in the regulation of visceral pain. *Front Mol Neurosci.* 7**,** 31. doi: 10.3389/fnmol.2014.00031

Hartmann M, Horst AK, Klemm P & Lindhorst TK (2010) A kit for the investigation of live *Escherichia coli* cell adhesion to glycosylated surfaces. *Chem Commun.* 46**,** 330-2. doi: 10.1039/b922525k

Havarstein LS, Diep DB & Nes IF (1995) A family of bacteriocin ABC transporters carry out proteolytic processing of their substrates concomitant with export. *Mol Microbiol.* 16**,** 229-40. doi: 10.1111/j.1365-2958.1995.tb02295.x

Hawkins TL, O'connor-Morin T, Roy A & Santillan C (1994) DNA purification and isolation using a solid-phase. *Nucleic Acids Res.* 22**,** 4543-4. doi: 10.1093/nar/22.21.4543

He B, Tjhung KF, Bennett NJ, Chou Y, Rau A, Huang J & Derda R (2018) Compositional bias in naive and chemically-modified phage-displayed libraries uncovered by paired-end deep sequencing. *Sci Rep.* 8**,** 1214. doi: 10.1038/s41598-018-19439-2

Hecker KH & Rill RL (1998) Error analysis of chemically synthesized polynucleotides. *Biotechniques.* 24**,** 256-60. doi: 10.2144/98242st01

Hedrick TL, Adams JD & Sawyer RG (2006) Implant-associated infections: an overview. *J Long Term Eff Med Implants.* 16**,** 83-99. doi: 10.1615/jlongtermeffmedimplants.v16.i1.90

Hnilova M, Oren EE, Seker UO, Wilson BR, Collino S, Evans JS, Tamerler C & Sarikaya M (2008) Effect of molecular conformations on the adsorption behavior of gold-binding peptides. *Langmuir.* 24**,** 12440-5. doi: 10.1021/la801468c

Holick MF (2005) PTH (1-34): a novel anabolic drug for the treatment of osteoporosis. *South Med J.* 98**,** 1114-7. doi: 10.1097/01.smj.0000140864.78760.8d

Hoogenboom HR, Griffiths AD, Johnson KS, Chiswell DJ, Hudson P & Winter G (1991) Multi-subunit proteins on the surface of filamentous phage: methodologies for displaying antibody (Fab) heavy and light chains. *Nucleic Acids Res.* 19**,** 4133-7. doi: 10.1093/nar/19.15.4133

Hoover DM, Wu Z, Tucker K, Lu W & Lubkowski J (2003) Antimicrobial characterization of human β-defensin 3 derivatives. *Antimicrob Agents Chemother.* 47**,** 2804-9. doi: 10.1128/AAC.47.9.2804-2809.2003

Horinek D, Serr A, Geisler M, Pirzer T, Slotta U, Lud SQ, Garrido JA, Scheibel T, Hugel T & Netz RR (2008) Peptide adsorption on a hydrophobic surface results from an interplay of solvation, surface, and intrapeptide forces. *PNAS.* 105**,** 2842-7. doi: 10.1073/pnas.0707879105

Hou W, Zhang X & Liu C-F (2017) Progress in chemical synthesis of peptides and proteins. *Trans Tianjin Univ.* 23**,** 401-19. doi: 10.1007/s12209-017-0068-8

Huan Y, Kong Q, Mou H & Yi H (2020) Antimicrobial peptides: Classification, design, application and research progress in multiple fields. *Front Microbiol.* 11**,** 582779. doi: 10.3389/fmicb.2020.582779

Hust M & Dubel S (2005) Phage display vectors for the *in vitro* generation of human antibody fragments. In: Burns R (ed.) *Immunochemical Protocols,* Methods In Molecular Biology, vol 295. Humana Press, Totowa, NJ. 71-96, doi: 10.1385/1-59259-873-0:071

Hust M, Meysing M, Schirrmann T, Selke M, Meens J, Gerlach GF & Dubel S (2006) Enrichment of open reading frames presented on bacteriophage M13 using hyperphage. *Biotechniques.* 41**,** 335-42. doi: 10.2144/000112225

Huzum B, Puha B, Necoara RM, Gheorghevici S, Puha G, Filip A, Sirbu PD & Alexa O (2021) Biocompatibility assessment of biomaterials used in orthopedic devices: An overview. *Exp Ther Med.* 22**,** 1315. doi: 10.3892/etm.2021.10750

Hwang J, Zhong X & Tai PC (1997) Interactions of dedicated export membrane proteins of the colicin V secretion system: CvaA, a member of the membrane fusion protein family, interacts with CvaB and TolC. *J Bacteriol.* 179**,** 6264-70. doi: 10.1128/jb.179.20.6264-6270.1997

Iannolo G, Minenkova O, Petruzzelli R & Cesareni G (1995) Modifying filamentous phage capsid: limits in the size of the major capsid protein. *J Mol Biol.* 248**,** 835-44. doi: 10.1006/jmbi.1995.0264

Implen (2022) OD_{600} Cell Density, Bacterial Growth, Yeast Growth [Online]. Accessed: 07 May 2023. Available: https://www.implen.de/od600-diluphotometer/od600/

Innovagen (2023) PepCalc.com - Peptide property calculator [Online]. Accessed: 23 Apr 2023. Available: https://pepcalc.com/

Ishikawa H, Kim S, Kwak K, Wakasugi K & Fayer MD (2007) Disulfide bond influence on protein structural dynamics probed with 2D-IR vibrational echo spectroscopy. *PNAS.* 104**,** 19309-14. doi: 10.1073/pnas.0709760104

Isidro-Llobet A, Kenworthy MN, Mukherjee S, Kopach ME, Wegner K, Gallou F, Smith AG & Roschangar F (2019) Sustainability challenges in peptide synthesis and purification: From R&D to production. *J Org Chem.* 84**,** 4615-28. doi: 10.1021/acs.joc.8b03001

Jakes KS (2017) The colicin E1 TolC box: Identification of a domain required for colicin E1 cytotoxicity and TolC binding. *J Bacteriol.* 199**,** e00412-16. doi: 10.1128/JB.00412-16

Johnson JR (1991) Virulence factors in *Escherichia coli* urinary tract infection. *Clin Microbiol Rev.* 4**,** 80-128. doi: 10.1128/CMR.4.1.80

Joly S, Maze C, Mccray PB, Jr. & Guthmiller JM (2004) Human β-defensins 2 and 3 demonstrate strain-selective activity against oral microorganisms. *J Clin Microbiol.* 42**,** 1024-9. doi: 10.1128/JCM.42.3.1024-1029.2004

Kanonenberg K, Spitz O, Erenburg IN, Beer T & Schmitt L (2018) Type I secretion system - it takes three and a substrate. *FEMS Microbiol Lett.* 365. doi: 10.1093/femsle/fny094

Kapust RB, Tozser J, Copeland TD & Waugh DS (2002) The P1' specificity of *tobacco etch virus* protease. *Biochem Biophys Res Commun.* 294**,** 949-55. doi: 10.1016/S0006-291X(02)00574-0

Kenny B, Haigh R & Holland IB (1991) Analysis of the haemolysin transport process through the secretion from *Escherichia coli* of PCM, CAT or β-galactosidase fused to the Hly C-terminal signal domain. *Mol Microbiol.* 5**,** 2557-68. doi: 10.1111/j.1365-2958.1991.tb02102.x

Khosa S, Scholz R, Schwarz C, Trilling M, Hengel H, Jaeger KE, Smits SHJ & Schmitt L (2018) An A/U-Rich enhancer region is required for high-level protein secretion through the HlyA Type I secretion system. *Appl Environ Microbiol.* 84. doi: 10.1128/AEM.01163-17

Kim YS, Lee HJ, Han MH, Yoon NK, Kim YC & Ahn J (2021) Effective production of human growth factors in *Escherichia coli* by fusing with small protein 6HFh8. *Microb Cell Fact.* 20**,** 9. doi: 10.1186/s12934-020-01502-1

King DS, Fields CG & Fields GB (1990) A cleavage method which minimizes side reactions following Fmoc solid phase peptide synthesis. *Int J Pept Protein Res.* 36**,** 255-66. doi: 10.1111/j.1399-3011.1990.tb00976.x

Kloft N, Busch T, Neukirch C, Weis S, Boukhallouk F, Bobkiewicz W, Cibis I, Bhakdi S & Husmann M (2009) Pore-forming toxins activate MAPK p38 by causing loss of cellular potassium. *Biochem Biophys Res Commun.* 385**,** 503-6. doi: 10.1016/j.bbrc.2009.05.121

Kobashi K (1968) Catalytic oxidation of sulfhydryl groups by o-phenanthroline copper complex. *Biochim Biophys Acta.* 158**,** 239-45. doi: 10.1016/0304-4165(68)90136-0

Koronakis V, Sharff A, Koronakis E, Luisi B & Hughes C (2000) Crystal structure of the bacterial membrane protein TolC central to multidrug efflux and protein export. *Nature.* 405**,** 914-9. doi: 10.1038/35016007

Koschinski A, Repp H, Unver B, Dreyer F, Brockmeier D, Valeva A, Bhakdi S & Walev I (2006) Why *Escherichia coli* alpha-hemolysin induces calcium oscillations in mammalian cells - the pore is on its own. *FASEB J.* 20**,** 973-5. doi: 10.1096/fj.05-4561fje

Kreis C, Aschenbrenner FK, Gunther D, Tholema-Hans N, Koeppe J, Rosslenbroich SB, Raschke MJ & Fuchs T (2022) Establishment of a reliable *in vivo* model of implant-associated infection to investigate innovative treatment options. *Sci Rep.* 12**,** 3979. doi: 10.1038/s41598-022-07673-8

Krumpe LR, Atkinson AJ, Smythers GW, Kandel A, Schumacher KM, Mcmahon JB, Makowski L & Mori T (2006) T7 lytic phage-displayed peptide libraries exhibit less sequence bias than M13 filamentous phage-displayed peptide libraries. *Proteomics.* 6**,** 4210-22. doi: 10.1002/pmic.200500606

Krumpe LR, Schumacher KM, Mcmahon JB, Makowski L & Mori T (2007) Trinucleotide cassettes increase diversity of T7 phage-displayed peptide library. *BMC Biotechnol.* 7**,** 65. doi: 10.1186/1472-6750-7-65

Kuhn A & Wickner W (1985) Isolation of mutants in M13 coat protein that affect its synthesis, processing, and assembly into phage. *J Biol Chem.* 260**,** 15907-13.

Lai YP, Peng YF, Zuo Y, Li J, Huang J, Wang LF & Wu ZR (2005) Functional and structural characterization of recombinant dermcidin-1L, a human antimicrobial peptide. *Biochem Biophys Res Commun.* 328**,** 243-50. doi: 10.1016/j.bbrc.2004.12.143

Lau JL & Dunn MK (2018) Therapeutic peptides: Historical perspectives, current development trends, and future directions. *Bioorg Med Chem.* 26**,** 2700-07. doi: 10.1016/j.bmc.2017.06.052

Lecher J, Schwarz CK, Stoldt M, Smits SH, Willbold D & Schmitt L (2012) An RTX transporter tethers its unfolded substrate during secretion via a unique N-terminal domain. *Structure.* 20**,** 1778-87. doi: 10.1016/j.str.2012.08.005

Ledsgaard L, Kilstrup M, Karatt-Vellatt A, Mccafferty J & Laustsen AH (2018) Basics of antibody phage display technology. *Toxins.* 10**,** 236. doi: 10.3390/toxins10060236

Lee BK, Yun Y & Park K (2016) PLA micro- and nano-particles. *Adv Drug Deliv Rev.* 107**,** 176-191. doi: 10.1016/j.addr.2016.05.020

Lee CM, Iorno N, Sierro F & Christ D (2007) Selection of human antibody fragments by phage display. *Nat Protoc.* 2**,** 3001-8. doi: 10.1038/nprot.2007.448

Leeds JA & Welch RA (1997) Enhancing transcription through the *Escherichia coli* hemolysin operon, hlyCABD: RfaH and upstream JUMPStart DNA sequences function together via a postinitiation mechanism. *J Bacteriol.* 179**,** 3519-27. doi: 10.1128/jb.179.11.3519-3527.1997

Lenders MH, Beer T, Smits SH & Schmitt L (2016) *In vivo* quantification of the secretion rates of the hemolysin A Type I secretion system. *Sci Rep.* 6**,** 33275. doi: 10.1038/srep33275

Lenders MH, Weidtkamp-Peters S, Kleinschrodt D, Jaeger KE, Smits SH & Schmitt L (2015) Directionality of substrate translocation of the hemolysin A Type I secretion system. *Sci Rep.* 5**,** 12470. doi: 10.1038/srep12470

Leproust EM, Peck BJ, Spirin K, Mccuen HB, Moore B, Namsaraev E & Caruthers MH (2010) Synthesis of high-quality libraries of long (150mer) oligonucleotides by a novel depurination controlled process. *Nucleic Acids Res.* 38**,** 2522-40. doi: 10.1093/nar/gkq163

Li H, Wang D, Zhang W, Xu G, Xu C, Liu W & Li J (2023) Potential side effects of antibacterial coatings in orthopaedic implants: A systematic review of clinical studies. *Front Bioeng Biotechnol.* 11**,** 1111386. doi: 10.3389/fbioe.2023.1111386

Lin YM, Boccaccini AR, Polak JM, Bishop AE & Maquet V (2006) Biocompatibility of poly-DL-lactic acid (PDLLA) for lung tissue engineering. *J Biomater Appl.* 21**,** 109-18. doi: 10.1177/0885328206057952

Linhartova I, Bumba L, Masin J, Basler M, Osicka R, Kamanova J, Prochazkova K, Adkins I, Hejnova-Holubova J, Sadilkova L, Morova J & Sebo P (2010) RTX proteins: a highly diverse family secreted by a common mechanism. *FEMS Microbiol Rev.* 34**,** 1076-112. doi: 10.1111/j.1574-6976.2010.00231.x

Liu J, Chang W, Pan L, Liu X, Su L, Zhang W, Li Q & Zheng Y (2018) An improved method of preparing high efficiency transformation *Escherichia coli* with both plasmids and larger DNA fragments. *Indian J Microbiol.* 58**,** 448-56. doi: 10.1007/s12088-018-0743-z

Liu KS, Lee CH, Wang YC & Liu SJ (2015) Sustained release of vancomycin from novel biodegradable nanofiber-loaded vascular prosthetic grafts: *in vitro* and *in vivo* study. *Int J Nanomedicine.* 10**,** 885-91. doi: 10.2147/IJN.S78675

Liu Y, Mao J, Zhou B, Wei W & Gong S (2010) Peptide aptamers against titanium-based implants identified through phage display. *J Mater Sci Mater Med.* 21**,** 1103-7. doi: 10.1007/s10856-009-3970-3

Lobstein J, Emrich CA, Jeans C, Faulkner M, Riggs P & Berkmen M (2012) SHuffle, a novel *Escherichia coli* protein expression strain capable of correctly folding disulfide bonded proteins in its cytoplasm. *Microb Cell Fact.* 11**,** 56. doi: 10.1186/1475-2859-11-56

Loh B, Kuhn A & Leptihn S (2019) The fascinating biology behind phage display: filamentous phage assembly. *Mol Microbiol.* 111**,** 1132-38. doi: 10.1111/mmi.14187

Lowman HB, Bass SH, Simpson N & Wells JA (1991) Selecting high-affinity binding proteins by monovalent phage display. *Biochemistry.* 30**,** 10832-8. doi: 10.1021/bi00109a004

Ludwig A, Jarchau T, Benz R & Goebel W (1988) The repeat domain of *Escherichia coli* haemolysin (HlyA) is responsible for its Ca^{2+}-dependent binding to erythrocytes. *Mol Gen Genet.* 214**,** 553-61. doi: 10.1007/BF00330494

Ma M, Kazemzadeh-Narbat M, Hui Y, Lu S, Ding C, Chen DD, Hancock RE & Wang R (2012) Local delivery of antimicrobial peptides using self-organized TiO_2 nanotube arrays for peri-implant infections. *J Biomed Mater Res A.* 100**,** 278-85. doi: 10.1002/jbm.a.33251

Ma Y, Lee CJ & Park JS (2020) Strategies for optimizing the production of proteins and peptides with multiple disulfide bonds. *Antibiotics.* 9**,** 541. doi: 10.3390/antibiotics9090541

Ma Y, Yu J, Lin J, Wu S, Li S & Wang J (2016) High efficient expression, purification, and functional characterization of native human epidermal growth factor in *Escherichia coli*. *Biomed Res Int.* 2016. doi: 10.1155/2016/3758941

Mackman N, Baker K, Gray L, Haigh R, Nicaud JM & Holland IB (1987) Release of a chimeric protein into the medium from *Escherichia coli* using the C-terminal secretion signal of haemolysin. *EMBO J.* 6**,** 2835-41. doi: 10.1002/j.1460-2075.1987.tb02580.x

Mahlapuu M, Hakansson J, Ringstad L & Bjorn C (2016) Antimicrobial peptides: An emerging category of therapeutic agents. *Front Cell Infect Microbiol.* 6**,** 194. doi: 10.3389/fcimb.2016.00194

Manta B, Boyd D & Berkmen M (2019) Disulfide bond formation in the periplasm of *Escherichia coli*. *EcoSal Plus.* 8. doi: 10.1128/ecosalplus.ESP-0012-2018

Masi M & Wandersman C (2010) Multiple signals direct the assembly and function of a type 1 secretion system. *J Bacteriol.* 192**,** 3861-9. doi: 10.1128/JB.00178-10

Mastnak T, Maver U & Finsgar M (2022) Addressing the needs of the rapidly aging society through the development of multifunctional bioactive coatings for orthopedic applications. *Int J Mol Sci.* 23**,** 2786. doi: 10.3390/ijms23052786

Matochko WL, Chu K, Jin B, Lee SW, Whitesides GM & Derda R (2012) Deep sequencing analysis of phage libraries using Illumina platform. *Methods.* 58**,** 47-55. doi: 10.1016/j.ymeth.2012.07.006

Matsuno H, Sekine J, Yajima H & Serizawa T (2008) Biological selection of peptides for poly(l-lactide) substrates. *Langmuir.* 24**,** 6399-403. doi: 10.1021/la8008442

Mccombie WR, Mcpherson JD & Mardis ER (2019) Next-generation sequencing technologies. *Cold Spring Harb Perspect Med.* 9**,** a036798. doi: 10.1101/cshperspect.a036798

Mcconnell SJ, Uveges AJ, Fowlkes DM & Spinella DG (1996) Construction and screening of M13 phage libraries displaying long random peptides. *Mol Divers.* 1**,** 165-76. doi: 10.1007/BF01544954

Mcindoe JS & Vikse KL (2019) Assigning the ESI mass spectra of organometallic and coordination compounds. *J Mass Spectro.* 54**,** 466-79. doi: 10.1002/jms.4359

Meek RL, Eriksen N & Benditt EP (1992) Murine serum amyloid A3 is a high density apolipoprotein and is secreted by macrophages. *PNAS.* 89**,** 7949-52. doi: 10.1073/pnas.89.17.7949

Meier R, Drepper T, Svensson V, Jaeger KE & Baumann U (2007) A calcium-gated lid and a large beta-roll sandwich are revealed by the crystal structure of extracellular lipase from *Serratia marcescens*. *J Biol Chem.* 282**,** 31477-83. doi: 10.1074/jbc.M704942200

Melino S, C S, Nardo P & Sarkar B (2013) Histatins: Salivary peptides with copper(II)- and zinc(II)- binding motifs. Perspectives for biomedical applications. *FEBS J.* 281**,** 657-72. doi: 10.1111/febs.12612

Menendez A & Scott JK (2005) The nature of target-unrelated peptides recovered in the screening of phage-displayed random peptide libraries with antibodies. *Anal Biochem.* 336**,** 145-57. doi: 10.1016/j.ab.2004.09.048

Merrifield RB (1963) Solid phase peptide synthesis. I. The synthesis of a tetrapeptide. *J Am Chem Soc.* 85**,** 2149-54. doi: 10.1021/ja00897a025

Midorikawa K, Ouhara K, Komatsuzawa H, Kawai T, Yamada S, Fujiwara T, Yamazaki K, Sayama K, Taubman MA, Kurihara H, Hashimoto K & Sugai M (2003) *Staphylococcus aureus* susceptibility to innate antimicrobial peptides, beta-defensins and CAP18, expressed by human keratinocytes. *Infect Immun.* 71**,** 3730-9. doi: 10.1128/IAI.71.7.3730-3739.2003

Minisola S, Cipriani C, Grotta GD, Colangelo L, Occhiuto M, Biondi P, Sonato C, Vigna E, Cilli M & Pepe J (2019) Update on the safety and efficacy of teriparatide in the treatment of osteoporosis. *Ther Adv Musculoskelet Dis.* 11**,** 1759720X19877994. doi: 10.1177/1759720X19877994

Morgan AA & Rubenstein E (2013) Proline: the distribution, frequency, positioning, and common functional roles of proline and polyproline sequences in the human proteome. *PLoS One.* 8**,** e53785. doi: 10.1371/journal.pone.0053785

Nicaud JM, Mackman N, Gray L & Holland IB (1985) Characterisation of HlyC and mechanism of activation and secretion of haemolysin from *E. coli* 2001. *FEBS Lett.* 187**,** 339-44. doi: 10.1016/0014-5793(85)81272-2

Nicaud JM, Mackman N, Gray L & Holland IB (1986) The C-terminal, 23 kDa peptide of *E. coli* haemolysin 2001 contains all the information necessary for its secretion by the haemolysin (Hly) export machinery. *FEBS Lett.* 204**,** 331-5. doi: 10.1016/0014-5793(86)80838-9

Nizak C, Martin-Lluesma S, Moutel S, Roux A, Kreis TE, Goud B & Perez F (2003) Recombinant antibodies against subcellular fractions used to track endogenous Golgi protein dynamics *in vivo*. *Traffic.* 4**,** 739-53. doi: 10.1034/j.1600-0854.2003.00132.x

Noren KA & Noren CJ (2001) Construction of high-complexity combinatorial phage display peptide libraries. *Methods.* 23**,** 169-78. doi: 10.1006/meth.2000.1118

O'callaghan R, Bradley R & Paranchych W (1973) The effect of M13 phage infection upon the F-pili of *E. coli*. *Virology.* 54**,** 220-9. doi: 10.1016/0042-6822(73)90131-1

Otvos L, Jr. & Wade JD (2014) Current challenges in peptide-based drug discovery. *Front Chem.* 2**,** 62. doi: 10.3389/fchem.2014.00062

Pan C, Weng J & Wang W (2016) ATP hydrolysis induced conformational changes in the vitamin B12 transporter BtuCD revealed by MD simulations. *PLoS One.* 11**,** e0166980. doi: 10.1371/journal.pone.0166980

Parks TD, Leuther KK, Howard ED, Johnston SA & Dougherty WG (1994) Release of proteins and peptides from fusion proteins using a recombinant plant virus proteinase. *Anal Biochem.* 216**,** 413-7. doi: 10.1006/abio.1994.1060

Parmley SF & Smith GP (1988) Antibody-selectable filamentous fd phage vectors: affinity purification of target genes. *Gene.* 73**,** 305-18. doi: 10.1016/0378-1119(88)90495-7

Pedersen SL, Tofteng AP, Malik L & Jensen KJ (2012) Microwave heating in solid-phase peptide synthesis. *Chem. Soc. Rev.* 41**,** 1826-44. doi: 10.1039/c1cs15214a

Pelzer A, Schwarz C, Knapp A, Wirtz A, Wilhelm S, Smits S, Schmitt L, Funken H & Jaeger KE (2015) Functional expression, purification, and biochemical properties of subtilase SprP from *Pseudomonas aeruginosa*. *Microbiologyopen.* 4**,** 743-52. doi: 10.1002/mbo3.275

Peschel A & Sahl HG (2006) The co-evolution of host cationic antimicrobial peptides and microbial resistance. *Nat Rev Microbiol.* 4**,** 529-36. doi: 10.1038/nrmicro1441

Peters EA, Schatz PJ, Johnson SS & Dower WJ (1994) Membrane insertion defects caused by positive charges in the early mature region of protein pIII of filamentous phage fd can be corrected by prlA suppressors. *J Bacteriol.* 176**,** 4296-305. doi: 10.1128/jb.176.14.4296-4305.1994

Piddock LJ (2006a) Clinically relevant chromosomally encoded multidrug resistance efflux pumps in bacteria. *Clin Microbiol Rev.* 19**,** 382-402. doi: 10.1128/CMR.19.2.382-402.2006

Piddock LJ (2006b) Multidrug-resistance efflux pumps - not just for resistance. *Nat Rev Microbiol.* 4**,** 629-36. doi: 10.1038/nrmicro1464

Pimenta AL, Racher K, Jamieson L, Blight MA & Holland IB (2005) Mutations in HlyD, part of the type 1 translocator for hemolysin secretion, affect the folding of the secreted toxin. *J Bacteriol.* 187**,** 7471-80. doi: 10.1128/JB.187.21.7471-7480.2005

Pirisi L, Pennestri F, Vigano M & Banfi G (2020) Prevalence and burden of orthopaedic implantable-device infections in Italy: a hospital-based national study. *BMC Infect Dis.* 20**,** 337. doi: 10.1186/s12879-020-05065-9

Plessers S, Van Deuren V, Lavigne R & Robben J (2021) High-throughput sequencing of phage display libraries reveals parasitic enrichment of indel mutants caused by amplification bias. *Int J Mol Sci.* 22**,** 5513. doi: 10.3390/ijms22115513

Portillo ME, Corvec S, Borens O & Trampuz A (2013) *Propionibacterium acnes*: an underestimated pathogen in implant-associated infections. *Biomed Res Int.* 2013**,** 804391. doi: 10.1155/2013/804391

Pourhassan NZ, Cui H, Khosa S, Davari MD, Jaeger KE, Smits SHJ, Schwaneberg U & Schmitt L (2022) Optimized hemolysin type 1 secretion system in *Escherichia coli* by directed evolution of the Hly enhancer fragment and including a terminator region. *Chembiochem.* 23**,** e202100702. doi: 10.1002/cbic.202100702

Qi H, Lu H, Qiu HJ, Petrenko V & Liu A (2012) Phagemid vectors for phage display: properties, characteristics and construction. *J Mol Biol.* 417**,** 129-43. doi: 10.1016/j.jmb.2012.01.038

Qi H, Ma M, Hu C, Xu ZW, Wu FL, Wang N, Lai DY, Li Y, Zhang H, Jiang HW, Meng QF, Guo S, Kang Y, Zhao X, Li H & Tao SC (2021) Antibody binding epitope mapping (AbMap) of hundred antibodies in a single run. *Mol Cell Proteomics.* 20**,** 100059. doi: 10.1074/mcp.RA120.002314

Rakonjac J, Feng J & Model P (1999) Filamentous phage are released from the bacterial membrane by a two-step mechanism involving a short C-terminal fragment of pIII. *J Mol Biol.* 289**,** 1253-65. doi: 10.1006/jmbi.1999.2851

Rakonjac J & Model P (1998) Roles of pIII in filamentous phage assembly. *J Mol Biol.* 282**,** 25-41. doi: 10.1006/jmbi.1998.2006

Rami A, Behdani M, Yardehnavi N, Habibi-Anbouhi M & Kazemi-Lomedasht F (2017) An overview on application of phage display technique in immunological studies. *Asian Pac J Trop Biomed.* 7**,** 599-602. doi: 10.1016/j.apjtb.2017.06.001

Ratner AJ, Hippe KR, Aguilar JL, Bender MH, Nelson AL & Weiser JN (2006) Epithelial cells are sensitive detectors of bacterial pore-forming toxins. *J Biol Chem.* 281**,** 12994-8. doi: 10.1074/jbc.M511431200

Ravn U, Gueneau F, Baerlocher L, Osteras M, Desmurs M, Malinge P, Magistrelli G, Farinelli L, Kosco-Vilbois MH & Fischer N (2010) By-passing *in vitro* screening - next generation sequencing technologies applied to antibody display and in silico candidate selection. *Nucleic Acids Res.* 38**,** e193. doi: 10.1093/nar/gkq789

Riechmann L & Holliger P (1997) The C-terminal domain of TolA is the coreceptor for filamentous phage infection of *E. coli*. *Cell.* 90**,** 351-60. doi: 10.1016/s0092-8674(00)80342-6

Rivera-De-Torre E, Rimbault C, Jenkins TP, Sorensen CV, Damsbo A, Saez NJ, Duhoo Y, Hackney CM, Ellgaard L & Laustsen AH (2021) Strategies for heterologous expression, synthesis, and purification of animal venom toxins. *Front Bioeng Biotechnol.* 9**,** 811905. doi: 10.3389/fbioe.2021.811905

Roca-Pinilla R, Lopez-Cano A, Saubi C, Garcia-Fruitos E & Aris A (2020) A new generation of recombinant polypeptides combines multiple protein domains for effective antimicrobial activity. *Microb Cell Fact.* 19**,** 122. doi: 10.1186/s12934-020-01380-7

Rodi DJ, Soares AS & Makowski L (2002) Quantitative assessment of peptide sequence diversity in M13 combinatorial peptide phage display libraries. *J Mol Biol.* 322**,** 1039–52. doi: 10.1016/s0022-2836(02)00844-6

Rondot S, Koch J, Breitling F & Dubel S (2001) A helper phage to improve single-chain antibody presentation in phage display. *Nat Biotechnol.* 19**,** 75-8. doi: 10.1038/83567

Roy A & Mitra S (1970) Increased fragility of *Escherichia coli* after infection with bacteriophage M13. *J Virol.* 6**,** 333-9. doi: 10.1128/JVI.6.3.333-339.1970

Ruano-Gallego D, Fraile S, Gutierrez C & Fernandez LA (2019) Screening and purification of nanobodies from *E. coli* culture supernatants using the hemolysin secretion system. *Microb Cell Fact.* 18**,** 47. doi: 10.1186/s12934-019-1094-0

Rubsam K, Davari MD, Jakob F & Schwaneberg U (2018) KnowVolution of the polymer-binding peptide LCI for improved polypropylene binding. *Polymers.* 10**,** 423. doi: 10.3390/polym10040423

Ryvkin A, Ashkenazy H, Weiss-Ottolenghi Y, Piller C, Pupko T & Gershoni JM (2018) Phage display peptide libraries: deviations from randomness and correctives. *Nucleic Acids Res.* 46**,** e52. doi: 10.1093/nar/gky077

Saeidnia S, Manayi A & Abdollahi M (2015) From *in vitro* experiments to *in vivo* and clinical studies; pros and cons. *Curr Drug Discov Technol.* 12**,** 218-24. doi: 10.2174/1570163813666160114093140

Sakagami-Yasui Y, Shirafuji Y, Yamasaki O, Morizane S, Hamada T, Umemura H & Iwatsuki K (2017) Two arginine residues in the COOH-terminal of human beta-defensin-3 constitute an essential motif for antimicrobial activity and IL-6 production. *Exp Dermatol.* 26**,** 1026-32. doi: 10.1111/exd.13361

Sanchez-Magraner L, Viguera AR, Garcia-Pacios M, Garcillan MP, Arrondo JL, De La Cruz F, Goni FM & Ostolaza H (2007) The calcium-binding C-terminal domain of *Escherichia coli* alpha-hemolysin is a major determinant in the surface-active properties of the protein. *J Biol Chem.* 282**,** 11827-35. doi: 10.1074/jbc.M700547200

Sass V, Pag U, Tossi A, Bierbaum G & Sahl HG (2008) Mode of action of human beta-defensin 3 against *Staphylococcus aureus* and transcriptional analysis of responses to defensin challenge. *Int J Med Microbiol.* 298**,** 619-33. doi: 10.1016/j.ijmm.2008.01.011

Schagger H & Von Jagow G (1987) Tricine-sodium dodecyl sulfate-polyacrylamide gel electrophoresis for the separation of proteins in the range from 1 to 100 kDa. *Anal Biochem.* 166**,** 368-79. doi: 10.1016/0003-2697(87)90587-2

Schittek B, Hipfel R, Sauer B, Bauer J, Kalbacher H, Stevanovic S, Schirle M, Schroeder K, Blin N, Meier F, Rassner G & Garbe C (2001) Dermcidin: a novel human antibiotic peptide secreted by sweat glands. *Nat Immunol.* 2**,** 1133-7. doi: 10.1038/ni732

Schnölzer M, Alewood P, Jones A, Alewood D & Kent SB (1992) *In situ* neutralization in Boc-chemistry solid phase peptide synthesis. Rapid, high yield assembly of difficult sequences. *Int J Pept Protein Res.* 40**,** 180-93. doi: 10.1111/j.1399-3011.1992.tb00291.x

Schulz E, Schumann M, Schneemann M, Dony V, Fromm A, Nagel O, Schulzke JD & Bucker R (2021) *Escherichia coli* alpha-hemolysin HlyA induces host cell polarity changes, epithelial barrier dysfunction and cell detachment in human colon carcinoma caco-2 cell model via PTEN-dependent dysregulation of cell junctions. *Toxins.* 13**,** 520. doi: 10.3390/toxins13080520

Schwarz CK, Landsberg CD, Lenders MH, Smits SH & Schmitt L (2012) Using an *E. coli* Type 1 secretion system to secrete the mammalian, intracellular protein IFABP in its active form. *J Biotechnol.* 159**,** 155-61. doi: 10.1016/j.jbiotec.2012.02.005

Schwinges P, Pariyar S, Jakob F, Rahimi M, Apitius L, Hunsche M, Schmitt L, Noga G, Langenbach C, Schwaneberg U & Conrath U (2019) A bifunctional dermaseptin–thanatin dipeptide functionalizes the crop surface for sustainable pest management. *Green Chemistry.* 21**,** 2316-25. doi: 10.1039/c9gc00457b

Serizawa T, Matsuno H & Sawada T (2011) Specific interfaces between synthetic polymers and biologically identified peptides. *J Mater Chem.* 21**,** 10252-260. doi: 10.1039/C1JM10602C

Shams D, Alizadeh M, Azari S, Hosseini S, Yasami-Khiabani S, Samani S & Shokrgozar MA (2019) High expression level of human epidermal growth factor (hEGF) using a well-designed fusion protein-tagged construct in *E. coli*. *Bratisl Lek Listy.* 120**,** 757-63. doi: 10.4149/BLL_2019_126

Shen LM, Lee JI, Cheng SY, Jutte H, Kuhn A & Dalbey RE (1991) Use of site-directed mutagenesis to define the limits of sequence variation tolerated for processing of the M13 procoat protein by the *Escherichia coli* leader peptidase. *Biochemistry.* 30**,** 11775-81. doi: 10.1021/bi00115a006

Sheng Y, Mancino V & Birren B (1995) Transformation of *Escherichia coli* with large DNA molecules by electroporation. *Nucleic Acids Res.* 23**,** 1990-6. doi: 10.1093/nar/23.11.1990

Siemann U (2005) Solvent cast technology – a versatile tool for thin film production. In: Stribeck N & Smarsly B (eds.) *Scattering Methods and the Properties of Polymer Materials,* vol 130. Springer, Berlin, Heidelberg. 1-14, doi: 10.1007/b107336

Silva RR, Avelino KY, Ribeiro KL, Franco OL, Oliveira MD & Andrade CA (2016) Chemical immobilization of antimicrobial peptides on biomaterial surfaces. *Front Biosci.* 8**,** 129-42. doi: 10.2741/s453

Singh A, Upadhyay V, Upadhyay AK, Singh SM & Panda AK (2015) Protein recovery from inclusion bodies of *Escherichia coli* using mild solubilization process. *Microb Cell Fact.* 14**,** 41. doi: 10.1186/s12934-015-0222-8

Singh SM & Panda AK (2005) Solubilization and refolding of bacterial inclusion body proteins. *J Biosci Bioeng.* 99**,** 303-10. doi: 10.1263/jbb.99.303

Singhvi P, Saneja A, Srichandan S & Panda AK (2020) Bacterial inclusion bodies: A treasure trove of bioactive proteins. *Trends Biotechnol.* 38**,** 474-486. doi: 10.1016/j.tibtech.2019.12.011

Sloth AB, Bakhshinejad B, Jensen M, Stavnsbjerg C, Liisberg MB, Rossing M & Kjaer A (2022) Analysis of compositional bias in a commercial phage display peptide library by next-generation sequencing. *Viruses.* 14**,** 2402. doi: 10.3390/v14112402

Slouka C, Kopp J, Spadiut O & Herwig C (2019) Perspectives of inclusion bodies for bio-based products: curse or blessing? *Appl Microbiol Biotechnol.* 103**,** 1143-53. doi: 10.1007/s00253-018-9569-1

Smeal SW, Schmitt MA, Pereira RR, Prasad A & Fisk JD (2017) Simulation of the M13 life cycle I: Assembly of a genetically-structured deterministic chemical kinetic simulation. *Virology.* 500**,** 259-74. doi: 10.1016/j.virol.2016.08.017

Smith DB & Johnson KS (1988) Single-step purification of polypeptides expressed in *Escherichia coli* as fusions with glutathione S-transferase. *Gene.* 67**,** 31-40. doi: 10.1016/0378-1119(88)90005-4

Smith GP (1985) Filamentous fusion phage: novel expression vectors that display cloned antigens on the virion surface. *Science.* 228**,** 1315-7. doi: 10.1126/science.4001944

Smith GP & Petrenko VA (1997) Phage Display. *Chem Rev.* 97**,** 391-410. doi: 10.1021/cr960065d

Smith TJ, Sondermann H & O'toole GA (2018) Type 1 does the two-step: Type 1 secretion substrates with a functional periplasmic intermediate. *J Bacteriol.* 200**,** e00168-18. doi: 10.1128/JB.00168-18

Soma T, Iwasaki R, Sato Y, Kobayashi T, Ito E, Matsumoto T, Kimura A, Homma F, Saiki K, Takahashi Y, Miyamoto K, Matsumoto M, Nakamura M, Morita M, Ishii K, Asoda S, Kawana H, Xingyu Z, Aizawa M, Nakagawa T & Miyamoto T (2022) An ionic silver coating prevents implant-associated infection by anaerobic bacteria *in vitro* and *in vivo* in mice. *Sci Rep.* 12**,** 18387. doi: 10.1038/s41598-022-23322-6

Song J, Winkeljann B & Lieleg O (2020) Biopolymer-based coatings: Promising strategies to improve the biocompatibility and functionality of materials used in biomedical engineering. *Adv Mater Interfaces.* 7**,** 2000850. doi: 10.1002/admi.202000850

Stanley P, Packman LC, Koronakis V & Hughes C (1994) Fatty acylation of two internal lysine residues required for the toxic activity of *Escherichia coli* hemolysin. *Science.* 266**,** 1992-6. doi: 10.1126/science.7801126

Stassen AP, Folmer RH, Hilbers CW & Konings RN (1994) Single-stranded DNA binding protein encoded by the filamentous bacteriophage M13: structural and functional characteristics. *Mol Biol Rep.* 20**,** 109-27. doi: 10.1007/BF00990543

Steffen H, Rieg S, Wiedemann I, Kalbacher H, Deeg M, Sahl HG, Peschel A, Gotz F, Garbe C & Schittek B (2006) Naturally processed dermcidin-derived peptides do not permeabilize bacterial membranes and kill microorganisms irrespective of their charge. *Antimicrob Agents Chemother.* 50**,** 2608-20. doi: 10.1128/AAC.00181-06

Steiner D, Forrer P, Stumpp MT & Pluckthun A (2006) Signal sequences directing cotranslational translocation expand the range of proteins amenable to phage display. *Nat Biotechnol.* 24**,** 823-31. doi: 10.1038/nbt1218

Storz G, Wolf YI & Ramamurthi KS (2014) Small proteins can no longer be ignored. *Annu Rev Biochem.* 83**,** 753-77. doi: 10.1146/annurev-biochem-070611-102400

Strobel C, Schmidmaier G & Wildemann B (2011) Changing the release kinetics of gentamicin from poly(D,L-lactide) implant coatings using only one polymer. *Int J Artif Organs.* 34**,** 304-16. doi: 10.5301/ijao.2011.6470

Su M, Ling Y, Yu J, Wu J & Xiao J (2013) Small proteins: untapped area of potential biological importance. *Front Genet.* 4**,** 286. doi: 10.3389/fgene.2013.00286

Sun L, Zhang W, Liu X & Sun J (2014) Preparation and evaluation of sustained-release azithromycin tablets in vitro and in vivo. *Asian J Pharm Sci.* 9**,** 155-61. doi: 10.1016/j.ajps.2014.03.003

Szostkova M & Horakova D (1998) The effect of plasmid DNA sizes and other factors on electrotransformation of *Escherichia coli* JM109. *Bioelectrochemistry and Bioenergetics.* 47**,** 319-323. doi: 10.1016/S0302-4598(98)00203-7

Teilum K, Ostergaard L & Welinder KG (1999) Disulfide bond formation and folding of plant peroxidases expressed as inclusion body protein in *Escherichia coli* thioredoxin reductase negative strains. *Protein Expr Purif.* 15**,** 77-82. doi: 10.1006/prep.1998.0985

Thamvasupong P & Viravaidya-Pasuwat K (2022) Controlled release mechanism of vancomycin from double-layer poly-L-lactic acid-coated implants for prevention of bacterial infection. *Polymers.* 14**,** 3493. doi: 10.3390/polym14173493

Thomas S, Bakkes PJ, Smits SH & Schmitt L (2014a) Equilibrium folding of pro-HlyA from *Escherichia coli* reveals a stable calcium ion dependent folding intermediate. *Biochim Biophys Acta.* 1844**,** 1500-10. doi: 10.1016/j.bbapap.2014.05.006

Thomas S, Holland IB & Schmitt L (2014b) The Type 1 secretion pathway - the hemolysin system and beyond. *Biochim Biophys Acta.* 1843**,** 1629-41. doi: 10.1016/j.bbamcr.2013.09.017

Thyparambil AA, Wei Y & Latour RA (2012) Determination of peptide-surface adsorption free energy for material surfaces not conducive to SPR or QCM using AFM. *Langmuir.* 28**,** 5687-94. doi: 10.1021/la300315r

Tikhonova EB & Zgurskaya HI (2004) AcrA, AcrB, and TolC of *Escherichia coli* form a stable intermembrane multidrug efflux complex. *J Biol Chem.* 279**,** 32116-24. doi: 10.1074/jbc.M402230200

Tripathi NK & Shrivastava A (2019) Recent developments in bioprocessing of recombinant proteins: expression hosts and process development. *Front Bioeng Biotechnol.* 7**,** 420. doi: 10.3389/fbioe.2019.00420

Uhlen P, Laestadius A, Jahnukainen T, Soderblom T, Backhed F, Celsi G, Brismar H, Normark S, Aperia A & Richter-Dahlfors A (2000) Alpha-haemolysin of uropathogenic *E. coli* induces Ca^{2+} oscillations in renal epithelial cells. *Nature.* 405**,** 694-7. doi: 10.1038/35015091

Van Wezenbeek PM, Hulsebos TJ & Schoenmakers JG (1980) Nucleotide sequence of the filamentous bacteriophage M13 DNA genome: comparison with phage fd. *Gene.* 11**,** 129-48. doi: 10.1016/0378-1119(80)90093-1

Vargas-Cortez T, Morones-Ramirez JR, Balderas-Renteria I & Zarate X (2017) Production of recombinant proteins in *Escherichia coli* tagged with the fusion protein CusF3H. *Protein Expr Purif.* 132**,** 44-49. doi: 10.1016/j.pep.2017.01.006

Vieira J & Messing J (1987) Production of single-stranded plasmid DNA. *Methods Enzymol.* 153**,** 3-11. doi: 10.1016/0076-6879(87)53044-0

Vodnik M, Zager U, Strukelj B & Lunder M (2011) Phage display: selecting straws instead of a needle from a haystack. *Molecules.* 16**,** 790-817. doi: 10.3390/molecules16010790

Von Burkersroda F, Schedl L & Gopferich A (2002) Why degradable polymers undergo surface erosion or bulk erosion. *Biomaterials.* 23**,** 4221-31. doi: 10.1016/s0142-9612(02)00170-9

Wandersman C & Delepelaire P (1990) TolC, an *Escherichia coli* outer membrane protein required for hemolysin secretion. *PNAS.* 87**,** 4776-80. doi: 10.1073/pnas.87.12.4776

Wang G (2014) Human antimicrobial peptides and proteins. *Pharmaceuticals.* 7**,** 545-94. doi: 10.3390/ph7050545

Wang L, Wang N, Zhang W, Cheng X, Yan Z, Shao G, Wang X, Wang R & Fu C (2022) Therapeutic peptides: current applications and future directions. *Sig Transduct Target Ther.* 7**,** 48. doi: 10.1038/s41392-022-00904-4

Wang Z, Li L, Hu R, Zhong P, Zhang Y, Cheng S, Jiang H, Liu R & Ding Y (2021) Structural insights into the binding of nanobodies LaM2 and LaM4 to the red fluorescent protein mCherry. *Protein Sci.* 30**,** 2298-2309. doi: 10.1002/pro.4194

Weber PC, Pantoliano MW & Thompson LD (1992) Crystal structure and ligand-binding studies of a screened peptide complexed with streptavidin. *Biochemistry.* 31**,** 9350-4. doi: 10.1021/bi00154a004

Wegmuller S & Schmid S (2014) Recombinant peptide production in microbial cells. *Curr Organic Chemistry.* 18**,** 1005-19. doi: 10.1007/978-1-60761-594-1_5

Weinstein RA (2001) Device-related infections. *Clin Infect Dis.* 33**,** 1386. doi: 10.1086/324190

Windolf CD, Logters T, Scholz M, Windolf J & Flohe S (2014) Lysostaphin-coated titan-implants preventing localized osteitis by *Staphylococcus aureus* in a mouse model. *PLoS One.* 9**,** e115940. doi: 10.1371/journal.pone.0115940

Wouters S, Eeltink S, Haselberg R, Somsen GW & Gargano AFG (2021) Microfluidic ion stripper for removal of trifluoroacetic acid from mobile phases used in HILIC-MS of intact proteins. *Anal Bioanal Chem.* 413**,** 4379-86. doi: 10.1007/s00216-021-03414-4

Wu CH, Liu IJ, Lu RM & Wu HC (2016) Advancement and applications of peptide phage display technology in biomedical science. *J Biomed Sci.* 23**,** 8. doi: 10.1186/s12929-016-0223-xWu N, Matand K, Kebede B, Acquaah G & Williams S (2010) Enhancing DNA electrotransformation efficiency in

Escherichia coli DH10B electrocompetent cells. *Electron J Biotechnol.* 13**,** 21-22. doi: 10.2225/vol13-issue5-fulltext-11

Wu Y, Ma Y, Li L & Yang X (2018) Molecular modification, expression and purification of new subtype antioxidant peptide from *Pinctada fucata* by recombinant *Escherichia coli* to improve antioxidant-activity. *J Food Sci Technol.* 55**,** 4266-75. doi: 10.1007/s13197-018-3365-x

Wu Z, Hoover DM, Yang D, Boulegue C, Santamaria F, Oppenheim JJ, Lubkowski J & Lu W (2003) Engineering disulfide bridges to dissect antimicrobial and chemotactic activities of human β-defensin 3. *PNAS.* 100**,** 8880-5. doi: 10.1073/pnas.1533186100

Xu Q, Chin SE, Wang CH & Pack DW (2013) Mechanism of drug release from double-walled PDLLA (PLGA) microspheres. *Biomaterials.* 34**,** 3902-11. doi: 10.1016/j.biomaterials.2013.02.015

Yadav DK, Yadav N, Yadav S, Haque S & Tuteja N (2016) An insight into fusion technology aiding efficient recombinant protein production for functional proteomics. *Arch Biochem Biophys.* 612**,** 57-77. doi: 10.1016/j.abb.2016.10.012

Yamane K & Mizushima S (1988) Introduction of basic amino acid residues after the signal peptide inhibits protein translocation across the cytoplasmic membrane of *Escherichia coli*. Relation to the orientation of membrane proteins. *J Biol Chem.* 263**,** 19690-6.

Yang LM, Wang JL, Kang L, Gao S, Liu YH & Hu TM (2008) Construction and analysis of high-complexity ribosome display random peptide libraries. *PLoS One.* 3**,** e2092. doi: 10.1371/journal.pone.0002092

Yazici H, O'neill MB, Kacar T, Wilson BR, Oren EE, Sarikaya M & Tamerler C (2016) Engineered chimeric peptides as antimicrobial surface coating agents toward infection-free implants. *ACS Appl Mater Interfaces.* 8**,** 5070-81. doi: 10.1021/acsami.5b03697

Zade HM, Keshavarz R, Shekarabi HSZ & Bakhshinejad B (2017) Biased selection of propagation-related TUPs from phage display peptide libraries. *Amino Acids.* 49**,** 1293-1308. doi: 10.1007/s00726-017-2452-z

Zaitseva J, Jenewein S, Oswald C, Jumpertz T, Holland IB & Schmitt L (2005) A molecular understanding of the catalytic cycle of the nucleotide-binding domain of the ABC transporter HlyB. *Biochem Soc Trans.* 33**,** 990-5. doi: 10.1042/bst20050990

Zavodszky M, Chen CW, Huang JK, Zolkiewski M, Wen L & Krishnamoorthi R (2001) Disulfide bond effects on protein stability: designed variants of *Cucurbita maxima* trypsin inhibitor-V. *Protein Sci.* 10**,** 149-60. doi: 10.1110/ps.26801

Zeng F & Harris RC (2014) Epidermal growth factor, from gene organization to bedside. *Semin Cell Dev Biol.* 28**,** 2-11. doi: 10.1016/j.semcdb.2014.01.011

Zhang Z, Peng F & Kornev KG (2022) The thickness and structure of dip-coated polymer films in the liquid and solid states. *Micromachines (Basel).* 13. doi: 10.3390/mi13070982

Zhao H, Lee J & Chen J (2022) The hemolysin A secretion system is a multi-engine pump containing three ABC transporters. *Cell.* 185**,** 3329-3340.e13. doi: 10.1016/j.cell.2022.07.017

Zompra AA, Galanis AS, Werbitzky O & Albericio F (2009) Manufacturing peptides as active pharmaceutical ingredients. *Future Med Chem.* 1**,** 361-77. doi: 10.4155/fmc.09.23

7 List of Publications

The following publications were published under the birth name "Nguyen":

Numaswitch, an efficient high-titer expression platform to produce peptides and small proteins
Nguyen BN, Tieves F, Rohr T, Wobst H, Schöpf FS, Solano JDM, Schneider J, Stock J, Uhde A, Kalthoff T, Jaeger KE, Schmitt L, Schwarz C. (2021) AMB Express. 11(1):48. doi: 10.1186/s13568-021-01204-w

Numaswitch, a biochemical platform for the efficient production of disulfide-rich pepteins
Nguyen BN, Tieves F, Neusius FG, Götzke H, Schmitt L, Schwarz C. (2023) Frontiers in Drug Discovery. 3. doi: 10.3389/fddsv.2023.1082058

IV. Supplementary Material

Renaturation and cleavage of truncated HlyA1 fusions

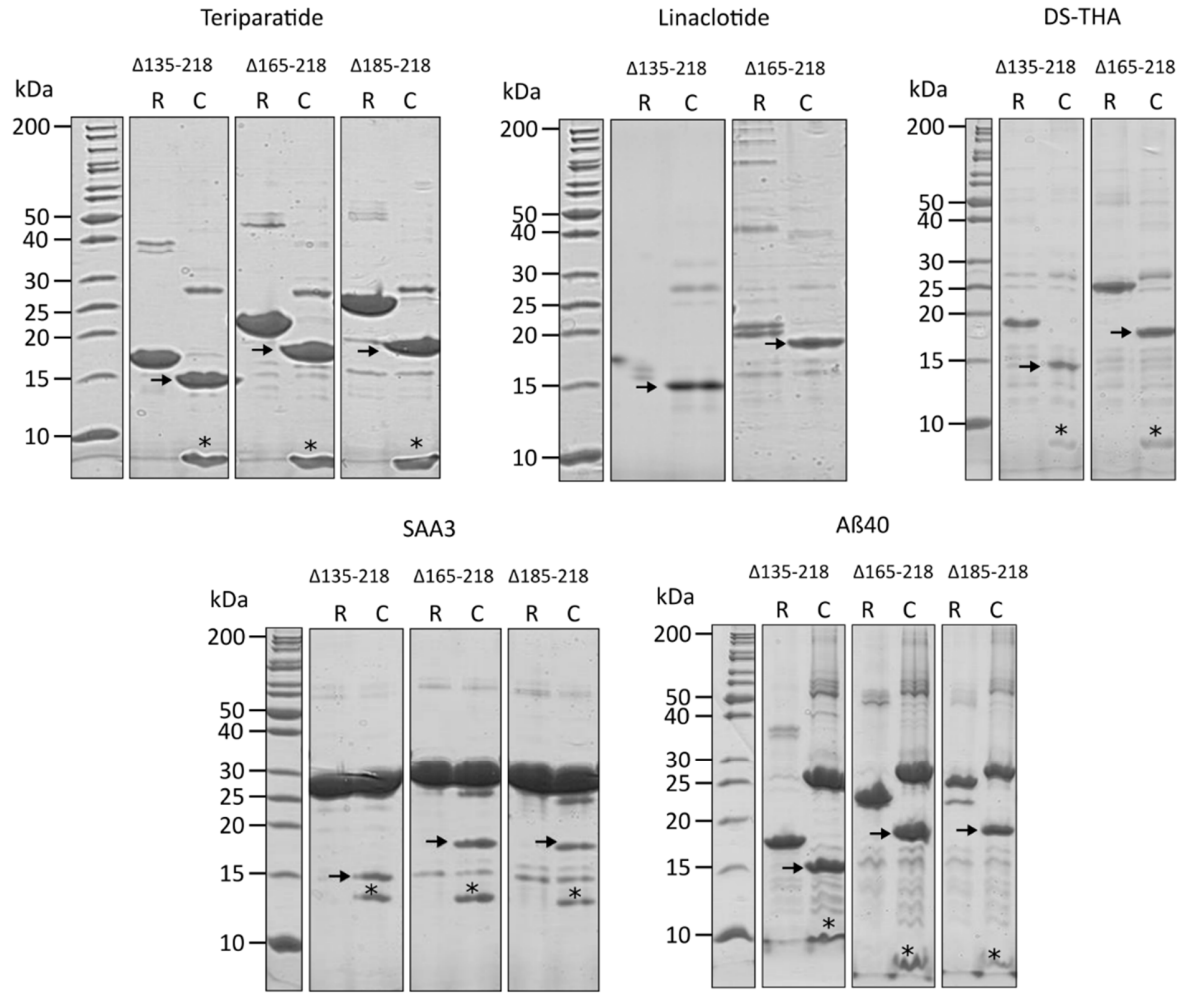

Figure S 1 | Analyses of renaturation and cleavage samples of truncated HlyA1 fusions

Renaturation (R) and TEV protease cleavage (C) reactions of truncated HlyA1 fusions were analyzed by SDS-PAGE. Arrows indicate the locations of truncated HlyA1 backbones (Δ135-218, Δ165-218 or Δ185-218) after TEV protease cleavage. The released targets are indicated (*).

Fed-batch high cell density fermentation of HlyA1 Δ165-218-Teriparatide

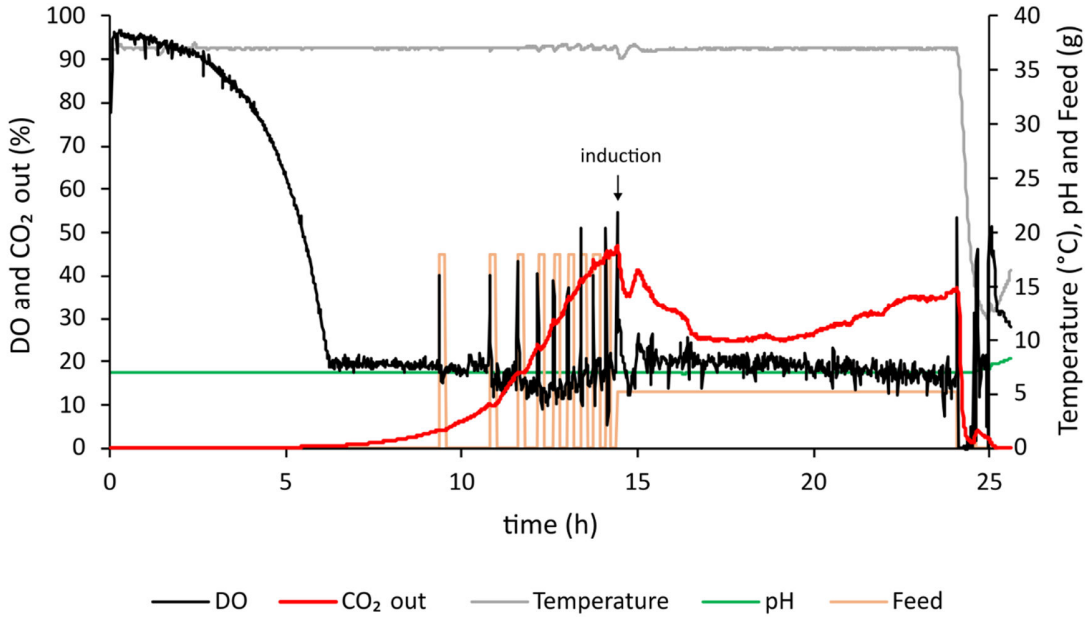

Figure S 2 | Fed-batch high cell density fermentation of HlyA1 Δ165-218-Teriparatide

High cell density fermentation was performed in a BioFlo® 320 Bioreactor by the Upstream division of Numaferm GmbH. For this, 750 mL of medium (17.7 g/L KH_2PO_4, 5.3 g/L $(NH_4)_2HPO_4$, 2.5 g/L citric acid, 10 mM $MgSO_4$) containing trace elements ($CaCl_2$, Fe_3Cl, $CoCl_2$, $MnCl_2$, $CuCl_2$, H_3BO_3, Na_2MoO_4, zinc acetate), antibiotics and glucose (20 g/L) were inoculated with pre-cultures of *E. coli* BL21 (DE3) containing the HlyA1 Δ165-218-Teriparatide plasmid to a final of OD_{600} of 0.25. The temperature, pH and dissolved oxygen (DO) level was maintained at 37 °C, 7.0 and 20 %, respectively. Cell growth phase was extended by adding glucose pulses of 20 g (Feed) when the DO level exceeded 40 %. Timepoint of expression induction is indicated (black arrow). Afterwards a constant glucose feed rate of 0.57 g/min was applied. Cell growth was monitored by measuring the CO_2 release (CO_2 out) and the OD_{600}.

Peptide mapping of purified Teriparatide and commercial drugs

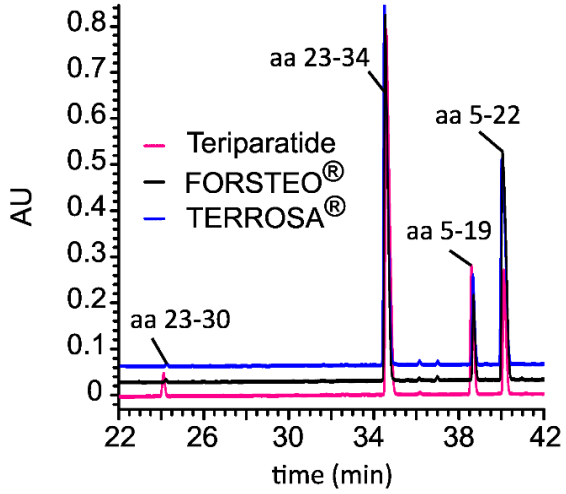

Figure S 3 | Peptide mapping of purified Teriparatide and commercial drugs

Peptide mapping by Glu-C digestion was performed with purified Teriparatide (section 4.4) and the commercial drugs FORSTEO® (Eli Lilly) and TERROSA® (Gedeon Richter). Teriparatides were digested with the endopeptidase Glu-C (Sigma-Aldrich) and the resulting peptide fragments were analyzed by RP-HPLC-MS, respectively (section 3.4.2). Chromatograms were monitored at 215 nm. The indicated elution peaks correspond to digested Teriparatide fragments of aa 23-30, aa 23-34, aa 5-19 and aa 5-22.

Purification of VHH, hEGF, scFv clone F2C and DS-THA

Individual purification strategies were developed to purify each target from crude cleavage reactions. The Figures S 4 to S 7 show the chromatograms and analysis data of fractions acquired during the purification process.

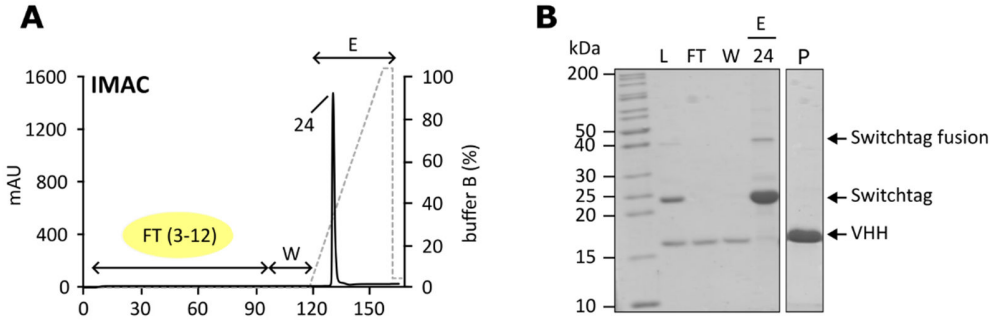

Figure S 4 | Purification process of VHH

(A) IMAC chromatogram of VHH purification monitored at 280 nm (section 3.7). The flow through (FT), wash (W) and elution (E) fractions and fraction numbers are indicated. The VHH-containing fractions are highlighted in yellow. **(B)** Coomassie-stained SDS-PAGE gel visualizing the load (L), flow through (FT), wash (W), elution (E) and final VHH product (P). Arrows indicate the locations of the Switchtag fusion, Switchtag and VHH.

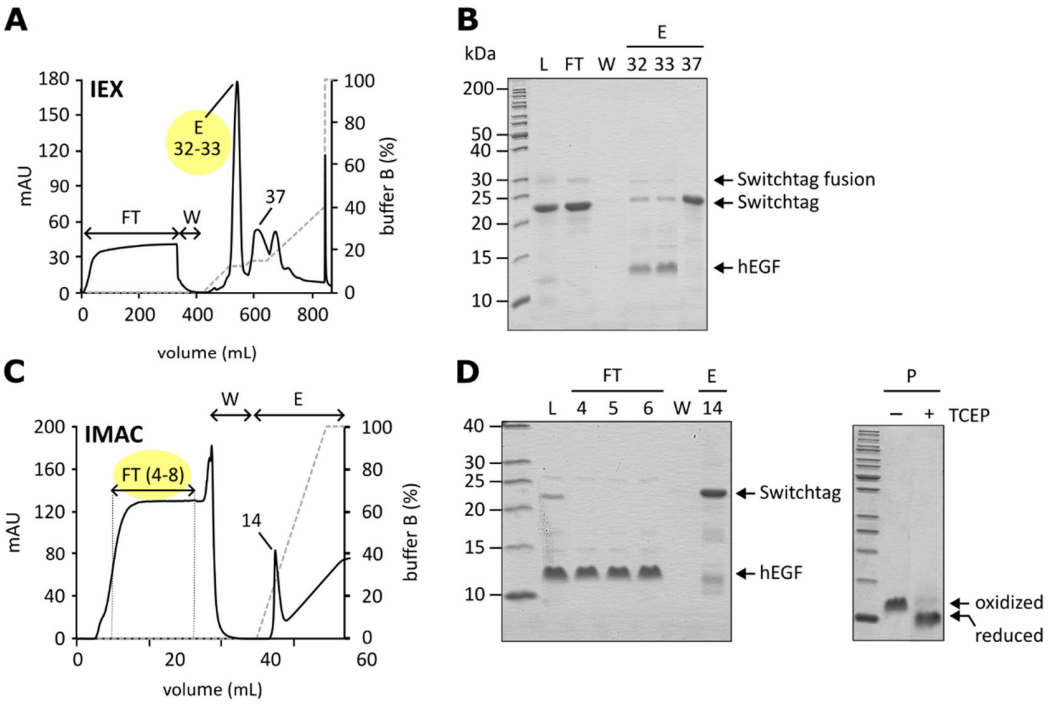

Figure S 5 | Purification process of hEGF

Purification of hEGF was performed in a two-step process (section 3.7). **(A)** IEX chromatogram of hEGF purification monitored at 280 nm. The flow through (FT), wash (W) and elution (E) fractions and fraction numbers are indicated. The hEGF-containing elution fractions are highlighted in yellow. **(B)** SDS-PAGE analysis of load (L) and respective FT, W and E fractions obtained during IEX purification. **(C)** IMAC chromatogram of hEGF purification monitored at 280 nm. As before, the hEGF-containing fraction is highlighted in yellow. **(D)** SDS-PAGE analysis of load (L) and respective FT, W and E fractions obtained during IMAC purification. The final hEGF product (P) was analyzed in the absence and presence of 5 mM TCEP leading to an oxidized and reduced isoform, respectively. Arrows indicate the locations of the Switchtag fusion, Switchtag and hEGF.

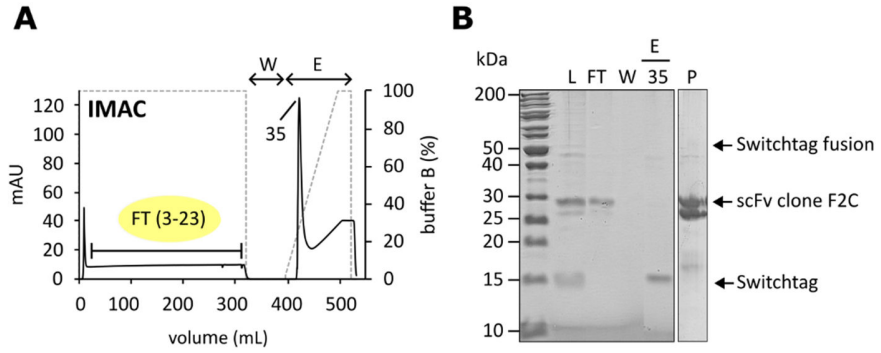

Figure S 6 | Purification process of scFv clone of F2C

(A) IMAC chromatogram of scFv clone F2C purification monitored at 280 nm (section 3.7). The flow through (FT), wash (W) and elution (E) fractions and fraction numbers are indicated. The scFv clone F2C-containing fractions are highlighted in yellow. **(B)** Coomassie-stained SDS-PAGE gel visualizing the load (L), flow through (FT), wash (W), elution (E) and final scFv clone F2C product (P). Arrows indicate the locations of the Switchtag fusion, scFv clone F2C and Switchtag.

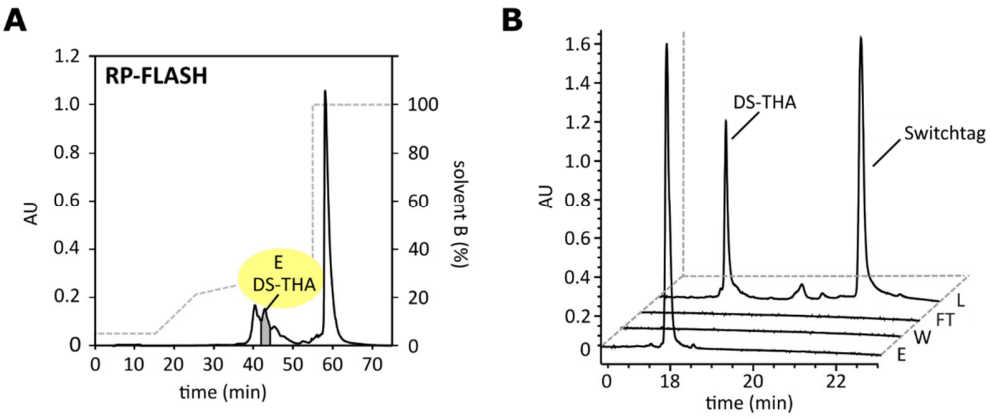

Figure S 7 | Purification process of DS-THA

(A) RP-FLASH chromatogram of DS-THA purification (section 3.7). The DS-THA-containing elution fraction (E) is highlighted in yellow. **(B)** RP-HPLC chromatograms of the load (L) or crude cleavage reaction, flow through (FT), wash (W) and pooled DS-THA elution fraction (E). Chromatograms obtained by RP-FLASH and RP-HPLC were monitored at 205 nm, respectively.

Oxidation of scFv clone F2C by Copper (II)-phenanthroline

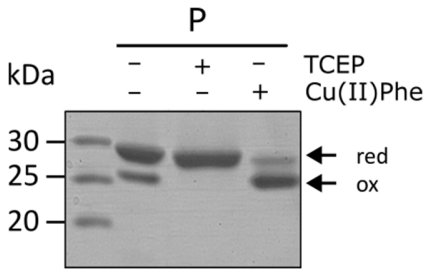

Figure S 8 │Oxidation of scFv clone F2C by Copper (II)-phenanthroline

Coomassie-stained SDS-PAGE gel visualizing the purified scFv clone F2C (P, section 3.7) treated with reducing agent TCEP or the oxidizing catalyst Copper (II)-phenanthroline (Cu (II)Phe). Arrows indicate the location of scFv clone F2C in its reduced (red) or oxidized (ox) state.

Biological function analyses of DS-THA, VHH, scFv clone F2C and hEGF

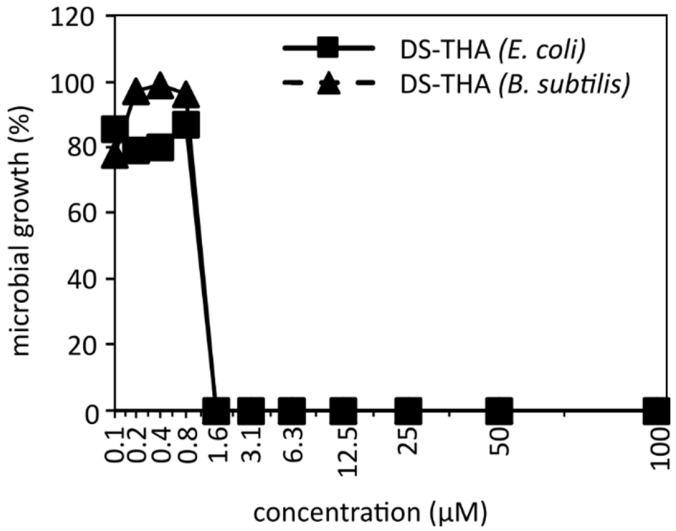

Figure S 9 │Growth curve of *E. coli* and *B. subtilis* in presence of DS-THA

The antimicrobial activity of DS-THA against *E. coli* and *B. subtilis* was investigated in a MIC assay (section 3.7). Microbial growth (%) in presence of different concentrations of DS-THA was determined by measuring the OD_{600} after 24 h of incubation.

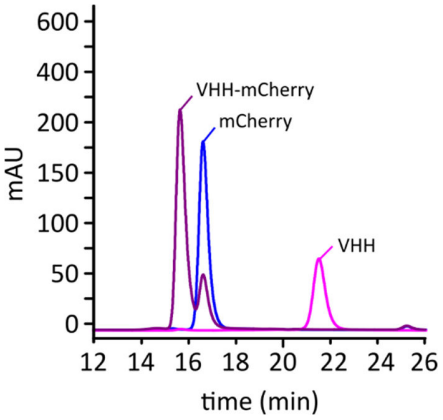

Figure S 10 | Investigation of VHH-mCherry heterodimer formation by SEC analysis

VHH binding to red fluorescence protein mCherry was analyzed by size exclusion chromatography (SEC). The binding assay was performed as described in section 3.9.2. Co-incubation of VHH and mCherry led to formation of VHH-mCherry heterodimers. Respective elution peaks of VHH, mCherry and VHH-mCherry are indicated. The chromatogram shows the elution signals at 280 nm.

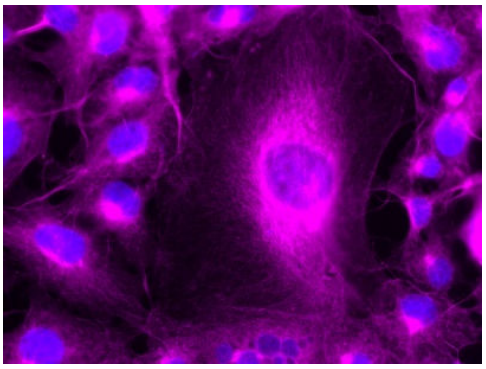

Figure S 11 | Epifluorescence imaging analysis of scFv clone F2C binding to α-tubulin

The biological activity of purified scFv clone F2C was analyzed by epifluorescence imaging performed by NanoTag Biotechnologies GmbH (section 3.9.4). For this, purified scFv clone F2C was coupled to Atto 647 fluorescent dye (magenta) and binding to α-tubulin in paraformaldehyde fixed COS-7 cells was detected by immunofluorescence (section 3.9.4). Nuclei of COS-7 cells were stained with fluorogenic DNA-binding dye DAPI (blue). The fluorescent images of scFv clone F2C and nuclei of COS-7 cell were merged.

Recombinantly purified hEGF was evaluated in an EGFR human receptor tyrosine kinase (RTK) cell-based assay.

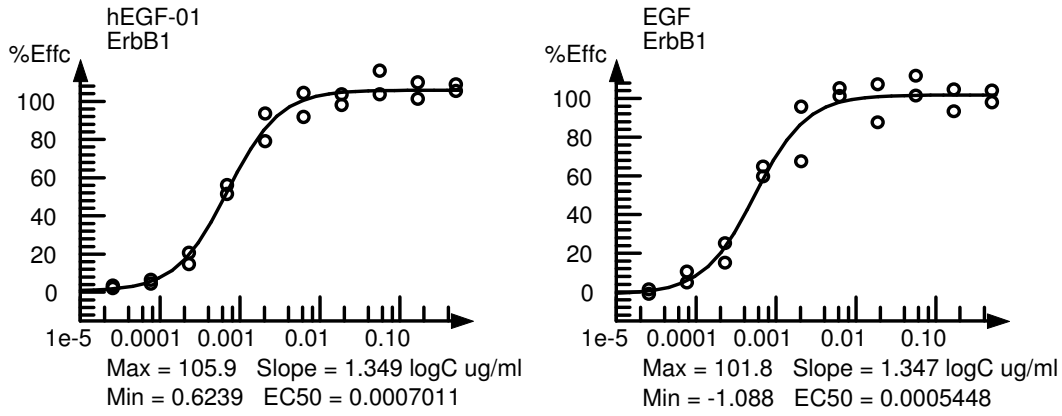

Figure S 12 │Dose-response curve for agonist hEGF in cell-based EGFR RTK assay

The activities of purified hEGF-01 (left) and reference standard EGF (right) were investigated in agonist (ErbB1) mode in a kinase biosensor assay (performed by Eurofins DiscoverX Corporation, Fremont USA). The data shown were normalized to the maximal (Max) and minimal (Min) response observed in the presence of control ligand and vehicle. Parameters like half maximal effective concentration (EC_{50}) and slope of dose-response curve are indicated.

Primers and oligonucleotides for phagemid library construction

Table S 1 │Name, DNA sequence and length of library oligonucleotides and primers

Name	DNA sequence (3'-5' direction)	Length (bp)
36-mer library oligonucleotide*	GACAGCTCTTGCTAGGGTACCGG $(NNM)_{36}$ CCACGCCGGCGACCTAGGTTTCCGG	156
extension primer	CCTAGCAAGAGCTGTC	16
–221 sequencing forward primer	CGAGAGCGGGCAGTGAG	17

* Reverse complement (MNN: Reverse complement of NNK codon)

Optimization of the transformation efficiency for 36-mer library production

The transformation efficiency, i.e. the number of transformants per µg input DNA, is a critical factor to construct phagemid libraries as it strongly affects their size, diversity and quality. It can be influenced by different parameters like the ligation temperature or the amount of input DNA used for electro-transformation (Sheng et al., 1995). Different ligation and transformation conditions were tested to determine the best experimental parameters to achieve high transformation efficiencies for the 36-mer library production (section 3.10.3).

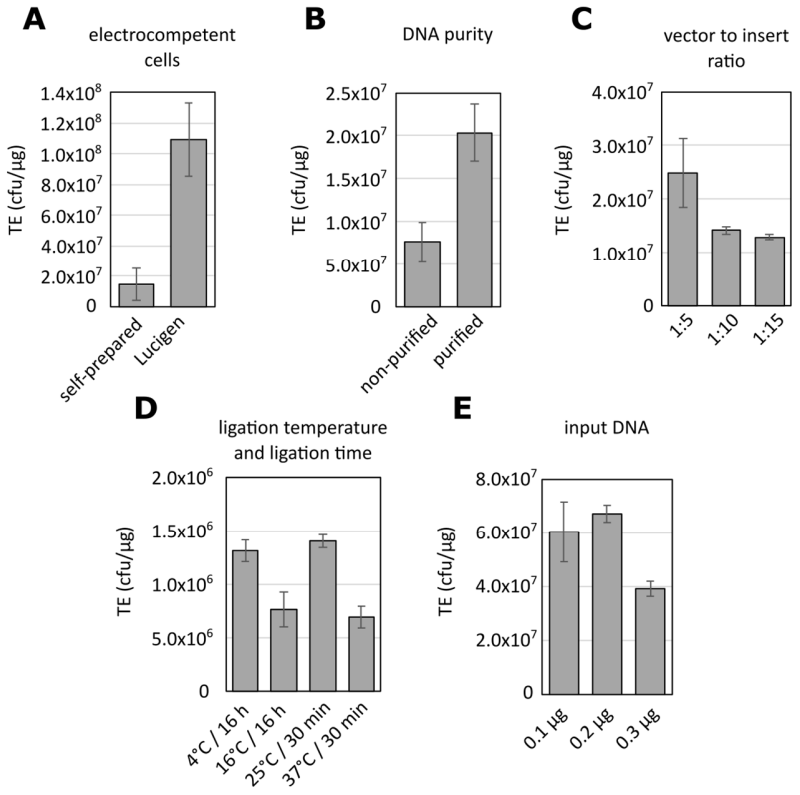

Figure S 13 │Transformation efficiency under different experimental conditions

Different experimental parameters were tested to assess their effect on the transformation efficiency (TE). Experiments were performed with either self-prepared or commercially available electrocompetent *E. coli* TG1 cells (Lucigen). **(A)** Self-prepared electrocompetent *E. coli* TG1 cells were compared to purchased ones ($\leq$ 4 x10^{10} cfu/µg). **(B)** The input DNA, i.e. pSEX81-36-mer phagemids were transformed either immediately after ligation (non-purified) or purified by Sera^{TM} Magnetic Beads (Hawkins et al., 1994) prior to electroporation. **(C)** Different vector to insert molar ratios and **(D)** different ligation temperatures and times were tested. **(E)** Different amounts of input DNA tested for electro-transformation. Transformation efficiencies were determined by colony counting (section 3.10.3). Error bars indicate the SD, measurements were performed in triplicates.

Phagemid library analyses

To analyze the 24-mer and 36-mer phagemid libraries roughly 60 randomly picked library clones were sent for DNA sequencing (Microsynth). In the 24-mer library, 48 out of 60 clones (Table S 2), and in the 36-mer library, 48 out of 64 clones (Table S 3) harbored properly inserted peptides. Information on the peptide sequences, the peptide lengths, the number of TAG stop codons and the number of Cys residues are detailed in Table S 2 and Table S 3.

Table S 2 | Correctly inserted peptides found in the 24-mer library

Clone-Nr.	Peptide sequence	Length (aa)	TAG stop codon	Cys
1	CHLPYPRGYLWTNVSTLWLCTLLH	24	0	2
2	WSEAVPTSSTMPQLCRKLPV*LTW	24	1	1
3	ATPQTSSYPFRLPTGDHPSGGAWS	24	0	0
4	RPGDQLSPIDFKFGPTWHTPSGYP	24	0	0
5	PAPRTSVGRRSCRHSLSPASHRQR	24	0	1
6	EWRLGPVAVGTRPRGRPGKSPRNS	24	0	0
7	RPLPRGDLSIIAPCTDYLNDPICL	24	0	2
8	SEYSNTVHKSPNSMTLRVKRIVL*	24	1	0
9	SQGMYAPADAAAAPLAFSRVW**A	24	2	0
10	G*WPATCPHWLY*TGDVQS*FDPL	24	3	1
11	LRWSKSPRRAADEYVITPMRFRLC	24	0	1
12	PPRRALVILLPVVTHPVVSRGSMA	24	0	0
13	RSNSISIQVNEN*TNRLPKQRVVD	24	1	0
14	NLDIGTSMTLHSYSFHR*QPGAMQ	24	1	0
15	TRLTV*NFPVLSALLWVSALKTRI	24	1	0
16	RPHPPQTVRTSTDPTCPV*MPLTL	24	1	1
17	TPNGPFAIPTLLRLSLCDLSQPLY	24	0	1
18	AFSPFTTNQHHLVL*LEGHDTHMF	24	1	0
19	GVCSAVVSLSSL*QLVMPDPRASL	24	1	1
20	RSPTQAGTHSHRCYAPPGAPVPAR	24	0	1

21	AGTRLSNTPLGYHVAP*GVSRYPN	24	1	0
22	LHAGSSHE*PVYLCKLMLDDNMCD	24	1	2
23	CVVVLPRNVSVSRCPMGTGYSP*S	24	1	2
24	QPHSCMRPWSPPASPSRTGS*AWA	24	1	1
25	RAGVYWG*SSRSL*ERNADAGQL	23	2	0
26	TCQVPNDPFDAYCFSTSRGQ*YLV	24	1	2
27	RPVLAMQQRGPTPLSHIAPRLLPS	24	0	0
28	RDASELAHTVRTGWPV*HLTVPRP	24	1	0
29	ESERSPDNLNGVGCRVLPNPRSCV	24	0	2
30	*VGGKADP*ESNPDPLPRGSPTSM	24	2	0
31	*PGSLGVFSVPALGPTPSHSAKRS	24	1	0
32	DGDCEVKFWAAA*R*TIVSFTNFA	24	2	1
33	GSGLHT**STFFAHKCSPEADCQD	24	2	2
34	GSMEYADLSRQKS**VYYDCHDKP	24	2	1
35	IRAGHPNRSL*RALPSGLSSATQW	24	1	0
36	TSGIMVKSKSLPARAHIGQANFRY	24	0	0
37	LPSPLYEYVYLLPLSTFRSTR*IN	24	1	0
38	DARSGFDG*GACERCGVLLLQTLQ	24	1	2
39	RDVFISSAQTADSRLHVEALAPSA	24	0	0
40	VLRLSTLPVAHNL*LPHAPSVNGL	24	1	0
41	HWGMTLPAPEQNYPLVTQTIPSLG	24	0	0
42	PGMPARAFFGPHTRAR*LEHKSGN	24	1	0
43	C*CTEPRQPLTPRRHSPMETWPSI	24	1	2
44	VLA*STPPHSLGRFQVGVTPRPRT	24	1	0
45	ASSELNAIANASRPGVRRPVRL*P	24	1	0
46	*PSSVVRPHAPRPHTQLP*SFRSP	24	2	0
47	WWSLWAVTSALRPRIVTSSDFPAK	24	0	0
48	PRPCSRPAMVPPSGRTRP*HRTRP	24	1	1

* Glutamine (Q) residues encoded by TAG stop codons.

Table S 3 | Correctly inserted peptides found in the 36-mer library

Clone-Nr.	Peptide sequence	Length (aa)	TAG stop codon	Cys
1	ACNANDPHFLVSQP*SAKTDSNRWKCDMRHTRSHHL	36	0	2
2	AQHIGMLSISTDRY*HMFAHKRFPTNDSPDLSPYPH	36	0	0
3	LLKGESRAKVSYTEYVYSAASTCHTYNQLMSSHSQD	36	0	1
4	LTTTRAMRFKLTHCTGLMLFMPLDAFHVKLYYDEP	35	0	1
5	TWKLRNLTSLSVRMLRLVRFRGFRSGHWHHPHL*Y	35	0	0
6	ALLNREHTTTGVPEPMNASDLLLTSRQGTIAKWNPA	36	0	0
7	TPQGAWARHTTGPCYYARWFVVHRRSVRCVPSAYFP	36	0	2
8	AA*PYKTPLRDMHLNS*SFRKYKSRELSHHILSMNQ	36	0	0
9	IKTQPHYDSRNVVGESMMIHMPPKKLGNTLSWSHWT	36	0	0
10	LPRLA*SRKAVNSLPGDIARLLDRPVPGSSQDKFTP	36	0	0
11	RFWH*DFSRPRTPSKIIVTLKRLIKPLKG*FW*TVV	36	0	0
12	ISIHPRSE*PESLLITEPIKQCYRQSLVPVPLELDT	36	0	1
13	TIHRQVVTYGRQHLRTIWKYLSPLDETYLDGLEATH	36	0	0
14	QVAVTE*NRLKSCTFSTPLTARPM*LWVWDSDSKHN	36	0	1
15	VFMNHWYELTSPIRLAIPMYPNLNQTLGSELTGSGP	36	0	0
16	KLVNRHQP*MRLKRLPKLLCNVIARTPNDVHCPPLT	36	0	2
17	NRALNGAPRVVVRCRELIR*RNIRFIVVRCKVS	33	0	2
18	KSGHLYLR*RSWRATSRHRHSRDRRQDRMKTFRTTG	36	0	0
19	TGWSWK*GTGPTIHAHTFNHALVRPCVVPPITCYFL	36	0	2
20	IIPSCTRN*IGPSLRIPRPNNVKMQPFKA*ARSEAP	36	0	1
21	FCPTPREKQRTYTCVGRPCISLSRDEYSPS*AWTPT	36	0	3
22	VCRRASRYEIFNVNKTRPEHTWSASYTATALKLNKS	36	0	1
23	PDDTEREA*TLKAVKYCDQSSTLNM*TMSIQGNRGS	36	0	1
24	GHATTDPSQNPFLPGHRRMVDGFLLTAEAAAFSCFY	36	0	1
25	LRKDLKYRYNILKYTSKTQKCSMPAAKESYRQRFLA	36	0	1
26	IDRWNDYRWAIR*ITHKSCEPNMP*QYIVAVPASLQ	36	0	1

27	YRHIDFHCT*CRLAGTNYHRMKTLRL*S*NLALKNM	36	0	2
28	PQISKQSKAPHNKVSRTKPQINMHRIVVSGSPTTS*	36	0	0
29	RMNTPSKP*RAGRPTARW*RVFSMEATMITPS*GAV	36	0	0
30	WMVDGFPERPFSAGPITSKSGSSDKEPR*SFNKEIA	36	0	0
31	DSNGAYIVRPPNYMNMLYRSTRIETTQELWKRSKHD	36	0	0
32	QRRFRDHGGLSKFPMGPNDSFLLEHLCPTTGDSYFA	36	0	1
33	PTRTHQDAKPSREAKNGNHLVEVRELQEMPDFLCSS	36	0	1
34	*MLSTRLDGPYCGSPSGNQSLKRWQFTDELWCRSVW	36	0	2
35	GRLHYGLTKLVQCNRTAFLSLLCNRPWFSLRLHAGN	36	0	2
36	GCS*HLR***TPEPCQEADFQYIHCCCLCQVPASWI	36	0	6
37	VG*DLTFL*KQSRPKRKSDMAYLPCVA**IPGHSTV	36	0	1
38	LTLLNTHTSRLYDSPLRPYGRRCLGSHHNT*CIELS	36	0	2
39	AMSHFTDSVPGLARTKKRLSNYRLLQTIEQTHRNIR	36	0	0
40	LGSTPVLFTSFSVLGMVSHCISMRHWVLLTPQSPQP	36	0	1
41	RQKQLSGGRMENSQTHTKSKGTMAPKSSKIETKQCP	36	0	1
42	PHKLLHSVPPHA*QGA*DSTKTRTPGRYWYHPPWPS	36	0	0
43	VSNYTRQGRLMASDQVPRHTRQFLHGTSMLTKFAYT	36	0	0
44	FVSAWRVVPPRITDLLCQYMCYGAMPTVSRV*RRPS	36	0	2
45	VRWPLPKQALSDFPLSKKTCLFNWPWMKSAIST	33	0	1
46	PMWQDASGCEMTQYDSFRRSSIRATCLYHTMAKQQI	36	0	2
47	AKNRIKLLSGNKTREHAMINSFKWRPVQLVF*TDTQ	36	0	0
48	FVTSHDRSALSILWNGP*SLVVLPLLSPVTSFGIGR	36	0	0

* Glutamine (Q) residues encoded by TAG stop codons.

Biopanning of the 24-mer library for identification of RBPs

The 24-mer library was screened against Resomer® surfaces to identify potential RBPs (section 3.13). Enrichment of Resomer® binding peptides after the 3rd and 4th biopanning round was assessed by re-infection of *E. coli* grown to OD_{600} 0.4–0.6 with phagemid elution pools. Library clones were grown on selective LB agar plates and ten randomly picked colonies were sent for DNA sequencing (Microsynth). Table S 4 and Table S 5 show details on the peptide sequences, the peptide lengths, the number of TAG stop codons, the number of Cys residues and the number of hits, respectively.

Table S 4 | Peptide sequences obtained after the 3rd biopanning round against Resomer® surfaces

Clone-Nr.	Peptide sequence	Length (aa)	TAG stop codon	Cys	number of hits
1	RWWSRPPAPSIHD*GSTFSSQPTS	36	1	0	9
2	RHLLWPGWAWNRFVP*SRPAAPAP	36	2	0	2
3	ELRYFRWPFIGIKRNYQSPQYYAG	36	0	0	1
4	RRFFGFPRLPSSIWTTPIPPQSTA	36	0	0	1
5	HSPPWSPPLIRTNPHSRRARE*RR	36	1	0	1
6	DHPHS*WFFPRWRWYHHPPAWITQ	36	1	0	1
7	MALPVLPAYAALRPLCSTFTVYMP	36	0	1	1
8	GPTLIRP*PQKRTT*LSLVRHM	34	2	0	1
9	*HQSHTRQLSRNLGCTYECDSHRA	36	1	2	1
10	NV*LHERNSQPLHISNIYNAATPP	36	1	0	1

* Glutamine (Q) residues encoded by TAG stop codons.

Table S 5 | Peptide sequences obtained after the 4th biopanning round against Resomer® surfaces

Clone-Nr.	Peptide sequence	Length (aa)	TAG stop codon	Cys	number of hits
1	RWWSRPPAPSIHD*GSTFSSQPTS	36	1	0	6
2	RHLLWPGWAWNRFVP*SRPAAPAP	36	1	0	6
3	RPWHRPRPNVDLGYMSTDKVAWP*	36	1	0	2
4	DHPHS*WFFPRWRWYHHPPAWITQ	36	1	0	1
5	SPTNPRVP*SEF*RNVSAGGKPDH	36	2	0	1
6	MNPRAGYQYDIVCRVSFTVLCA	34	0	2	1
7	H*YGWLSAFRSYSPWSALPFPSST	36	1	0	1

* Glutamine (Q) residues encoded by TAG stop codons.

Physicochemical properties of RBP1 and RBP2

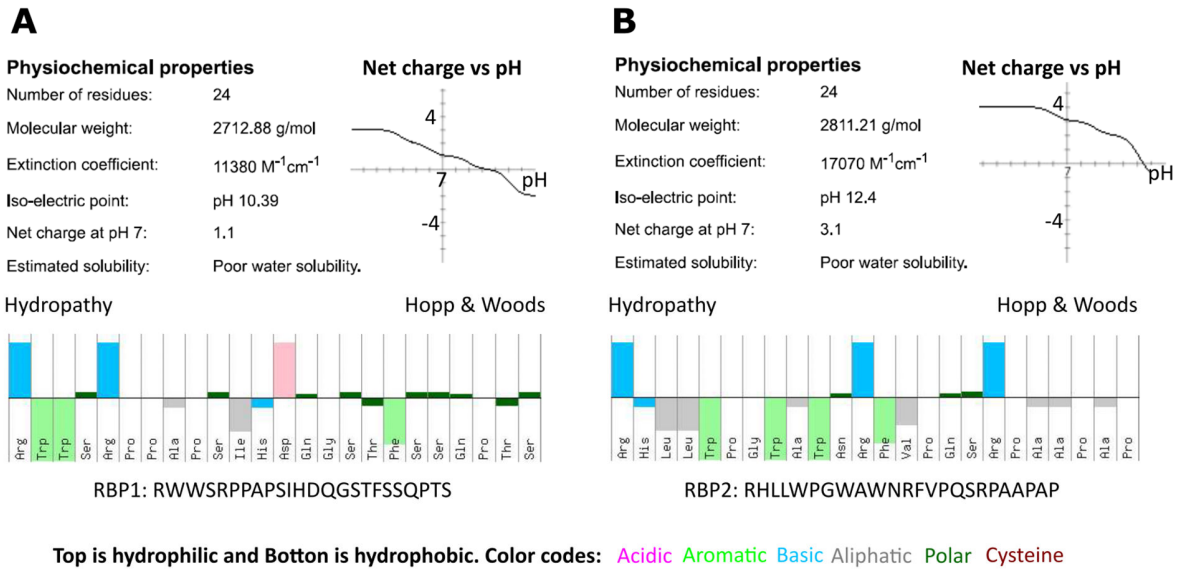

Figure S 14 | Physicochemical properties of RBP1 and RBP2

The theoretical physicochemical properties of **(A)** RBP1 and **(B)** RBP2 were predicted using the peptide calculator PepCalc (Innovagen, 2023).

Biopanning of the 36-mer library for streptavidin binding peptides

The 36-mer library was screened against streptavidin and non-coated microtiter plate wells (section 3.14). Enrichment of binding phagemid particle clones after the 2nd biopanning round was assessed by re-infection of *E. coli* grown to OD_{600} 0.4–0.6 with phagemid elution pools, respectively. The library clones were grown on selective LB agar plates and ten randomly picked colonies were sent for DNA sequencing (Microsynth). Table S 6 show the peptide sequences obtained after the 2nd biopanning round against non-coated wells. Among ten picked clones nine were positively returned.

Table S 6 | Peptide sequences obtained after the 2nd biopanning round against non-coated wells

Nr.	Peptide sequence	Length (aa)	HPM	HPQ
1	EKLEVAFTQRGIMLGLMSHLWEPYAWNS*VFYAML*	36	0	0
2	KTKMKRFLQVPSANA*AWTMPHSGPYRILWKFN*LW	36	0	0
3	GDGTSTSTADTLTSVRPWLLRWYLLWD*AK*SSQGT	36	0	0
4	MLLLWPYKAMSTRGDVKI*AQPAMNDVNKKHYFPGC	36	0	0
5	ILPTVSYPKVWTIDEL*QAMNALTRTRTAHKPSNKR	36	0	0
6	AGPFLLQSKHWYRTGGPLPMKLHLIWFTWGK*PPRG	36	0	0
7	RHLVWWGSIVTPTQWAWLFYNPNWFARQWNAKV*TR	36	0	0
8	*HSRHALWIEPHWTVPSLS*KRGTFLWKWRAGYFSP	36	0	0
9	PF*FPYALSWPGWQPHYSP*D*KLCSELTLSNMEAL	36	0	0

* Glutamine (Q) residues encoded by TAG stop codons.

Overview of designed Switchtag fusions

Table S 7 | Structure, amino acid sequence and MWs of designed Switchtag fusions

Name of Switchtag fusions	Structure and Amino acid sequence (one letter code)	MW (kDa)
Switchtag – RBP2-HBD3	Switchtag– ENLYFQRHLLWPGWAWNRFVPQSRPAAPAPGGGGSGIINTLQK YYCRVRGGRCAVLSCLPKEEQIGKCSTRGRKCCRRKK	33.1
Switchtag – RBP2-HTN3	Switchtag– ENLYFQRHLLWPGWAWNRFVPQSRPAAPAPGGGGSDSHAKRH HGYKRKFHEKHHSHRGYRSNYLYDN	32.0
Switchtag – RBP2-DCD-1L	Switchtag– ENLYFQRHLLWPGWAWNRFVPQSRPAAPAPGGGGSSSLLEKGL DGAKKAVGGLGKLGKDAVEDLESVGKGAVHDVKDVLDSVL	32.9
Switchtag – HBD3-RBP2	Switchtag– ENLYFQGIINTLQKYYCRVRGGRCAVLSCLPKEEQIGKCSTRGR KCCRRKKGGGGSRHLLWPGWAWNRFVPQSRPAAPAP	33.1
Switchtag – HTN3-RBP2	Switchtag – ENLYFQDSHAKRHHGYKRKFHEKHHSHRGYRSNYLYDNGGGG SRHLLWPGWAWNRFVPQSRPAAPAP	32.0
Switchtag – DCD-1L-RBP2	Switchtag– ENLYFQSSLLEKGLDGAKKAVGGLGKLGKDAVEDLESVGKGA VHDVKDVLDSVLGGGGSRHLLWPGWAWNRFVPQSRPAAPAP	33.1

ENLYFQ: Cleavage site of the TEV protease, Underlined: Amino acid sequence of the bifunctional peptide

Solubilization, renaturation and cleavage of Switchtag fusions

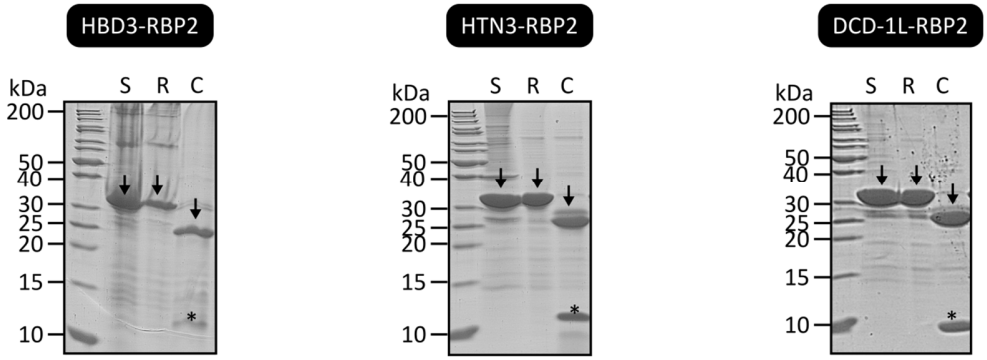

Figure S 15 | SDS-PAGE analysis of HBD3-RBP2, HTN3-RBP2 and DCD-1L-RBP2 preparations

Solubilized (S), renatured (R) and TEV protease cleaved (C) Switchtag-HBD3-RBP2, Switchtag-HTN3-RBP2 and Switchtag-DCD-1L-RBP2 were analyzed by SDS-PAGE (section 3.17). The arrows indicate the locations of Switchtag fusions after solubilization in chaotropic agents, their subsequent refolding, and the Switchtag following TEV protease cleavage. Protein bands corresponding to each target peptide after TEV protease cleavage are highlighted (*).

RP-UPLC-MS analysis of purified HBD3-RBP2

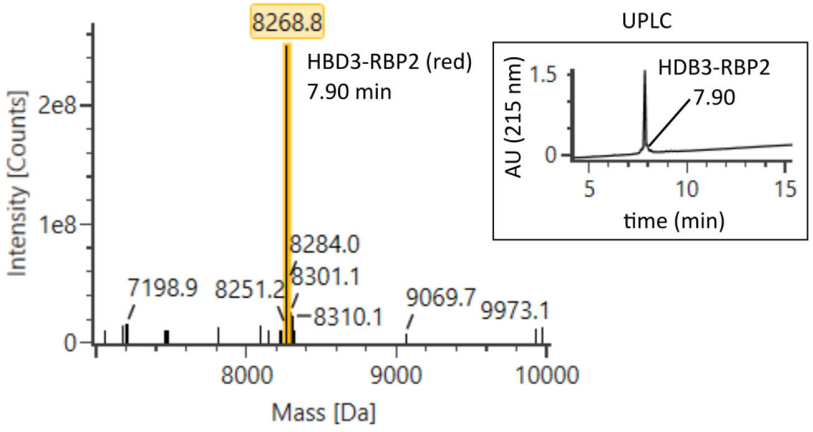

Figure S 16 | RP-UPLC-MS analysis of purified HBD3-RBP2

The identity of purified HBD3-RBP2 was confirmed by RP-UPLC-MS (section 3.18). The UPLC chromatogram monitored at 215 nm indicate the target elution peak and the retention time. Mass chromatogram of the elution signal at 7.90 min was obtained by ESI-TOF mass spectrometric analysis. The observed mass for HBD3-RBP2 is highlighted (yellow) and corresponds to the MW calculated for reduced (red) HBD3-RBP2 (8,269.64 Da, see Table 15).

MIC assays of HBD3-RBP2, HTN3-RBP2 and DCD-1L-RBP2

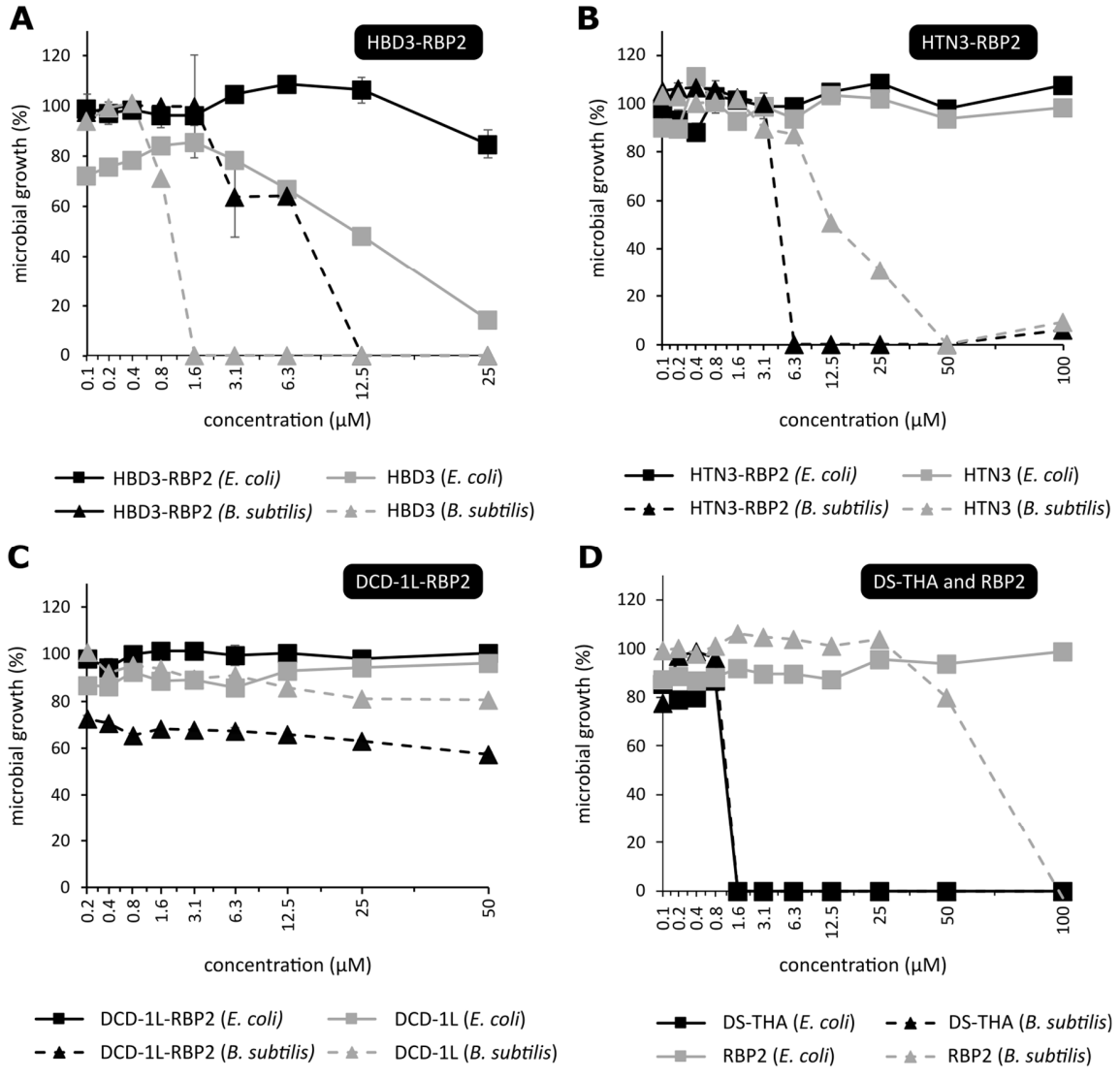

Figure S 17 | Killing curves of different peptides against *E. coli* and *B. subtilis*

In MIC assays the antimicrobial activities of **(A)** HBD3-RBP2 and HBD3, **(B)** HTN3-RBP2 and HTN3, **(C)** DCD-1L-RBP2 and DCD-1L and the peptides **(D)** DS-THA and RBP2 were investigated against *E. coli* and *B. subtilis* (section 3.19.2). Error bars indicate the SD, measurements were performed in duplicates.

Investigation of bacterial growth in absence and presence of mannan

The main objective of this study was to determine if *E. coli* PKL1162 adheres to Resomer® coatings in the absence of the polysaccharide mannan. Mannan's presence on Resomer® coatings may form a barrier, reducing the antimicrobial effect and affecting the contact-killing capabilities of bifunctional peptides in Resomer® coatings. To find this out, bacterial growth on Resomer® surfaces both with and without mannan was explored as described in the following abstracts.

Preparation of mannan-coated Resomer® coatings: Wells of black microtiter plates coated with Resomer® (section 3.20) were incubated with 100 µL of mannan from *S. cerevisiae* in carbonate buffer pH 9.5 (1.2 mg/mL) at 37 °C overnight. The next day, the wells were washed three times with 200 µL of PBS before dried under laminar flow.

Preparation of bacterial solution: Pre-cultures of GFP-expressing *E. coli* PKL1162 were grown from cryo stock in LB medium supplemented with 100 µg/mL ampicillin and 25 µg/mL chloramphenicol at 37 °C and 180 rpm overnight. 25 mL of selective MHB medium in a 250 mL shaking flask was inoculated with pre-culture to a starting OD_{600} of 0.1. The culture was cultivated to OD_{600} 0.4–0.6, the cells were harvested by centrifugation (4,000 *g*, 15 min, RT) and washed two times with PBS before adjusted to OD_{600} 0.4 (corresponds to 3.2 x10^8 cells/mL) and 0.004 (corresponds to 3.2 x10^6 cells/mL) with PBS, respectively.

Bacterial adhesion assay: 50 µL of the bacterial solutions were applied onto Resomer® surfaces coated with mannan and onto uncoated Resomer® surfaces, respectively. Subsequently, the cells were permitted to adhere by incubation at 37 °C for 2 h. Afterwards, the bacterial solution was removed, and the surfaces were washed three times with 300 µL of PBS to get rid of non-adherent bacteria. Then, 200 µL MHB media supplemented with 100 µg/mL ampicillin and 25 µg/mL chloramphenicol were added to induce growth of adherent bacteria. Cell growth on mannan-coated and uncoated Resomer® surfaces was monitored at 37 °C for 16 hours by fluorescence readout (Figure S 18).

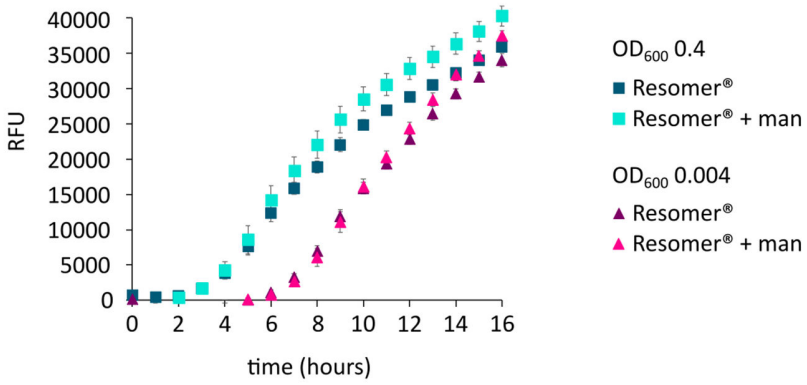

Figure S 18 | Growth of adherent *E. coli* PKL1162 in presence and absence of mannan

Growth of adherent *E. coli* PKL1162 cells on Resomer® coatings in the presence (+ man) and absence of mannan were monitored for 16 hours by fluorescence readout (section 3.20). Fluorescence signal is indicated as RFU (Relative Fluorescence Units). Different inoculum concentrations like 3.2 $x10^8$ cells/mL (OD_{600} of 0.4, light and dark blue) or 3.2 $x10^6$ cells/mL (OD_{600} of 0.004 pink and purple) were employed to evaluate its effect on bacterial growth. Error bars indicate the SD, measurements were performed in triplicates.

V. List of Supplementary Figures and Tables

List of Supplementary Figures

List of Supplementary Tables

VI. Acknowledgements

First of all, I would like to thank my doctoral supervisor **Prof. Dr. Lutz Schmitt**, not only for his willingness to accept me as an external PhD student and to assess my dissertation, but also for his guidance and support throughout my work. Thank you for always having an open ear for scientific discussions and for allowing us to draw on your immense wealth of experience.

I would also like to extend my thanks to **Prof. Dr. Karl-Erich Jaeger** who kindly accepted to be the co-referee of this dissertation. Furthermore, I really appreciate the helpful recommendations and advice you provided in contribution to this work.

In particular, I would like to express my sincere gratitude to my mentor **Dr. Christian Schwarz**, the managing director of Numaferm GmbH, primarily for giving me the opportunity to do my PhD research in his facilities. Back then, when I was unsure whether to embark on this journey you encouraged and placed your faith in me. Now, four years later I can say that engaging in academic research within an industrial environment was amazing and a rewarding experience. I am grateful that you granted me this opportunity and I deeply appreciate your guidance and support throughout these years. Your persistent optimism in every situation is inspiring.

Furthermore, I would like to extend my thanks to all my colleagues at Numaferm GmbH. Especially, to **Dr. Florian Tieves** who immensely contributed to the two publications and supported me with words and deeds, to **Dr. José Montoya** who I had numerous fruitful scientific discussions about Phage Display with, but also to **Dr. Andreas Uhde, Dr. Hilke Thron and Dr. Janpeter Stock** for their constant support in every aspect. Honestly, I cannot think of better colleagues, thank you for always encouraging me throughout these years. I would also like to thank my former student **Florian Neusius** who did a fantastic job at Numaferm GmbH, and I really enjoyed supervising you.

My sincere thanks also go to **Jun.-Prof. Dr. Stephan Schmidt** and **Prof. Dr. Laura Hartmann** for providing me with the *E. coli* PKL1162 strain to perform the bacterial adhesion assays. I would also like to thank you both for the scientific discussions and helpful advice you provided related to materials and strategies for the implant surface coating.

My thanks also go to **Dr. Hansjörg Götze**, the managing director of NanoTag Biotechnologies GmbH, who performed the functional studies of the purified anti-α-tubulin scFv clone F2C.

I would also like to express my special appreciation to my husband **Dr. David Wetzel**, who has accompanied me along my adventurous journey. Thank you for always showing interest and enthusiasm in my work and for your great support both scientifically and in everyday life. We have been through many ups and downs together, thank you, for being my rock on which I can always rely.

Lastly, I am grateful for my **Family and Friends** for their unconditional love and emotional support. You have been behind my back when needed and kept me grounded, I deeply appreciate it.

VII. Declaration

Ich versichere an Eides statt, dass die vorliegende Dissertation von mir selbständig und ohne unzulässige fremde Hilfe unter Beachtung der „Grundsätze zur Sicherung guter wissenschaftlicher Praxis an der Heinrich-Heine-Universität Düsseldorf“ erstellt worden ist. Diese Dissertation wurde in der vorgelegten oder in ähnlicher Form noch bei keiner anderen Institution eingereicht. Ich habe bisher keine erfolglosen oder erfolgreichen Promotionsversuche unternommen.

_____ _____

(Ort, Datum) Bach-Ngan Wetzel